

# User Guide to the PDS Dataset for the Cassini Composite Infrared Spectrometer (CIRS)



Conor A. Nixon, Monte S. Kaelberer, Nicolas Gorius  
And The CIRS Instrument Team

NASA Goddard Space Flight Center  
Greenbelt, MD 20771

V11.6 November 13<sup>th</sup> 2012

GSFC STI/DAA Release Authorization #20120809115444

## Frontispiece

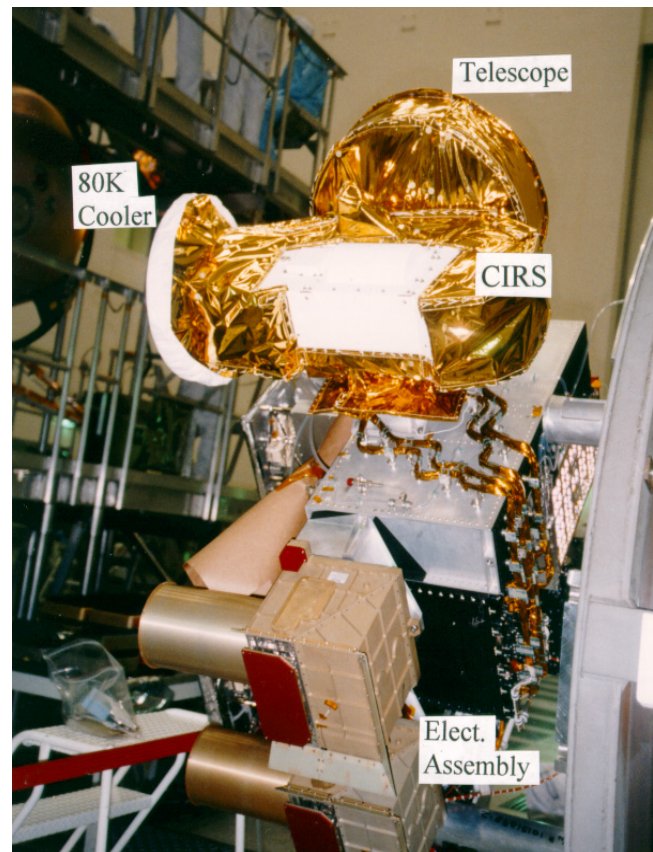
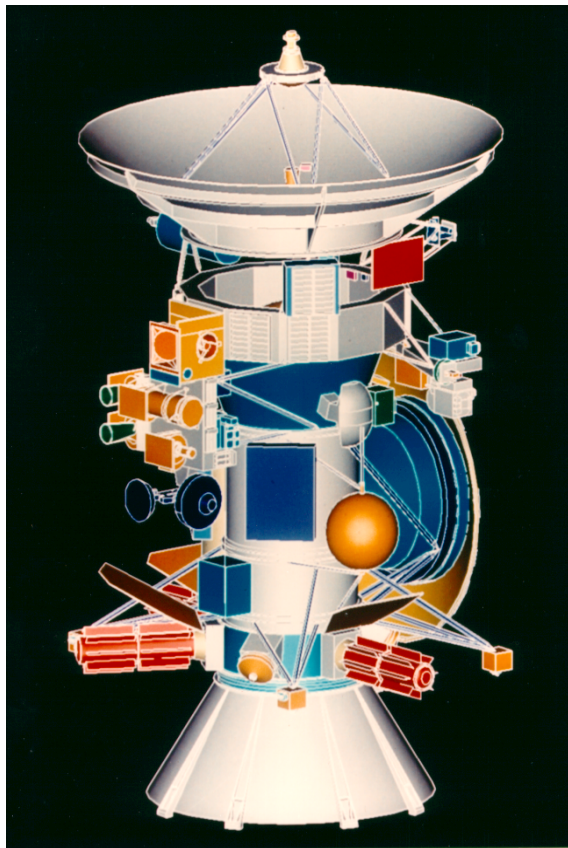


Figure 1: (left) The Cassini spacecraft showing location of CIRS (blue) on the Remote Sensing Palette (RSP). (Right) photograph of CIRS mounted on the spacecraft before launch.

# Table of Contents

<b>FRONTISPIECE</b>	<b>I</b>
<b>PREFACE</b>	<b>V</b>
<b>WRITING AND REVIEWING TEAM</b>	<b>VI</b>
<b>LIST OF ACRONYMS AND ABBREVIATIONS</b>	<b>VII</b>
<b>LIST OF FIGURES</b>	<b>XI</b>
<b>LIST OF TABLES</b>	<b>XVI</b>
<b>VERSION HISTORY</b>	<b>XVIII</b>
<b>1.0 INTRODUCTION</b>	<b>1</b>
1.1 WELCOME	1
1.2 PURPOSE	1
1.3 SCOPE	1
1.4 HOW TO USE THIS GUIDE	1
<b>2.0 GENERAL INFORMATION</b>	<b>3</b>
<b>2.1 INSTRUMENT CHARACTERISTICS</b>	<b>3</b>
2.1.1 CASSINI MISSION	3
2.1.2 INSTRUMENT DESIGN	5
2.1.3 INSTRUMENT OPERATION MODES	8
2.1.4 TYPES OF DATA AT PDS	12
2.1.5 DATA UNIT DEFINITION	13
<b>2.2 SCIENCE OBJECTIVES</b>	<b>16</b>
<b>2.3 OBSERVATION STRATEGIES</b>	<b>17</b>
2.3.1 SATURN	17
2.3.2 RINGS	19
2.3.3 TITAN	24
2.3.4 ICY SATELLITES	27
2.3.5 OTHER TWTs AND WGS	30
2.3.6 PRIMES AND RIDERS	30
<b>2.4 DATA GAPS</b>	<b>30</b>
2.4.1 DATA THAT DID NOT REACH THE GROUND	30
2.4.2 DATA THAT COULD NOT BE CALIBRATED	31
2.4.3 LIST OF ANOMALIES	31
<b>2.5 ELECTRICAL INTERFERENCES (SPIKES) AND OTHER DATA ISSUES</b>	<b>32</b>
2.5.1 BACKGROUND	32
2.5.2 MITIGATION	36
<b>3.0 CALIBRATION OF THE INSTRUMENT</b>	<b>42</b>

<b>3.1 OVERVIEW OF DATA FLOW</b>	<b>42</b>
<b>3.2 INSTRUMENT READOUT TO RAW TABLES</b>	<b>43</b>
3.2.1 RAW DATA TABLES	44
3.2.2 NAVIGATION DATA TABLES	44
<b>3.3 CLEANING AND FILTERING OF INTERFEROGRAMS</b>	<b>50</b>
3.3.1 OVERVIEW	51
3.3.2 SUPPRESSION OF FP1 SPIKES: INTRODUCTION	51
<b>3.4 CALIBRATION OF THE DATA</b>	<b>52</b>
3.4.1 WAVELENGTH CALIBRATION	52
3.4.2 RADIOMETRIC CALIBRATION	54
<b>3.5 POST-PROCESSING: RESAMPLING AND APODIZATION</b>	<b>59</b>
3.5.1 APODIZATION	59
3.5.2 RESAMPLING	61
<b>3.6 ESTIMATION OF NOISE EQUIVALENT SPECTRAL RADIANCE (NESR)</b>	<b>62</b>
3.6.1 NESR CONVERSIONS	63
3.6.2 NESR SPREADSHEETS AND PLOTS	64
<b>3.7 DISCUSSION: LIMITATIONS OF STANDARD SPECTRA PRODUCTS</b>	<b>66</b>
<b>3.7.1 BANDPASS AND ALIASING</b>	<b>66</b>
<b>3.7.2 FP1 LONG WAVELENGTH CALIBRATION</b>	<b>68</b>
<b>3.7.3 DEEP SPACE CALIBRATION BLOCKS</b>	<b>69</b>
<b>4.0 HOW TO SEARCH AND EXTRACT DATA</b>	<b>70</b>
<hr/>	
<b>4.1 DATA FORMAT DESCRIPTION</b>	<b>70</b>
4.1.1 DATA LEVELS	71
4.1.2 VANILLA DATABASE	72
<b>4.2 VANILLA SEARCH TOOL: OVERVIEW</b>	<b>72</b>
4.2.1 VANILLA HELP	73
4.2.2 DATABASE STRUCTURE	74
4.2.3 DATASET USAGE	74
4.2.4 ‘FIELDS’ PARAMETER	76
4.2.5 ‘SELECT’ PARAMETER	76
4.2.6 VANILLA OUTPUT	77
4.2.7 TIPS AND TRICKS	77
<b>4.3 VANILLA AND THE CIRS DATABASE</b>	<b>78</b>
<b>4.4 VANILLA EXTRACTION OF POINTING/GEOMETRY</b>	<b>81</b>
<b>4.5 FINAL WORDS ON VANILLA</b>	<b>86</b>
<b>4.6 OTHER EXTRACTION TOOLS</b>	<b>87</b>
<b>5.0 END-TO-END EXAMPLES OF DATA USE</b>	<b>88</b>
<hr/>	
<b>5.1 OVERVIEW AND GENERAL ALGORITHM</b>	<b>88</b>
5.1.1 SELECTION OF OBSERVATIONS	88
5.1.2 SUBSET OBSERVATIONS	89
5.1.3 BAD DATA CHECK	90
5.1.4 AVERAGE SPECTRA	90
5.1.5 FIELD OF VIEW MODELING	91
5.1.6 RADIANCE MODELING OF THE SPECTRUM	91
5.1.7 VANILLA END-TO-END GENERIC EXAMPLE	92



<b>5.2 WORKED EXAMPLE 1: ICY SATELLITE SCIENCE</b>	<b>95</b>
5.2.1 INTRODUCTION	95
5.2.2 DECIDING WHICH OBSERVATIONS TO USE	95
5.2.3 POINTING ADJUSTMENTS	96
5.2.4 REJECTION OF BAD DATA.	97
5.2.5 DATA ANALYSIS	98
<b>5.3 WORKED EXAMPLE 2: SATURN SCIENCE</b>	<b>99</b>
5.3.1 OVERVIEW	99
5.3.2 SATURN DATA SELECTION	100
5.3.3 ESTIMATION OF SPECTRAL NOISE	103
5.3.4 POSSIBLE SYSTEMATIC ERRORS	104
5.3.5 DATA ANALYSIS	105
<b>FURTHER INFORMATION SOURCES</b>	<b>109</b>
<b>BIBLIOGRAPHY</b>	<b>111</b>
<b>APPENDIX</b>	<b>113</b>
<b>A. EXAMPLE PDT DESIGNS FOR OBSERVATIONS</b>	<b>113</b>
A.1 SATURN	113
A.2 RINGS	119
A.3 TITAN	123
A.4 SATELLITES	128
<b>B. LIST OF MAJOR DATA GAPS</b>	<b>134</b>
<b>C. THE CIRS FP1 SPIKE SUPPRESSION ALGORITHM: METHODOLOGY</b>	<b>138</b>
C.1 CALCULATION OF THE 0.5 HZ AND 8.0 HZ REFERENCE WAVEFORMS (“COMBS”)	140
C.2 CALCULATION OF DE-SPIKED FILTERED INTERFEROGRAMS (FIFMS)	140
<b>D. EFFECTIVE INTEGRATION TIMES</b>	<b>142</b>
<b>E. CONTACT INFORMATION</b>	<b>145</b>

## Preface

By 2010, an important topic of discussion within the Cassini Project Science Group (PSG) was how best to improve accessibility for non-Cassini insiders to the public Cassini data archive at the Planetary Data System (PDS). The result was an initiative to produce User Guides for the datasets of each of the twelve Cassini instruments, including this one for the Composite Infrared Spectrometer (CIRS). This Guide has been written with two communities in mind. First and foremost, scientists external to the Cassini Project who seek to use the CIRS data as archived in the Planetary Data System (PDS). In addition, it is intended to be a reference guide for those internal to the CIRS team.

The writing, editing and review process (with multiple iterations) took two years to finally complete, and was the result of a collective effort from a large number of CIRS team members – see the list on the next page. We also wish to express our sincere express thanks to the five external reviewers (Katia Macheva, Tom Mommary, and three anonymous) whose comments were invaluable in helping to refine this product.

We hope you find this Guide to be useful, intelligible and comprehensive. However, we – the writing team – consider this to be a living breath work-in-progress, and look forward to updating, amending and expanding the Guide in response to comments we receive from the readership. Please tell us how to improve it!

Conor A. Nixon, NASA GSFC

Monte S. Kaelberer, ADNET Systems

Nicolas Gorius, Catholic University of America

December 1<sup>st</sup> 2012

## Writing and Reviewing Team

This document is the result of the combined efforts of a large number of persons associated with the CIRS team, who contributed to diverse aspects of the writing, figures, editing.

Achterberg, Richard K.	<i>Rings science, apodization example</i>
Albright, Shane	<i>Instrument operating modes/Data gaps and anomalies</i>
Ansty, Todd M.	<i>Titan science/observation design</i>
Brasunas, John C.	<i>Calibration method</i>
Brooks, Shawn	<i>Rings science/observations</i>
Carlson, Ronald C.	<i>Data flow/preprocessing</i>
Fletcher, Leigh N.	<i>Saturn worked example</i>
Guandique, Ever	<i>Calibration pipeline</i>
Gorius, Nicolas	<i>Calibration pipeline</i>
Hesman, Brigitte	<i>Saturn observations</i>
Howett, Carly	<i>Icy satellites worked example</i>
Flasar, F. Michael	<i>Editorial direction</i>
Kaelberer, Monte S.	<i>Lead author/editorial</i>
Nixon, Conor A.	<i>Lead author/editorial</i>
Pilorz, Stuart	<i>Rings science/observations</i>
Schinder, Paul	<i>Navigation tables description</i>
Segura, Marcia	<i>Icy satellite science/data gaps</i>
Simon-Miller, Amy	<i>Saturn Observations</i>

The document also benefited greatly from careful proof-reading and suggestions from: Bruno Bézard, Frederic Taylor and Nick Teanby. If your name has been accidentally omitted, thank-you, and tell us!

## List of Acronyms and Abbreviations

Acronyms and abbreviations are color-coded as follows:

BLUE	Cassini
RED	CIRS
BLACK	other

---

Abbrev.	Long Form	Notes
AD	Analog-(to)-Digital (Converter)	
AWG	Atmospheres Working Group	Until 2005. Replaced with SWG (Saturn) and TWG.
BIU	Bus Interface Unit	Hardware for communicating between CIRS and spacecraft data bus.
B/S	Beam-Splitter	
CDS	Command and Data System	Spacecraft data-handling pathway
CIRS	Composite Infrared Spectrometer	
CML	Central Meridian Longitude	
CSM	Cassini Solstice Mission	Synonym for XXM
DSN	Deep Space Network	
DWG	Discipline Working Group	(AWG, RWG etc)
EM	Equinox Mission	Same as XM
FFT	Fast Fourier Transform	a.k.a. Cooley-Tukey algorithm
FP	Focal Plane	
FPA	(mid-IR) Focal Plane Assembly	

FOV	Field of View	
FSW	Flight Software	
HGA	High Gain Antenna	
ICO	Instrument Check-Out	
IFM/IFGM	Interferogram	
ILS	Instrumental Line Shape	Apodized or Unapodized spectral line shape
IR	Infrared	
ISS	Imaging Science Subsystem	Not to be confused with the International Space Station
ISWG	Icy Satellites Working Group	From 2005, replacing SWG.
MUX	Multiplexer	
NAC	Narrow Angle Camera	Part of the ISS instrument
NAIF	Navigation and Ancillary In-Formation	NASA ephemeris system for computing positions of spacecraft and solar system bodies
OST	Orbiter Science Team	TOST, SOST etc
PC	Photoconductive (detectors)	CIRS FP3
PDS	Planetary Data System	
PIE	Pre-Integrated	
PM	Prime Mission	
PV	Photovoltaic (detectors)	CIRS FP4
RCS	Reaction Control Systems	a.k.a. spacecraft reaction wheels
RBOT	RWA Bias Optimization Tool	
RMS	Root Mean Square	Standard mathematical term
RPM	Revolutions per minute	
RSP	Remote Sensing Palette	CIRS, ISS, VIMS, UVIS

RTI	Real Time Interrupt	1/8 sec signal from spacecraft clock
RWA	Reaction Wheel Assembly	
RWG	Rings Working Group	
SC	Spacecraft	
SCET	Spacecraft Event Time	
SM	Solstice Mission	Equivalent to XXM
SNR or S/N	Signal to Noise Ratio	Standard mathematical definition
SOI	Saturn Orbit Insertion	
SOPC	Science Operations and Planning Computer	
SOST	Satellites Orbiter Science Team	
SPICE	(not an acronym but a useful mnemonic is "Spacecraft, Planetary, Instrument, Camera, Event")	Navigation 'kernel' data files that are inputs to NAIF
SWG	Surfaces Working Group	Until 2005. Replaced with ISWG.
SWG	Saturn Working Group	Post-2005, replacing AWG.
TEA	Titan Exploration at Apoapsis	Another type of Cassini timeline segment
TOST	Titan Orbiter Science Team	
TWG	Titan Working Group	Formed 2005 (see AWG & SWG)
TWT	Target Working Team	
UVIS	Ultraviolet Imaging Spectrometer	Cassini instrument
VIMS	Visible and Infrared Mapping Spectrometer	Cassini instrument
WAC	Wide-Angle Camera	Part of the ISS instrument
XM	(Cassini) extended mission	2008-2010
XXM	(Cassini) extended extended mission	2010-2017



ZPD      Zero Path Difference



## List of Figures

Figure 1: (left) The Cassini spacecraft showing location of CIRS (blue) on the Remote Sensing Palette (RSP). (Right) photograph of CIRS mounted on the spacecraft before launch. ...	i
Figure 2: Cassini mission overview showing Saturn orbits and satellite encounters, as of April 22 <sup>nd</sup> 2012. ....	4
Figure 3: CIRS mechanical layout from Kunde et al. (1996). ....	6
Figure 4: schematic layout of the CIRS instrument optical pathways. Incoming light from the telescope (not shown) at top is split into the mid-IR (left path) and far-IR (right path) interferometers. Both interferometers share a common scan mechanism. ....	7
Figure 5: CIRS mid-infrared focal plane layout, showing detector spacing and numbering. ....	8
Figure 6: Modeled thermal heating on mid-IR FPA during rolling downlinks with an equilibrium temperature of 74.6 K. ....	10
Figure 7: Modeled thermal heating on mid-IR FPA during rolling downlinks using setpoint 20. ....	10
Figure 8: schematic summary of CIRS Titan observations (not all shown).....	27
Figure 9 - BIU average power consumption. ....	33
Figure 10 - sample BIU transient waveforms showing the BIU in-rush current (a) and supply voltage, Vcc (b) versus time.....	34
Figure 11 – plot of averaged FP1 interferogram data showing electrical interferences (spikes) .....	35
Figure 12 – comparison of averaged FP1 interferogram data from different mission periods	38
Figure 13 – FP1 uncalibrated spectrum before (blue) and after (red) despiking.....	39
Figure 14 – raw FP3 uncalibrated spectrum before (blue) and after (red) despiking.....	40
Figure 15 – Saturn spectrum before and after despiking .....	41
Figure 16: block diagram of data flow from the CIRS instrument to the eventual user. ....	42
Figure 17: flowchart of CIRS data at GSFC. For definition of Vanilla see Section 4.1.2 .....	43
Figure 18: block diagram showing checks performed on raw interferogram data.....	50
Figure 19: CIRS laser modes .....	54

Figure 20: simple model of interferometer.....	55
Figure 21: apodization functions in the spatial and spectral domains .....	59
Figure 22: example of Titan T23 FIRNADCMP north polar spectrum (average of 800 FP3 spectra), showing the effect of apodization (blue) versus the unapodized spectrum (red). .....	61
Figure 23: NESR for FP1 versus spectral resolution .....	65
Figure 24: NESR for FP3 versus spectral resolution.....	65
Figure 25: NESR for FP4 versus spectral resolution.....	66
Figure 26: frequency filter applied to short wavelength end of CIRS FP4. ....	67
Figure 27: example CIRS high resolution ( $0.5 \text{ cm}^{-1}$ ) spectrum, with ‘clean’ bandpasses for each focal plane in blue and ‘aliased’ ranges in red. ....	68
Figure 28: schematic of CIRS archive volume creation.....	70
Figure 29: relative locations of CIRS detectors, showing numbering of pixels and q-points...71	
Figure 30: temperatures across Mimas from Rev 144, plotted in RA/DEC space with the expected limb location depicted by the white circle.....	97
Figure 31 - Temperature RA/DEC plot for Rev 126 Mimas, showing hot bad pixels in the center of the disk. ....	98
Figure 32 - Surface temperature map of Mimas, produced using Rev 144 data. For full description of this plot see Figure 2 of Howett et al., 2011.....	99
Figure 33: Example of CIRS $2.5 \text{ cm}^{-1}$ spectra of Saturn using the mid-infrared focal planes, FP3 and FP4. The upper abscissa shows wavelengths in $\mu\text{m}$ . Emission features of $\text{CH}_4$ ( $7.7 \mu\text{m}$ ), ethane ( $12.3 \mu\text{m}$ ) and acetylene ( $13.8 \mu\text{m}$ ) are visible, along with absorptions due to $\text{PH}_3$ and $\text{NH}_3$ ( $8\text{-}11 \mu\text{m}$ ) and the collision-induced continuum of $\text{H}_2$ ( $15+ \mu\text{m}$ ).....	100
Figure 34: diagram showing three types of observations used - COMPSIT $0.5 \text{ cm}^{-1}$ ‘sit-and-stare’ integrations at specific latitudes, MIRMAP $2.5 \text{ cm}^{-1}$ integrations using the same technique, and hemispherical FIRMAPs at $15.0 \text{ cm}^{-1}$ resolution where the arrays are scanned north-south over the central meridian. ....	101
Figure 35: FIRMAP $15 \text{ cm}^{-1}$ observations of Saturn’s methane emission associated with the eruption of the storm in 2010 (Fletcher et al., 2011). Each FIRMAP focuses on a single hemisphere, but captures all longitudes.....	102
Figure 36: MIRMAPs can also be used to map out contrasts in thermal emission for a narrow latitudinal width. This figure shows two MIRMAPs from July 2011, focusing on methane emission from Saturn’s storm.....	102

Figure 37: Example of MIRTMAP observations at 2.5 cm<sup>-1</sup> for the northern hemisphere, showing how the arrays are stepped from north to south as Saturn rotates beneath the spacecraft. .... 103

Figure 38: Saturn’s temperature field derived from a co-addition of all available FIRMAP observations from the prime mission. The region between 10-80 mbar is a smooth interpolation between the two regions of CIRS sensitivity. Temperatures below 800 mbar are a smooth relaxation back to the a priori profile. See (Fletcher L. N., 2010) for details..... 106

Figure 39: The meridional distribution of PH<sub>3</sub> derived from CIRS 1100-1200 cm<sup>-1</sup> FP4 observations at 2.5 cm<sup>-1</sup> using a parameterized profile (Fletcher L. N., Phosphine on Jupiter and Saturn from Cassini/CIRS, 2009). .....107

Figure 40: COMPSIT with the focal planes on the central meridian. Also shows the deep space position..... 113

Figure 41: COMPSIT with FP1 offset for high emission angle studies. Also shows deep space position. .... 114

Figure 42: COMPSIT with FP3 offset for high-emission angle studies. Also shows deep space position. .... 114

Figure 43: MIRMAMP on the central meridian. Also shows deep space position..... 115

Figure 44: MIRTMAP with focal planes at multiple latitude positions on the central meridian. Also shows the deep space positions. .... 115

Figure 45: FIRMAP showing the targeting positions and deep space position. .... 116

Figure 46: FIRMAP showing the focal planes for part of an observation. This shows the slewing across the northern hemisphere. .... 116

Figure 47: LIMBINT showing the entire observation and deep space position. Please note that LIMBMAP's also look like this except they have many target latitudes..... 117

Figure 48: LIMBINT at altitude position 1. Focal planes are oriented normal to the local latitude limb to sound the first altitude position. This will be the same for LIMBMAP's. .... 117

Figure 49: LIMBINT at the second altitude position..... 118

Figure 50: NADIROCC shown along with the deep space positions. .... 118

Figure 51 - A TEMP, CIRS\_074RI\_TEMPL13LP001\_PRIME, showing four radial scans taken from a relatively low spacecraft emission angle. .... 119

Figure 52 - A TDIF, CIRS\_089RI\_TDIFN45HP001\_PRIME. ....120

Figure 53 - A TDIF is composed of two scans: one on the lit side of the rings, the other on the unlit side of the rings but with an otherwise comparable geometry. In this case the rings have been scanned at a local hour angle of 12h and 18h from both the lit and unlit side of the rings. ....120

Figure 54 - Temperatures within Saturn's shadow are measured by scanning the FP1 detector in the vicinity of and within the planet's shadow. Each point in each scan is offset in longitude from the edge of the planet's shadow by an amount determined by the distance of that point from Saturn. The time it would take a ring particle moving on a circular Keplerian orbit to traverse the longitudinal offset at a given radial distance is identical across an individual scan. Offsets used in these PSHAD scans can be calculated relative to the egress or ingress shadow boundary. .... 121

Figure 55 - Azimuthal scans reveal temperature variations in the course of an orbit around Saturn. Due to RBOT considerations, such long duration azimuthal scans are no longer performed..... 122

Figure 56 - During POLARIZ observations CIRS integrates on the rings from three distinct orientations in order to look for any polarization in the signal originating from the rings. The outer C ring is being targeted in CIRS\_113RI\_POLARIZ181\_PRIME. Deep space spectra are also obtained at the same three spacecraft orientations. .... 122

Figure 57: T6 FIRLMBT ..... 123

Figure 58: T6 FIRLMBBAER .....124

Figure 59: T6 FIRLMBINT .....124

Figure 60: T6 FIRNADMAP .....125

Figure 61: T6 MIRLMBINT ..... 125

Figure 62: T6 MIRLMBMAP.....126

Figure 63: T6 FIRNADCMP .....126

Figure 64: T6 MIDIRTMAP ..... 127

Figure 65: Mimas FP3DAYMAP in Rev 126A.4 SATELLITES.....128

Figure 66: Enceladus FP1DRKMAP Rev 131.....128

Figure 67: Enceladus SECLNX in Rev 8.....129

Figure 68: Iapetus FP13MAPS Rev 00C.....129

Figure 69: Hyperion FP1GREEN Rev 15 ..... 130

Figure 70: Tethys FP1FP3MAP Rev 15 ..... 130

Figure 71: Enceladus Collaborative Observation taken in Rev 28. Includes ISS, UVIS, and VIMS pointing as well as CIRS FP1, FP3, and FP4..... 131

Figure 72: Rhea FP1SECLNX - Rhea eclipse exit on REV 71 ..... 131

Figure 73: Tethys FP13STARE taken in Rev 73 .....132

Figure 74: Enceladus distant FP3/4 map and FP1 Stare taken in Rev 74 .....132

Figure 75: Enceladus FP1 Eclipse Scan/Map of the South Pole on Rev 80 .....133

Figure 76: CIRS spike suppression algorithm block diagram ..... 139

Figure 77: anatomy of an asymmetric interferogram.....142

Figure 78: inverse polynomial fit of scan time to spectral resolution..... 144



## List of Tables

Table 1: Cassini Mission Phases .....	3
Table 2: CIRS set point temperatures (all in Kelvin) .....	9
Table 3: pixel modes.....	11
Table 4: PDS directories .....	13
Table 5: CIRS PDS data object types.....	13
Table 6: CIRS Saturn observation types .....	17
Table 7: summary of CIRS Prime Mission rings observations and scientific objectives.....	20
Table 8: summary of CIRS XM Mission rings observations and objectives. ....	23
Table 9: summary of CIRS XXM mission rings observations and objectives .....	23
Table 10: historical summary of CIRS rings naming conventions.....	24
Table 11: CIRS Titan observation descriptions.....	24
Table 12: CIRS icy satellite observation descriptions .....	28
Table 13: a list of the possible stellar targets that could be used for testing purposes that could have entries in the POI tables. The numerical id's are artificial, and have nothing to do with NAIF id's. Not all of these were used during the mission.....	47
Table 14: list of objects that were included in the NAV tables during the Jupiter flyby. The body/target id is identical with the NAIF id of the body.....	48
Table 15: list of objects that are included in the NAV tables from the Saturnian system. The body/target id is identical with the NAIF id of the body.....	48
Table 16: native and resampled spectrum point spacings .....	62
Table 17: spectral resolution, scan time (RTI), effective integration and frame times .....	63
Table 18: actual and clean bandpasses for each focal plane .....	67
Table 19: table keys at a glance.....	72
Table 20: Details of the CIRS FP3 observations used in this analysis. Local time is defined as the angular rotation of the body, in degrees, since local midnight. The names of the observations used are (corresponding from top to bottom in the table):	

CIRS_126MI_FP3DAYMAP001_PRIME, CIRS_139MI_MIMAS001_PRIME and CIRS_144MI_MIMAS001_PRIME.....	96
Table 21: list of major data gaps.....	134
Table 22: Coefficients for the inverse 5th order polynomial fit to effective integration time as a function of spectral resolution .....	145

## Version History

<b>Date</b>	<b>Version</b>	<b>Notes</b>
13-Nov-2012	11.6	First public release version

## 1.0 Introduction

### 1.1 Welcome

This is the User Guide to the CIRS instrument of the Cassini spacecraft. A User Guide is being prepared for each of the Cassini instruments by the instrument science teams. We hope you find this guide useful, and that it enables you to conduct research and publish findings based on the Cassini CIRS public dataset. Enjoy!

### 1.2 Purpose

This guide is written for scientists who are using, or contemplating the use of publicly available CIRS data in the Atmosphere's Node of the Planetary Data System (PDS). It is intended to pass along the 'corporate knowledge' of CIRS-team insiders to the wider scientific community, especially in the longer term when the Cassini mission has ended and the instrument teams disbanded. Specific goals of this document include:

- An introduction to the instrument, and the types of observations made for different target bodies and various science goals.
- What data is available and how to extract the particular subset you are interested in.
- Examples of how the data can be used.
- Pitfalls and traps, especially calibration uncertainties and noise interferences in the data.

This guide for the CIRS instrument is one of several guides available, for various instruments on the Cassini orbiter and Huygens probe.

### 1.3 Scope

This guide focuses on CIRS data: its acquisition; organization, including ancillary information such as pointing, and metadata; some details of data processing (cleaning/calibration); extraction of data, especially binary data; and some examples of usage. However this document is not intended to be a detailed technical guide to the instrument itself, nor a mathematical or computer algorithm guide to the details of the Fourier Transform and calibration process.

### 1.4 How to use this guide

This user guide may be either read end-to-end as a complete introduction to the CIRS PDS dataset, or used as a reference guide for the experienced user to consult regarding details of specific topics.



## 2.0 General Information

This chapter first describes the Cassini Mission in general and the CIRS instrument in particular. That is followed by a detailed account of the various scientific objectives and measurements made by CIRS, and then we tackle the topics of data gaps and instrument performance, including interferences and other artifacts that affect the data.

### 2.1 Instrument Characteristics

This section describes the Cassini mission and CIRS instrument.

#### 2.1.1 Cassini Mission

The Composite Infrared Spectrometer is a dual-interferometer carried on the Cassini spacecraft Remote Sensing Palette (RSP). Cassini was launched on 15th October 1997 and made four gravity assist maneuvers before reaching Saturn: Venus (twice), Earth and finally Jupiter. The slow, distant Jupiter flyby (137 RJ) at the end of 2000 allowed for a six-month observing campaign that was used to evaluate the performance of the Cassini instruments, and achieve some early science. The CIRS Jovian dataset forms the first part of the CIRS archive.

After achieving Saturn orbit on July 1<sup>st</sup> 2004, Cassini commenced a four-year ‘Prime Mission’ lasting until July 2008. It included 75 spacecraft orbits (or revolutions: ‘revs’) of Saturn known as 0, A, B, C, 3 ... 74. The original orbits 1 and 2 were replaced with A, B and C when the mission was redesigned in order to accommodate radio link issues with the Huygens probe, discovered after launch. The probe delivery to Titan occurred on rev C. There were 45 targeted (i.e. close) fly-bys of Titan during the first 75 orbits.

**Table 1: Cassini Mission Phases**

Phase	Dates	Orbits (revs)	Sequences	Titan Flybys	Other Encounters
Prime	07/01/04-06/30/08	0-74	S1-S41	T0-T44	See Figure 2
Extended (EM)	07/01/08-10/10/10	75-133	S42-S60	T45-T70	See Figure 2
Solstice (SM)	10/10/10-	134-270	S61-S99	T71-T126	See Figure 2

The second mission phase was the Equinox Mission (EM), sometimes called the Extended Mission (XM), over 2 years from July 2008 to October 2010. This mission phase was designed to reach the Saturn northern spring equinox in August 2009, and comprised a



further 55 orbits and 26 further flybys of Titan (T45 to T70). At the time of writing, the third, and final anticipated mission phase is the Solstice Mission (SM, CSM, or XXM for second extended mission), which began in October 2010 and continues through to the anticipated spacecraft disposal in Saturn's atmosphere in mid-2017. This phase will encompass the northern summer solstice of Saturn in early 2017, and includes 136 orbits, 56 further Titan encounters, and multiple encounters with other moons (see Table 1 and Figure 2 below). The last part of the mission features 'proximal orbits', where the spacecraft periapse (closest approach to Saturn) will be moved from outside to inside the main rings, providing a very close look at Saturn's atmosphere.

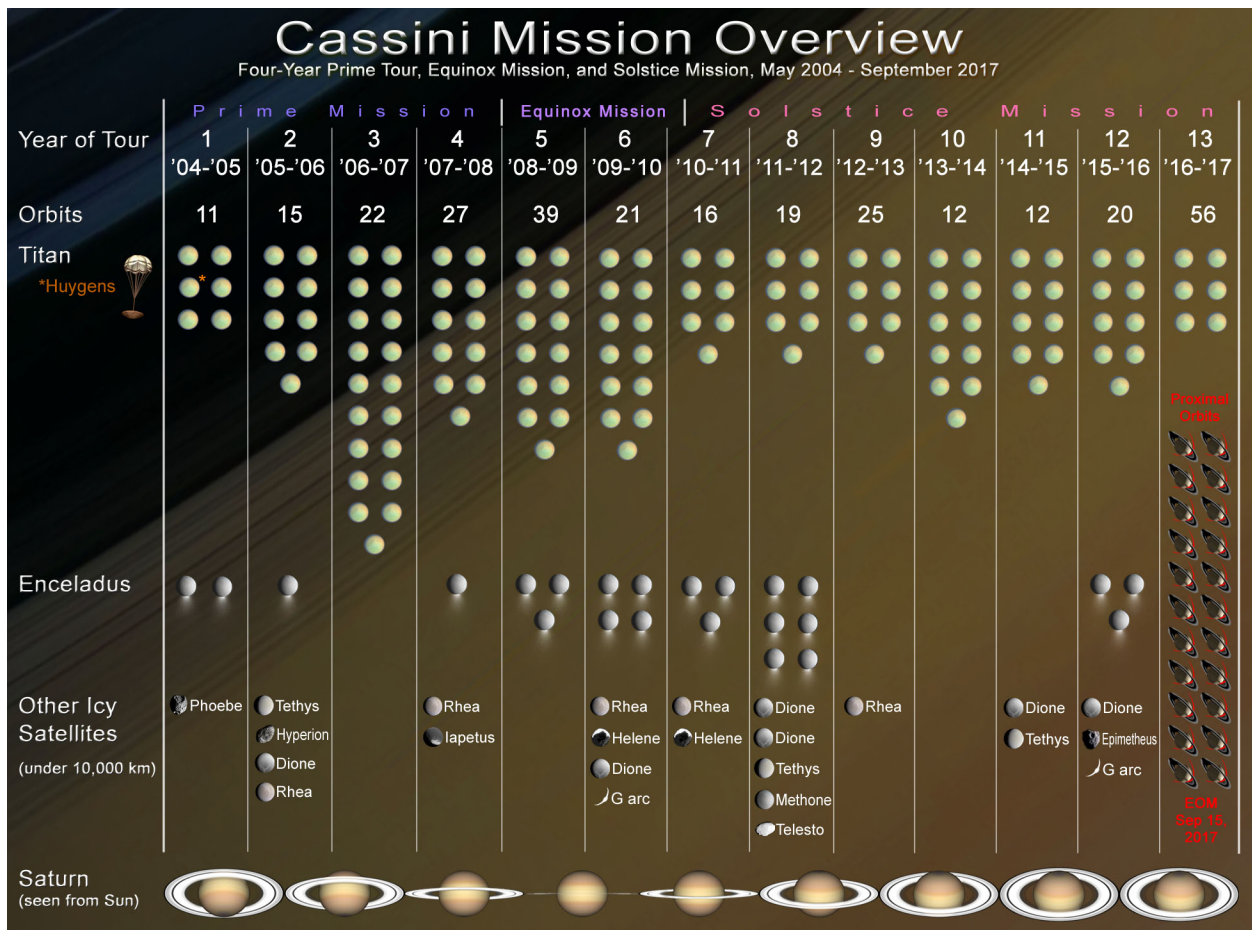


Figure 2: Cassini mission overview showing Saturn orbits and satellite encounters, as of April 22<sup>nd</sup> 2012.

### TWTs and OSTs

The time allocation between various Cassini instruments (also known as the time-line 'integration' process, as opposed to the later 'implementation' process, which developed actual pointing designs) was carried out by a number of virtual teams, known as either TWTs (Target Working Teams) or OSTs (Orbiter Science Teams). These were:

- **TOST** – the Titan Orbiter Science Team
- **SOST** – the Satellites Orbiter Science Team
- **XD TWT** – the Cross-Discipline Target Working Team
- **Saturn TWT** – the Saturn Target Working Team
- **Rings TWT** – the Rings Target Working Team
- **MAG TWT** – the Magnetospheres Target Working Team

CIRS maintained representation on all of these virtual (not physically co-located) working teams that met by teleconference at regular intervals. Following timeline integration, it was the responsibility of each team to develop spacecraft pointing commands for the allocated time-period, rather than by request to a central design office (as on the Galileo Mission) a system known as ‘Distributed Operations’ (Distributed Ops).

For further information on the Cassini mission, see the MISSION.CAT file in any of the Cassini PDS volumes.

### **2.1.2 Instrument Design**

CIRS consists of two interferometers; a far-IR polarizing interferometer sensitive from 10-600  $\text{cm}^{-1}$  (1000-17  $\mu\text{m}$ ), and a mid-IR interferometer sensitive from 600-1400  $\text{cm}^{-1}$  (17-7  $\mu\text{m}$ ) (see Figure 3 and Figure 4 below). These two share common components including the telescope (Cassegrain, with 508 mm primary beryllium mirror, and 76 mm secondary), fore-optics, reference laser and scan mechanism, which moves the retroreflectors of both interferometers simultaneously. Engineering details are given in (Kunde et al., 1996).

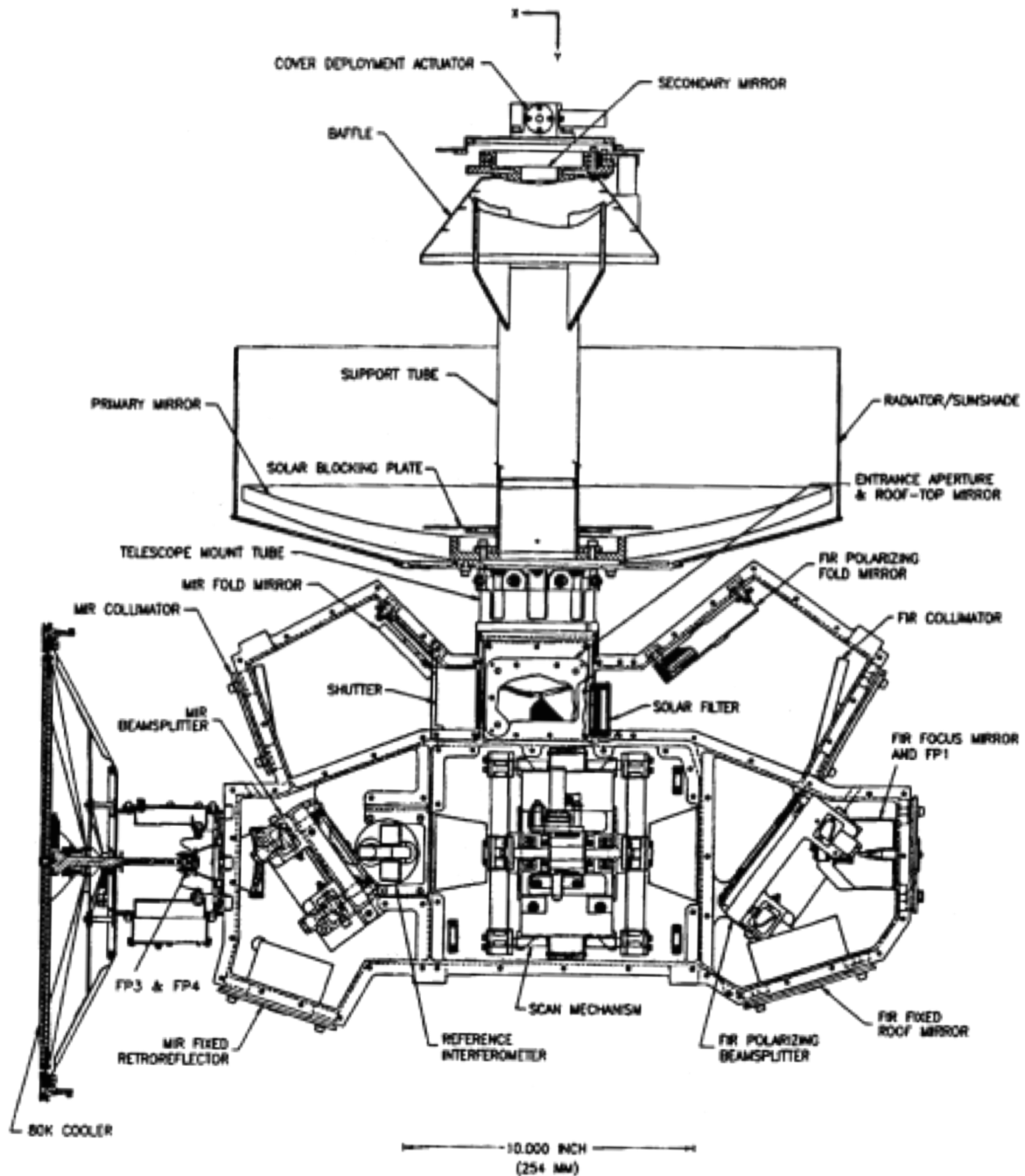


Figure 3: CIRS mechanical layout from Kunde et al. (1996).

The far-IR radiation is sensed by a large (3.9 mrad FWHM) thermopile detector (actually two, one for reflected and one for transmitted beam at the polarizer/analyzer), known as FP1. The mid-IR radiation falls on two  $1 \times 10$  pixel HgCdTe arrays, known as focal planes 3 & 4. FP3 is an array of photoconductive (PC) detectors sensitive from  $600\text{-}1100\text{ cm}^{-1}$  ( $17\text{-}9\text{ }\mu\text{m}$ ), and FP4 is an array of photovoltaic (PV) detectors sensitive from  $1100\text{-}1400\text{ cm}^{-1}$  ( $9\text{-}7\text{ }\mu\text{m}$ ).

There is no 'FP2' as it was dropped from the original design. Further details of the mid-IR arrays can be found in (Nixon, Infrared Limb Sounding of Titan with Cassini CIRS, 2009).

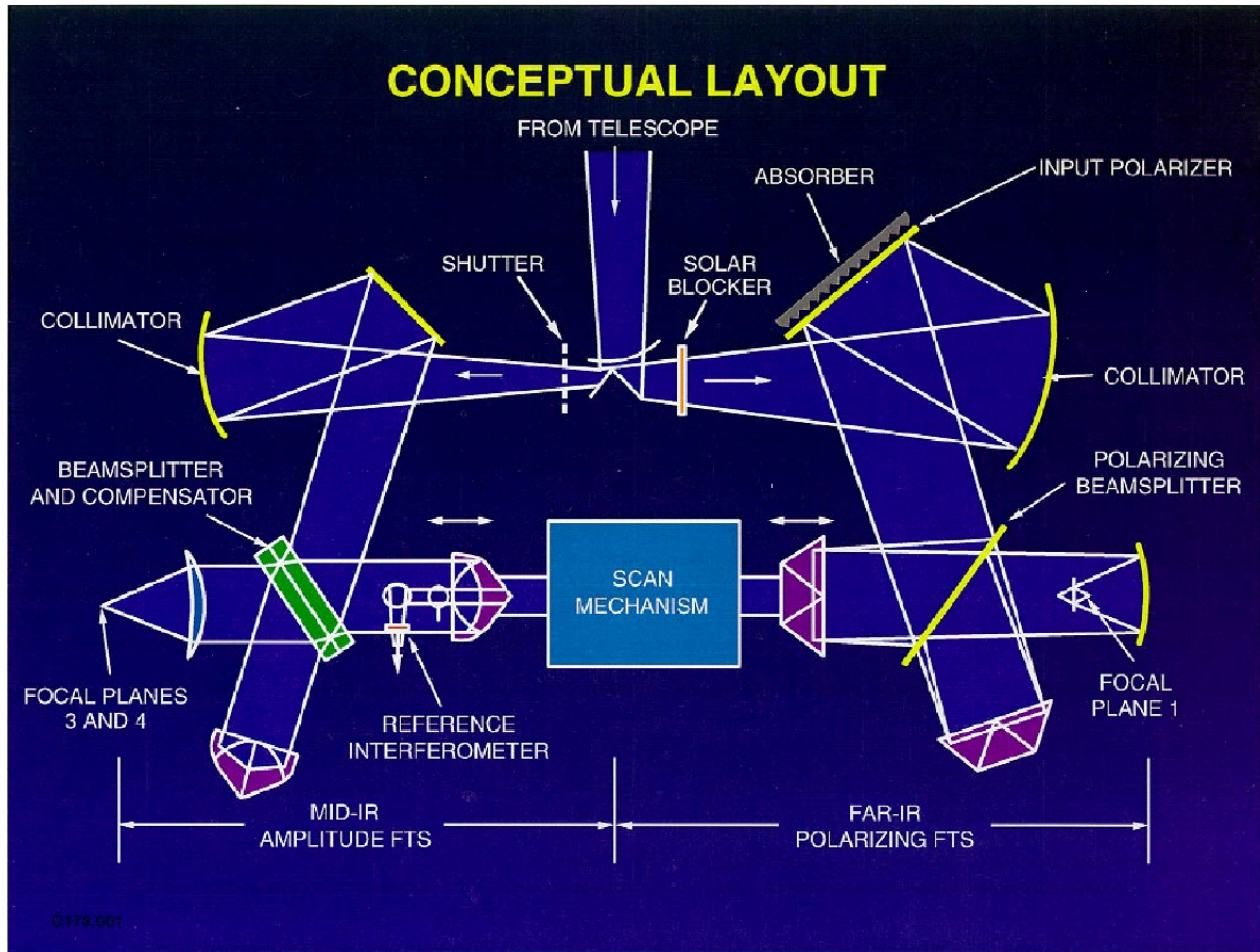
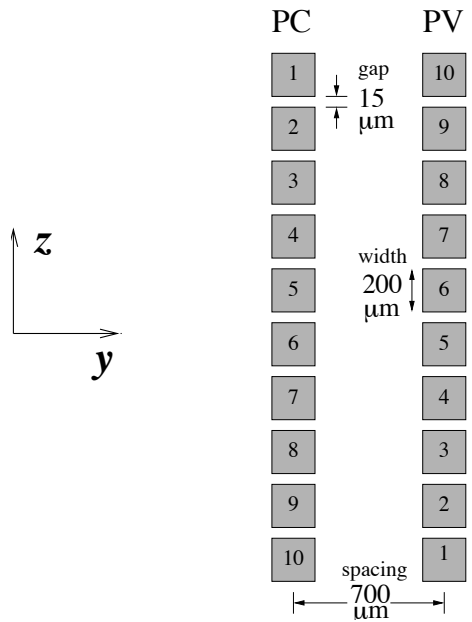


Figure 4: schematic layout of the CIRS instrument optical pathways. Incoming light from the telescope (not shown) at top is split into the mid-IR (left path) and far-IR (right path) interferometers. Both interferometers share a common scan mechanism.

Each of the 1x10 mid-IR arrays (Figure 5) has a 5-channel amplifier/signal processor, meaning that only 5 outputs from the 10 detectors in each array can be recorded at a time. The maximum number of simultaneous interferograms from CIRS is therefore 11 (1 from FP1, 5 from FP4, 5 from FP4). However, there are observing modes in which some of the focal planes are not used, leading to a lesser number of active channels.





**Figure 5: CIRS mid-infrared focal plane layout, showing detector spacing and numbering.**

Sampling is triggered by fringes of a reference red laser ( $784.5 \pm 0.3$ ) nm and the raw interferogram is later decimated by a numerical filter (factors 18, 4.5, 5.0 for FP1, 3, 4 respectively). A white light source is used to sense the zero-path-difference (ZPD) point when both arms of the interferometer are equal length. Scanning occurs over a maximum path difference of about 2 cm, but may be less. Spectral resolution is determined by the mirror travel distance. Velocity is constant,<sup>1</sup> so this equates to scan time, in units of 1/8 second (1 RTI, or ‘real time interrupt’, from the spacecraft clock).<sup>2</sup> The resolution is varied from approximately  $15.5 \text{ cm}^{-1}$  (lowest resolution, for a  $\sim 5$  sec scan, or 40 RTI) to  $0.5 \text{ cm}^{-1}$  (highest resolution, from a 50 s scan, 400 RTI).<sup>3</sup>

See the INST.CAT file on the archive volumes for additional details.

### 2.1.3 Instrument operation modes

#### *Set-point and thermal stability*

While most of the instrument operates at  $\sim 170$  K, stabilized by heaters, in contrast the mid-IR focal plane is cooled to 75-85 K by a passive radiative cooler, which is linked to the thermally-isolated mid-infrared focal plane assembly (FPA) by a ‘cold finger’. This operating temperature is controlled by replacement heaters commanded to different set-points (see Table 2) beginning with SP 22 (76.22 K) and rising in increments of 0.4 K. Note that the actual temperatures achieved by the instrument at the various set-points differ from the commanded value: for example at set-point 22 CIRS actually stabilizes at 76.301.

<sup>1</sup> Nominally at least. Practically, it is feedback-controlled to within  $\pm 1\%$ .

<sup>2</sup> Really, the scan time is controlled in Flight Software to the millisecond level. As of FSW v6, 5 ms is added to each scan to help control spike artifacts, see “2.5 Electrical interferences (spikes) and other data issues”.

<sup>3</sup> Maximum allowed range is 16-416 RTI (FSW v1-v5) and 24-416 RTI (FSW v6 on).

**Table 2: CIRS set point temperatures (all in Kelvin)**

Set Point #	FPA Temp	Min Temp	Max Temp	Set Point #	FPA Temp	Min Temp	Max Temp
31	69.52	69.32	69.72	15	81.37	81.17	81.57
30	70.27	70.07	70.47	14	82.10	81.90	82.30
29	71.02	70.82	71.22	13	82.83	82.63	83.03
28	71.77	71.57	71.97	12	83.56	83.36	83.76
27	72.52	72.32	72.72	11	84.28	84.08	84.48
26	73.26	73.06	73.46	10	85.01	84.81	85.21
25	74.00	73.80	74.20	09	85.74	85.54	85.94
24	74.75	74.55	74.95	08	86.47	86.27	86.67
23	75.49	75.29	75.69	07	87.19	86.99	87.39
22	76.22	76.02	76.42	06	87.92	87.72	88.12
21	76.96	76.76	77.16	05	88.64	88.44	88.84
20	77.70	77.50	77.90	04	89.37	89.17	89.57
19	78.43	78.23	78.63	03	90.10	89.90	90.30
18	79.17	78.97	79.37	02	90.90	90.70	91.10
17	79.90	79.70	80.10	01	91.60	91.40	91.80
16	80.63	80.43	80.83	00	92.30	92.10	92.50

The set-point is usually set to be as low as possible for best detector performance, subject to the expected heating load on the passive radiative cooler. For example, during a ‘rolling downlink’ (spacecraft pointed with  $-Z$  to Earth, high gain antenna (HGA) to Earth, but rolling about the Z-axis for fields and particles science) the cooler may experience small, cyclic heating flux from a warm body (Sun, Saturn, or rings) in excess of its capacity to shed. This case is shown in Figure 6 where the black line is the modeled mid-IR FPA temperature resulting from heating due to Saturn and the sun, and an equilibrium temperature of 74.6 K is assumed. The rolling downlink periods are evident at times 1800 on day of year 5 and again at 1800 on day of year 7. Therefore, during these events, CIRS may either not take



data, or take data but with an elevated set-point, commanded to be above the maximum temperature excursion predicted (Figure 7).

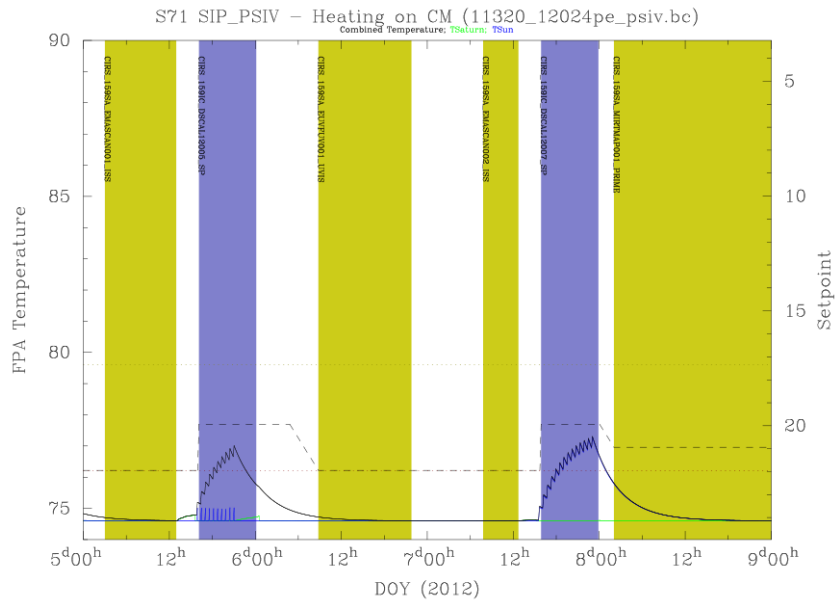


**Figure 6: Modeled thermal heating on mid-IR FPA during rolling downlinks with an equilibrium temperature of 74.6 K.**

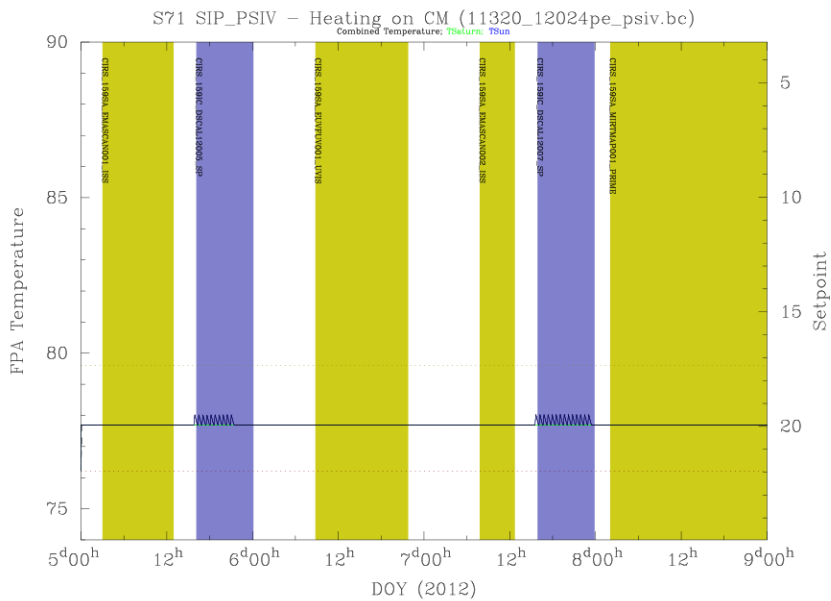


**Figure 7: Modeled thermal heating on mid-IR FPA during rolling downlinks using setpoint 20.**

### Shutter

The instrument may command the shutter closed (for calibration) or open (default). The shutter affects only the mid-infrared detectors (FP3 and FP4), not the far-infrared detector (FP1). The shutter temperature is close to the stabilized instrument temperature (~170 K). Shutter open and closed modes appear to cause different baselines (‘shape functions’) in

the FP1 interferograms for electrical reasons (or possibly stray light?), although the optical path has not been occluded. See “5.1.5 Field of view modeling” for further details.

### FP3 and FP4 Pixel Modes

Due to the fact that fewer amplification channels are available (5) than the numbers of detectors on each focal plane (10), a choice must be made about which detectors are in use at any given time. The choices are ‘ODD’, ‘EVEN’, ‘CENTERS’ and ‘PAIRS’. In the ‘ODD’ mode, odd numbered detectors are used (1,3,5,7,9) and in the even mode, even-numbered detectors are used (2,4,6,8,10). As the numbering of the FP3 and FP4 detectors is reversed, FP3 detector 1 is side-by-side with FP4 detector 10. Therefore, to match spatial positioning, FP3 EVEN is usually selected along with FP4 ODD, and vice versa. In ‘CENTERS’ mode detectors 3-7 are used from FP3 and detectors 4-8 are used from FP4, which are again co-located. In ‘PAIRS’ mode, the signals from each pair of detectors within each array - 1&2, 3&4, 5&6, 7&8, 9&10 – are co-added before being sent into the amplifier, so that the arrays function as five-element arrays with 2x larger rectangular pixels but increased S/N sensitivity. The modes and their definition with respect to both physical and virtual detector numbering are shown in Table 3.

**Table 3: pixel modes**

Virtual Detector Number	Focal Plane	FP3 Physical Detector	FP3 Mode	Virtual Detector Number	Focal Plane	FP4 Physical Detector	FP4 Mode
00	1	1					
01	3	1&2	PAIR	21	4	1	ODD
02	3	3&4	PAIR	22	4	2	EVEN
03	3	5&6	PAIR	23	4	3	ODD
04	3	7&8	PAIR	24	4	4	EVEN
05	3	9&10	PAIR	25	4	5	ODD
06	3	3	CENTER	26	4	6	EVEN
07	3	4	CENTER	27	4	7	ODD
08	3	5	CENTER	28	4	8	EVEN
09	3	6	CENTER	29	4	9	ODD

10	3	7	CENTER	30	4	10	EVEN
11	3	1	ODD	31	4	4	CENTER
12	3	2	EVEN	32	4	5	CENTER
13	3	3	ODD	33	4	6	CENTER
14	3	4	EVEN	34	4	7	CENTER
15	3	5	ODD	35	4	8	CENTER
16	3	6	EVEN	36	4	1&2	PAIR
17	3	7	ODD	37	4	3&4	PAIR
18	3	8	EVEN	38	4	5&6	PAIR
19	3	9	ODD	39	4	7&8	PAIR
20	3	10	EVEN	40	4	9&10	PAIR

### *Co-add mode*

The co-add mode is either ‘on’ or ‘off’. If co-add is ‘on’ then an interferogram is stored in a buffer, and co-added to the next interferogram from the same detector, before being passed along the data chain. This reduces effective temporal sampling, but reduces the data volume by a factor 2 when data volume limitations are imposed. The length of an interferogram from two coadded scans corresponds to the length of the shorter of the two scans being coadded. The data from a coadded interferogram includes the frame scan diagnostics data block and frame scan ID block information from both of the original scans, but only one frame scan data block containing the coadded data.

### **2.1.4 Types of Data at PDS**

The data selected for submission to the PDS falls into four broad categories. Housekeeping tables (HSK) are included to provide insight into the health and status of the instrument. Interferogram-related tables (DIAG, FRV, IFGM, IHSK, and OBS) provide the interferograms themselves plus a wide-range of parameters describing the instrument modes, conditions, and settings that occurred during the scan. The navigational tables (GEO, POI, RIN, and TAR) detail the positions of the major bodies, describe where the instrument was pointed, and what bodies were within the FOV. Finally, the ISPM tables provide the calibrated spectra resampled onto standardized wavenumber grids. This information is summarized in Table 4 below.

**Table 4: PDS directories**

<b>PDS Volume Directory</b>	<b>Description</b>	<b>Data Table Types</b>
DATA/HSK_DATA	Raw housekeeping data at 64 sec intervals.	HSK
DATA/UNCALIBR	Unprocessed raw interferograms (IFGM), basic instrument parameters (IHSK, OBS, FRV) and preliminary assessment of quality (DIAG).	IFGM, IHSK, OBS, DIAG, FRV
DATA/NAV_DATA	Navigation and pointing data derived from the Cassini SPICE kernels and computed for the CIRS observations.	GEO, POI, RIN, TAR
DATA/APODSPEC	Calibrated and apodized spectra	ISPM

Descriptions of the fields within each table as well as the binary format of the tables are given in the DATASIS.PDF document available at any of the CIRS PDS node sites.

### 2.1.5 Data Unit Definition

The following table lists the types of data units that can be found in the DATA directory. These are delivered to the PDS, and archived at the PDS Atmospheres Node, in variable-length binary form. However the tables have been translated into a mixture of ASCII and fixed-length binary records for increased accessibility, and are available in this form at the PDS Rings Node.

**Table 5: CIRS PDS data object types**

<b>Data Object</b>	<b>Description</b>
HSK	These tables store the data from the housekeeping packets (e.g., instrument temperatures, voltages, and currents) that are required for the calibration of IFMs. Note that the housekeeping packets are created every 64 seconds, and records do not have a direct one-to-one or one-to-many correspondence to science scans, as all other table records do. A full description of this data is in the CIRS flight software documentation.
DIAG	These tables contain diagnostic information determined regarding the raw interferograms, including the presence or absence of noise interferences (e.g., spikes, velocity variations, RWA), the identification of the laser mode, and the location of the ZPD.
FRV	These tables store the voltages of the central fringe of the CIRS white-light

	interferometer, sampled at 1 second intervals after mirror flyback.
IFGM	These tables store the actual IFM records. Note that there will typically be eleven IFM records (one per signal channel) for a given SCET time.
IHSK	These tables store interpolated housekeeping data for use in the calibration. A small subset of fields from the HSK housekeeping tables are interpolated to the times of the actual scans.
OBS	These tables store information relating to the instrument data-taking settings for each scan (e.g., RTI, co-add, shutter status) and the values of warning and indicator flags.
GEO	These tables store the geometry, the relative positions and orientations of the spacecraft, primary body, and object bodies (which may include the primary, e.g. Saturn), usually at the time of the zero path difference (ZPD) of the interferogram (when most of the signal is collected). One entry is generated for every body in the target list.
POI	These tables store the pointing for each active detector at the ZPD of the IFM and at scan's end. One POI entry is generated for each detector and each non-rings non-primary target in the field of view. An entry is always generated for the primary as the target, whether or not it is in the field of view. Rings are described in a separate RIN table rather than as entries in the POI tables.
RIN	These tables contain the pointing information for the rings. One entry is generated for each detector at all times. For the purpose of this table, the rings are assumed to fill the equatorial plane of the primary ( $z = 0$ in the coordinate system of the primary with $z$ along the rotation axis) out to a selected cutoff radius. If a line of sight intersects the primary body before intersecting the rings, or if the line of sight falls outside the cutoff radius, the values for most fields for that line of sight are set to -200.
TAR	These tables describe which, if any, of the various targets are in the field of view of a given detector. Individual fields (e.g. TITAN) are set to 1 or 0 according to whether the body appears in the FOV or not. Any, all, or none of these fields may be specified individually to select data with a particular subset of bodies in the FOV. Additionally, the field FOV TARGETS contains the same information as the individual byte fields, except stored as bits in a single 4-byte integer. This may provide a useful shorthand for selecting an exact target body combination.
ISPM	These tables contain the interpolated (resampled) calibrated spectra. The older SPM type created formerly used a natural wavelength index resulting from the instrument, which meant that the final spectrum fell on irrational

	<p>wavenumber values such 577.3256, 577.7792, instead of 577.250, 577.500, 577.750 etc. The ISPM type contains the same spectra, but interpolated and re-sampled onto a more user-friendly grid. There is no loss of resolution or data in this process. <b>NOTE:</b> the point spacing of the ISPM tables does <u>not</u> correspond to the spectral resolution, nor is it half the resolution (Nyquist spacing). In practice the over-sampling is always smaller than <math>\frac{1}{2}</math> the spectral resolution. The 'real' resolution is contained in a table field (Nyquist, Rayleigh or FWHM, depending on which definition you prefer).</p>
--	--

## 2.2 Science Objectives

For a detailed description of the science objectives, see (Flasar, 2004). A short description is included here for guidance. The Cassini/Huygens mission to the Saturnian system is designed to investigate the following targets:

1. **Saturn:** Sensing of tropospheric and stratospheric temperatures, dynamics, and composition. This includes abundances of the major and minor species, the hunt for new gaseous species, the ortho-to-para ratio for hydrogen, isotope ratios for major species. Allocating time for Saturn observations was the responsibility of the Saturn TWT (Target Working Team), which had orbit (rev) and segment allocations divided up through negotiation with other working groups. The Atmospheres Working Group (AWG) also provided input and dealt with high-level science recommendations and mission objectives. In 2005 the AWG was replaced with a Saturn Working Group (SWG) and Titan Working Group (TWG).
2. **Rings:** Measurement of the infrared spectrum at varying phases, leading to conclusions about ring particle size, shape, composition, distribution and dynamics. Allocation of time for rings observing was carried out by the Rings TWT, in conjunction with the Rings Working Group (RWG).
3. **Titan:** Sensing of tropospheric and stratospheric temperatures and composition. This includes abundances of the major and minor species, the hunt for new gaseous species, isotope ratios for major species, and dynamics. CIRS is also able to sense the surface near  $530\text{ cm}^{-1}$ . Allocation of time for Titan observations was primarily done in the TOST group (Titan Orbiter Science Team), in conjunction with recommendations from the AWG, the Surfaces Working Group (SWG). In 2005 the TWG replaced the AWG and SWG for directing Titan science.
4. **Other ('icy') satellites:** Surface mapping in the infrared provides information on the surface composition, temperature, morphology, and age. Close passes of icy satellites resulted in time being allocated to the SOST (Satellites Orbiter Science Team), which in turn divided the time between teams. This effort was done with the oversight and guidance of the Surfaces Working Group (SWG). In 2005 the SWG became the ISWG (Icy Satellites Working Group) and the term SWG was used for Saturn Working Group.

The overall mission may also be broken in physical target types:

1. Atmospheres (Saturn and Titan)
2. Surfaces (Titan, and other satellites).
3. Magnetosphere: fields, particles and solar wind interaction (Sun-Saturn)
4. Orbital mechanics (rings, satellites especially Hyperion).

CIRS contributes to the investigation of many of these areas.

## 2.3 Observation Strategies

Here follows a description of how the various science investigations are implemented in terms of actual spacecraft pointing. Accompanying figures are provided in Appendix A.

### 2.3.1 Saturn

CIRS Saturn atmospheric science goals are met with observations at a variety of inclinations, ranges from Saturn and, in some cases, in conjunction with other teams' observations. The standard CIRS requests include those shown in Table 6.

**Table 6: CIRS Saturn observation types**

Name	Range ( $R_S = 1$ Saturn radius)	Details
COMPSIT	All ranges of $R_S$	Composition sit and stare at $0.5 \text{ cm}^{-1}$ spectral resolution with FP3/4 paired detector mode using either nadir viewing for low emission angle studies, or FP3 or FP1 offset to obtain high emission angles. Uses all 3 focal planes. Search for oxygen compounds ( $\text{CO}_2$ and $\text{H}_2\text{O}$ ) and new molecules (Figure 40, Figure 41, Figure 42).
MIRMAP	25-50 $R_S$	Mid-IR maps, centered at a single latitude, with the focal planes oriented N-S on Saturn to allow the planet's rotation to map out a latitude band. Uses all three focal planes and $3 \text{ cm}^{-1}$ resolution using FP3/4 paired detector mode. Arrays are centered on the central meridian (Figure 43).
MIRTMAP	25-50 $R_S$	Mid-IR maps that step across multiple latitudes with the focal planes oriented N-S on Saturn. Hybrid of MIRMAP's to allow mapping temperatures across the entire planet regularly. Latitudes from $75^\circ\text{N}$ to $75^\circ\text{S}$ are covered with approximately 2hrs of longitude coverage per latitude pointing. Uses all three focal planes and $3 \text{ cm}^{-1}$ resolution using FP3/4 paired detectors. Arrays always centered on the central meridian at each latitude position (Figure 44).



FIRMAP	15-30 $R_S$	Far-IR maps, constructed by slewing equator-ward over a single hemisphere. Slews overlap and repeat to map out the entire hemisphere. 15 $\text{cm}^{-1}$ spectral resolution and FP3/4 paired detector mode. Some short temporal spacing between FIRMAPs of the same hemisphere to search for thermal waves (Figure 45, Figure 46).
FTRACK	< 10 $R_S$	Campaign with VIMS and ISS to track features across the disk from limb to limb, including limb sounding. FP1 nadir sounding at 3 $\text{cm}^{-1}$ , FP3/4 limb sounding at 15 $\text{cm}^{-1}$ . FP3/4 paired and blink detector modes. The goal is to study vertical structure and pole-ward heat transport. Only performed in the prime mission.
LIMBMAP	< 6 $R_S$	Vertical sounding at multiple latitudes on the limb at 15 $\text{cm}^{-1}$ . FP3/4 blink detector mode. Focal planes are placed normal to the local latitude limb to sound multiple altitudes. All 3 focal planes are used. Sometimes are labeled LIMBINT, if repurposed during the design phase.
LIMBINT	< 6 $R_S$	Long integrations for vertical composition at one location on the limb, with 2 or 3 altitude positions. A spectral resolution of 0.5 $\text{cm}^{-1}$ until mid-2008 and 1 $\text{cm}^{-1}$ thereafter. FP3/4 blink detector mode (Figure 47, Figure 48, Figure 49).
NADIROCC	< 10 $R_S$	Helium abundance measurements taken by following the Radio Science Team's occultation points across the disk. Observations performed at 3 latitude positions displaced by -2, 0, +2 mrad along the central meridian longitude (CML) to allow for pointing uncertainties. Using 3 $\text{cm}^{-1}$ spectral resolution and FP3/4 paired detector mode (Figure 50).
OCCLIMB	< 6 $R_S$	Independent verification of vertical temperature profile at Radio Science's occultation latitudes. Observations performed at 0.5 and 2.5 mrad above the 1 bar level (100 and 1 mbar?). 15 $\text{cm}^{-1}$ spectral resolution and FP3/4 blink detector mode.
REGMAP/ COMPFT	< 10 $R_S$	Regional mapping and/or composition feature tracks, to fill in coverage not obtained by the other observations (0.5 or 3 $\text{cm}^{-1}$ spectral resolution and blink detector mode). Primarily used in the prime mission.
TEMPSIT		Saturn approach temperature map. 3 $\text{cm}^{-1}$ spectral resolution and paired detector mode. Focal planes oriented N-S on the central meridian. Planet rotates to cover all longitudes. Arrays

	cover Southern Hemisphere (north blocked by rings).
MIRCMPSIT	Saturn approach composition sit and stare. $0.5 \text{ cm}^{-1}$ spectral resolution and paired detector mode. Focal planes oriented N-S on the central meridian. Arrays cover Southern Hemisphere (north blocked by rings).
FIRCMPSIT	Saturn approach far-IR composition. $0.5 \text{ cm}^{-1}$ spectral resolution and paired detector mode. FP1 centered on South Pole and on mid-Southern latitudes.

---

### 2.3.2 Rings

The name conventions for the ring observations have changed during the mission, driven partially by the team discovering that certain objectives were beyond the sensitivity of the instrument, and partially by the unanticipated degree of variation in effective temperature and emissivity with illumination conditions and observation geometry. With the exception of a few shifts of policy in observation planning that were made during main mission, most of the new naming conventions commenced with XM, and a few more with XXM.

The science objectives are discussed individually in the first sub-section, below, and the main events driving the name changes that took place during the mission are discussed afterwards. Table 7, Table 8, and Table 9 summarize the science objectives by observation name, and Table 10 presents a summary for how the naming conventions associated with the science objectives have changed with each mission phase.

#### *Science Objectives and Observing Strategies*

**Faint Ring Long Integrations:** To observe the low optical depths of the faint rings, observations used  $15 \text{ cm}^{-1}$  integrations with FP1. The FMOVIE and FMONITOR observations taken during the Main Mission detected the F Ring only when averaging over many hours. The original geometry planned for nearly edge-on viewing, however it was discovered that, due to the thickness of the F ring, viewing from an inclination of 1.5 to 2 degrees maximized signal by allowing the ring to fill substantial portions of the FP1 FOV. No opportunities were found for F Ring observations in XM, with the XXM still pending as of the time of this report.

**Composition Integrations:** These observations were designed to search for absorption features between 50 and 1000 microns. Three observation types were planned. Long integrations at  $0.5 \text{ cm}^{-1}$  would target each of the main rings at ansa, from 20-40 Rs using FP1 and FP3; FP3 measurements would take long integrations of the rings against Saturn, so that absorption features might be catalogued; and certain radial scans, “submillimeter” scans, would be made at  $1 \text{ cm}^{-1}$  spectral resolution of the lit and unlit sides of the rings to map the thermal characteristics and composition of the ring particles out to 1 mm.

**Stellar Occultations:** These observations provide a direct measurement of the IR opacity of the rings. The only two targets that have been identified as being observable by CIRS are

CW Leo (FP3) and Eta Carinae (FP4). They used  $15 \text{ cm}^{-1}$  spectral resolution, centering the star in a single pixel of the array.

**Ring Thermal Properties:** Observational goal was to constrain the overall thermal budget of the rings to determine how it drives the emission seasonally and during orbital periods. The flux into the rings depends upon the Solar elevation, distance from Saturn, and azimuthal location at points along the orbit, and the emission of the rings should vary in step with this. This variation was catalogued using radial scans typically executed between 5 and 20 Rs over a range of spacecraft inclinations, from the lowest ( $5^\circ$ ) to the highest possible inclination ( $75^\circ$ ). Radial mapping (FP1, FP3) of the rings, on both lit and unlit sides, over a range of spacecraft elevations, inclinations, local times and phase angles, was performed to obtain broadband radiometric measurements of the total flux in the CIRS wavelength range. Sets of observations were obtained in each of the inclined orbit intervals to map the temperature variation in the rings with changing solar illumination. Two types of scans were implemented. The temperature scans consisted of spectra at  $15 \text{ cm}^{-1}$  spectral resolution of the lit and unlit sides of the rings at many incidence and emission angles and provided prime information on the ring thermal gradient as a function of radial distance to Saturn.

**Ring Particle Thermal and Dynamical Properties:** Observations were designed to infer surface properties, vertical dynamics and spin of ring particles. Observations of the cooling and heating of the ring particles entering and emerging from the planetary shadow were used to derive particle thermal inertias for all three main rings. This allowed measurements at moderate radial resolution (typically 1000 km) across the shadow boundaries at low spectral resolution ( $15 \text{ cm}^{-1}$ ) with the FP1 field of view. To constrain the vertical dynamics of ring particles, the temperatures of the main rings were measured by CIRS along the ring azimuth of the main rings, from the exit of the shadow (morning) to the evening ansa, both on the unlit and unlit faces. This unique experiment was designed using spectra at low spectral resolution ( $15 \text{ cm}^{-1}$ ). Spins create both an azimuthal asymmetry in the ring temperature and a dependence of the temperature with the emission angle, due to day/night contrast. Circumferential scans at a variety of phase and emission angles were executed to detect azimuthal asymmetries and the anisotropy in the ring particle emission function which are both function of particles spin and thermal inertia. Occasionally, when observing time is highly disputed, long azimuthal scans (8-to-20 hours long depending on geometry and face) were replaced by a series of radial scans at different azimuths.

### Observation Types

A summary of the observation names associated with the Prime Mission science objectives is listed in Table 7.

**Table 7: summary of CIRS Prime Mission rings observations and scientific objectives**

Name:	Scan Type:	Objectives
COMP	Stare at A, B, or C ring ansa, $1 \text{ cm}^{-1}$	Detect bands due to

	resolution.	contaminants.
SUBM	Radial scans at ansae, $1 \text{ cm}^{-1}$ resolution, slow scans.	Scan slowly at high resolution to map radial contaminants.
TEMP	Radial scans at $15 \text{ cm}^{-1}$ resolution (Figure 51).	Map radial variations of temperature.
SHAD	Azimuthal scans at fixed radii (usually $R=82000 \text{ km}$ , $108000 \text{ km}$ , $132000 \text{ km}$ ), $15 \text{ cm}^{-1}$ resolution.	Observe azimuthal heating and cooling to constrain thermal inertia.
VERT	Azimuthal scans at fixed radii, planned in pairs for lit and unlit comparison, $15 \text{ cm}^{-1}$ resolution.	Observe azimuthal heating and cooling on both sides of thick rings to find evidence for vertical transport of particles.
FMOVIE	Fixed spot on F ring for duration of orbit.	Observe azimuthal variation and clumpiness.
FMONITOR	Shorter version of F Movie.	
CWLEOCC	Fix on RA/DEC of target star as it occults rings.	Determine optical thickness of rings in IR.
ZEROPHAS	Map several locations in B ring to assemble phase curves near 0 phase.	A one-off follow-up discovery mode which failed to detect a thermal phase surge.

During the mission the team learned the following lessons that changed the observation strategies during design implementation as follows:

- (i) Long integrations showed no hint of bands from contaminants; some SUBM radial scans became TEMP scans; fewer COMP scans were scheduled (except when, due to geometry, only the ansae were available).
- (ii) Noise limitations at low wavenumbers were prohibitive for observing the change from emission to reflection spectrum in the  $5\text{-}20 \text{ cm}^{-1}$  range. This resulted in further curtailment of the SUBM scans.
- (iii) The effective temperature and emissivity have much more directional variation and detailed dependence on illumination conditions, radius, and resolution than had been anticipated; in contrast, the azimuthal curves could be over-fit, for cooling and thermal properties. Consequently, at the onset of XM it was decided

that fine radial resolution scans contained more information than fine azimuthal resolution at a given radius. The TMAP observations were started as thermal mapping campaigns to take multiple radial scans so as to provide more information on radial structure and use less time for over-fit azimuthal curves.

- (iv) The optimal viewing geometry for faint rings is not edge-on, but at a slight elevation so that the ring fills the FOV. The spectra from the original FMOVIES had to be averaged over whole orbital periods in order to get a signal at all, so more of these were not scheduled.
- (v) Some observations suggested a thermal phase surge. One observation, a ZEROPHAS, was created to catalogue this peak at the end of Prime Mission, but obtained a null result and was not repeated.
- (vi) The phase behavior of the thermal emission and filling factor came to be of interest for fitting comprehensive models of ring emission. Consequently, in the XXM, observations are labeled by the phase/latitude bin that they cover. The [N,S]PXXLXX observations were designed to complete phase curve studies started at the end of the PM. The PIE observations in this category were specifically designed to capture the phase variation at Solar elevations where the spacecraft was in equatorial orbit during MM (i.e., for which there was no rings data).
- (vii) The competition for time around Saturn Equinox prompted the design of the EQ[N,S][L,S]B observations, short for EQUinox North/South Long/Short baseline. These were designed to detect the overall cooling rates of the rings on timescales of hundreds of days (Long Baseline) and hours or days (Short Baseline) around equinox. They are radial scans at  $15 \text{ cm}^{-1}$  scheduled at geometries as self-similar as tour constraints allow.
- (viii) TDIFF measurements are designed in pairs to constrain vertical transport by observing radial scans at the same Hour Angle from the lit- and unlit sides of the rings at similar spacecraft elevations, solar elevations and phase angle. While vertical transport was an objective of the azimuthal VERT scans, the unanticipated variation in thermal emission with illumination and observation geometry resulted in these being somewhat ineffectual because the different geometries often resulted in a multiplicity of potentially influential parameters varying between the lit- and unlit observations.
- (ix) SHAD[UN,LIT] were introduced in XXM to make up for a lack of high-latitude radial scans of the shadow region during PM and XM.

Summaries of the observation names associated with the science objectives for XM and XXM are in Table 8 and Table 9. A tabulation of how the science objectives and observation names changed during the full mission is in Table 10.

**Table 8: summary of CIRS XM Mission rings observations and objectives.**

<b>Name:</b>	<b>Scan Type:</b>	<b>Objectives:</b>
TMAP	Use several radial scans at various azimuths; azimuthal scans included on opportunity basis; 15 cm <sup>-1</sup>	Optimize observations to divulge both radial structure and cooling curve information.
TDIFF	Radial scans 15 cm <sup>-1</sup> . Planned in pairs, carefully designed so unlit and lit sides are observed at the same geometry (Figure 52, Figure 53, Figure 54).	Constrain the thermal budget due to vertical transport of heat through the rings.
POLARIZ	Stare at each main ring using 3 different orientations, with copious deep space interleaved. 15 cm <sup>-1</sup> (Figure 56).	Determine whether any polarization signal is emitted from the rings.
EQLBN	Radial scans 15 cm <sup>-1</sup> .	Establish a “long baseline” record of cooling and heating in the months before and after equinox.
EQSBN	Radial scans 15 cm <sup>-1</sup> .	Establish a “short baseline” record of heating and cooling in the days around equinox.

**Table 9: summary of CIRS XXM mission rings observations and objectives**

<b>Name:</b>	<b>Scan Type:</b>	<b>Objectives:</b>
[N,S]PXXLXX	Radial scans at 15 cm <sup>-1</sup> . Azimuthal scans on opportunity basis.	Complete the phase/lat coverage started during main mission, extend to missed solar geometries (PIE’s); take over the previous TMAP objectives (non-PIE’s).
SHADUN, SHADLIT	Shadow ingress and egress scans and/or radial scans at 15cm <sup>-1</sup> , high latitude.	Map the temperature variation around the shadow region for determining thermal inertia.

**Table 10: historical summary of CIRS rings naming conventions**

Science goal:	Main Mission:	XM:	XXM:
Composition	COMP SUBM		
Radial Temperature	SUBM TEMP	TMAP	[NS]PXXLXX
Azimuthal Temperature and Vertical Transport	SHAD VERT	TDIFF VERT	TDIFF SHADUN SHADLIT
Temperature response around equinox		EQSB[N,S] EQLB[N,S]	
Seeking polarization		POLARIZ	
Faint ring Observations	FMOVIE FMONITOR		
Star occultations	CWLEOCC		
A one-off discovery mode	ZEROPHAS		

### 2.3.3 Titan

CIRS achieves different science goals at different distances from Titan (see Figure 8). Typically, CIRS makes the following requests (symmetric about closest approach):

**Table 11: CIRS Titan observation descriptions**

TIME FROM C/A	NAME	DETAILS
0 to 10 mins	HIRES	Surface mapping (e.g. slew over south pole).

10 to 45 mins	FIRLMBT	1-2 radial limb scans with FP1 to derive temperatures in the 8--100 mbar region via the N <sub>2</sub> -N <sub>2</sub> collision-induced absorption between 20--100 cm <sup>-1</sup> (Figure 57).  <b>[resol: 15.5 cm<sup>-1</sup>; max rate: 40 μrad/s; angle: ~25 mrad or ~ 0-250 km altitude]</b>
45 to 75 mins	FIRL MBAER	1-2 radial limb scans with FP1 to measure/characterize particulate and condensate distributions, abundances and properties (Figure 58).  <b>[resol: 15.5 cm<sup>-1</sup>; max rate: 50 μrad/s; angle: ~40 mrad or ~ -100-700 km altitude]</b>
75 to 135 mins	FIRLMBINT	Integrate at two altitudes on the limb (125 km, 225 km) with FP1 to search for signals of CO, H <sub>2</sub> O and new species (Figure 59). <b>[resol: 0.5 cm<sup>-1</sup>]</b>
2:25 hrs to 5 hrs	FIRNADMAP	Slow scan spanning the disk to sound tropospheric temperatures at 40—200 mbar, via the N <sub>2</sub> -N <sub>2</sub> absorption, and to retrieve surface temperatures in the presence of aerosols around 520 cm <sup>-1</sup> (Figure 60).  <b>[resol: 15.5 cm<sup>-1</sup>; max rate: 12 μrad/s, set by 1 FOV in 5 mins]</b>
5 to 9 hrs (type 1)	MIRLMBMAP	Map 1/4 limb using the FP3 and FP4 arrays, to infer stratospheric temperatures via the 1304 cm <sup>-1</sup> band of CH <sub>4</sub> . The arrays are placed perpendicular to the limb at two altitudes (~350 km, 100 km), chosen to provide overlapping coverage of the altitude range 150 to 420 km. The arrays are used in blink (ODD-EVEN) mode. After mapping both altitudes, the arrays are stepped 5 degrees in latitudes for the next step (Figure 62). <b>[resol: 15.5 cm<sup>-1</sup>]</b>
5 to 9 hrs (type 2)	MIRLMBINT	As in MIRLMBMAP, except that only a single latitude is covered, at two overlapping altitudes (~350 km, 100 km) for 2 hrs in each position. To search for and measure new species in the mid-IR: methyl, benzene etc. (Figure 61). <b>[resol: 0.5 cm<sup>-1</sup>]</b>
5 to 9 hrs (type	MIRLMPAIR	Arrays are placed <i>parallel</i> to limb at a specific altitude, continuous integration for 4 hrs using



3)		mid-IR PAIR detector mode. Purpose is to achieve highest possible S/N for trace species by co-adding all detectors (same altitude). [ <b>resol: 0.5 cm<sup>-1</sup></b> ]
9 to 13 hrs	FIRNADCMP	Integrate on the disk at emission angle approximately 60 degrees with the FP1 detector, in order to measure spatial abundance distribution of weak species and search for new species in the far-IR. Use some nodding on/off disk to get deep space for reference/calibration (Figure 63). [ <b>resol: 0.5 cm<sup>-1</sup></b> ]
13 to 22 hrs	MIDIRTMAP	Scan the entire visible disk with the FP3/FP4 arrays perpendicular to the scan direction ('push-broom'), to measure stratospheric temperatures via the CH <sub>4</sub> ν <sub>4</sub> band. Used for later dynamical analysis, for winds, waves etc. (Figure 64). [ <b>resol: 0.5 cm<sup>-1</sup>; rate: max 10 μrad/s; TOST type M2 includes 30-min ISS dwells at start and end for cloud search; M3 has 1 ISS dwell at start or end; M4 is all CIRS</b> ]
22 to 48 hrs	COMPMAP or TEMPMAP	Map a meridian across the planet either E-W or N-S, using the Fp3/FP4 arrays in one to five positions longwise. To search for new species, and/or monitor temperatures.
Away from closest approach	TEA (Titan Exploration at Apoapse)	Long-duration (12-36 hours) stare at Titan at long range. Typically one FP3/FP4 footprint. May include an ISS NAC mosaic if Titan's angular diameter exceeds 6 mrad.

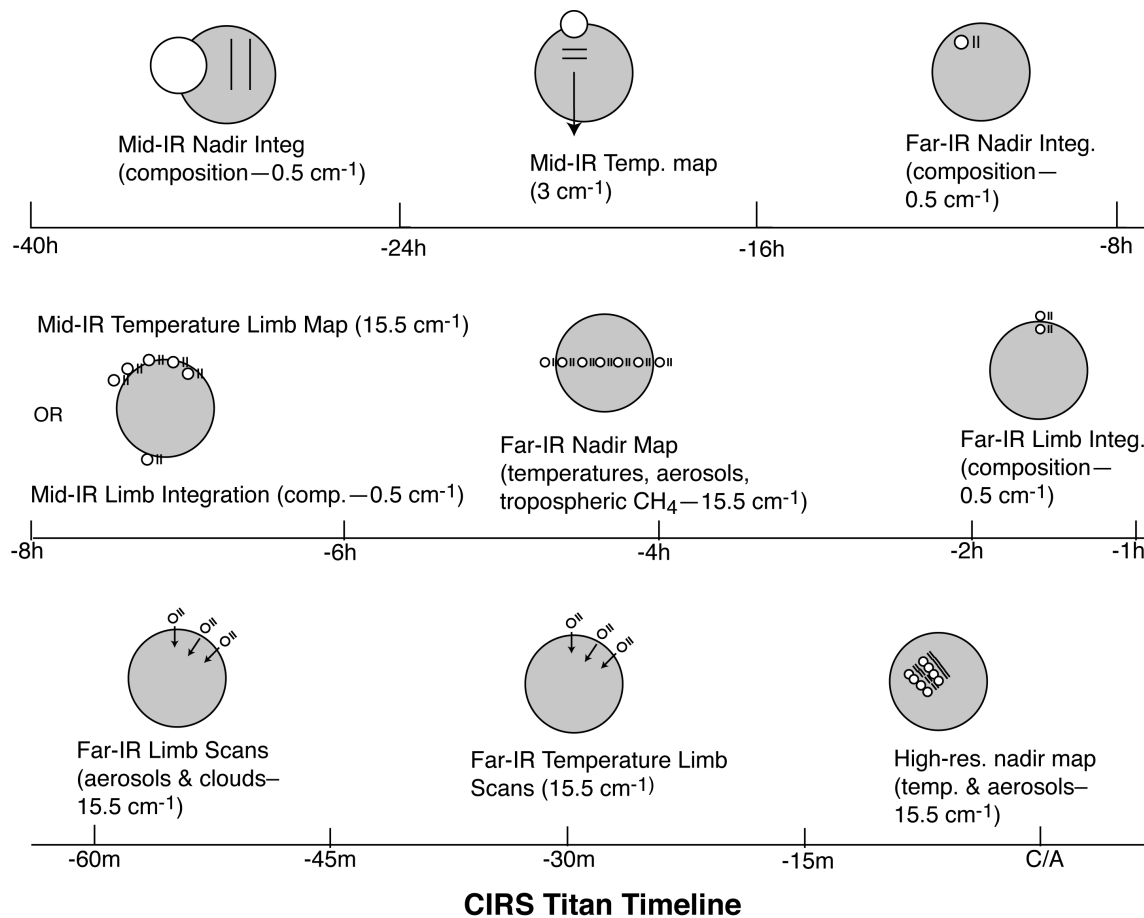


Figure 8: schematic summary of CIRS Titan observations (not all shown)

### 2.3.4 Icy Satellites

During the Cassini prime mission, there were eight flybys of the classical icy satellites targeted at 1000 km or less, as well as a number of 'Voyager-class' (less than 300,000 km) encounters. There were also flybys of several much smaller satellites, such as Janus and Epimetheus, at various distances. The dimensions of these objects range from less than 100 km to as much as 1530 km (for Rhea). Consequently, it is most useful to discuss CIRS observations in terms of the angular diameter of the object, rather than its distance from the spacecraft.

Normally the spacecraft orientation is controlled by momentum wheels (RWA), which provide pointing accuracy and precision of  $\sim 2$  mrad and  $\sim 0.04$  mrad, respectively. Consequently, the full spatial resolution of the FP3 and FP4 pixels (0.3 mrad) cannot be utilized with reasonable confidence until the target exceeds 1 mrad in diameter. At that point, the separation of focal planes 3 and 4 (0.9 mrad), and the large size of FP1 (nominally 3.9 mrad) offer reasonable assurance of obtaining useful data in either FP1 or at least one of FP3 and FP4. As with the planet and the rings, the order of magnitude difference in FOV scale between FP1 and the other focal planes plays heavily in the design of the icy satellite

observations. Approaching from a distance, CIRS observations proceeded roughly in the following order. As the observation plan matured, the naming convention gradually changed to reflect the multi-purpose nature of the data.

**Table 12: CIRS icy satellite observation descriptions**

<b>NAME</b>	<b>REQUIREMENTS</b>	<b>DESCRIPTION</b>
FP1INT, FP34INT FP1GLOBAL FP34GLOBAL FP13STARE	1-3 cm <sup>-1</sup> resolution $\Omega = 1-3$ mrad	Compositional integrations (typically performed at ranges where the target angular diameter ( $\Omega$ ) is 1-3 mrad). Because spectral features of solid materials are generally broader than those of molecular lines, these observations are made at 1-3 cm <sup>-1</sup> resolution. Conducted in staring mode, using FP1 and center detectors of FP3 and FP4, these are concentrated in geometries with low phase angles, so as to view the icy satellite surfaces at their warmest and maximize the signal-to-noise ratio. The steep roll off of intensity with increasing wavenumber requires increasing integration time to extend the spectrum. For a 100 K surface and a spectral resolution of 3 cm <sup>-1</sup> , a SNR of 10 at 600 cm <sup>-1</sup> can be obtained with 1 minute of integration, but extending the spectrum to 800 cm <sup>-1</sup> with the same SNR requires integration of 100 minutes. Therefore, extending the spectrum to the highest wavenumbers will involve coadding spectra over the entire tour.
SECLN, SECLX		Satellite eclipse entry (N) or exit (X) observations ( $\Omega > 1$ mrad, phase angle $\phi < 100^\circ$ , spectral resolution $\Delta\nu = 15.5$ cm <sup>-1</sup> ; a typical eclipse duration is ~2 hours). The high sensitivity of FP1 permits observations of objects even when the FOV is incompletely filled, or when the phase angle is moderately high. At low phase angles, even FP3 can be used to follow the initial portion of the cooling curve for relatively dark objects; this allows observations with body-centric spatial resolution better than 100 to be made when the apparent target size exceeds ~3 mrad. Eclipses provide the thermal inertia of the upper mm or so of the surface, as well as estimates of surface coverage by relatively large fragments of consolidated material (Figure 67, Figure 72).
FP1FAZ		Phase/longitude (diurnal cycle) coverage ( $\Omega > 1$

---

FP1MAP	mrad, $\Delta\nu=15.5\text{ cm}^{-1}$ , 10-20 minutes). Focal plane 1 will be utilized to determine the disk-averaged temperature of the satellites. From the resulting diurnal behavior, mean thermal inertias in the upper cm or so of the surface will be derived.
FP34FAZ, FP34MAP, FP34REG	Global thermal inertia mapping and/or hot spot monitoring ( $\Omega>3\text{ mrad}$ , $\Delta\nu=15.5\text{ cm}^{-1}$ ). Maps are made by slewing and rastering FP3 and FP4 across the disk at rates not to exceed that for Nyquist sampling ( $16\text{ }\mu\text{rad/s}$ in blink mode); observation durations will typically be 10-30 minutes. These maps will be successful for varying portions of a satellite, depending on its albedo and thermal inertia. The exception is Enceladus, which is so cold that even the subsolar regions will be barely detectable in an individual measurement. In this case, mapping will serve to monitor the satellite for ongoing endogenic activity; for example, active sources at or above the $\text{NH}_3\text{-H}_2\text{O}$ eutectic temperature will be easily observed if they fill more than a few percent of an FP3 or FP4 pixel.
FPGREEN	Search for a solid state greenhouse ( $\Omega>10\text{ mrad}$ , $\phi<40^\circ$ , $\Delta\nu=15.5\text{ cm}^{-1}$ , 15 minutes). The decreasing absorption coefficient of water ice with decreasing wavenumber in the far-IR permits detection of radiation from increasingly far below the surface, reaching as deep as 1 cm at $10\text{ cm}^{-1}$ . Slow east-west slews using FP1 allow following the daily penetration of the thermal wave into the regolith (Figure 69).
FP1POLE FP1MAP	Polar night (annual cycle) coverage ( $\Omega>10\text{ mrad}$ , $\Delta\nu=15.5\text{ cm}^{-1}$ , 15 minutes). FP1 observations of the dark winter polar region from high latitude permit determination of the seasonal cooling curve. This enables an estimate of thermal inertia in the upper tens of cm of the polar regolith.
FP1DAYMAP, FP1DRKMAP	Hemispheric FP1 mapping near closest approach ( $\Omega>10\text{ mrad}$ , $\Delta\nu=15.5\text{ cm}^{-1}$ ). The high sensitivity of FP1 permits rapid mapping of satellite disks near closest approach, where time is at a premium.

---

---

Nyquist-sampled maps at low spectral resolution (slew rate 400  $\mu$ rad/sec) will typically take 10-30 minutes. These permit identification of minor thermal anomalies, even on the night hemisphere (Figure 66).

---

### **2.3.5 Other TWTs and WGs**

The cross-discipline TWT (XD TWT) allocated time near apoapse on some revs. The magnetospheres TWT allocated critical time for magnetospheric observations, such as time near critical transition boundaries.

### **2.3.6 Primes and Riders**

CIRS may operate either as the 'prime' instrument, in which case it controls the spacecraft attitude by a set of uplinked pointing commands, or else as a 'ride-along' partner when another team is 'prime'. As the mission progressed, the approach to observing also matured to include "collaborative" observations in which either CIRS or another instrument may serve as the PRIME team responsible for the developing the designs but all rider instruments' pointing requirements were accommodated. Late in the mission, PIES were established in the science integration part of the uplink process – these observations are considered of highest priority in the acquisition of the data to provide some level of protection against deletion. The data is collected and processed in the same manner as all other data.

## **2.4 Data Gaps**

Gaps in the calibrated CIRS data fall into two categories: data that never reached the ground and data that could not be calibrated.

### **2.4.1 Data that did not reach the ground**

There are four primary reasons for missing data from CIRS observations: Spacecraft anomaly, instrument anomaly, the Deep Space Network (DSN) being unable to receive the data, and onboard data policing due to CIRS exceeding its allowed data volume.

A spacecraft anomaly can present three ways. The anomaly can force the instrument to turn off, thus no data is taken; and an anomaly could require the spacecraft to alter its pointing, thus CIRS may have produced data but not at the desired target; and an anomaly can cause transmission of data to fail, thus preventing it from reaching the ground.

Similarly, instrument anomalies can cause data corruption, or a complete lack of data output. The anomalies can be of hardware or software in nature. A hardware anomaly can sometimes correct itself or be corrected by the flight software, but when that does not occur, or when the anomaly is in the software, the solution is typically to reboot the instrument.

DSN issues can be a result of hardware malfunctions with the antenna arrays, weather (rain and other atmospheric conditions can cause packets to be dropped), and packets are

typically lost at higher rates when the spacecraft is within a few degrees of solar conjunction.

Data policing is rare. The standard CIRS data rate requested is 4000 bps for noadd and 2000 bps for coadded data. CIRS flight software, however, has a data compression algorithm that makes the normal output between 2800 bps and 3600 bps for noadd data and between 1700 and 1900 for coadded data. The signal from a specific target is one of the primary factors in determining where in those ranges the actual data would fall. On some observations CIRS has concluded it would have extra data volume available after an observation that could be applied to a future observation. In those situations, CIRS would run at a higher data rate than requested and would therefore risk being data policed. On most occasions of data policing, it is a deep space observation run at the no-add rate but with a request of only 3000 bps that is curtailed. This is designed intentionally so that CIRS could take data for as long as possible and obtain as much data as was allowed.

#### **2.4.2 Data that could not be calibrated**

There are several factors that may lead to data that cannot be calibrated. Chief among these is interference. Interference in the raw data has been known to occur when there is vibration induced in the instrument scan mechanism. The most common source of vibration has been the spacecraft reaction wheels operating at certain angular velocities. Interference has also been observed during thruster firing and from malfunctioning actuators on other instruments (MIMI LEMMS).

Instrument temperatures also affect the ability to calibrate the data. CIRS attempts to stabilize its focal plane assembly temperature; however, during heating, the temperature will rise and can be at a temperature that doesn't correspond to a set-point. In those situations, the data is bypassed and does not get calibrated.

Unusual laser modes can also prevent data from being calibrated. When the CIRS laser is turned off (generally only when the instrument is powered off or rebooted for anomalies), the laser can switch to a different configuration. It is impossible to know ahead of time what the configuration will be, but it often takes several days or weeks to stabilize. When a known laser mode is in use, data can be calibrated normally. However, in unknown modes or when the laser is drifting between modes, proper wavenumber correction of the data is impossible.

#### **2.4.3 List of Anomalies**

Below is a list of time periods and observations with significant or total data loss due to one of the above causes. Times listed for anomalies are the times of the last CIRS packet that reached the ground prior to the anomaly and the first packet received after the anomaly recovery had begun.

Spacecraft Anomalies:

9/11/2007 5:48:35	9/15/2007 16:30:47	Spacecraft safing due to TWTA anomaly
11/2/2010 21:28:49	11/15/2010 19:30:10	Spacecraft safing due to CDS anomaly

Instrument Anomalies:

10/25/2004 17:28:44	10/28/2004 2:39:05	Commanding error triggered FSW buffer overflow
12/10/2006 4:51:21	12/11/2006 9:18:49	BIU Anomaly
12/16/2006 5:43:53	12/17/2006 9:43:20	BIU Anomaly
4/4/2007 7:30:19	4/5/2007 5:04:10	Instrument turned off by accidental contingency uplink
5/19/2007 23:37:32	5/20/2007 23:01:33	BIU Anomaly
11/2/2008 9:36:02	11/4/2008 17:33:58	BIU Anomaly
2/6/2009 12:41:48	2/10/2009 6:57:13	BIU Anomaly

DSN and Data Policing Issues:

Data policing issues are extremely rare on science observations, but since there is no simple way to distinguish them from DSN issues, they are lumped together. A list of major gaps is given in Appendix B. Note that only observations with less than 10% of the data making it to the ground are listed.

## **2.5 Electrical interferences (spikes) and other data issues**

### **2.5.1 Background**

There are several known interference patterns in the CIRS science data. Some of them have been identified as relating to externally controlled hardware, others are internally controlled, and the source of one has never been identified.

For interferences external to the instrument, and regulated elsewhere on the spacecraft, two patterns have been identified. Both are tied to communications with the CIRS Bus Interface Unit (BIU), which shares a power source with the instrument and provides the only means of communication between the instrument and the spacecraft.

The first interference pattern is tied to the telemetry packet collection cycle. During the first Instrument Check-Out test (ICO1) performed after launch, it was noticed that a pattern of large spikes at quasi-regular intervals was evident on the FP1 interferograms. These occurred with intervals of 11, 11, 10, 11, 11, 10 (repeated) RTIs and were soon determined to originate in the Bus Interface Unit (BIU). Querying of the BIU by the spacecraft Command and Data System (CDS) at a frequency of 0.75 Hz to transfer cached science packet data, led to interferences at 1.333 second intervals, which was subsequently discretized to the nearest 1/8 of a second (1 RTI). The CIRS telemetry rates were later redefined to be consistently 16 RTIs apart, so from the Cooler Cover Release Checkout onwards, the interference rate was changed to 0.5 Hz.

The second noise pattern that is controlled externally is tied to the spacecraft communications cycle; it has always been fixed at 8 Hz. Every 125 ms, the spacecraft notifies the instrument that it is time to check the BIU for transactions such as new commands, updated clock time, and to upload any housekeeping or science-engineering data. Each time there are transactions BIU power consumption increases linearly as data throughput increases. Since the science packets transactions are approximately 5 times the size of any other transactions, they produce greater and more sustained power transients than the 8 Hz transactions. As a result, the 0.5 Hz noise pattern creates stronger spikes in the science data than the 8 Hz pattern of the rest of the transactions. In the figures below, you can see how average data rates affect power consumption, and how transmissions affect current and voltage.

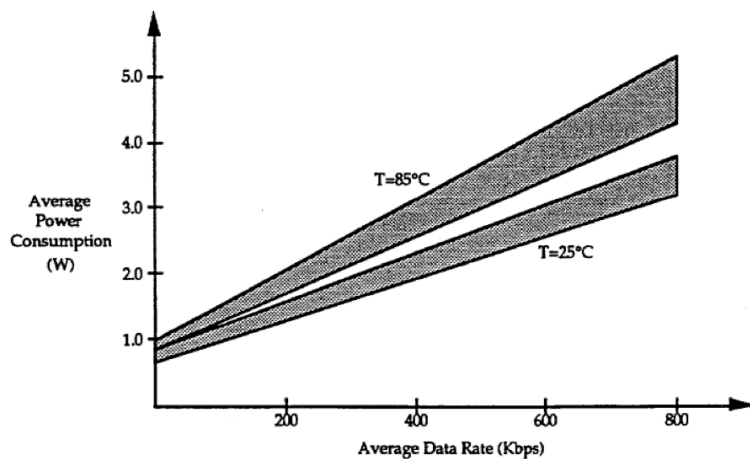
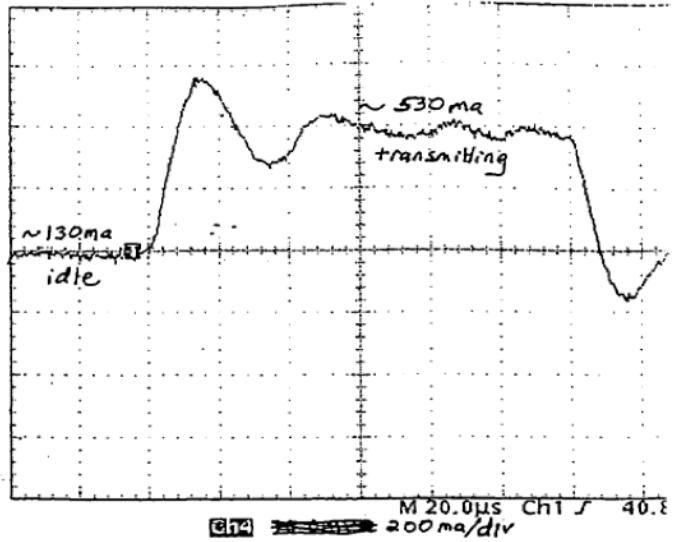


Figure 9 - BIU average power consumption.



SAMPLE BIU POWER  
TRANSIENT WAVEFORMS

- a) In-rush current from host supply  
X: 20 $\mu$ sec/div  
Y: 200ma/div



- b) Vcc transients at host supply output  
X: 20 $\mu$ sec/div  
Y: 20mv/div

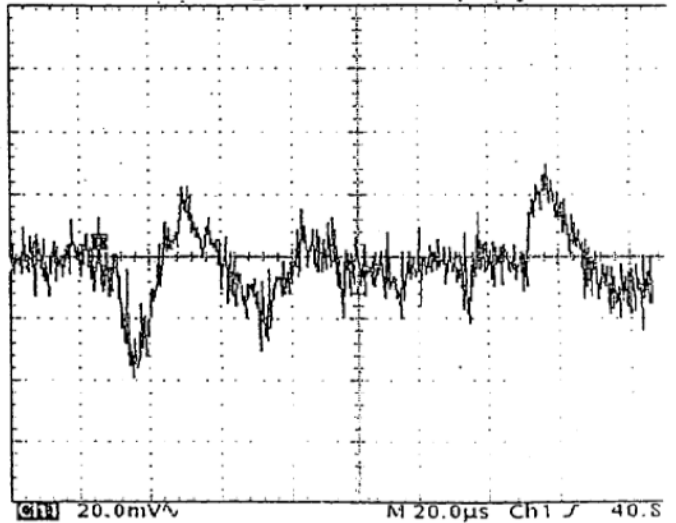


Figure 10 - sample BIU transient waveforms showing the BIU in-rush current (a) and supply voltage, Vcc (b) versus time.

Complicating the issues for 8 Hz noise is an additional source of interference. This, second source of 8 Hz noise is one of two known noise patterns that are controlled by timing established in the CIRS flight software (FSW). The first FSW regulated noise follows the schedule of the numerical filtering and compression cycles of the instrument. Traditionally, this timing was linked by the FSW to the same 8 Hz cycle used for communications. Through on board experimentation, it was discovered that this internal 8 Hz noise could be separated from the externally controlled 8 Hz noise. The FSW was updated in July 2010 to implement that separation so that the internally controlled noise could be averaged out over multiple interferograms.

The other source of noise with a FSW controllable rate is noise caused by performing analog MUX data readouts. The noise was discovered after a FSW change caused internal timing to be more tightly controlled. As a result, the noise no longer averaged out over a large number of scans, it appeared in the same positions on each scan. The resulting fixed

pattern produced a spike in the spectra. This noise is the weakest of the known noise patterns and is nearly impossible to see in uncalibrated instrument data.

Figure 11 below is a plot of averaged interferogram data from focal plane 1 in early 2005. The 0.5 Hz spikes stand out on the sides, with the fifteen 8 Hz spikes between them (The sixteenth 8 Hz spike coincides with the 0.5 Hz spike so it is masked.) The MUX related noise, which would have been observed in individual interferograms at 0.77-1.0 Hz is not discernible.

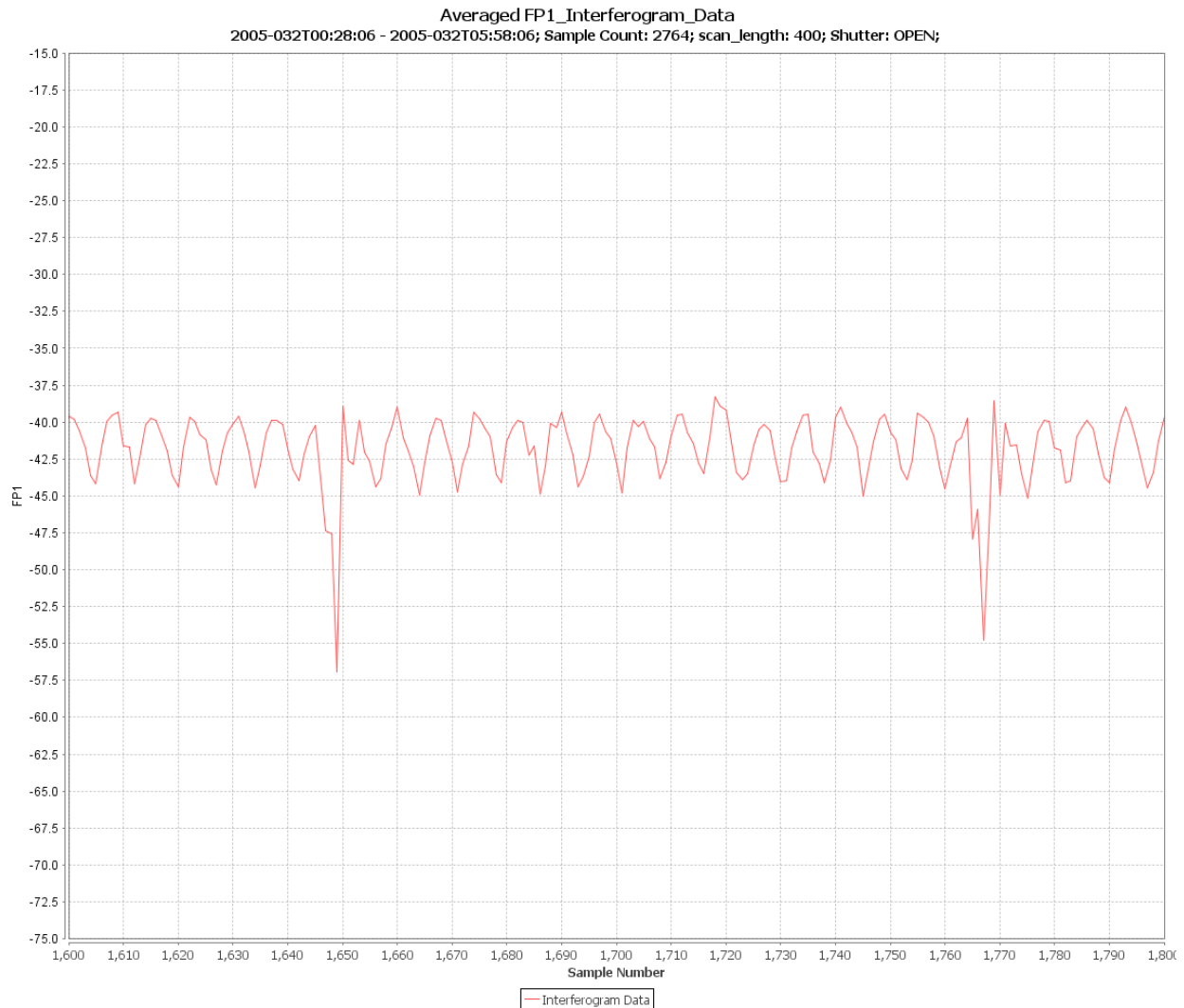


**Figure 11 – plot of averaged FP1 interferogram data showing electrical interferences (spikes)**

Each of the above noises has been observed in focal planes 1 and 3. The internal filtering related noise has also been observed in FP4 during a noise experiment, but no noise has been seen in FP4 under normal operating conditions.

A further ‘spike’ pattern only affects FP3. It occurs at a rate of approximately 8.33 Hz. The CIRS team has performed experiments in attempts to affect the timing of the noise;

however, none of the experiments have had any affect. All that can be learned was that the timing of the noise is relative to the start of the scan.

In addition to spikes occurring in the spectra at positions corresponding to these frequencies, additional spikes occur at the harmonics of each frequency. For example, in FP1, the 8 Hz noise appears at  $191.38 \text{ cm}^{-1}$ , but it also appears at  $382.62 \text{ cm}^{-1}$  and  $573.93 \text{ cm}^{-1}$ , corresponding to the 16 Hz and 24 Hz harmonics. While easily identifiable, the spikes in the spectra are not the same size for each harmonic. The conversion between the frequency of the noise in the interferogram and the location in the spectra of the corresponding spike is approximately  $23.91375 \text{ cm}^{-1}$  per 1 Hz (though it is affected by the laser mode which was active at the time the data was recorded).

The final interference pattern does not consist of a spike comb. Two sine waves (at least) are present: one in FP1 and one in FP3 interferogram data. This interference presents itself as large spikes in the spectra. Its frequency changes over time, so the spike moves within the spectra. For FP1 it has been seen in the range  $\sim 23 - 430 \text{ cm}^{-1}$  range (at least), and for FP3 between  $880$  and  $1020 \text{ cm}^{-1}$  (at least). The FP3 sine wave spike is a harmonic of the one in FP1. The exact cause of the sine waves is unknown; however, it is known that the frequencies decrease as the CIRS electronics board temperatures increase.

### 2.5.2 Mitigation

Over the years, several steps were taken to eliminate or average out the noise spikes. In 2005, CIRS began using scan lengths that would create 16 positions for the 0.5 Hz noise spikes (39, 57, 97, 225, & 401 RTIs). Algorithms were also introduced into the ground data processing to (i) locate the spikes, and then (ii) to subtract out a typical shape ('comb') of the noise from the interferogram, thereby greatly reducing the appearance of the noise.

In FSW Version 6.0.0 (uploaded July 2010), the ability to manipulate the timing of events that affect the position of noise spikes relative to the start of an interferogram was introduced. To that end, the noise spike that occurs in FSW Version 5 at a 1 Hz rate, and the stronger of the two observed {8, 16, 24} Hz interference sources, have their rates randomized. The positions of the noise spikes that occur at 0.5 Hz, as well as the positions of a second, weaker, noise pattern occurring at {8, 16, 24} Hz, are manipulated by adding 5 ms to the scan length. For example, in versions of the FSW previous to FSW 6.0.0, a 401 RTI scan was approximately 50.125 seconds in duration; in FSW 6.0.0 the duration is 50.130 seconds.

The result of this additional time being added to each scan is that the 0.5 Hz and {8, 16, 24} Hz noise patterns are shifted within the interferogram relative to the start of fly back, and thus to the start of scanning. The 5 ms shift quantity creates 200 potential time delays from the start of the scan to the first 0.5 Hz noise spike in the interferogram. Assuming perfect timing, when 200 consecutive scans are averaged the combined noise pattern would appear to be a 100 Hz pattern. With the {8, 16, 24} Hz noise, there would be 25 potential positions inside the interferogram for the noise, which would produce a 200 Hz noise pattern when averaged. Both the 100 Hz and 200 Hz noise patterns lie outside the

bandwidth of CIRS Focal Planes 1 and 3 and therefore do not show up in the interferogram. The full amplitude 0.5 Hz spikes and a much diminished {8, 16, 24} Hz spike sequence are present in each individual interferogram.

In summary, the new timing configuration was as follows:

- Science packet collection, ½ Hz noise, shifted 5ms per scan
  - Individual scans: 200 noise positions; but ½ Hz noises still present in each individual scan.
  - Averaged scans: 200 positions average to a 100 Hz noise; outside the band pass
- Analog MUX channel data collection, 1 Hz noise
  - Individual scans: randomized noise positions; noise outside band pass
  - Averaged scans: randomized noise positions; noise outside band pass
- Spacecraft communications cycle, 8 Hz noise 1, shifted 5 ms per scan
  - Individual scans: 25 noise positions; but 8 Hz noise still present in each individual scan.
  - Averaged scans: 25 positions average to a 200 Hz noise; outside the band pass.
- Internal/numerical filter related, 8 Hz noise 2.
  - Individual scans: randomized noise positions; noise outside band pass.
  - Averaged scans: randomized noise positions; noise outside band pass.
- Internal/FP3 only, ~8.33 Hz noise
  - No change – still always 8.33 Hz

The effects of the changes were positive and are shown below. Averaging scans with noise in the above configurations reduces the spikes to levels smaller than the already despiked data from earlier versions of flight software.

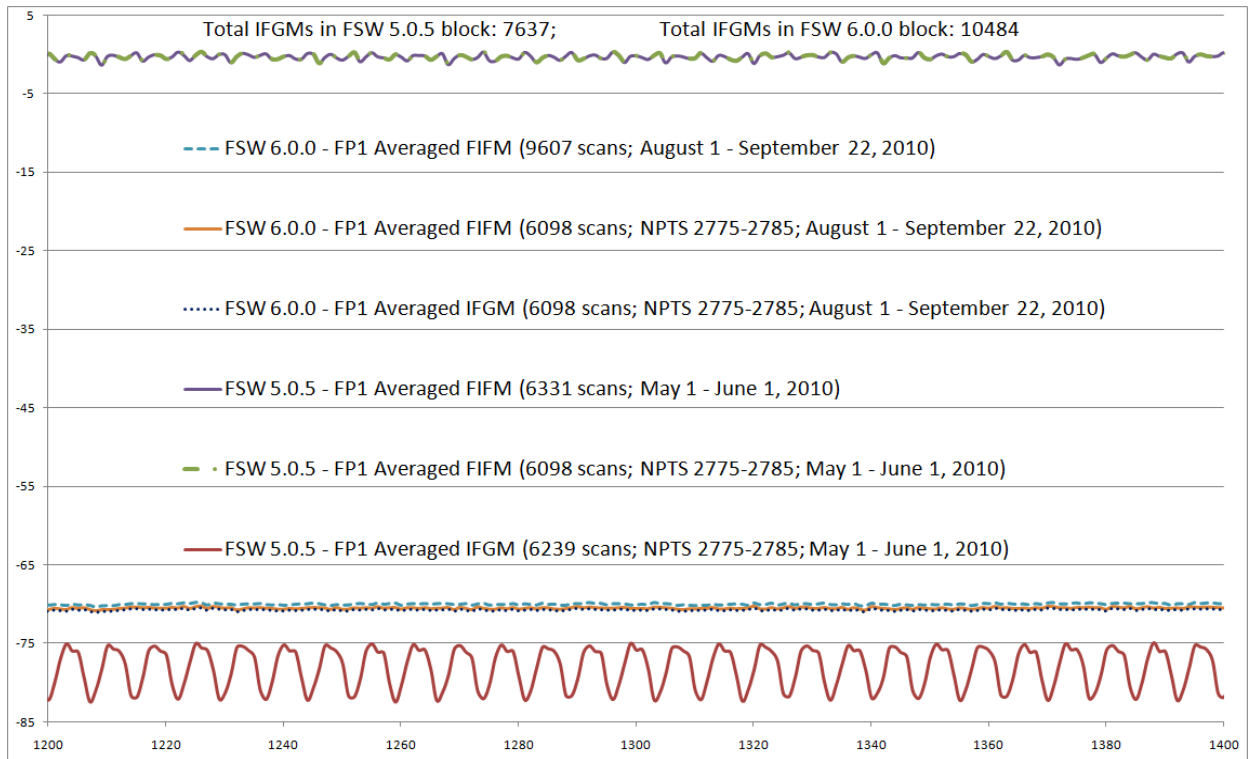


Figure 12 – comparison of averaged FP1 interferogram data from different mission periods

In the FP1 and FP3 average spectra the results were even more pronounced. Figure 13 shows both pre- and post-FSW 6.0 spectra (where only the 8.0 Hz noise is visible). Note that the large 8.0 Hz spikes in the blue line (pre-FSW 6.0) are not present in the red line (post FSW 6.0):

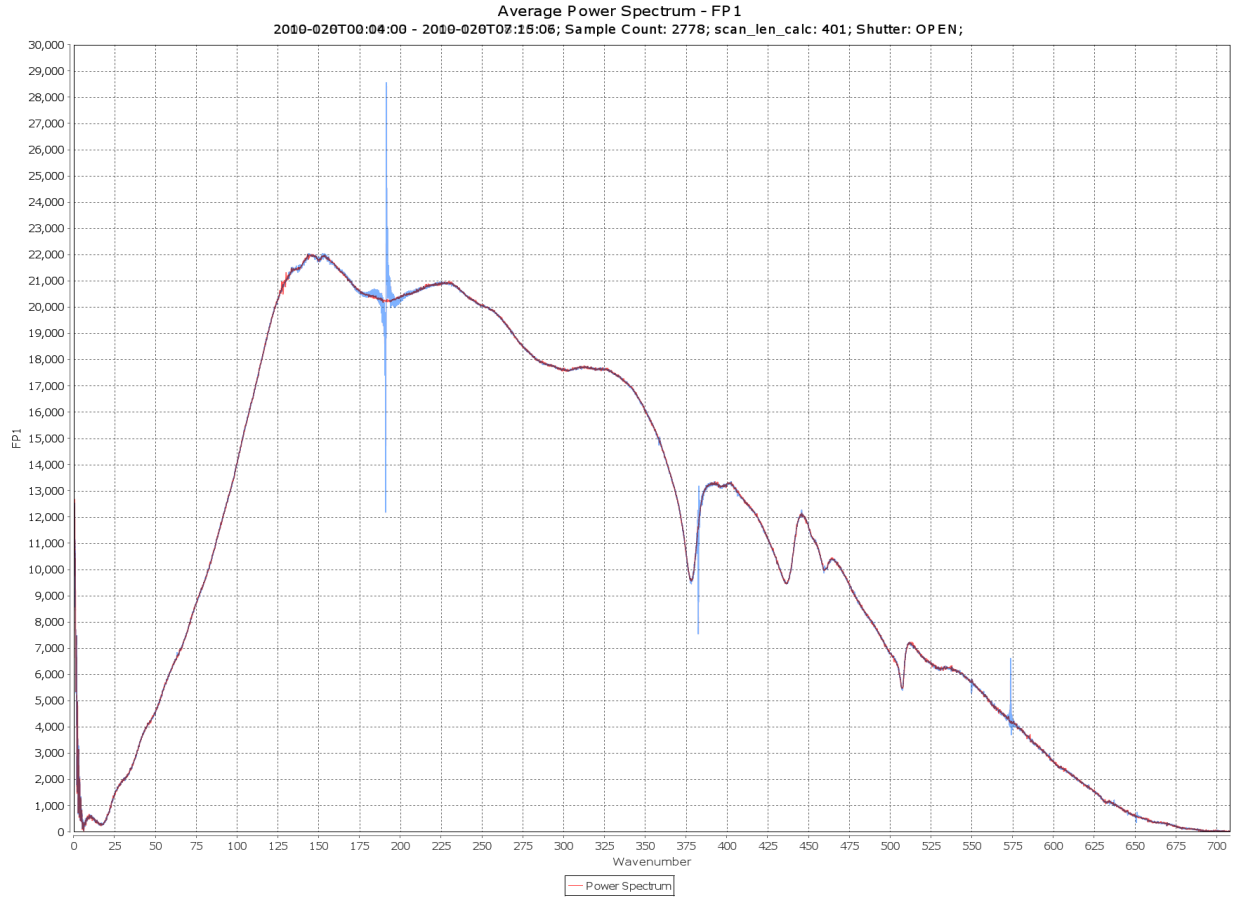
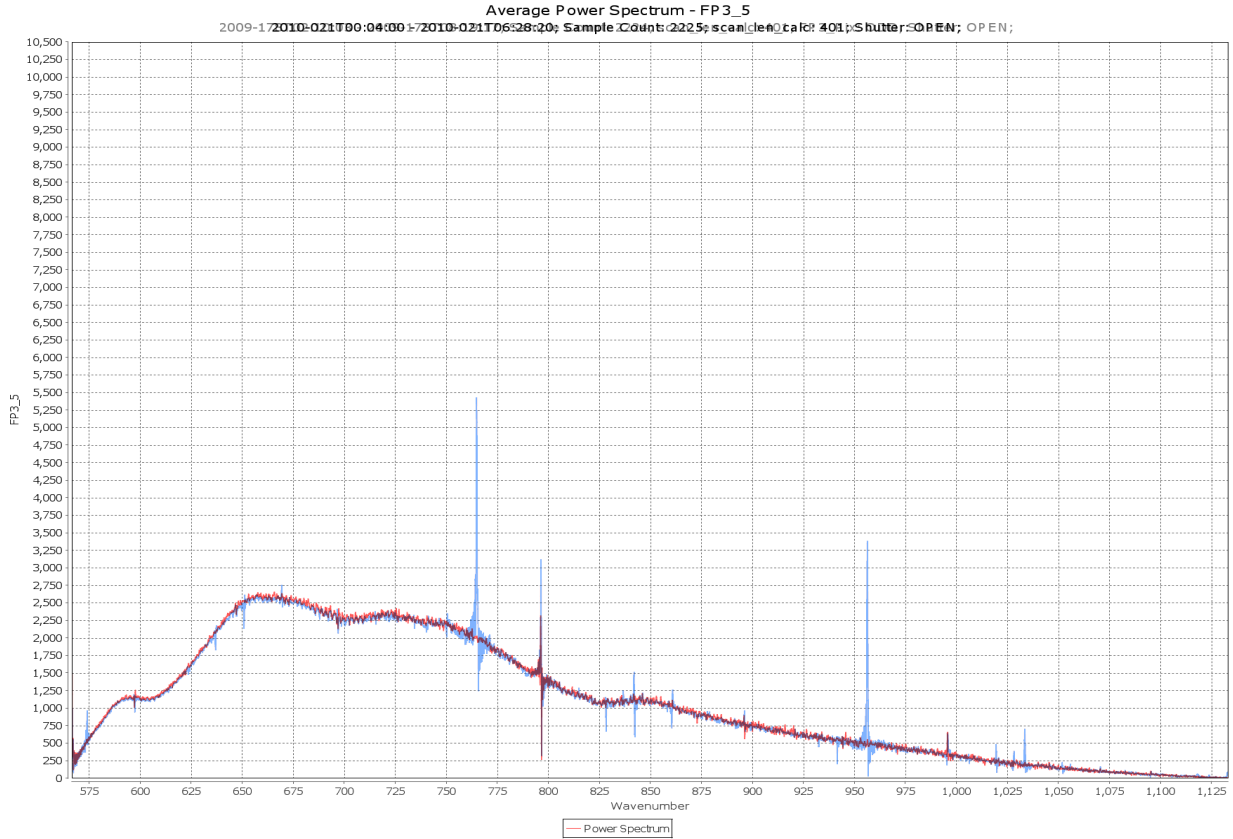


Figure 13 – FP1 uncalibrated spectrum before (blue) and after (red) despiking.

Similarly in FP3, the 8 Hz spikes are essentially gone, while the 8.33 Hz spikes (at 598, 797, 996  $\text{cm}^{-1}$ ) are visible (Figure 14), as expected, in data acquired with both versions of the flight software. Note that in Figure 14 only noise at 8.0 Hz and 8.3 Hz is visible with noise at other frequencies being too low to see.



**Figure 14 – raw FP3 uncalibrated spectrum before (blue) and after (red) despiking**

The solution is not, however, perfect. By randomizing the positions of some spikes and shifting others within the interferograms, the standard deviations of the samples at each position are increased. In Figure 15 below, you can see that the 8 Hz spikes in green (pre-FSW 6.0) are much larger than the 8 Hz spikes in black (from a test of the FSW 6 configuration). A similar statement can be made about the pre-FSW 6.0 standard deviation in red and the standard deviation of the FSW 6.0 test, in purple. However, the baseline of the new configuration's standard deviation is higher in the regions without a spike.

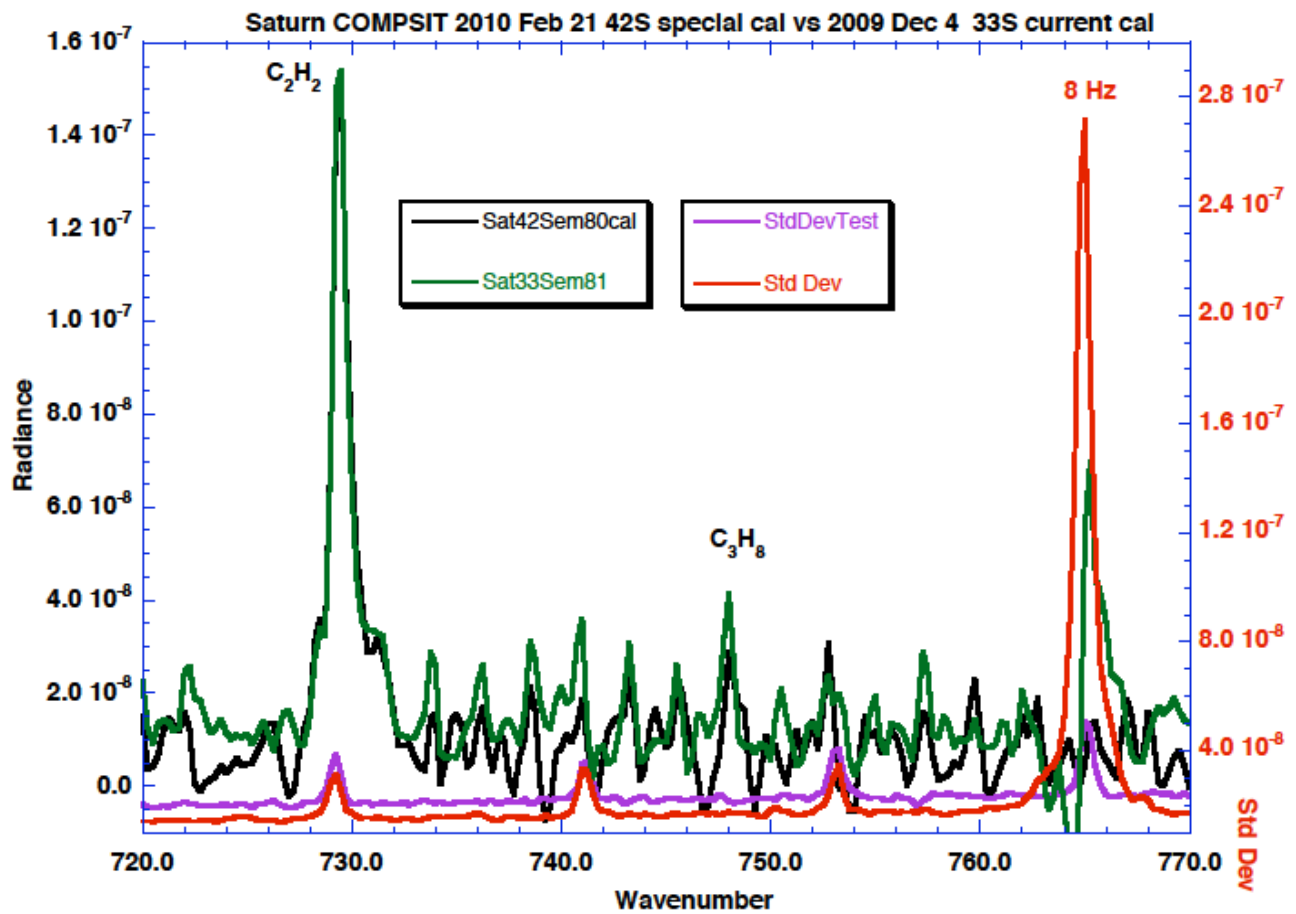


Figure 15 – Saturn spectrum before and after despiking

Note: since both the amplitude and phase of the noise spikes are variable, it is usually necessary to confirm the presence of an apparent artifact in the spectrum by looking for a spike in the standard deviation at the same wavenumber position. The effect is especially clear on averages of deep space spectra.



## 3.0 Calibration of the instrument

### 3.1 Overview of data flow

The block diagram in Figure 16 schematically illustrates the overall flow of data from the spacecraft, through various transfers on the ground, to reach the user. In this document we will focus only on the part of the data pipeline that occurs at GSFC (top center dashed box).

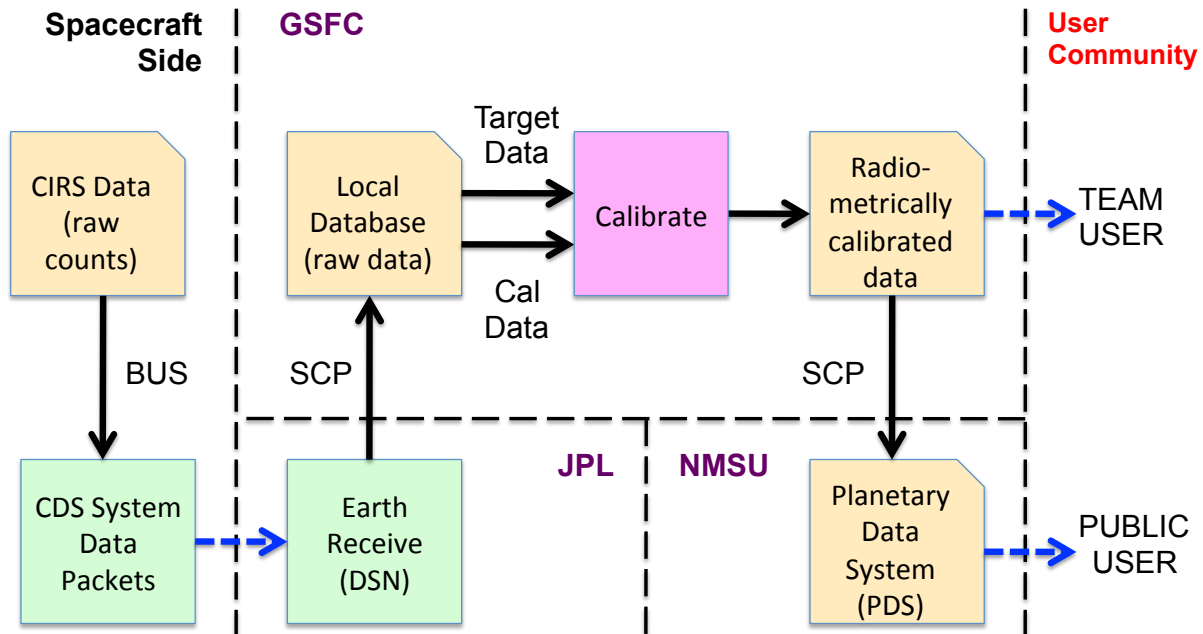


Figure 16: block diagram of data flow from the CIRS instrument to the eventual user.

A more detailed picture of the data flow at NASA GSFC is shown in Figure 17.

Raw compressed instrument data packets arrive from the spacecraft, via the DSN, at NASA JPL. An automated query program brings all new or changed packets via secure copy to the GSFC SOPC computer, shown in the upper left behind the firewall. At this point they are requested to an archive computer, and across the firewall to the main data server computer (cirsdata). Decompression of the data to form raw table blocks is performed here automatically every night. Following the creation of the raw interferograms (IFM), pointing and geometry data is automatically generated based on spacecraft ephemeris data (see Section...). At this point the level o ‘raw’ database is complete.

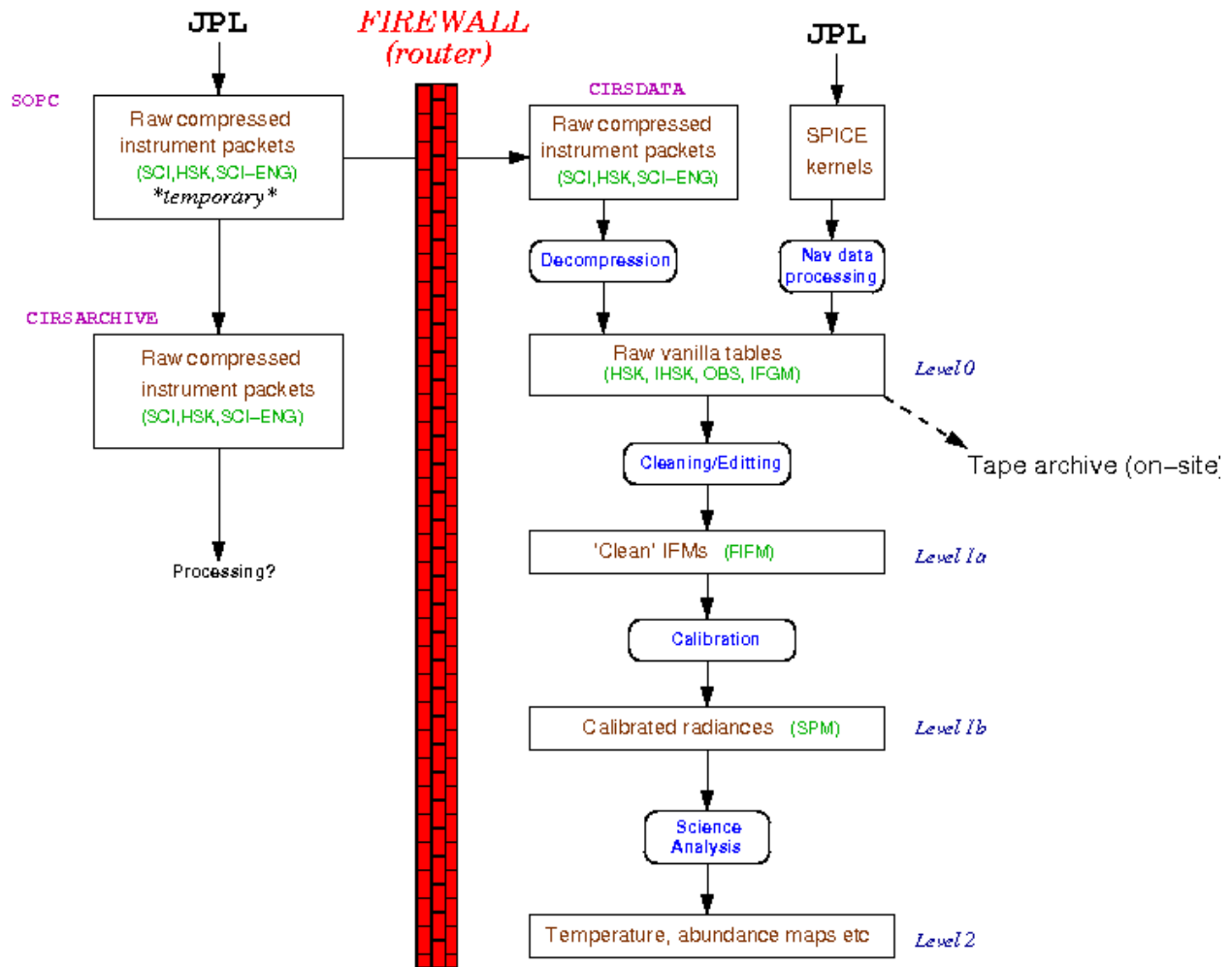


Figure 17: flowchart of CIRS data at GSFC. For definition of Vanilla see Section 4.1.2

The second part of the data flow takes the level 0 (integer count) interferogram data and filters out bad data, applies some ‘cleaning’ algorithms to the good data, creates a record of any potential issues for calibration (e.g. scan mechanism out of lock), and re-writes the interferograms as floating point data. See Section 3.3 for further details.

The third and final process is the calibration, which combines interferograms of reference temperature sources (space for FP1, space and shutter for FP3/4) with the on-target data, and then calibrates both the radiance (from counts to physical units) and the wavenumber axis (from sample number to inverse centimeters). See Section 3.4 for details.

### 3.2 Instrument readout to raw tables

CIRS data is normally read out at a rate of 4 kbits per second (kbps)<sup>4</sup> and 8 kbit packets are transferred via the Bus Interface Unit (BIU) to the spacecraft Command Data Subsystem (CDS) every 2 seconds. CIRS has many ways of reducing data rate, such as co-adding IFMs (reduces rate by factor 2), dropping FP3 or FP4 readout (reduces by 45%), dropping FP3 and

<sup>4</sup> 6 kbps during the Jupiter encounter.

FP4 readout (reduces by 91%), or going to housekeeping only mode. Data packets are compressed in the instrument electronics, packetized on the spacecraft, transmitted to the Earth via the Deep Space Network (DSN) and then decompressed by software on the ground. At this stage, the data goes into a processing pipeline, which organizes the science data into binary tables and interpolates housekeeping records. Pointing and geometry tables are also produced when the NAIF data becomes available.

### 3.2.1 Raw data tables

The raw data tables are fixed or variable-length binary tables in the Vanilla format, created by simply uncompressing the instrument packets from the spacecraft and writing the data as binary files. There are four types:

- OBS: observation data. A fixed-length record binary table containing basic information about the data modes during the observation, including which detectors are active, whether COADD mode is activated, the scan length (spectral resolution) and so on.
- IFGM: variable-length binary records containing the raw interferogram data, in units of detector counts.
- FRV: fringe voltage data.
- IHSK: interpolated housekeeping data, including the temperatures recorded by sensors on various parts of the instrument, which is needed for eventual calibration. Housekeeping data packets are created every 64 seconds, however to align this information with the individual interferograms (4.5 to 52 seconds in length), the housekeeping data is interpolated to match the start times of each interferogram.

Further information about the Vanilla tables, how to read them and their contents, is given in “Section 4.0 How to search and extract data”.

### 3.2.2 Navigation data tables

The NAV tables take as input various *kernels* provided by the Cassini Navigation Team and produce various quantities related to the location and velocity of Cassini and other bodies in the target system and the orientation of CIRS. This is done almost entirely by using the *NAIF toolkit*, a collection of software which is written by JPL’s Navigation and Ancillary Information Facility, which reads the various formats that the kernels come in and performs various operations on that data. (A list of the kernels used for every NAV table and the version of the NAIF toolkit that was used to produce a given table is entered in the text .LBL file associated with each binary .DAT file which contains the actual table.) Important types of kernels are the SP kernels, binary kernels which contain the ephemeris for Cassini, the Earth, the Sun, and the bodies in the target (either Jupiter or Saturn) system, the C kernels, binary kernels which contain information about the orientation of Cassini at any given time, and the PC kernels, text kernels which contain the masses, rotation rates and axes, shapes (as modeled by triaxial ellipsoids), etc., for the bodies in the target system. Other kernels

contain the details of the spacecraft and instrument coordinate systems, and the relationship between spacecraft event time and the “spacecraft clock”.

It is important to keep in mind that the software that produces the NAV tables has no knowledge of what a particular observation is for or what the intended target is. For that reason, entries in the NAV tables may seem to be extraneous. For example, an entry in the RIN (rings) table is always made, even if the rings aren’t a target and even if CIRS is pointed away from the rings.

Another important point to keep in mind is the use of *NAIF reference ellipsoids* by the NAIF toolkit. For bodies with solid surfaces, those surfaces are modeled by a triaxial ellipsoid, with axes contained in the planetary constants (PC) kernels. For gas giants (Saturn and Jupiter), the NAIF reference ellipsoid is suppose to model the 1 bar surface. However, using the reference ellipsoid as the one bar surface is a very poor choice, since, because of the subtleties of the atmospheres (winds, deviations from axisymmetry, etc.) the NAIF reference ellipsoid can deviate from the actual one bar surface by over 100 km. The NAV tables always use the NAIF reference ellipsoids as references, but keep in mind they may be inadequate for the problem you are trying to solve.

#### *The GEO (geometry) tables*

The GEO tables are unique among the NAV tables in that they do not depend at all on the orientation of Cassini, but only upon its *state vector* (location + velocity) and the state vectors of the Sun and all of the bodies specified in table 4.4.1. The list of quantities included in the GEO tables can be found in the file GEO.FMT, and are more fully described in DATASIS.CAT. The field keys for the GEO tables are scet and body\_id. body\_id is similar to target\_id for the POI, RIN, and TAR tables, but is called body\_id because there is no “target” to speak of. All of the bodies in table 4.4.1 have an entry in the GEO tables for every scet. The entries in the GEO tables are independent of a particular CIRS detector.

Note that the quantities in the GEO tables are computed not at the scet, but at the time\_zpd, the time of Zero Path Difference where the majority of the signal is collected, typically a few seconds after the scet. Also note that while the .LBL files for the GEO tables list C kernels in the collection of kernels used to create an individual table, the C kernels are not actually used.

#### *The POI (pointing) tables*

The POI tables contain quantities that depend on the orientation of CIRS and on the individual detectors. The three field keys are scet, det, and target\_id. (However, as with the GEO tables, many of the quantities in the POI tables are actually computed at time\_zpd, and a few at time\_end, the end time of the scan.) The entries in the POI tables are found in the file POI.FMT.

Entries are made in the POI tables for all active detectors and for every body that is in the field of view of an active detector. One exception is the primary (Saturn), for which an entry is always made at every scet and det, whether or not it is in the field of view of a detector. “Field of view” also requires a little explanation. Every body gets a “penumbra” attached to it before it is determined whether it is in the field of view or not. For airless bodies, a penumbra of 0.001 mrad is added to the three axes of the triaxial ellipsoid defining the surface of the body. For bodies with atmospheres (Saturn and Titan), the penumbra is larger, and depends on the detector. For FP1, the penumbra is  $600 \text{ km} + 0.004 \text{ mrad}$  (i.e.,  $600 + [0.004 * \text{distance to target}]$  is added to each axis). For FP3 and FP4, 0.003 mrad is used in addition to the 600 km. Then we check to see whether this new object (target + penumbra) is in the field of view. If any Q point (grid of nine points defining the outline of the detectors: see Figure 29) intersects the object, then it’s in the field of view. If the entire object is within the field of view but not touching any Q points, then it’s within the field of view. Otherwise, it’s out of the field of view. Note that, even though an entry is always generated in the POI table for Saturn, it is only marked as in the field of view if it actually is.

The POI tables have many entries that are computed at each Q point for the active detectors, but some are computed only for the boresight of the detector (Q point 5). Two quantities, `filling_factor` and `emission_angle_fov_average` merit special attention because they are computed by doing a Monte Carlo estimate. The field of view of the detector in question is filled with rays randomly chosen in the field of view, and then we determine whether or not the ray intersects the target in question. Unlike the field of view computation for the Q points, we do not add the penumbra and use the NAIF reference ellipsoid as the target’s surface. Then the `filling_factor` is computed by taking the ratio of rays that intersect to the total number of rays, and `emission_angle_fov_average` simply averages the emission angle for the rays that intersect. There’s an additional complication for FP1. FP1 is more sensitive toward the center than toward the edges. This can be modeled as a Gaussian response, and we use this Gaussian to bias the selection of the random rays toward the more sensitive part of the detector in the center. So while `filling_factor` for FP3 and FP4 is simply an approximation to the area of the detector that is filled with the target, for FP1 weight is given to the more sensitive part of the detector. For purposes of speed, a modest number of random rays is used. We stop whenever 1000 points have intersected. If 5000 points have been tried before 1000 points have intersected, both `filling_factor` and `emission_angle_fov_average` are set to -200, an otherwise impossible value. So the formal statistical error for these quantities is on the order of a few percent.

The smear is defined in the following manner. The position of the boresight on the target at `time_zpd` is computed and saved. Then, at `time_end`, the angle between that point and the position of the boresight at `time_zpd` is computed. `smear` is the ratio of this angle with the angular width of the field of view of the detector, or in other words, is the fraction of the field of view over which the original intersection point of the boresight has moved between `time_zpd` and `time_end`. If the boresight at either `time_zpd` or `time_end` is off the target, then this is set to -200.

Latitudes in the POI tables are given in two systems, planetocentric and planetographic. For spherical bodies they will be identical.

The POI tables are also unique in that they may contain entries for targets that are fixed stars, which are used occasionally for testing. The list of potential fixed star targets is in Table 13. Since many of the entries have no meaning when referred to a star (for example, latitude and longitude), these are set to the usual “CIRS bad value”, -200. Stars were given artificial target\_id’s which have nothing to do with actual NAIF id’s in this case.

**Table 13: a list of the possible stellar targets that could be used for testing purposes that could have entries in the POI tables. The numerical id’s are artificial, and have nothing to do with NAIF id’s. Not all of these were used during the mission.**

body_id/target_id	Object
10101011	VY CMa
10101012	eta Car
10101013	CW Leo
10101014	A Ori
10101015	A Sco
10101016	R Dor
10101017	O Ceti
10101018	NML Tauri
10101019	W Hya
10101020	Gamma Cru

### *The RIN (rings) tables*

The RIN tables contain quantities describing the rings of Saturn as the target. Like the POI tables, the RIN tables depend on the orientation of CIRS aboard Cassini. Unlike the POI table, no effort is made to determine whether or not the rings are actually in the field of view of a detector. An entry in RIN is made for every active detector at every scet. The field variables are scet and det. As required by the Planetary Data System, the coordinate system used to describe the rings is an inertial coordinate system centered on Saturn, with the z axis aligned with Saturn’s rotational axis. The rings are assumed to be in the z=0 plane, out to 140270 km. Longitudes are measured eastwards from the ascending node of the “intersection of the ring plane with J2000”, or, in other words, the intersection of the ring plane with a plane parallel to the ecliptic plane of the J2000 coordinate system.

### The TAR (target) tables

The TAR tables answer a simple question, whether a given object is in the field of view of a detector at a given scet. The field variables are scet and det. The TAR tables consist of single byte entries containing either a one (true) or a zero (false) for each body in

Table 14 or Table 15, a single byte containing either one or zero which says whether any of the stars in Table 13 are in the field of view, and a byte that says whether or not the rings (Saturn or Jupiter) are in the field of view. In addition, the TAR tables contain fov\_targets, an integer in which each bit is a separate entry for each body identical with the byte fields. The bit values are fully described in DATASIS.CAT.

In the TAR tables, a satellite that is being eclipsed by its primary (e.g. Titan behind Saturn) is not marked in the field of view. However, a satellite being eclipsed by another satellite will still be marked in the field of view; i.e. if Enceladus is completely behind Titan, it will still be marked in the field of view if it otherwise would be if Titan weren't there.

**Table 14: list of objects that were included in the NAV tables during the Jupiter flyby. The body/target id is identical with the NAIF id of the body.**

body_id/target_id	Object
501	Io
502	Europa
503	Ganymede
504	Callisto
599	Jupiter

**Table 15: list of objects that are included in the NAV tables from the Saturnian system. The body/target id is identical with the NAIF id of the body.**

body_id/target_id	Object
601	Mimas
602	Enceladus
603	Tethys
604	Dione
605	Rhea
606	Titan

<b>body_id/target_id</b>	<b>Object</b>
607	Hyperion
608	Iapetus
609	Phoebe
610	Janus
611	Epimetheus
612	Helene
613	Telesto
614	Calypso
615	Atlas
616	Prometheus
617	Pandora
618	Pan
699	Saturn



### 3.3 Cleaning and filtering of interferograms

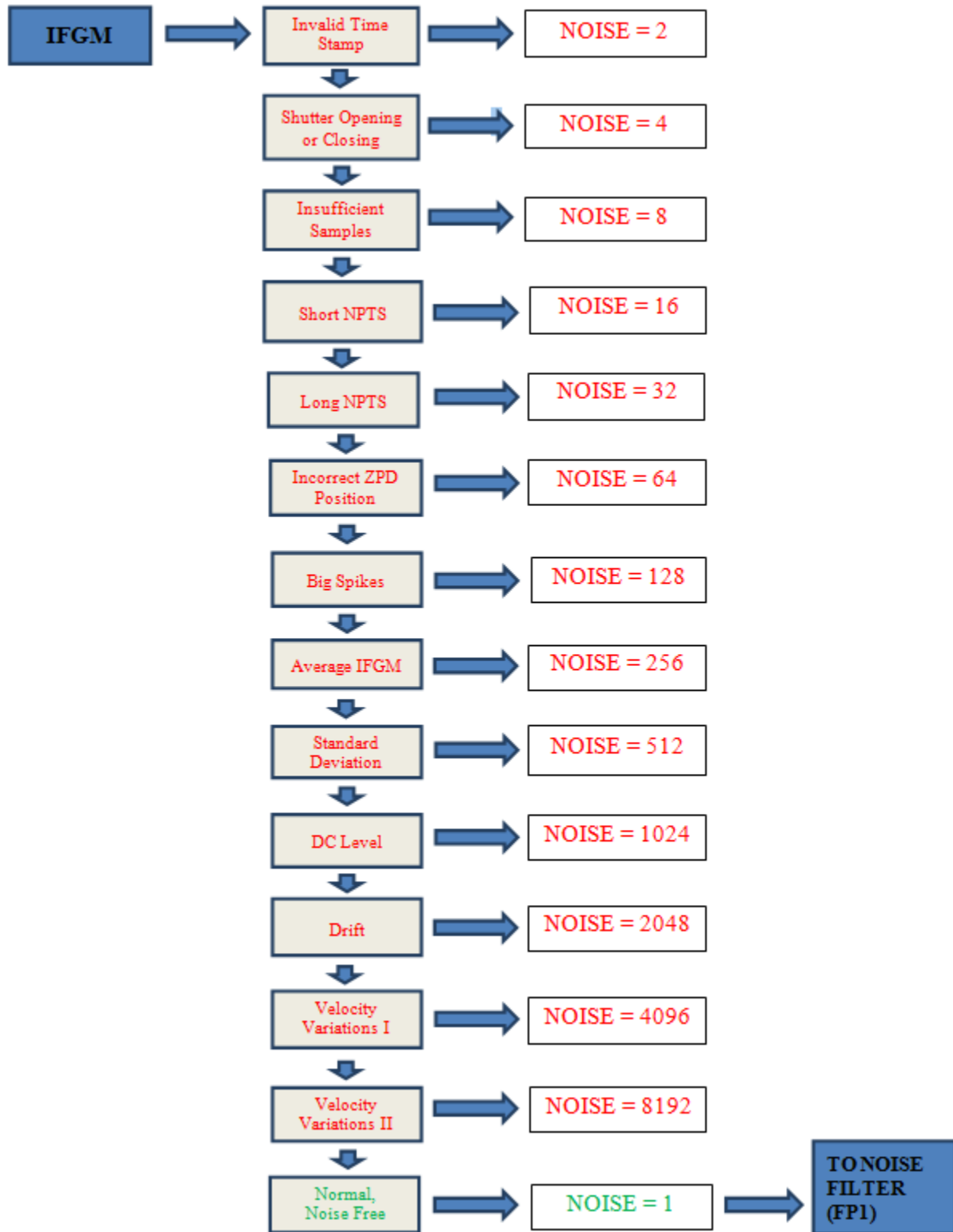


Figure 18: block diagram showing checks performed on raw interferogram data

### 3.3.1 Overview

The first stage in the conversion of an FP1, FP3, or FP4 raw interferogram (IFGM) to a filtered interferogram (FIFM) suitable for calibration is to send the IFGM through the CIRS noise detector algorithm. This algorithm tests each IFGM for disturbances from external noise effects, such as transient spikes, ZPD shifts, laser mode drifts, and scan mirror velocity variations. The logic of the algorithm is illustrated in Figure 18 (above).

Once an FP1 IFGM passes successfully through the noise detector with a value of NOISE = 1 (NORMAL IFGM), it is sent to the CIRS FP1 spike suppression algorithm. If the IFGM is successfully de-spiked by the spike suppression algorithm it is written to Vanilla tables as an FIFM. FP3 and FP4 IFGMs are presently converted directly to FIFMs by simply converting their amplitudes from integer to floating point format, and they are then written to Vanilla tables. A summary of the issues involved in suppression of FP1 spikes follows; a fuller description of the present spike suppression algorithm is given in Appendix C.

### 3.3.2 Suppression of FP1 Spikes: Introduction

Interferograms from the CIRS FP1 and FP3 detectors are contaminated by two series of prominent 0.5 Hz and 8.0 Hz noise spikes that are caused by electrical interference due to real-time interrupt (RTI) signals from the Cassini spacecraft bus interface unit (BIU). The spikes are spaced in time during every interferogram by the RTI period of 1/8 second, and their intensities are enhanced every 2 seconds by a data transfer event. The phase of the spike pattern in each interferogram, i.e., the position of the spikes relative to the zero path difference (ZPD), depends upon the starting time of the scan, which can be controlled to some extent through selection of the interferogram length. The 0.5 Hz spike pattern in the interferogram results in a series of spikes in the spectrum spaced by  $12 \text{ cm}^{-1}$ , corresponding to the harmonics of 0.5 Hz. The 8.0 Hz spike at  $191.38 \text{ cm}^{-1}$  also appears in FP1 spectra as strong harmonics at 16.0 Hz ( $382.76 \text{ cm}^{-1}$ ) and 24.0 Hz ( $574.14 \text{ cm}^{-1}$ ). Both the 0.5 Hz and 8.0 Hz spikes coincide with certain spectral features and can make atmospheric retrievals difficult. In addition, FP1 far-infrared interferograms are contaminated by a prominent single frequency (“sine wave”) feature of unknown origin that has been observed between  $18 \text{ cm}^{-1}$  and  $400 \text{ cm}^{-1}$ . FP3 interferograms and spectra also exhibit a harmonic series of 8.3 Hz spikes (see Section 2.5 Electrical interferences (spikes) and other data issues” for further details).

The CIRS FP1 multi-parameter spike suppression algorithm utilizes high fidelity empirical 0.5 Hz and 8.0 Hz spike waveforms (“combs”) created from real deep-space data using large averages of FP1 interferograms. The algorithm matches the positions and intensities of the spike combs to the observed spikes in each individual interferogram and performs checks to optimize and characterize the quality of the fitting process. Before de-spiking, each interferogram is over-sampled by a factor of 8.

The CIRS noise suppression algorithm has proven extremely successful in reducing 0.5 Hz and 8.0 Hz electrical noise spikes, as well as ripples  $< 50 \text{ cm}^{-1}$  and  $> 300 \text{ cm}^{-1}$ , in a variety of Focal Plane 1 spectra calculated from interferograms recorded at 96, 97, 224, 225, 400 and 401 RTI scan lengths.

Since October 2004 (Titan observations) and March 2005 (Saturn and all other observations), CIRS has been employing an additional technique for suppressing 0.5 Hz spikes. The 0.5 Hz spike pattern is effectively suppressed in averages of  $\geq 16$  scans by recording interferograms with  $16N+1$  RTI, e. g. 97, 225, and 401 RTI. The 0.5 Hz suppression is affected by the 0.5 Hz spike pattern being averaged into the 8.0 Hz pattern in the course of the averaging. Unfortunately this technique is not applicable to the 96, 224, and 400 RTI interferograms that were acquired before the above dates. In addition, the 8.0 Hz spikes remain in the spectra.

It was necessary to modify the FP1 0.5 Hz and {8.0, 16.0, 24.0} Hz spike suppression algorithm after CIRS flight software (FSW) Version 6.0.0 was uploaded and implemented on July 28, 2010 (see Section “2.5.2 Mitigation”). FSW 6.0.0 significantly reduces 8, 16, and 24 Hz electrical interference noise spikes in both individual and average FP1 interferograms. 0.5 Hz noise spikes are still present at their pre-FSW 6.0.0 shapes and amplitudes in individual interferograms, but their positions relative to the start of each scan are changed.

In light of the changes to the spike patterns resulting from FSW 6.0.0, the FP1 spike suppression algorithm was modified to bypass {8.0, 16.0, 24.0} Hz spike suppression for each NOADD interferogram recorded post-FSW 6.0.0. As with earlier FSW versions, the algorithm subtracts out the interferogram’s D. C. baseline and deep-space shape function prior to suppressing the 0.5 Hz spikes. Due to the difficulty of discerning 0.5 Hz spike patterns in individual and average post-FSW 6.0.0 FP1 COADD interferograms, both 0.5 Hz and {8.0, 16.0, 24.0} Hz spike suppression are bypassed for COADDs. The spike suppression algorithm only subtracts out each COADD interferogram’s D. C. baseline and deep-space shape function.

### **3.4 Calibration of the data**

This section describes the wavelength and radiometric calibration of the data.

#### **3.4.1 Wavelength calibration**

Wavelength calibration is achieved by use of a reference diode laser (783 nm) interferometer that uses the same scan mechanism as the IR interferometer. The scan mirror moves at a constant speed of 0.0208 cm/s. While the mirror is moving, data are logged at every zero-crossing of the laser intensity, i.e. every 391.5 nm of light path difference, or every 195.75 nm of mirror travel.

#### *Number of samples returned*

FP3 and FP4 in the mid-infrared each sample from five detectors out of a possible ten, depending on the selected observation mode (see Section “2.1.3 Instrument operation modes”). Each detector is sampled in turn, so that the number of points per mid-IR spectrum is 5x less than in the far-IR (FP1) spectrum. Finally, all the channels are further decimated by resampling factors of 18, 4.5 and 5 respectively for FP1, FP3 and FP4, so as not to exceed the necessary Nyquist sampling rate for the spectrum.

The final number of points in the spectrum is therefore:

$$n_p = \frac{\text{light path change}}{\text{logging interval}} \times \frac{1}{\text{resample factor}} \quad (1)$$

$$n_p = \frac{(2 \times 0.0208 \times t)}{(783/2 \times 10^{-7})} \times \frac{1}{(n_d \times n_{\text{resamp}})} \quad (2)$$

where  $n_d$  is the number of detector elements switched between, and  $n_{\text{resamp}}$  is the resampling factor given above. For example, a 10 s scan with FP4 would have  $n_p=425$ . In fact, the above formulae only provide an approximate guide to the number of samples that are returned from a scan of given length. This is due primarily to mirror fly-back time (at start of scan) which shortens the effective scan duration, and moreover requires an amount of time that is variable depending on the length of the *preceding* scan – i.e. where the mirror was left prior to the current scan. In addition, loss of scan mechanism phase lock due to spacecraft vibrations (mainly from the reaction wheels) and inherent velocity variations in the scan mechanism can lead to variations of ~1% in the amount of samples returned.

### Sample point spacing

The spacing of output points on the power spectrum is the reciprocal of the maximum path difference of the beam,  $X$ :

$$\delta\nu = \frac{1}{2X}; \quad X = 2 \times 0.0208 \times (t - t_0) \quad (3)$$

where  $t_0$  is the time after scan start when the mirror reaches the zero path difference (ZPD) point, equality in the light path in both interferometer arms. This is triggered by the white light fringe of a reference source. Alternatively, substituting for  $t$  in Eq. (2) we arrive at:

$$\delta\nu = \frac{1}{2 \times c_{FP} \times n_L} \quad (4)$$

where  $n_L$  is the actual (returned) number of samples in the long side of the interferogram (after ZPD), and we define the constant  $c_{FP}$  for each focal plane as follows:

$$c_{FP} \equiv n_d \times n_{\text{resamp}} \times \frac{783}{2} \times 10^{-7} \quad (5)$$

For example,  $c_{FP4}=9.7875 \times 10^{-4} \text{ cm}^{-1}$ , so if there were 350 actual samples after ZPD in a 10 s scan on FP4, the point spacing in the final power spectrum would be  $1.46 \text{ cm}^{-1}$ . Note that this Nyquist point spacing is about half the spectral resolution, depending on definition. So in this example the spectral resolution is about  $2.92 \text{ cm}^{-1}$ .

In practice, Fourier transforms are often made using an array size that is some power of 2: i.e. 512, 1024 etc. Therefore, the *zero-padding* that occurs to the interferogram in the array results in an oversampling on the resultant power spectrum. In this case, the 350-point array would be padded to 512 and the resulting point spacing would be  $0.998 \text{ cm}^{-1}$ , less than half the resolution. This topic is discussed in greater detail later (Section “3.5.1”).

### Laser modes

A further complexity is added to the wavelength calibration due to the fact that the diode laser may ‘mode-hop’ to different frequencies. This occurs infrequently, and modes generally persist for months or years. However even within the modes there is some smaller drift over time that may be due to thermal effects. Modes are generally determined by monitoring the fringe voltages returned in the housekeeping data packets. Therefore, care must be taken to match laser modes/fringe voltages of target scans, and blackbody reference scans, during calibration. See Figure 19 for an overview of the modes.

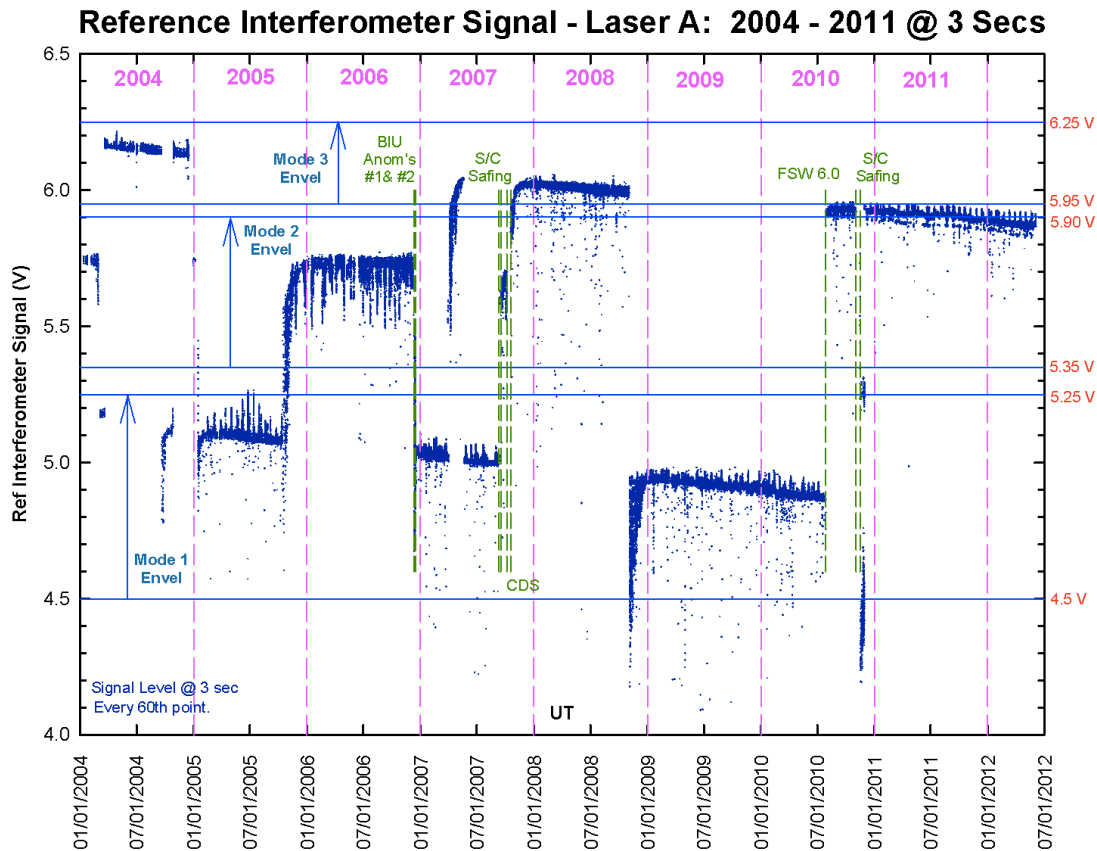


Figure 19: CIRS laser modes

Further discussion of laser modes is beyond the scope of the User Guide.

### 3.4.2 Radiometric calibration

Radiometric calibration in the far-IR (FP1) is simplified due to the fact that there is only one temperature inside the instrument. Therefore, use of a deep space (2.7 K) reference target is sufficient to calibrate radiance. The fact that the mid-IR has two temperatures to contend with means that a second reference target is required. Therefore, in the mid-IR optical path, a shutter may be lowered for calibration purposes, which gives a 170 K reference body. Due to phase differences that may arise in the beamsplitter, differencing of

target-space and target-shutter is conducted in the interferogram domain, prior to Fourier transforming.

A somewhat idealized description of the radiometric calibration is included hereafter. In the real pipeline, additional complexities must be accounted for, including apodization to reduce ringing (Gibbs Phenomenon) in the final result.

### 3.4.2.1 Idealized Interferometer Model

Consider the following simplified radiometric model for CIRS, from (Brasunas, 2002).

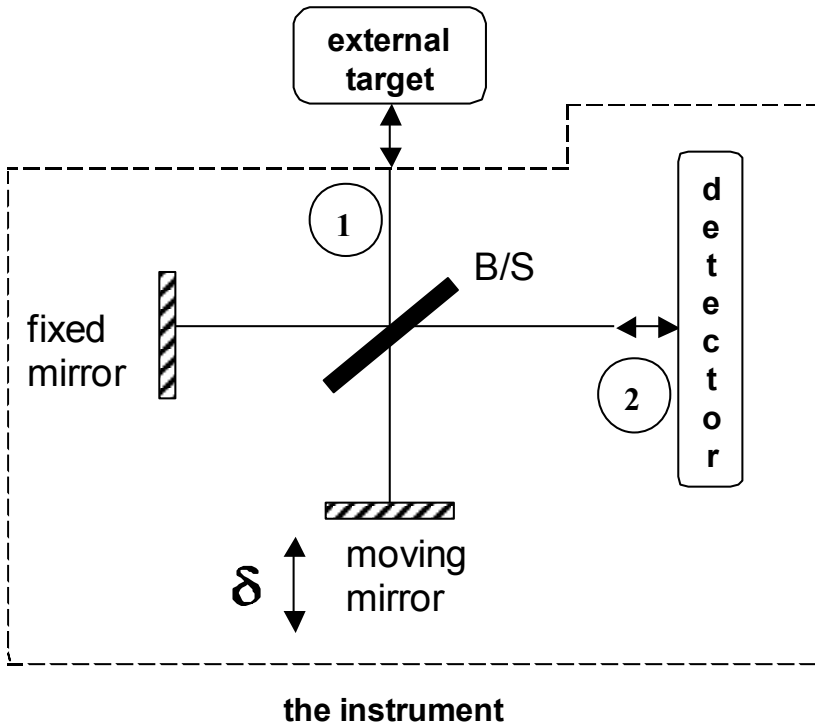


Figure 20: simple model of interferometer

Instrument self-emission includes emission from the detector, and from the beam splitter (B/S) if it is absorbing. As the optical path difference  $\delta$  ( $\delta$  is the two-way difference, expressed as a phase) changes, the received signal (interferogram) at the detector changes.

Let the complex reflection amplitude  $\vec{r}$  of the B/S be  $r \exp(i\delta r)$ , and the transmission amplitude  $\vec{t}$  be  $t \exp(i\delta t)$  (assume either TM or TE polarization). Let  $a_{11}$  be the propagation amplitude from port 1 back to port 1, thus:

$$a_{11} = ( r^2 \exp(i2\delta r) + t^2 \exp(i2\delta t) \exp(i\delta) ) \exp(i\delta_0) \quad (6)$$

where  $\delta_0$  is round-trip travel common to each of the two arms. Thus the fraction of the input power returned to port 1,  $P_{11}$ , is:

$$P_{11} = |a_{11}|^2 = R^2 + T^2 + 2RT \cos(\delta + 2(\delta t - \delta r)) \quad (7)$$

where  $R = r^2$  and  $T = t^2$  ( $r, R, t$  and  $T$  are all real). Similarly, the propagation amplitude  $a_{12}$  from port 1 to port 2 is

$$a_{12} = a_{21} = rt \exp(i(\delta r + \delta t))(1 + \exp(i\delta)) \exp(i\delta_0) \quad (8)$$

and the fraction of the power transferred from port 1 to port 2 is

$$P_{12} = P_{21} = 2RT (\cos(\delta) + 1) \quad (9)$$

Lastly  $a_{22}$  and  $P_{22}$  are

$$a_{22} = (r^2 \exp(i2\delta r) \exp(i\delta) + t^2 \exp(i2\delta t)) \exp(i\delta_0) \quad (10)$$

$$P_{22} = |a_{22}|^2 = R^2 + T^2 + 2RT \cos(\delta - 2(\delta t - \delta r)) \quad (11)$$

Eqs. (6) through (11) are not restricted to a loss-less dielectric, but they do assume a specific polarization state. For a loss-less dielectric  $(\delta t - \delta r)$  is  $\pi/2$ , thus the two modulated output signals due to the target are complementary, as can be seen from  $P_{11}$  and  $P_{12}$ . Define  $\Delta$  to be  $2(\delta t - \delta r)$ , which is  $\pi$  for a dielectric.

Now let the B/S be absorbing. Consider radiant flux emitted into the FTS from port 2: the total fraction transmitted or returned is  $P_{21} + P_{22}$ . Therefore the absorption of the B/S on side 2,  $A_2$ , satisfies the equation

$$A_2 = (1 - P_{21} - P_{22}). \quad (12)$$

Similarly the side 1 absorption of the B/S is

$$A_1 = (1 - P_{12} - P_{11}). \quad (13)$$

By Kirchoff's law, the emissivity equals the absorption coefficient. Now consider the flux balance at port 2: flux is lost (the flux from port 2 that is not returned) and flux is gained

both from port 1 and from the B/S emission. Let the unity emissivity fluxes from target, detector and B/S be  $F_{tar}$ ,  $F_{det}$  and  $F_{B/S}$ , all assumed to be in thermal equilibrium and therefore functions of their respective temperatures (through the Planck function). The flux net gain or loss  $dF$  at port 2 is:

$$dF = F_{tar}P_{12} + F_{B/S}(1 - P_{21} - P_{22}) - F_{det}(1 - P_{22}). \quad (14)$$

Using Eqs. (9) and (11) in Eq. (14), and considering only the modulated part  $dF_{mod}$  of the net flux ( $dF$  is a narrow spectral slice of the modulated part of the interferogram), we have

$$dF_{mod} = 2RT(F_{tar} \cos \delta - F_{B/S}(\cos \delta + \cos(\delta - \Delta)) + F_{det} \cos(\delta - \Delta)), \quad (15)$$

$$dF_{mod} = 2RT((F_{tar} - F_{B/S}) \cos \delta + (F_{det} - F_{B/S}) \cos(\delta - \Delta)) \quad (16)$$

Thus the self-emission anomalous phase (when  $\Delta$  is not  $\pi$ ) becomes associated both with the B/S emission and with the detector emission. This model correctly shows zero net flux when the target, B/S and detector are all at the same temperature.

### 3.4.2.2 Calibration Equations

$I_{Targ}$  interferogram recorded when viewing a target of interest at temperature =  $T_{Targ}$

$I_{Cold}$  interferogram recorded when viewing a cold blackbody calibration target at temperature =  $T_{Cold}$

$I_{Warm}$  interferogram recorded when viewing a warm blackbody calibration target at temperature =  $T_{Warm}$

$\nu$  frequency in wavenumbers ( $cm^{-1}$ )

$c_{Targ}(\nu)$   $FFT(I_{Targ})$  = uncalibrated complex spectrum of the target of interest at temperature =  $T_{Targ}$

$c_{Cold}(\nu)$   $FFT(I_{Cold})$  = uncalibrated complex spectrum of the cold blackbody calibration target at temperature =  $T_{Cold}$

$c_{Warm}(\nu)$   $FFT(I_{Warm})$  = uncalibrated complex spectrum of the warm blackbody calibration target at temperature =  $T_{Warm}$

$\theta$  instrument phase = the small angle of rotation of the instrument emission spectrum from  $180^\circ$

$r(\nu)$  complex instrument spectral response



$R(\nu)$  scalar instrument spectral response

$I_{\text{Instr}}$  interferogram due to instrument emission = the instrument (self-emission) contribution to  $I_{\text{Targ}}$

$B_{\text{Instr}}(\nu)$  spectral radiance of the instrument (self-emission) in  $\text{W cm}^{-2} \text{ster}^{-1}/\text{cm}^{-1}$

$B_{\text{Targ}}(\nu)$  spectral radiance of the target of interest in  $\text{W cm}^{-2} \text{ster}^{-1}/\text{cm}^{-1}$  at temperature =  $T_{\text{Targ}}$

$B_{\text{Cold}}(\nu)$  spectral radiance of the cold blackbody calibration target in  $\text{W cm}^{-2} \text{ster}^{-1}/\text{cm}^{-1}$  = the Planck function at temperature =  $T_{\text{Cold}}$

$B_{\text{Warm}}(\nu)$  spectral radiance of the warm blackbody calibration target in  $\text{W cm}^{-2} \text{ster}^{-1}/\text{cm}^{-1}$  = the Planck function at temperature =  $T_{\text{Warm}}$

$T_{\text{Instr}}$  the temperature of the CIRS instrument  $\sim 170.0\text{K}$

The “target” can either be a nominally unknown science target, the “cold” target (deep space at 3K), or the “warm” on-board target at the optics temperature, nominally 170K. Following (Carlson, 2005) defining  $c(\nu)$  to be the uncalibrated spectrum (FFT of the interferogram  $I$ ,  $c = \text{FFT}(I)$ ), and proceeding from Eq. 16 above,

$$c_{\text{targ}} = r(\nu) \left( (B_{\text{targ}} - B_{\text{B/S}}) + (B_{\text{det}} - B_{\text{B/S}}) \exp(-i\Delta) \right). \quad (17)$$

$\Delta$  is the constant  $\pi$  in the case of a dielectric; in the case of a thin metal film B/S (Brasunas, 2002)  $\Delta$  has a term linear in wavenumber, indicating a relative shift of the interferogram corresponding to the  $2^{\text{nd}}$  term in (17), compared with the first term.

We then derive calibration equations identical to those of (Carlson, 2005):

$$r(\nu) = \text{FFT} ( I_{\text{warm}} - I_{\text{cold}} ) / ( B_{\text{warm}} - B_{\text{cold}} ), \text{ and} \quad (18)$$

$$B_{\text{targ}} = \text{FFT} ( I_{\text{targ}} - I_{\text{cold}} ) / r(\nu), \quad (19)$$

ignoring  $B_{\text{cold}}$  (B at 2.7K). These are the calibration equations for FP 3 and 4.

For FP1, the isothermal instrument means  $F_{\text{B/S}} = F_{\text{det}}$ , and (16) becomes:

$$dF_{\text{mod}} = 2RT(F_{\text{tar}} - F_{\text{det}}) \cos \delta. \quad (20)$$

For an external blackbody target at the optics temperature  $T_{\text{inst}}$  (nominally 170K for FP1),  $I_{\text{targ}}$  is identically zero. Thus the FP1 version of Eq. 18 is:

$$r(u) = \text{FFT}(-I_{\text{cold}}) / (B_{\text{Instr}} - B_{\text{cold}}) = -\text{FFT}(I_{\text{cold}}) / B_{\text{Instr}} \quad (21)$$

the same as (Carlson, 2005). The equation for  $B_{\text{targ}}$  is the same as (19).

### 3.5 Post-processing: resampling and apodization

After the calibrated power spectrum has been computed, with radiometric and wavelength calibration, two further processes are applied that affect (i) the spectral resolution and (ii) the sampling grid. In fact, these are applied during the Fourier Transform process that creates the power spectrum, to avoid unnecessary repetition of forward and reverse transforms, but for simplicity we will present these as independent additional processes.

#### 3.5.1 Apodization

Apodization (literally ‘removal of feet’) is a process that smooths the power spectrum, dampening down ripples/ringing that are due to the bandwidth limitations of the finite Fourier Transform, at the expense of broadening spectral lines. A detailed discussion of this topic is beyond the scope of this User Guide (see for example Section 13.4.1 of (Press, 2007)), but a short description is necessary, as the user needs to understand how to model the data.

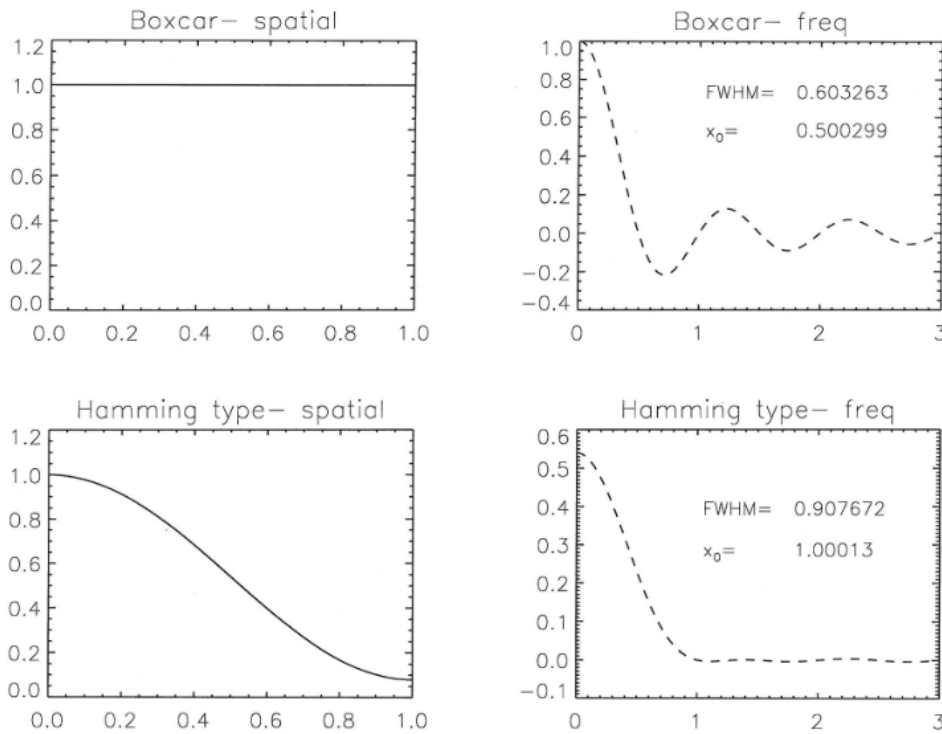


**Figure 21: apodization functions in the spatial and spectral domains**

Figure 21 shows the two apodization functions used by CIRS. In the spatial domain an apodization functions  $f$  is applied to the interferogram by pointwise multiplication. In the spectral domain, this convolves the spectrum with a smoothing function  $F$  (columns 2&4). So:

$$S * F = FFT\{I \times f\} \quad (22)$$

where  $f$  and  $F$  are a Fourier pair. The boxcar function corresponds to the ‘no apodization’ case, and results in a sharply-peaked spectral line (the Instrumental Line Shape, or ILS, is a sinc function,  $(\sin x)/x$  with significant side-lobes, or ‘ripples’. However application of the Hamming apodization function reduces the side-lobes very substantially, at the cost of widening the main lineshape. Quantitatively the FWHM of the Hamming-apodized ILS is  $(0.907/0.603)$  or 50% greater than for the sinc function, while the distance to first ‘null’ ( $x$ -axis crossing of the ILS) has doubled. This latter quantity is sometimes loosely referred to as the Rayleigh definition for spectral resolution, although Rayleigh’s definition technically referred to diffraction-limited imaging (when the maximum of the image of one point source falls on the first minimum of the second point source).

In the spatial domain Hamming apodization is applied by the formula:

$$f(x) = 0.54 - 0.46 \cos\left(\frac{\pi x}{a}\right) \quad (23)$$

where  $a$  is the maximum path difference. CIRS spectra are computed for unapodized (boxcar) and apodized (Hamming) interferograms; however only the apodized spectra are provided on the PDS volumes (in DATA/APODSPEC) as apodized spectra are almost exclusively used for science. The user must convolve any spectral models accordingly (see the ‘Nyquist’, ‘FWHM’ and ‘Rayleigh’ fields for information on spectral resolution). The convolution function, which is the Fast Fourier Transform of the Hamming function, is given by:

$$F(\nu) = \frac{a(1.08 - 0.64a^2\nu^2)\text{sinc}(2\pi a\nu)}{1 - 4a^2\nu^2} \quad (24)$$

The respective Rayleigh resolutions are:  $\Delta\nu=1/2a$  (Boxcar) (25)

And  $\Delta\nu=1/a$  (Hamming) (26)

Figure 22 shows an example of the effect of apodization on a typical Titan spectrum.

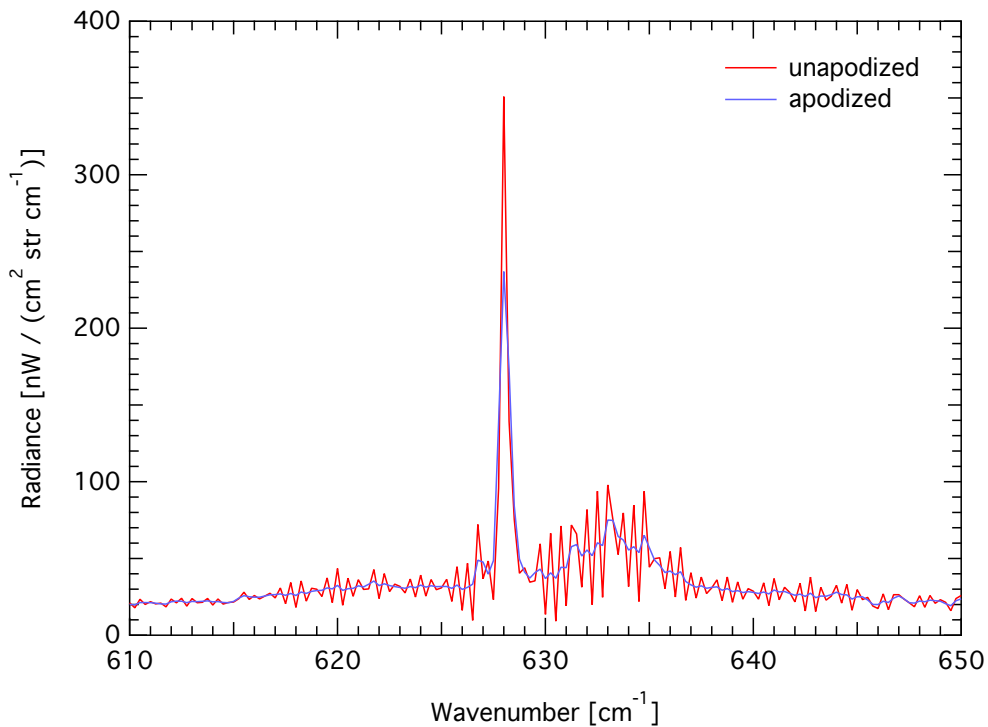


Figure 22: example of Titan T23 FIRNADCMP north polar spectrum (average of 800 FP3 spectra), showing the effect of apodization (blue) versus the unapodized spectrum (red).

### 3.5.2 Resampling

Whereas the spectral bandpass of each focal plane is set by the interferogram data sampling rate (after resampling), the spectrum point spacing is the reciprocal of twice the length of the scan ( $1/2L'$ ), where  $L'$  is measured after ZPD. This typically results in a non-integer native point spacing (the 'Nquist' value in the database). For ease of modeling therefore, the data are resampled to integer values (or simple fraction thereof) grid. To avoid losing information, the resampling grid must be at least as dense as the resolution (e.g.  $1/L'$  in the unapodized case).

As previously mentioned, Fast Fourier Transforms typically use arrays sizes that are  $2^n$  in size, therefore simply zero-padding the interferogram to the next larger  $2^n$  array size rarely gives the desired point spacing either. Therefore, a two-step process is used.

- 1) the interferogram is zero-padded by a large amount (typically a factor  $\sim 8$ ), to create a resulting over-sampled spectrum on an (8x) finer grid than previously, then:

- 2) the over-sampled spectrum is interpolated onto the exact wavenumber grid desired. Linear interpolation is used, to avoid introducing unwanted artifacts that could be caused by use of higher-order functions.

Table 16 lists the native and resampled point spacings in the CIRS dataset.

**Table 16: native and resampled spectrum point spacings**

RTI (scan length in 1/8 s units)	Native point spacing ('Nquist') (cm <sup>-1</sup> )	Resampled Point Spacing (cm <sup>-1</sup> )
38 & 39	7.96	5.00
40	6.53	5.00
56	3.25	2.50
96 & 97	1.39	1.00
224 & 225	0.497	0.250
400 & 401	0.263	0.250

### 3.6 Estimation of Noise Equivalent Spectral Radiance (NESR)

The sensitivity of the CIRS instrument is specified by the Noise Equivalent Spectral Radiance (NESR). The NESR is the target radiance level for which the instrumental signal to noise (S/N) ratio is unity. The NESR is defined as:

$$\text{NESR}(\nu) = \text{NEP}(\nu) / [\eta_{\text{Sys}} \eta_{\text{Opt}} \eta_{\text{Diff}} A \Omega \Delta\nu \text{SQRT}(t_{\text{Eff}})] \quad (27)$$

where

- NESR( $\nu$ ) is the Noise Equivalent Spectral Radiance in W cm<sup>-2</sup> sr<sup>-1</sup> / cm<sup>-1</sup>
- NEP( $\nu$ ) is the noise equivalent power of the detector in W Hz<sup>-0.5</sup>
- $\nu$  is the frequency in wavenumbers (cm<sup>-1</sup>)
- $\eta_{\text{Sys}}$  is the system efficiency
- $\eta_{\text{Opt}}$  is the optical efficiency
- $1 - \eta_{\text{Diff}}$  is the loss due to diffraction
- $A$  is the telescope area (cm<sup>2</sup>)
- $\Omega$  is the solid angle of the field of view (sr)
- $\Delta\nu$  is the spectral resolution (cm<sup>-1</sup>)
- $t_{\text{Eff}}$  is the effective integration time (sec)

The instrument has the capability for any unapodized spectral resolution from 0.25 to 10.0  $\text{cm}^{-1}$ , by commanding the scan time. The apodized spectral resolutions 0.53, 1.00, 2.85, 6.60, and 15.67  $\text{cm}^{-1}$  have been selected as representative base resolutions for carrying out the majority of the CIRS science observations. The measurement parameters for these CIRS observing modes and their associated integration times are given in Table 17.

**Table 17: spectral resolution, scan time (RTI), effective integration and frame times**

Unapodized Resolution $= 1/4L_2 (\text{cm}^{-1})^3$	Apodized Resolution $= 1/2L_2 (\text{cm}^{-1})$	Required RTI ( $1/8 \text{ sec}$ )	$t_{\text{Frame}}$ (sec)	$t_{\text{Eff}}$ (sec) <sup>1</sup>	$t_{\text{Dead}} = t_{\text{Frame}} - t_{\text{Eff}}$ (sec)
0.27	0.53	400	50.000	47.10	2.90
0.50	1.00	224	28.000	26.11	1.89
1.43	2.85	96	12.000	11.00	1.00
3.30	6.60	56	7.000	5.93	1.07
7.85 <sup>2</sup>	15.67 <sup>2</sup>	38	4.750	3.10	1.65

<sup>1</sup> $t_{\text{Eff}}$  = Effective integration time

<sup>2</sup>Symmetrical two-sided interferogram

<sup>3</sup> $L_2$  = scan length from ZPD to the end of scan (cm); resolution is here defined as distance from peak to first null of the instrument function (Rayleigh definition)

The calculation of the effective integration time ( $t_{\text{Eff}}$ ) is discussed in Appendix D. The frame time is the repeat cycle for the scan and is approximate.

### 3.6.1 NESR Conversions

#### Spectral Resolution

The NESR for a given spectral resolution ( $\text{NESR}_2$ ) may be calculated from the NESR for the reference resolution ( $\text{NESR}_1 = 0.53 \text{ cm}^{-1}$ ) by:

$$\text{NESR}_2 = (\Delta v_1 / \Delta v_2) * [\text{SQRT}(t_{\text{Eff}1} / t_{\text{Eff}2})] * \text{NESR}_1 \quad (28)$$

Using Table 17, the conversion factors are:

$$\text{NESR}(1.00 \text{ cm}^{-1}) = 0.7118 * \text{NESR}(0.53 \text{ cm}^{-1}) \quad (29a)$$

$$\text{NESR}(2.85 \text{ cm}^{-1}) = 0.3848 * \text{NESR}(0.53 \text{ cm}^{-1}) \quad (29b)$$

$$\text{NESR}(6.60 \text{ cm}^{-1}) = 0.2263 * \text{NESR}(0.53 \text{ cm}^{-1}) \quad (29c)$$

$$\text{NESR}(15.67 \text{ cm}^{-1}) = 0.1318 * \text{NESR}(0.53 \text{ cm}^{-1}) \quad (29d)$$

### Number of Pixels

For FP3 and FP4 scans, individual pixels may be summed together. The improved NESR would then be:

$$\text{NESR}(N \text{ pixels}) = [1/\text{SQRT}(N)] * \text{NESR}(1 \text{ pixel}) \quad (30)$$

For example, if the detectors are used in PAIR mode then the NESR is the single pixel NESR/ $\sqrt{2}$ .

### 3.6.2 NESR Spreadsheets and Plots

The CIRS NESRs were calculated from 100 scan averages of deep-space interferograms recorded during the Jupiter encounter on days 330 and 332, 2000. Each NESR is apodized and corresponds to a single scan. The measurement conditions were:

Target temperature = 2.7 K (deep space)

FP1: Far-IR polarizer temperature = 170.04 K

FP3 & FP4: average optics assembly temperature = 169.84 K; FPA temperature = 77.74 K

NESRs for apodized spectral resolutions 0.53, 1.00, 2.85, 6.60, and 15.67  $\text{cm}^{-1}$  are tabulated for focal planes 1, 3, and 4 in files provided in the CALIB directory of the CIRS PDS archive volumes (CIRS\_NESR\_FPn.ASC, where n=1,3,4). Plots of the FP1, FP3, and FP4 NESRs for each spectral resolution are shown in Figs. 21-23.

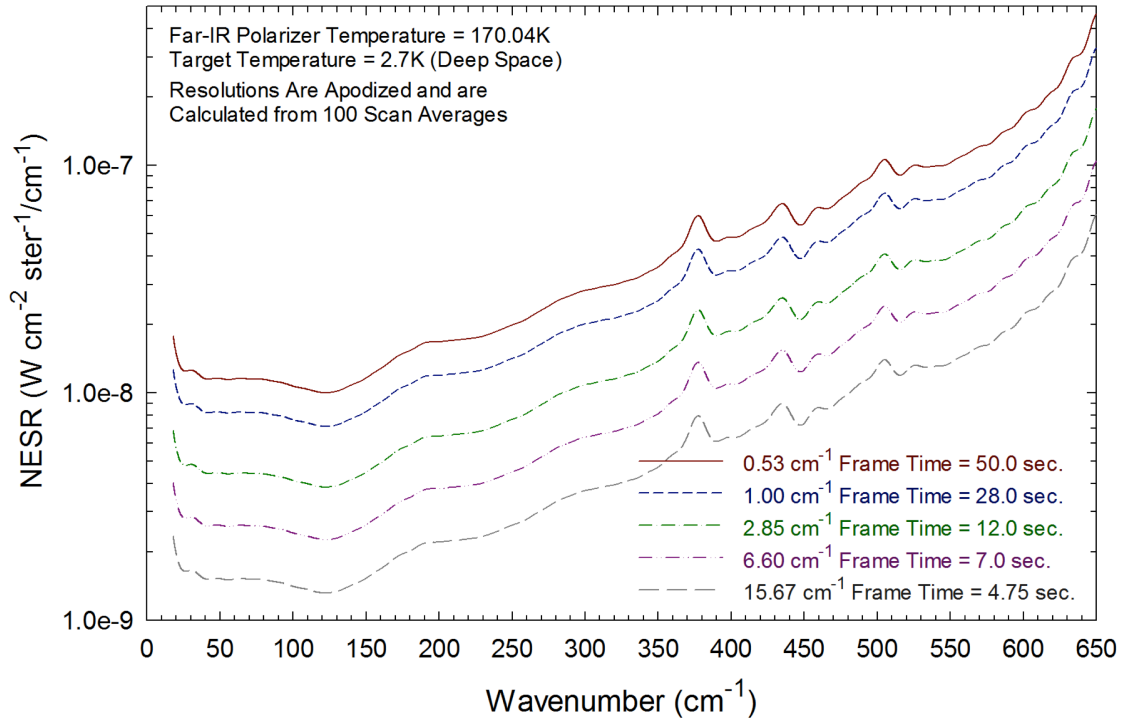


Figure 23: NESR for FP1 versus spectral resolution

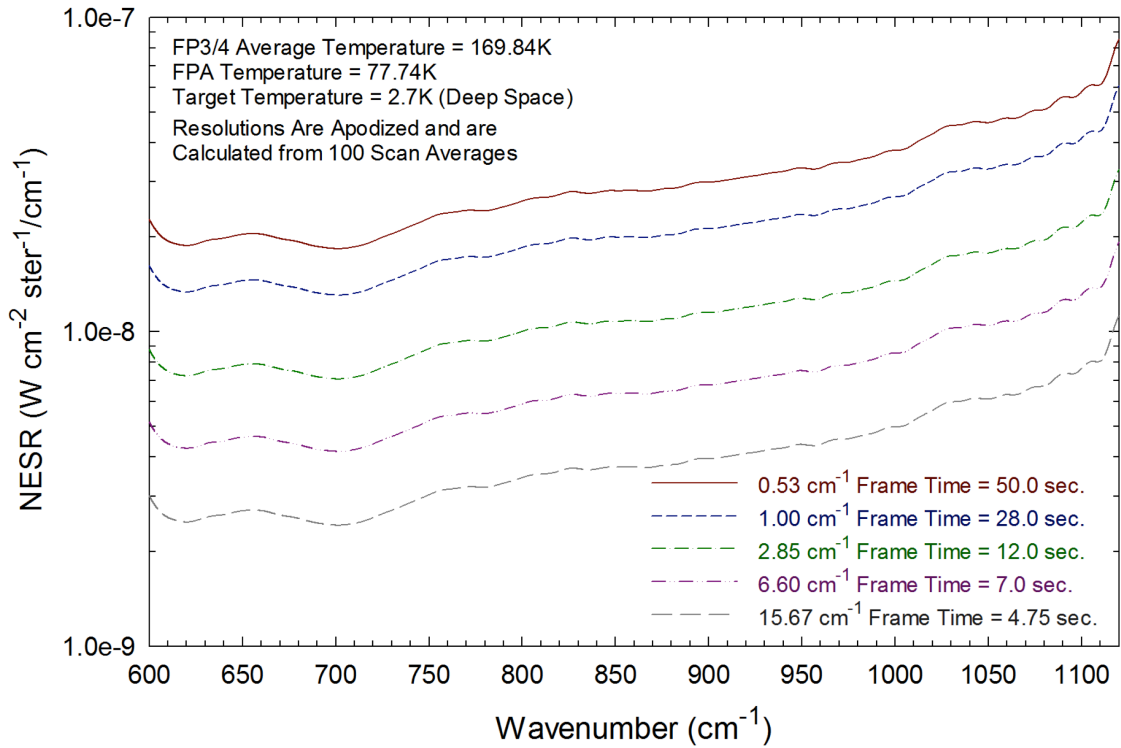


Figure 24: NESR for FP3 versus spectral resolution



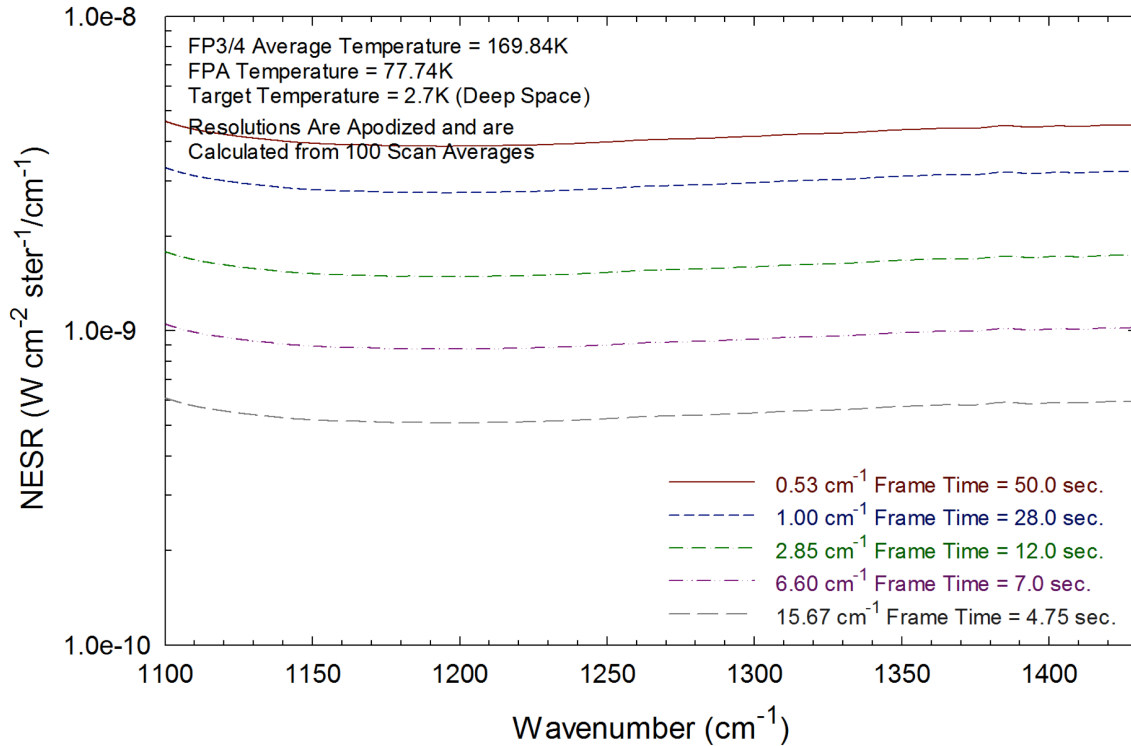


Figure 25: NESR for FP4 versus spectral resolution

### 3.7 Discussion: limitations of standard spectra products

Several final notes and caveats are given here about the limitations of the standard spectral data products, above and beyond previous discussions of noise, interferences etc.

#### 3.7.1 Bandpass and aliasing

CIRS is a Fourier Transform Spectrometer (FTS), so the bandpass of each focal plane is set by the sample spacing of the native interferogram. The highest wavenumber uniquely measured is  $\nu_{NY} = (0.5/\Delta L) \text{ cm}^{-1}$ , where  $\Delta L$  is the sample spacing in cm. For example FP1 acquires  $\sim 2800$  samples over  $\sim 1$  cm of mirror travel (2 cm of light path difference), so  $\Delta L = 0.000714$  cm and the Nyquist frequency (wavenumber) is  $\sim 700 \text{ cm}^{-1}$ . Light at higher wavenumbers  $\nu'$  is aliased into the FP1 band at frequency  $\nu$ , where:  $\nu = 2\nu_{NY} - \nu'$ . E.g.  $1000 \text{ cm}^{-1}$  is the alias of  $(2 \times 700 - 1000) = 400 \text{ cm}^{-1}$ . To avoid the uncertainty caused by aliasing, a filter must be applied to block the unwanted higher frequencies: CIRS achieves this in the receiver electronics by numerical filtering.

FP3 and FP4 are similar to FP1, except that they are designed to operate in the second ( $\nu_{NY} - 2\nu_{NY}$ ) and third ( $2\nu_{NY} - 3\nu_{NY}$ ) orders respectively, so must be filtered at both the high and low ends of the bandpass. In practice, no filter  $F(\nu)$  has an infinitely-sharp cut-off, rather there is a gradual roll-off. Figure 26 shows the high-frequency end of the FP4 range. This gradual cut-off requires us to have some criterion for defining the acceptable 'clean' spectral range. The CIRS definition is such that  $F(\nu')/F(\nu) < 1\%$  - i.e. the spectral range where the ratio

of the weighting of the aliased frequency ( $\nu'$ ) is less than 1% of the in-band frequency ( $\nu$ ) weighting.

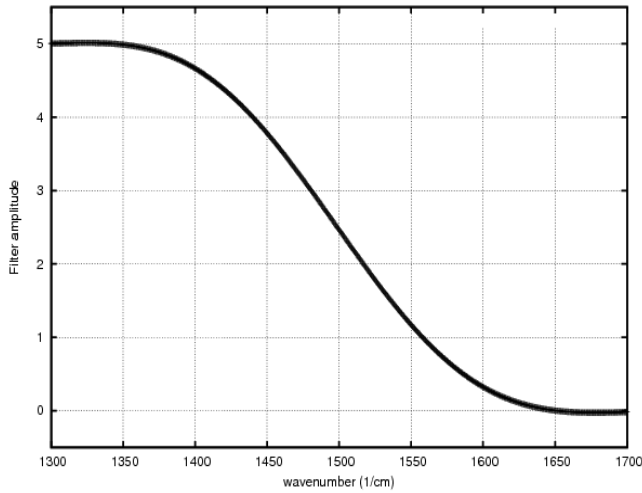


**Figure 26: frequency filter applied to short wavelength end of CIRS FP4.**

**Table 18: actual and clean bandpasses for each focal plane**

FP	Signal bandpass	Clean Bandpass
1	0-708	0-651
3	556-1133	604-1094
4	1020-1529	1131-1433

The nominal and clean bandpasses for each focal plane are given in Table 18. One point of particular concern is that, while the ‘clean’ ranges of FP1 and FP3 overlap, those of FP3 and FP4 do not: meaning that there is a spectral range from 1094-1131  $\text{cm}^{-1}$  where aliasing may become significant. However, any signal seen at, for example, 1110  $\text{cm}^{-1}$  on FP3 may be checked for reality by looking at the same frequency on FP4. More problematic is the range from 1433-1529  $\text{cm}^{-1}$  on FP4, as there is no second measurement with which to compare the spectrum. The only solution is to model the aliasing: to extend the range of the spectral calculation to the highest aliased frequency, and then to combine the nominal and aliased ranges with the appropriate scaling  $F(\nu)$ :

$$I'(\nu) = [F(\nu)I(\nu)] + [F(2\nu NY - \nu)I(2\nu NY - \nu)] \quad (31)$$

Figure 27 shows an example Titan spectrum, with the ‘clean’ bandpasses shown in blue and the compromised bandpass in red. The aliased bandpass of FP4 includes the  $\nu_8$  band of  $\text{C}_2\text{H}_6$  (1468  $\text{cm}^{-1}$ ) and the  $\nu_7$  (1464  $\text{cm}^{-1}$ ) and  $\nu_{24}$  (1472  $\text{cm}^{-1}$ ) emission bands of  $\text{C}_3\text{H}_8$ . It is an area of on-going work at this time to add a model of the aliasing behaviour into spectral synthesis models.

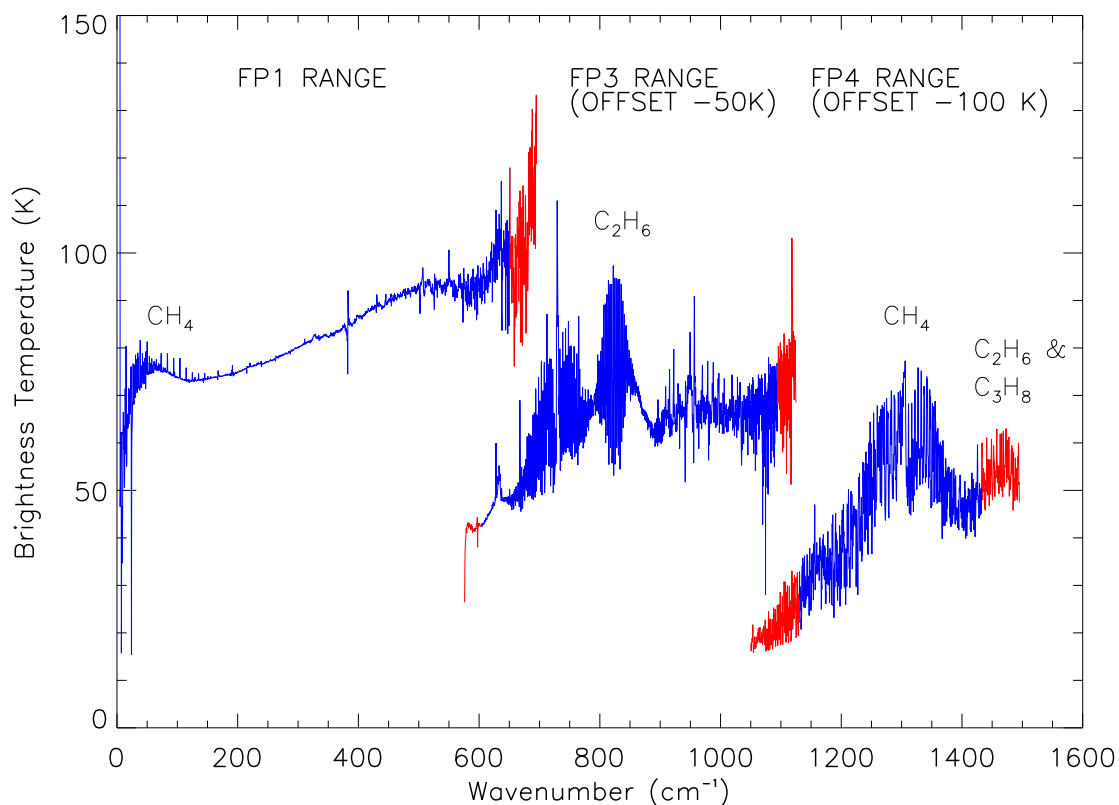


Figure 27: example CIRS high resolution ( $0.5 \text{ cm}^{-1}$ ) spectrum, with ‘clean’ bandpasses for each focal plane in blue and ‘aliased’ ranges in red.

### 3.7.2 FP1 Long Wavelength Calibration

At the time of writing, a problem has been identified at the long-wavelength end of the FP1 spectral range, approximately  $1000\text{--}200 \mu\text{m}$  ( $10\text{--}50 \text{ cm}^{-1}$ ), whereby the continuum radiances typically appear lower than physically realistic (‘FP1 droop’). See **Error! Reference source not found.**, from (Teanby, 2010), which shows the very far-IR continuum of Titan at three low southern latitudes near the Huygens landing site ( $12^\circ\text{S}$ ) in units of equivalent brightness temperature ( $B_T$ ). The horizontal line at  $70.3\text{K}$  corresponds to the coldest temperature measured by Huygens (at the tropopause). Therefore, all brightness temperatures should be at least  $70.3\text{K}$ . However, below  $30 \text{ cm}^{-1}$  many brightness temperatures are significantly ( $10\text{--}20\text{K}$ ) below this level, confirming problems with the continuum level in this wavelength region.

The cause of this calibration issue is currently not known: presumably an unidentified thermal effect in the instrument. Therefore, until this problem is finally resolved it is recommended that this spectral region is used in line-to-continuum ratio mode only. Please refer to ERRATA.TXT in the PDS volumes for most up to date status information.

### 3.7.3 Deep Space Calibration Blocks

During the observation design stage, every effort is made to ensure an adequate number of deep space data is recorded in order to fully and accurately calibrate the on-target interferograms. However, the number of available deep space interferograms can be reduced for a number of reasons including design constraints, lost data (see 2.4 Data Gaps), and noise (2.5 Electrical interferences (spikes) and other data issues). The use of small deep space blocks causes known systematic errors in the calibrated data such as:

- deep space blocks with one, or even two, orders of magnitude fewer interferograms than the target data they are applied to
- jumps of 2 - 4 K in brightness temperature within a given observational map when multiple deep space blocks are used to calibrate different sections of the map
- differences of up to 5 K in the zonal mean brightness temperature ( $1392 \text{ cm}^{-1}$ ) between consecutive maps, making map-to-map latitudinal studies difficult

These issues are being actively addressed and are expected to be resolved in future versions of the database.

## 4.0 How to search and extract data

### 4.1 Data Format Description

The CIRS PDS dataset is divided into volumes, each of which is a self-contained unit comprised of CIRS and ancillary data for one month of the Cassini mission. The volumes are composed of data, formally known as ‘Time Sequential Data Records’ (TSDR), related search software, and other documentation. A schematic diagram of the creation of the CIRS archive volumes is shown below (Figure 28).

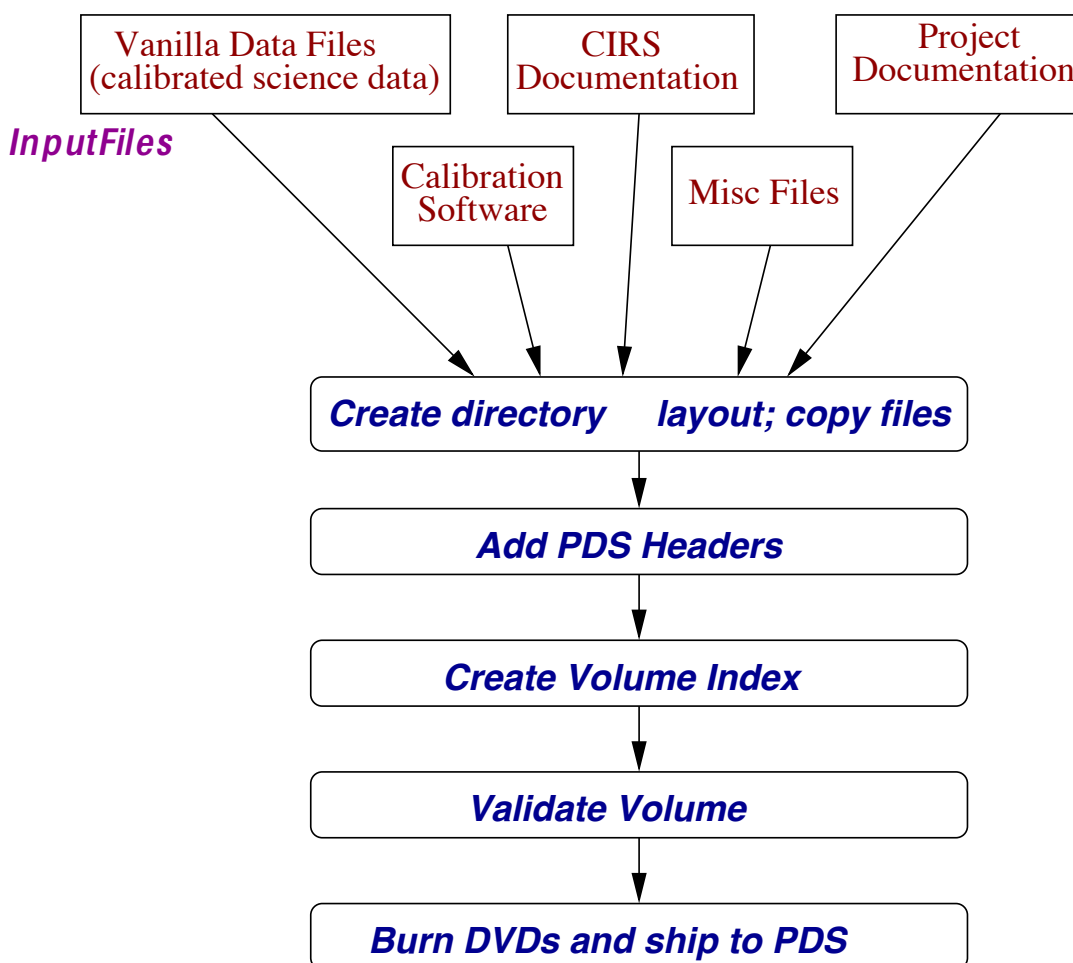


Figure 28: schematic of CIRS archive volume creation

The organization of the database is now described in more detail.

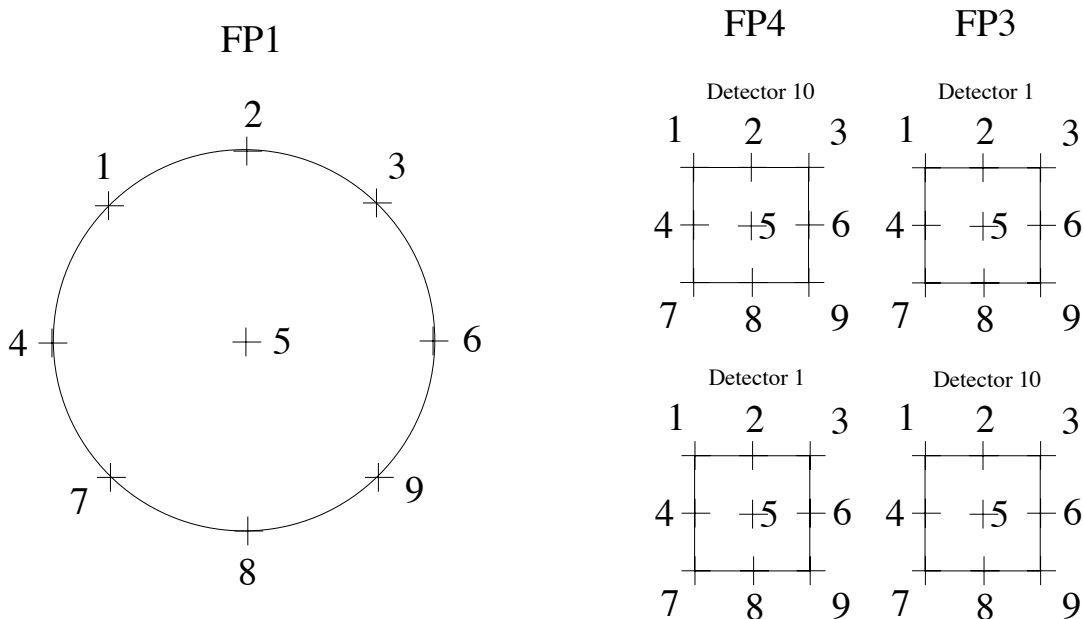
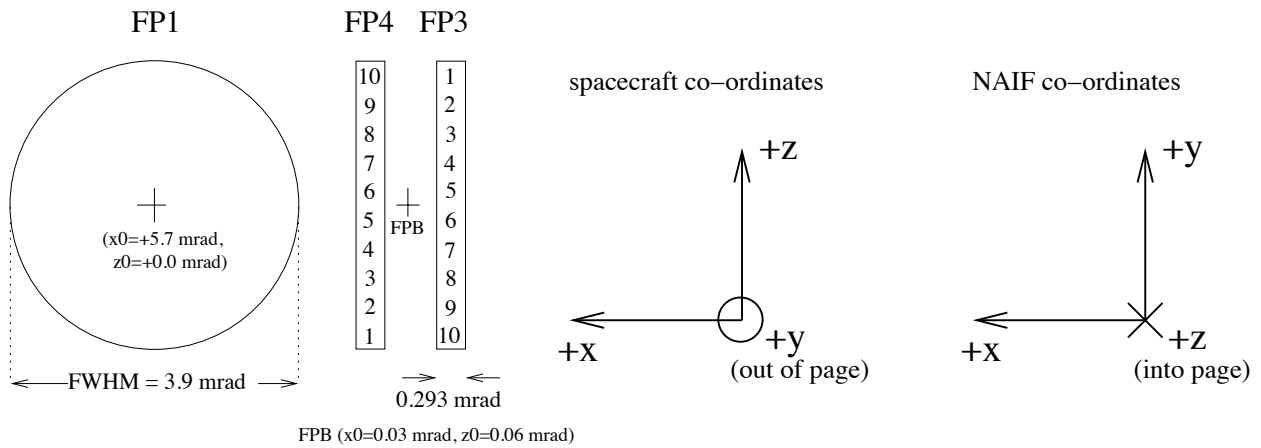


Figure 29: relative locations of CIRS detectors, showing numbering of pixels and q-points.

#### 4.1.1 Data Levels

The level-0 tables (base level) are contained in /DATA/UNCALIBR/. These are described in detail in the document file in /DOCUMENT/DATASIS.PDF. These tables types (IFGM, OBS, IHSK, FRV) are essentially the raw-level information which came from the instrument: the only process applied was unpacking (uncompressing) the instrument packets and, in the case of the housekeeping data, interpolating the 64-sec interval housekeeping data onto the science scan intervals. Original housekeeping data is stored in /DATA/HSK\_DATA/, which is read out at 64-sec intervals when the instrument is either ON or in SLEEP mode. Pointing and geometry information is stored in /DATA/NAV\_DATA/. These tables are described in detail in the DATASIS document, and also in the FMT format files in the NAV\_DATA/ area. Primarily, these store the spacecraft attitude and position with respect to major bodies (GEO file type), the position of the 11 detectors (99 q-points, or fiducial reference marks) on all

bodies in the FOV (POI file type, see Figure 29), the list of bodies seen in each detector (TAR type), and the observational information of rings (RIN file type).

Pointing and geometry information is derived from the spacecraft re-constructed attitude ('C') and trajectory ('SPK') kernels, using NAIF (Navigation and Ancillary Information Facility) toolkit routines supplied by JPL. Calibrated spectra, apodized with a Hamming function are stored in /DATA/APODSPEC/. Apodization is the process of mathematical filtering or smoothing, which removes 'ringing' effects from finite-width mathematical FFTs, widening the instrument line shape in the process.

#### 4.1.2 Vanilla Database

The data is in the form of binary tables, also known as the Vanilla database. Vanilla is a simple database access tool, also included on each volume as both source and executable. Note however that the Vanilla software is NOT REQUIRED in order to read the binary data, but it may simplify the task. Vanilla links together all binary files into a large, 'logical' table, which can be searched based on key fields. However, the user may read the binary data directly, using any programming language desired. If this approach is taken it is extremely important to pay attention to binary field widths: field widths vary, and, typically, trying to read an entire record into a data structure will fail if it assumes padding of fields. The user must read the data in field-by-field, specifying width. Field widths are described in the \*.FMT files, which are placed in each data directory. Some tables have both fixed-length and variable-length fields. In this case, the variable length part of the record is stored separately, in a file with the same name but an extension .VAR, instead of .DAT. The third type of file extension is .LBL, which is the PDS detached label.

**Important note:** by convention hereafter we will refer to tables by uppercase names (IFGM, TAR, RIN, etc) and fields within the tables by lowercase names (scet, det etc). This is to avoid the confusion that may arise when the same term is used for both a table type, and a field within that table (ifgm, fifm, ispm, etc.).

#### 4.2 Vanilla Search Tool: Overview

The Vanilla tables were designed to be a relational database, with different tables linked by keys (i.e., fields common among some or all of the various tables, Table 19). There are several important advantages to this approach. Being able to store the data in a binary format without having to repeat all fields for every possible combination of scet, detector, and Saturnian body produces enormous savings in storage space. By storing a given table in multiple file fragments, search times are minimized by specifying only the applicable fragment or fragments on the vanilla command line. Finally, because the source code is available, modifications were possible that allowed customization of the database for CIRS-specific needs and for PDS standards compliance.

Table 19: table keys at a glance

TABLE NAME	KEY 1	KEY 2	KEY 3
DIAG	scet	det	
FRV	scet		

GEO	scet	body_id	
HSK	scet	det	
IFGM	scet	det	
IHSK	scet		
ISPM	scet	det	
OBS	scet		
POI	scet	det	target_id
RIN	scet	det	
TAR	scet	det	

---

An Excel spreadsheet with all fields and brief descriptions is in VanillaFieldList.xls.

Vanilla is a command line program. This enables it to be easily used within other programs and scripts by "piping" its output to the next process. To use it you'll need access on your computer to a terminal (or command) window from which you can enter the commands, the vanilla executable file, and the vanilla executable command within your shell's command search path.

The vanilla executable file is available on PDS volumes in the SOFTWARE/BIN directory and has been precompiled for the Linux and Solaris operating systems. The source code is available in the SOFTWARE/SRC/VANILLA directory if you have an operating system different from the above and want to compile it by yourself. Only a single executable file is needed to run the vanilla database query program.

#### 4.2.1 Vanilla Help

Typing only the vanilla command name at the command prompt will give you a quick syntactical description of how to use the program. It will look similar to:

```
-----
Vanilla version 3.4.21
Usage: vanilla [options] dataset

dataset:                               (required)
  directory-name  containing the DATASET file  -OR-
  dataset-file-name          -OR-
  -files data-file1 [data-file2 data-file3 ...]

query options:
  -fields 'field1 field2 ...'          (required)
  -select 'field1 low high field2 low high ...'  (optional)

  -Bfm filename  binary output, cooked 4 byte words
  -Bdm filename  binary output, cooked 8 byte words

index generation options:
```



-index 'field1 field2 ...' (required)

index based count options:

-select 'field1 low high field2 low high ...' (required)  
-count

-OR-

-select 'field1 low high field2 low high ...' (required)  
-idxstats

Note:

Use one type of option at one time, i.e. don't use query with index etc.

-----

Of these many possibilities, by far the most commonly used are just the "dataset" specification and the "-fields" and "-select" query options which means your query line will look more like:

vanilla -fields "field1 field2 ..." -select "select1 select1min select1max ..." dataset\_path

where:

field1... are the fields you would like extracted from the database

selectX is a field which you would like to restrict to a range

selectXmin is the minimum value allowed for selectX

selectXmax is the maximum value allowed for selectX

dataset\_path is the path to the DATASET file

#### 4.2.2 Database Structure

Each CIRS PDS volume contains extensive documentation on its structure. For a detailed description of the CIRS database including its file structure in the volume, the table layout, and the data fields available within each table, see the DATASIS.PDF document

#### 4.2.3 Dataset Usage

The dataset\_path mentioned above in the vanilla command description can be specified several different ways, and, depending on which you choose, can dramatically shorten the time necessary to complete a query. The dataset\_path can either point to a directory with a dataset file in it or it can point to a dataset file outside of the PDS volume. A dataset file is

used to tell vanilla what tables should be included in the search and/or where to search for another dataset file.

For example, the dataset file in the PDS volume's data/apodspec/ directory is

```
ISPM
../NAV_DATA/
```

This tells vanilla to look in the current directory for the ISPM tables and to look in the NAV\_DATA directory for another dataset file. The dataset file in NAV\_DATA contains

```
../UNCALIBR/
TAR
RIN
POI
GEO
```

and the dataset in UNCALIBR is

```
OBS
IHSK
IFGM
FRV
DIAG
```

Therefore, by pointing to the dataset file in the apodspec/ directory, you will be searching across all available tables in the database. However, if you only wanted to query for fields contained in the OBS table, you could just point to the dataset file in the UNCALIBR directory, allowing vanilla to skip the overhead of including the navigation and spectra tables.

If your output fields are restricted to only a single table, there is one more way to greatly decrease the number of files to be searched. By using the "-files" option (see the full vanilla help output) rather than a dataset specification, you can specify exactly which files to search. For example, if you knew your data was completely self-contained within the OBS table for 4 January 2008, in the command line instead of dataset\_file you would specify

```
-files path/OBS08010400.LBL path/OBS08010404.LBL path/OBS08010408.LBL
path/OBS08010412.LBL path/OBS08010416.LBL path/OBS08010420.LBL
```

where path is the path to the label files of interest. While it is an extremely restrictive case, it will result in a very fast search. Another advantage of using this approach is that wildcards are allowed. So the above could have been shortened to

-files path/OBS080104??

At the other extreme, suppose you wanted to query the entire database consisting of multiple PDS volumes. Assuming you've copied all the volumes to your hard drive at /data, then the dataset file would look like

```
/data/cocirs_0401/data/apod_spec/  
/data/cocirs_0402/ data/apod_spec/  
/data/cocirs_0403/ data/apod_spec/  
. . .  
/data/cocirs_1705/ data/apod_spec/  
/data/cocirs_1706/ data/apod_spec/
```

Note, when specifying a directory within a dataset file, always place a "/" at the end of the path. If you don't, vanilla will output a cryptic "No tables in dataset." message.

#### 4.2.4 '-fields' parameter

The fields listed with the fields parameter specify the columns that will be output to the screen. Any field listed in the .FMT file for each table can be used. In addition, if that field is an array, you can specify a single element using square brackets or a ":" if a range of elements is used. For example, ispm[1:10] would extract the first 10 elements of the spectrum while spm[99] would extract only the 99th (vanilla array indices start at 1). Typically the entire array can be extracted with just its name, but in the case of a variable length array (like ispm), the entire array can only be output if "ispm[]" is used. It does not matter whether you use upper- or lower-case to specify the field. The field can be specified by either using its field name alone or using both the table name and the field name together, separated by a ".", e.g., "OBS.scet".

#### 4.2.5 '-select' Parameter

The selections listed with the select parameter will restrict the output field columns to only those records matching the selection range. Any field listed in the .FMT files for each table can be used. In addition, if that field is a fixed-length array, you can specify an element of the array, for example, "POI.latitude\_zpd[5] -10 10". Multiple selection parameters are logically "AND'ed" together, however, if two or more of the selection fields are the same (e.g., when you want multiple, disjoint scet ranges) those fields are logically "OR'ed". Like the fields parameter, case does not matter, and the field can be specified either alone or with its table name.

#### 4.2.6 Vanilla Output

By default, all vanilla output is ASCII text written to screen with tab characters separating output fields and a return character at the end of each line (i.e. a "record"). The very first line of output will always be a listing of the field names requested.

#### 4.2.7 Tips and Tricks

These are tips that may help when creating vanilla queries. Some have already been mentioned above but are repeated here because of their usefulness.

1. A directory path in a dataset file ALWAYS needs a trailing "/".
2. Double quotes (" ") or single quotes ( ' ') can be used to enclose the fields and/or the selections on the vanilla command line.
3. The dataset\_path, fields, and select parameters can appear in any order on the command line.
4. You CANNOT specify a single element from an array in the selection parameter of the vanilla command line if that array has variable length. In short, this means you cannot use single elements from the calibrated spectrum (ispm) or interferogram (ifgm, fifm) arrays in the select parameter. For example:

```
vanilla myDatasetPath -fields "field1 field2..." -select "ispm[99] 5e-8 6e-8"
```

will not work!

5. To shorten your query time, if you need data from only a single month or a subset of months, create a dataset file with only those months listed.
6. If the field or selection you want is an entire array, you can specify it just with its name. But if it's a variable length array, square brackets must be included. The only variable length field arrays are currently frv, ifgm, and ispm.
7. To prevent confusion, it is recommended that a field that is also a key be qualified with its table name, e.g., OBS.scet.
8. Note that scet, as used in the tables, typically implies when the measurement was taken, at what time the value was calculated, or with what time the field should be associated (usually that of an IFM). For example, IFGM.scet indicates the time at the start of the interferometer's scan, POI.scet gives the time at which the pointing information is applicable (specifically chosen to be that of an interferogram), and the scet time for DIAG.tzpd indicates which IFM it applies to.

9. The tool used to query the CIRS data set was designed to be a generic, simple, lean program for querying data with few frills. Thus the name "vanilla" was chosen.
10. Vanilla is case insensitive with the "fields" and "select" query strings (enclosed in ""), although the directory/dataset file name is case sensitive on UNIX operating systems.
11. In some cases, the parameters in "-fields" and "-select" result in a vanilla command string that is very long. In these instances it may be more convenient to break the command, which includes data path, parameters of "-fields", parameters of "-select", and an optional output directory/file, into a few relatively short strings. Language-specific string concatenation techniques can then be used to combine the short strings together to make the long vanilla command.

### 4.3 Vanilla and the CIRS Database

Another of the great advantages of a relational database is that each table does not need to be one to one with the other tables, i.e., they may not all have the same number of records. However, to be useful, a large number of their keys should match across tables (Table 19). It is through the concept of "keys" that a relational database can match records from one table to those in another. Understanding how keys are implemented within the CIRS database is crucial to creating meaningful queries with the intended output.

The primary key field, used to cross-link CIRS data in different files together, is spacecraft event time (scet) stored as an integer number of seconds since 1/1/1970 00:00:00 UT, ignoring leap seconds. Also stored as retrievable fields, but not key fields, are spacecraft clock (sclk), and the sclk partition number. These are stored as two integers.

sclk is essentially an integer number related to oscillations of the on-board quartz crystal clock. Partition number is advanced by one when the sclk count is reset, expected to be a rare event, if ever. sclk ticks are not even linearly related to universal time, and the conversion between the two requires a polynomial to account for drifts in the sclk oscillation frequency. scet on the other hand is linearly related to universal time.

scet is used as the primary time key field rather than sclk for two reasons: firstly, sclk may reset, and not be monotonically increasing, in which case the partition number also changes; and secondly, scet may easily and conveniently be converted to text time using standard computer library functions, whereas interpreting sclk requires the NAIF toolkit and Cassini time kernel (SCLKSCET) files.

At the time of writing, standard computer library routines are available which facilitate the conversion to and from text time to scet number, such as the C and Perl functions gmtime and timegm.

The golden rule that vanilla will use when searching through records from different tables is simple - when the selection criteria are satisfied, IT WILL ONLY COMBINE RECORDS IF THE COMMON KEYS AMONG THE TABLES CAN BE MATCHED. A key or keys within a table are used to uniquely identify a record (consisting of those keys plus all the other fields in the table). For tables using only a single key, each key value is unique. For tables with multiple keys, their key combinations are unique. Some CIRS-specific examples should help make this clear. (Note that because of improvements we continually make to our database, you may not be able to exactly replicate these results.)

**Example 1:**

Query a single table (OBS) for a single field given a selection criteria on scet.

```
vanilla /data/cocirs_0501/data/apodspec/ -fields "OBS.scet" -select "OBS.scet 1104538500 1104538542"
```

yields

```
OBS.scet
1104538500
1104538506
1104538542
```

The OBS table has only 1 key ("scet"). This output implies there are 3 records in the OBS table that match the selection criteria. Of course, if any of the other OBS fields had been included in the query, they would have been output as well.

**Example 2:**

Query a single table (ISPM) for two fields given a selection criteria on scet.

```
vanilla /data/cocirs_0501/data/apodspec/ -fields "ISPM.scet ISPM.det" -select "ISPM.scet 1104538500 1104538542"
```

yields

ISPM.scet	ISPM.det
1104538500	0
1104538500	11
1104538500	13
1104538500	15
1104538500	17
1104538500	19
1104538500	22
1104538500	24
1104538500	26

```

1104538500  28
1104538500  30
1104538542   0

```

Here it is clearly evident why ISPM needs two keys to keep each key combination unique. If the table had been designed with only scet used as a key, multiple records for the same time but different detector numbers would have the same key (“degeneracy”).

**Example 3:**

Query fields from two tables given a selection criteria on scet.

```

vanilla /data/cocirs_0501/data/apodspec/ -fields 'OBS.scet OBS.rti ISPM.scet ISPM.det
ISPM.ispts' -select "ISPM.scet 1104538500 1104538542"

```

yields

OBS.scet	OBS.rti	ISPM.scet	ISPM.det	ISPM.ispts
1104538500	38	1104538500	0	139
1104538500	38	1104538500	11	112
1104538500	38	1104538500	13	112
1104538500	38	1104538500	15	112
1104538500	38	1104538500	17	112
1104538500	38	1104538500	19	112
1104538500	38	1104538500	22	95
1104538500	38	1104538500	24	95
1104538500	38	1104538500	26	95
1104538500	38	1104538500	28	95
1104538500	38	1104538500	30	95
1104538542	38	1104538542	0	139

Comparing the output of examples 1 and 2 shows that the time for scet = 1104538506, from Example 1, is not listed. It has been excluded because there is no matching scet in the ISPM table. This is an example of the golden rule in practice - records from both tables are combined only if the values of their common keys match (the only common key here is scet).

**Example 4:**

Query a single table with a key field, THE TABLE UNDESIGNATED, and a scet selection.

```

vanilla /data/cocirs_0501/data/apodspec/ -fields 'scet' -select "scet 1104538500 1104538542"

```

yields

```

scet
1104538500

```

1104538500  
1104538500  
1104538500  
1104538500  
1104538500  
1104538500  
1104538500  
1104538500  
1104538500  
1104538500  
1104538542

This example illustrates how vanilla handles ambiguities that arise when the requested field occurs in more than one table. The query above returned the scets from the ISPM table. The duplicate scets are returned because using scet alone is not sufficient to identify a unique record; in the ISPM table, both scet and det (the table key set) are required. If vanilla encounters a field common to more than one table, it will search the list of tables and directories listed in the dataset file and use the first table that has that field. In this case, ISPM is the first table in the dataset list and therefore ISPM.scet is used. If you want to avoid this type of ambiguity and prevent possible confusion in your query's output, just USE THE TABLE NAME WITH THE FIELD WHEN THAT FIELD OCCURS IN MULTIPLE TABLES. In most practical cases, this means the fields "scet" and "det" should be qualified with the table name in your queries.

#### **4.4 Vanilla Extraction of Pointing/Geometry**

##### **NAVIGATION TABLE QUERIES, GEO:**

Of the navigational tables, the RIN and TAR tables both use scet and det fields as the keys to identify a unique table record. However, the GEO and POI tables each use a very different key set and require special consideration when used in vanilla queries.

The GEO table was designed to provide information on the positions and orientations of the local object bodies and the spacecraft. As seen in Table 19, the field keys for the GEO table are scet and body\_id. The field "det" is not needed as a key, nor even as a field in the table, because the relative positions between the spacecraft and a body are independent of detector. The body\_id field is a subset of the bodies in the Jupiter and Saturn systems with values defined by the NAIF ID for those bodies (see Table 3 "Selected NAIF IDS of relevance to Cassini CIRS" in the DATASIS.PDF PDS document). The GEO table's primary\_id field identifies which system is relevant for that scet. For each scet, information for all bodies within the primary\_id field's designation will be available. Therefore, for the relatively brief period that Jupiter was encountered, each scet will have entries for body id's of 501-516 and 599. Likewise, for the prime mission and beyond, the primary\_id field will be 699 (Saturn) and each scet will have entries for body\_id's of 601-618 and 699. This means at Saturn, each scet in the GEO table will have 19 entries! Not specifying a body\_id when using fields from



the GEO table is a common cause of confusion as many more records will be produced than expected with, seemingly, duplicate scet times. Example 5 demonstrates this.

**Example 5:**

Query for the GEO key set fields using a selection criteria on scet.

```
vanilla /data/cocirs_0501/data/apodspec/ -fields 'GEO.scet body_id' -select "GEO.scet  
1104538500 1104538506"
```

yields

GEO.scet	body_id
1104538500	601
1104538500	602
1104538500	603
1104538500	604
1104538500	605
1104538500	606
1104538500	607
1104538500	608
1104538500	609
1104538500	610
1104538500	611
1104538500	612
1104538500	613
1104538500	614
1104538500	615
1104538500	616
1104538500	617
1104538500	618
1104538500	699
1104538506	601
1104538506	602
1104538506	603
1104538506	604
1104538506	605
1104538506	606
1104538506	607
1104538506	608
1104538506	609
1104538506	610
1104538506	611
1104538506	612
1104538506	613

1104538506 614  
 1104538506 615  
 1104538506 616  
 1104538506 617  
 1104538506 618

Another important concept within the GEO table is that of timing. In order for different tables to be joined productively, the majority of the scets within each table should be the same. The scet for the ISPM table refers to the first recorded raw sample of the interferogram. Values of fields in other tables for scet are then either for measurements taken at that scet time or interpolated to it (as in the IHSK table). However, in the GEO table it is often more important to know the location of an object during the period at which the interferometer is at Zero Path Difference (ZPD) because during this time the great majority of the signal is being collected. So while GEO.scet indicates to which interferogram the GEO field should be associated, the actual positions are calculated at the time of ZPD, typically a few seconds later than the scet. In this way the functionality of the database is maintained while providing the highest degree of navigational accuracy.

**NAVIGATION TABLE QUERIES, POI:**

The POI tables store the pointing for each active detector at the ZPD of the IFM. One POI record is produced for each active detector and each non-rings non-primary target body in the field of view plus a record for the primary body (either Saturn or Jupiter) whether or not it is in the field of view. The POI table therefore requires 3 fields within its key set to uniquely identify a record: scet, det, and target\_id. There are typically 11 channels (detectors) active during a given time. The number of targets within the field of view varies from observation to observation and therefore so does the number of records with a given scet. Example 6 displays the available, unique records for the scet range used in Example 5.

**Example 6:**

```
vanilla /data/cocirs_0501/data/apodspec/ -fields 'POI.scet POI.det POI.target_id' -select "POI.scet 1104538500 1104538506"
```

yields

POI.scet	POI.det	POI.target_id
1104538500	0	608
1104538500	0	699
1104538500	11	608
1104538500	11	699
1104538500	13	608
1104538500	13	699
1104538500	15	608
1104538500	15	699
1104538500	17	608

1104538500	17	699
1104538500	19	608
1104538500	19	699
1104538500	22	608
1104538500	22	699
1104538500	24	608
1104538500	24	699
1104538500	26	608
1104538500	26	699
1104538500	28	608
1104538500	28	699
1104538500	30	608
1104538500	30	699
1104538506	0	608
1104538506	0	699
1104538506	12	608
1104538506	12	699
1104538506	14	608
1104538506	14	699
1104538506	16	608
1104538506	16	699
1104538506	18	608
1104538506	18	699
1104538506	20	608
1104538506	20	699
1104538506	22	608
1104538506	22	699
1104538506	24	608
1104538506	24	699
1104538506	26	608
1104538506	26	699
1104538506	28	608
1104538506	28	699
1104538506	30	608
1104538506	30	699

The output shows that there are 11 different vanilla detectors per scet, as expected, plus an entry for the primary target body (Saturn) which may or may not be in the field of view, and for lapetus (target\_id = 608=NAIF ID) which is in the field of view.

#### **NAVIGATION TABLE QUERIES, TAR:**

To find out if Saturn is in the field of view, you can use the TAR table field, TAR.saturn. It will be one if in the field of view and zero if not (Example 7).

**Example 7:**

```
vanilla /data/cocirs_0501/data/apodspec/ -fields POI.scet POI.det POI.target_id saturn  
iapetus' -select "POI.scet 1104538500 1104538506"
```

yields

POI.scet	POI.det	POI.target_id	saturn	iapetus
1104538500	0	608	0	1
1104538500	0	699	0	1
1104538500	11	608	0	1
1104538500	11	699	0	1
1104538500	13	608	0	1
1104538500	13	699	0	1
1104538500	15	608	0	1
1104538500	15	699	0	1
1104538500	17	608	0	1
1104538500	17	699	0	1
1104538500	19	608	0	1
1104538500	19	699	0	1
1104538500	22	608	0	1
1104538500	22	699	0	1
1104538500	24	608	0	1
1104538500	24	699	0	1
1104538500	26	608	0	1
1104538500	26	699	0	1
1104538500	28	608	0	1
1104538500	28	699	0	1
1104538500	30	608	0	1
1104538500	30	699	0	1
1104538506	0	608	0	1
1104538506	0	699	0	1
1104538506	12	608	0	1
1104538506	12	699	0	1
1104538506	14	608	0	1
1104538506	14	699	0	1
1104538506	16	608	0	1
1104538506	16	699	0	1
1104538506	18	608	0	1
1104538506	18	699	0	1
1104538506	20	608	0	1
1104538506	20	699	0	1
1104538506	22	608	0	1
1104538506	22	699	0	1
1104538506	24	608	0	1

1104538506	24	699	0	1
1104538506	26	608	0	1
1104538506	26	699	0	1
1104538506	28	608	0	1
1104538506	28	699	0	1
1104538506	30	608	0	1
1104538506	30	699	0	1

So Saturn was not in the field of view and was only included because it was the primary target body.

The distinction between the `fov_targets` field in the TAR tables, and the individual bytes for each target can also be useful, since it allows searches that isolate times when two objects are in the field of view, or times when *only* one object is in the field of view. For example, the search:

```
vanilla . -fields "TAR.scet TAR.det" -select "titan 1 1"
```

will find all entries in which Titan is in the field of view, while

```
vanilla . -fields "TAR.scet TAR.det" -select "fov_targets 4096 4096"
```

finds all entries in which *only* Titan is in the field of view.

#### 4.5 Final Words On Vanilla

Additional material on the vanilla database search engine and its use with the CIRS database are available within each CIRS PDS volume. The file `vanilla-guide.pdf` in `SOFTWARE/DOC/` gives a description of the vanilla search engine as well as a detailed explanation of the generic database file format required by vanilla. In the same directory, the file `cirs_vanilla_examples.pdf` expands on the examples above, providing further guidance on querying the CIRS database using more detailed queries.

Also provided with PDS volumes is a text file, `vanilla_fields.txt`, listing all the fields available within the database. Located within the `DOCUMENT/` directory, it is a comma separated value (CSV) file, easily imported into most spreadsheet programs. Each line in the file is a record describing a given field as well as additional information. In order, the values within a record are: table name, field name, data type, total number of bytes in the field, number of items in the field, and a description (enclosed in double quotes). Note that when the number of items is greater than one (i.e., it's an array), dividing the total number bytes by the number of items gives you the individual element size in bytes.

#### **4.6 Other Extraction Tools**

The CIRS team uses a variety of scripts and programs that either supplement or directly operate on vanilla output. Their functions include conversions between scet (i.e., UNIX time) and a human-readable UTC time, plus a utility to average spectra returned from a vanilla query. While currently only being utilized within the team, based on user interest, they may be provided on PDS volumes at a later date.

## 5.0 End-to-end examples of data use

In previous sections of this document, we have described in detail the background about CIRS and diverse topics about the instrument, observation designs, operations, calibration and how to extract data from the binary records. In this section we finally come to the core purpose of this CIRS User's Guide, a detailed discussion of how you – the reader and hopefully scientific user – can select the data you want, subset the data in different ways, comprehend the limits to the data and instrument modeling specifics, and finally reverse engineer the infrared spectrum to find scientific data regarding the target of interest. This section begins with an overview of the tasks required and their ordering, to achieve this goal.

### 5.1 Overview and general algorithm

A high-level overview of the steps involved from the very beginning of contemplating what CIRS data might be useful for a particular scientific investigation, to acquiring the final results of the study, are as follows:

- 1) **Selection of observations:** beginning with target, determine types of observations available, and then research specific instances of those observations to find the most appropriate.
- 2) **Subset spectra:** beginning with all potentially relevant spectra, list their characteristics including geometrical parameters, and exclude or subset the spectra as required.
- 3) **Bad data check:** check the subsetted spectra more rigorously for bad data.
- 4) **Average spectra:** similar spectra are added together, if required, to increase signal-to-noise ratio (SNR), prior to modeling. A detailed assessment of SNR for the average is made at this time.
- 5) **Determine field-of-view model:** if the finite field-of-view of the detector convolves an inhomogeneous area, then the user needs to consider whether to explicitly model this (e.g. by inclusion of multiple ray paths), or estimate it as a systematic error.
- 6) **Spectral modeling and inversion:** the final stage is to model the spectrum, adjusting parameters iteratively until a good fit is made. At this point the parameters' final values are set and the error bars are estimated.

The following sub-sections will describe each of these topics in more detail.

#### 5.1.1 Selection of observations

In Section “2.2 Science Objectives” the broad scientific objectives of CIRS are summarized, while in Section “2.3 Observation Strategies” the actual implementation of

these objectives in terms of planned observations are described in depth. If you are new to using CIRS data, you should familiarize yourself at this point with the various observation types, and determine which you are interested in studying.

Next comes the issue of finding exactly when these observations were conducted, and what the pointing and other parameters were. All CIRS observations implemented and archived are listed in a *Time Ordered Listing (TOL)* file, which can be found in the INDEX directory on the PDS archive volumes. The TOL files have a name such as C23\_TOL.ASC or S49\_TOL.ASC, where the first three characters of the name correspond to the spacecraft execution sequence, simply a block of time for which the spacecraft executes a pre-set series of maneuvers. The earliest sequences (prior to SOI) had names beginning with 'C' for cruise, while those after SOI had names beginning with 'S' for Saturn. The TOL files were created by direct export from the Cassini Information Management System (CIMS), an on-line database available during the Cassini Mission to all teams, and keep track of all planned and executed observations and maneuvers by all instruments and engineering teams.

The TOLs are text files of a specific text-table format, known as CSV, for comma separated values. Each line in the file, known as a record, consists of an identical number of data fields, delimited by double quotes, "" and separated from the other fields by a comma. Together all the records form a table, which can be read by standard spreadsheet programs such as *Excel* and *Open Office Calc*. The TOL records contain the start time and end time of each observation in a format yyyy-doyThh:mm:ss, where yyyy=year, doy=day of year (beginning with Jan 1<sup>st</sup> =001), hh=hour, mm=minute, ss=second. The observation name is also recorded.

Therefore, either by reading the TOLs into a text editor and using standard search commands, or by reading into a spreadsheet program, the entire observational database may be searched for specific instances of any observation type, using the 9-character stem of the observation instance, such as FIRNADMAP or MIDIRTMAP.

The next task is to convert the DOY-style date and time into a SCET time, as described in Section 4.3 "Vanilla and the CIRS Database". Finally, the Vanilla software tool may be used to query the database for records between the start and end scet time of the observation, to extract pointing information such as latitude, longitude, local time, altitude at FOV center, and other parameters.

### **5.1.2 Subset observations**

The user should begin by initially extracting all the spectra for the desired observation(s), including necessary pointing and ancillary information, using the '-fields' parameter of Vanilla. These fields should then be examined closely to find out the max and min of the ranges of important parameters such as latitude, longitude and local time. The term "ispm[]" should be included to print out the calibrated, interpolated spectrum.

Questions the user may wish to research at this point include:



- Which bodies are visible in the FOV (FOV\_TARGETS)?
- What are the target coordinates of the observation, including latitude (LATITUDE\_ZPD[5]), longitude (LONGITUDE\_ZPD[5]), altitude (ALTITUDE\_ZPD[5]) etc and are they appropriate?
- What is the distance to the target (BODY\_SPACECRAFT\_RANGE), which sets the FOV footprint size?
- What are the viewing parameters, such as emission angle (EMISSION\_ANGLE[5]) and phase? (PHASE\_ANGLE[5])
- Are the Q-points all on the planet, if required (ALL\_Q\_ON)?

Finally, the '-select' parameter of Vanilla can be used to narrow the range of data to be used in the scientific investigation, using the same fields, with a min and max range specified: Vanilla -select "<param> <pmin> <pmax>" (quotes are required). If a specific value is required, both min and max ranges have to be set to the same value.

### 5.1.3 Bad data check

There are several methods of checking the data that may be employed:

- Viewing individual spectra to look for gross distortions/noise.
- Computing the RMS (standard deviation) of a set of similar spectra: electrical interferences (noise spikes) often show up as large departures in the standard deviation at certain wavenumbers. See also Section "2.5 Electrical interferences (spikes) and other data issues".
- Checking that the number of overall raw samples (npts) on each IFGM falls within 3-sigma of the mean number (may indicate scan mechanism out of phase lock).
- Modeling the spectrum with a radiative transfer model. If the model is trusted, then it can sometimes show up problems with the data continuum calibration, including ripples and sag/droop (unphysical gradients).

### 5.1.4 Average spectra

After the final subset of spectra has been selected, most users will wish to average spectra together in one or more 'bins' to improve S/N. A common example might be to add together all spectra taken during an integration (static dwell observation), for example at a particular altitude on Titan's limb, or for a feature track on Saturn. However, even mapping observations are commonly binned, adding together spectra that are recorded at very close spatial positions during a slow-moving scan. Often these observations are designed so that the movement rate is slow enough that adequate S/N can be obtained post facto by binning in spatial bins where the range of FOV center location is equivalent to the FOV size (width). For example, a Titan FIRNADMAP is designed so that about 60 5-sec spectra are taken in 300 seconds, with a FOV movement in this time equal to 4 mrad: the same size as the detector. Therefore 60 spectra can be co-added while losing only a factor 2 in spatial resolution.

To assess the noise level at each spectral point, the standard deviation ( $\sigma$ ) may be used as a first order-estimate. However, if the spectra being averaged are not homogeneous to a high-degree (i.e. if the ‘signal’ is changing from scan to scan as well as the random noise), then  $\sigma$  will over-estimate the noise level. For this reason it may be desirable to estimate the random noise from the  $\sigma$  of space calibration spectra, which are taken at very frequent intervals (near daily) and included in the database. Note that the expected random noise on an average of  $N$  spectra is equal to  $\sigma/\sqrt{N}$ .

### 5.1.5 Field of view modeling

Before modeling the spectrum, the investigator must also consider whether the field sampled by the detector is significantly uniform or non-uniform. By ‘significantly’ we mean that the signal non-uniformity is larger than the expected random errors in the spectrum. For example, the large FP1 footprint (3.9 mrad) when directed to Titan’s limb samples 39 km at 10000 km distance (FWHM size), or somewhat less than one atmospheric scale height (~50 km). However the time spent at this range is very short, so more typically FP1 limb observations maybe taken at ranges up to 50000 km, when the FOV is already ~200 km in size and much larger than a scale height. So in this case, accounting for the non-uniformity of the stratified atmosphere within the footprint size when modeling the spectrum would be desirable.

Several journal papers have dealt with this topic in detail, including giving precise information on the FOV spatial response functions (Nixon, Infrared Limb Sounding of Titan with Cassini CIRS, 2009) (Teauby, 2007), and should be consulted for detailed modeling instructions.

### 5.1.6 Radiance modeling of the spectrum

Modeling infrared spectra of planetary atmospheres, surfaces and rings is a large field within planetary sciences. Typically this problem can be broken down into two parts (1) the **forward problem**: calculating a reference synthetic spectrum based on a set of model parameters, e.g. planetary temperature field and gas composition, and (2) the **inverse problem**, which attempts to adjust the model parameters iteratively, to minimize the model-data spectrum mismatch, and thus ‘fit’ the spectrum and derive useful information about the emitting object (the model parameters). There are a number of useful textbooks on this subject (Goody and Yung, 1989) (Hanel, 2003) (Liou, 2002) (Rodgers, 2000).

In addition, the CIRS data user is advised to carefully read a sample of the already published analyses of CIRS data, which give details of several different approaches to spectral synthesis. These include the Oxford model NEMESIS, which has been applied to model the atmospheres of Jupiter, Saturn and Titan using the correlated-k method (Irwin, 2008); several line-by-line models used at Observatoire de Paris, Meudon, e.g. AART (Coustenis, 2010); a second correlated-k model at NASA GSFC (Achterberg, 2011); and other models.

While a full discussion of radiative transfer modeling is beyond the scope of this document, a few key pointers specific to modeling the CIRS spectra can be mentioned.

- The user should be aware of the aliased and unaliased bandpasses of CIRS. See Appendix A of (Nixon, Titan's Prolific Propane: The Cassini CIRS Perspective, 2009).
- The finite field of view of CIRS which convolves the source may need to be modeled explicitly, by treating the spectrum as the weighted average of multiple rays emanating from different points on the source, if inhomogeneous. See Section "5.1.5 Field of view modeling" of this document for further details.
- The spectral line shape and FWHM should be explicitly modeled. A description of the apodization leading to the final shape (Hamming Function) is discussed in Section "3.5 Post-processing: resampling and apodization".

### 5.1.7 Vanilla end-to-end generic example

As an example of how to use the PDS TOL files and Vanilla to extract spectra of interest from the database, suppose, after reviewing Section "2.3 Observation Strategies", you decide to use data of Saturn from a FIRMAP-type observation taken in October 2010. To determine if data of this type exists, you would first scan the TOL files under the INDEX directory at PDS identifying those TOL files that corresponded to October 2010. As discussed in Section "5.1.1 Selection of observations", the start and stop time for each observation is included in the TOL files, and in this case, files S63\_TOL.ASC and S64\_TOL.ASC apply. Searching for "FIRMAP" in these two files produces one matching record:

```
"CIRS_139SA_FIRMAP002_PRIME", "CIRS_4000", ,"2010-291T22:00:00", ,"000T12:00:00",  
"2010-292T10:00:00",...
```

The information in this record tells you the observation was a CIRS prime request occurring on orbit 139 with the principal target being Saturn. It also tells you that the observation started on day of year 291 (October 18) at 22:00:00, had a duration of 12 hours, and ended on day of year 292 (October 19) at 10:00:00.

To extract the spectra and ancillary data from the database, the start and end times will need to be converted to scet (i.e., the number of seconds elapsed since 1 January 1970, excluding leap seconds). While you could calculate this yourself, it's easier if you use the `timegm` and `gmtime` functions found in the C or Perl programming languages. For example, in Perl the two lines needed to do the conversion for the start time are:

```
use Time::Local;  
print timegm(0, 0, 22, 18, 9, 110);
```

where the arguments to the `timegm` function are:

```
arg 1 = second  
arg 2 = minute
```

arg3 = hour  
arg4 = day of month  
arg5 = month (Note: this counter starts at 0 so valid inputs are 0-11.)  
arg6 = year - 1900

Using the above plus a second call (`timegm(0, 0, 10, 19, 9, 110)`) to find the end time produces start/end scet times of 1287439200 and 1287482400, respectively. To do the conversion in reverse, use "`($second, $minute, $hour, $dayOfMonth, $month, $year, $dayOfWeek, $dayOfYear, $isDST) = gmtime(scet)`" where `$dayOfWeek` is in the range 0 - 6.

Now Vanilla queries can be done to determine how much data is available and its quality. Because the period of interest has been restricted to October 2010, the only PDS volume needed is `cocirs_1010` (which translates into "Cassini Orbiter, CIRS, 2010, October"). From here on in this example it is assumed you have downloaded this volume from the PDS to a local drive and have made `DATA/APODSPEC` your current working directory. By doing this, the dataset argument to the Vanilla call can be specified simply as "." (this tells Vanilla to look in the current directory for a `dataset.txt` file). It's also assumed you've read Section "4.0 How to search and extract data".

To find the number of spectra in this time range, the command would be

```
vanilla . -fields "ISPM.scet ISPM.det" -select "ISPM.scet 1287439200 1287482400"
```

which produces 97,027 data records (where I've counted records by piping the output to Unix's `wc` (word count) command). But if you look at the detector field values, you'll notice all detectors are represented here. `FIRMAP`'s are geared toward focal plane 1 so restrict the output to only an `ISPM.det` of 0 using:

```
vanilla . -fields "ISPM.scet ISPM.det" -select "ISPM.scet 1287439200 1287482400 ISPM.det 0 0"
```

The number of records is now reduced to 8,727.

Next weed out the shutter closed and noisy spectra by using `OBS.shutter` equal to 0, `DIAG.noise` equal to 1, and `DIAG.rwa_noise_flag` equal to 0:

```
vanilla . -fields "ISPM.scet" -select "ISPM.scet 1287439200 1287482400 ISPM.det 0 0  
OBS.shutter 0 0 DIAG.noise 1 1 DIAG.rwa_noise_flag 0 0"
```

This gets the count down to 8,652 records.

Another quality-type check can be done using the number of points in the raw interferogram (`IFGM.npts`). Values that are more than  $3\sigma$  from the average may indicate the scan was affected by unrecognized sources of additional noise. By finding the average and standard deviation of the output from

```
vanilla . -fields "IFGM.npts" -select "ISPM.scet 1287439200 1287482400 ISPM.det 0 0  
OBS.shutter 0 0 DIAG.noise 1 1 DIAG.rwa_noise_flag 0 0",
```

a new selection criteria based on the npts field can be created. In this case, the average is 194 with a standard deviation of 1.5. Our new spectra query then becomes

```
vanilla . -fields "ISPM.scet" -select "ISPM.scet 1287439200 1287482400 ISPM.det 0 0  
OBS.shutter 0 0 DIAG.noise 1 1 DIAG.rwa_noise_flag 0 0 IFGM.npts 189.5 198.5"
```

with an output of 8,272 records.

The only step left to do is restrict the subset to your desired instrument mode and pointing limits. This is, of course, highly dependent on the particular study you're trying to do. In this case, let's suppose you want all 39 RTI data with a latitude range of -5 to 0 degrees, a longitude range of 265 to 270 degrees, and a low emission angle. Because geometry and pointing information is now being included, the selection part of the Vanilla command must take into account the target we're interested in:

```
vanilla . -fields "ISPM.scet OBS.rti GEO.body_spacecraft_range POI.emission_angle[5]  
POI.latitude_zpd[5] POI.longitude_zpd[5]" -select "ISPM.scet 1287439200 1287482400  
ISPM.det 0 0 OBS.shutter 0 0 DIAG.noise 1 1 DIAG.rwa_noise_flag 0 0 IFGM.npts 189.5 198.5  
POI.latitude_zpd[5] -5 0 POI.longitude_zpd[5] 265 270 GEO.body_id 699 699 POI.target_id  
699 699 OBS.rti 39 39"
```

This command produces 247 records, but if you look at the field `body_spacecraft_range` values, you'll notice they fall into two distinct sections, while the emission angle is very variable at first, stays fairly constant for a while, and then gradually increases. To produce the cleanest subset, restrict the range to distances greater than 1560000 km and restrict the emission angle to between 0.0 and 0.5 degrees and force all Q-points to be on the target

```
vanilla . -fields "ISPM.scet OBS.rti GEO.body_spacecraft_range POI.emission_angle[5]  
POI.latitude_zpd[5] POI.longitude_zpd[5]" -select "ISPM.scet 1287439200 1287482400  
ISPM.det 0 0 OBS.shutter 0 0 DIAG.noise 1 1 DIAG.rwa_noise_flag 0 0 IFGM.npts 189.5 198.5  
POI.latitude_zpd[5] -5 0 POI.longitude_zpd[5] 265 270 GEO.body_id 699 699 POI.target_id  
699 699 OBS.rti 39 39 GEO.body_spacecraft_range 1.56e6 1.56e7 POI.emission_angle[5] 0 .5  
POI.all_q_on 1 1"
```

This leaves 77 records, corresponding to 77 spectra, that can now be processed.

The spectra, along with the fields used to create the wavenumbers, can be extracted using

```
vanilla . -fields "ISPM.iwn_start ISPM.iwn_step ISPM.ispts ispm.ispm[]" -select "ISPM.scet  
1287439200 1287482400 ISPM.det 0 0 OBS.shutter 0 0 DIAG.noise 1 1 DIAG.rwa_noise_flag 0  
0 IFGM.npts 189.5 198.5 POI.latitude_zpd[5] -5 0 POI.longitude_zpd[5] 265 270 GEO.body_id  
699 699 POI.target_id 699 699 OBS.rti 39 39 GEO.body_spacecraft_range 1.56e6 1.56e7  
POI.emission_angle[5] 0 .5 POI.all_q_on 1 1"
```

where the wavenumber set can be created using  $iwn\_start + (iwn\_step * i)$  for  $i$  equal 0 to  $ispts - 1$ . Note that the wavenumber set won't change for a given RTI value so if you already

have created the wavenumbers, you won't need to include those fields in the query for spectra.

This was just one example of how a CIRS data user could select the type of data needed from the database. There are many other fields that can be used to restrict the data to different subsets, but the procedure in all remains the same - use the TOL files to find suitable observations and then use Vanilla quality and geometry fields to restrict the data to only what is needed. You may often find that your selection criteria are so restrictive that few or no spectra are returned. In those cases the criteria will need to be relaxed until an appropriate numbers of matching records are found.

## 5.2 Worked Example 1: Icy Satellite Science

### 5.2.1 Introduction

This example gives an overview of how the temperature maps of Mimas, used in (Howett, 2011) were produced. In this example capitalized words are used to show when fields in the pointing, geometry or spectral files are being referred to. FP3 is short for the CIRS focal plane 3 detector (similarly for FP1 and FP4), NAIF stands for NASA's *Navigation and Ancillary Information Facility* and NAIFID is the NAIF's identification code for solar system objects. SPICE is NAIF's toolkit for interpreting spacecraft data. More details of SPICE can be found in (Acton, 1996). RA and DEC are short for Right Ascension and Declination respectively.

### 5.2.2 Deciding which observations to use

Icy satellite encounters by Cassini are infrequent enough that the times and dates of the encounters are relatively well known. Satellite observations can be searched for using the name of the observation since the orbit and target are given in the observation title (e.g. CIRS\_126MI\_X\_PRIME will be CIRS PRIME Rev 126 observation of Mimas). SPICE, using the Cassini kernels can be used to determine when close encounters between Cassini and a target of interest occur. On most encounters some remote sensing occurs, although no CIRS data will exist for some gravity or radar focused encounters. At the time of writing Cassini SPICE kernels could be downloaded from here:

[https://naif.jpl.nasa.gov/pub/naif/pds/data/co-s\\_j\\_e\\_v-spice-6-v1.0/cosp\\_1000/](https://naif.jpl.nasa.gov/pub/naif/pds/data/co-s_j_e_v-spice-6-v1.0/cosp_1000/)

Orbit	Date	Time (UTC)	Sub-Solar Longitude	Local Time Coverage between $\pm 20$ Latitude (°)	Range (km)	Average Spatial Resolution (km/pixel)
126	13 Feb 2010	19:10 – 20:30	164 – 170	127-264	37,510 - 65,826	9.0
139	16 Oct 2010	14:27 – 16:53	85 - 90	4 - 130	73,167 - 101,071	16.0
144	31 Jan 2011	01:30 – 03:05	34 - 53	40 -207	138,88 - 141,011	42.2

**Table 20: Details of the CIRS FP3 observations used in this analysis. Local time is defined as the angular rotation of the body, in degrees, since local midnight. The names of the observations used are (corresponding from top to bottom in the table): CIRS\_126MI\_FP3DAYMAP001\_PRIME, CIRS\_139MI\_MIMAS001\_PRIME and CIRS\_144MI\_MIMAS001\_PRIME.**

In (Howett C. e., 2011) data from three flybys of Mimas by Cassini are used, which occurred on 13 Feb 2010, 16 Oct 2010 and 31 Jan 2011 and are referred to as Rev. or orbits 126, 139 and 144 respectively. Details of the observations used, including their full names, are given in the paper. However, here we will concentrate on the analysis on Rev 144, since the process was the same for all three data sets. The first step in analyzing any data is to download it; in this case the pointing, geometry and spectral files (the POI, GEO and ISPM files) were downloaded.

The data was then subsetting to include only observations of Mimas by selecting in the pointing information those data that had TARGET\_BODY for NAIFID of 601 (Mimas), and with DET values between 1 and 20 (FP3). Within a single icy satellite encounter there are often many types of observations made by CIRS. Usually (where data volume and timing allow) an FP3/4 global map is made by slowly scanning across the target at 6  $\mu$  radian per second, and an FP1 raster scan is made at Nyquist sampling at 40  $\mu$  radian per second. When making a temperature map each of the observations is considered separately, since local time changes throughout an encounter smears surface temperatures.

During an encounter each of the different observations that occurred can be determined by looking at the SCET (CIRS time stamp) versus RA and DEC variations in the pointing information. Integrations will have little change in the RA and DEC with SCET, whereas global scans will have smoothly varying values. In this example a global FP3 scan is used, which is comprised of two limb to limb swaths obtained on the 31<sup>st</sup> Jan 2011 between 02:54:35 and 03:05:30 UTC (i.e. SCET 1296442474 to 1296443130).

### **5.2.3 Pointing Adjustments**

Since the icy satellites are much smaller than other targets in the Saturnian system, such as Titan or Saturn, pointing errors correlate to greater longitude/latitude errors. Thus, when working on icy satellite data pointing tweaks are often required. How these tweaks are determined will depend on the target itself, the type of encounter and required output. For example on Enceladus it may be acceptable to tweak the pointing so that the warmest observed temperatures coincide with the hot sulci on Enceladus' South Polar Terrain (often dubbed tiger stripes). However, since the accurate determination of the boundary of Mimas' thermal anomaly was a key goal of this work, accurate absolute pointing was very important.

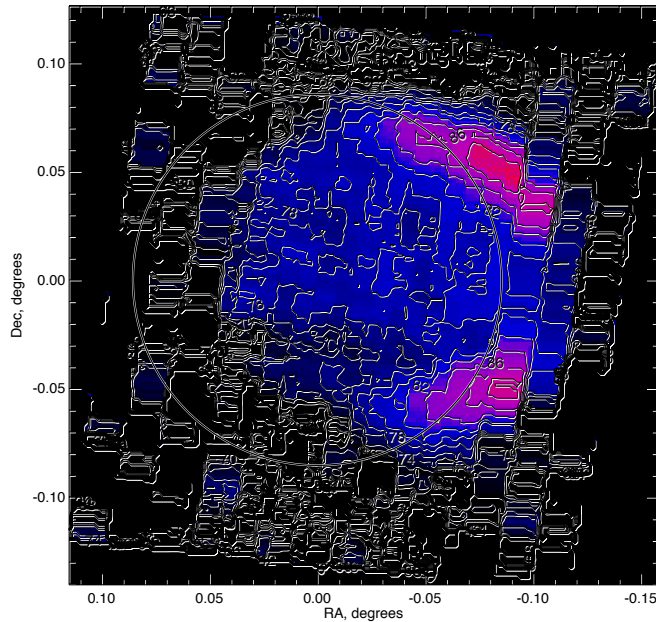


**Figure 30: temperatures across Mimas from Rev 144, plotted in RA/DEC space with the expected limb location depicted by the white circle.**

The best fitting blackbody temperature curve was found for each spectrum in the designated time frame, and the RA and DEC of each observation read from the pointing files. The expected limb location in RA and DEC space at the start of the observation was determined using SPICE and the Cassini kernels. Using this information a temperature map versus RA/DEC was determined, with the limb prediction overlaid, as shown in Fig. 28. The limb position is shown at the start of the scanning time and the fields of view have been scaled to this time to account for the changing distance of the observation.

If the fitted blackbody temperatures show a dramatic variation where the limb is predicted to occur then no tweaks are required. However, as Figure 30 shows, the predicted and observed limbs don't always overlap. So tweaks in RA and DEC space can be performed until the expected limb location from SPICE overlays the temperature limb. Using further SPICE routines these RA/DEC tweaks can be translated into longitude and latitude tweaks.

#### 5.2.4 Rejection of bad data.

Occasionally hot pixels make it into the CIRS data set. These individual data points are usually extremely obvious in an observation, having much higher temperatures than their neighboring, often spatially overlapping, observations. An easy check for these is to plot the SCET time against the SPECTRUM radiance (found in the spectral files) at a high signal to noise wavenumber (e.g. at  $\sim 200 \text{ cm}^{-1}$  for FP1), or plot this radiance value or its corresponding temperature against RA and DEC. As Figure 31 shows, any bad scans are likely to be very obvious outliers on these plots and once identified they can be excluded from the analysis.

Currently SPICE is used to check the pointing, however other systems exist that could perform this function. The method used here lines up the predicted limb location to that observed in the temperature information. This works well for a global or limb-to-limb daytime observation against dark sky, or for a nighttime observation during a Saturn transit. It is more limited for a nighttime observation against dark sky, where there is no large temperature variation at the limb or for an observation that does not scan off the limb (e.g. a stare). However, since FP3 global scans were made of Mimas the data technique above could be used.

The best fitting blackbody temperature curve was found for each spectrum in the designated time frame, and the RA and DEC of each observation read from the pointing files.



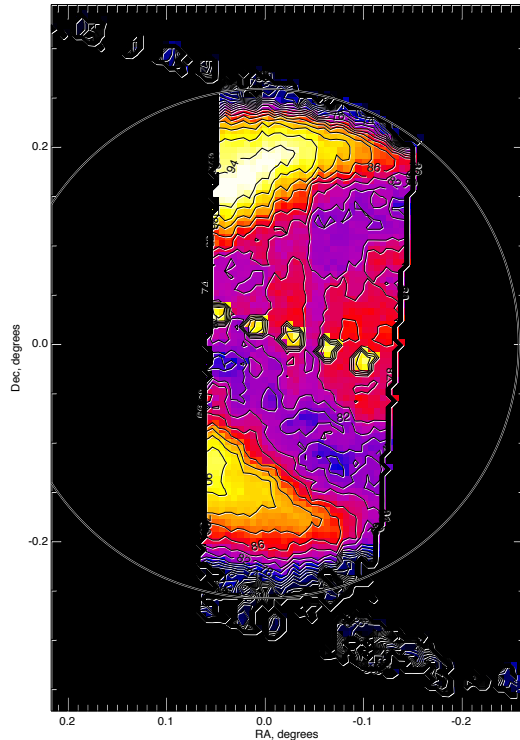


**Figure 31 - Temperature RA/DEC plot for Rev 126 Mimas, showing hot bad pixels in the center of the disk.**

### 5.2.5 Data Analysis

The first data product produced for icy satellite surfaces from CIRS data is often a surface temperature map (and is the goal of this example analysis).

In the event that pointing tweaks were not required then the data is further limited to ensure that the fields of view of the data used lie on the surface of the target. This is achieved by selecting data that has pointing information with a FILLING\_FACTOR greater than 0.99, ALL\_Q\_ON equal to 1 and ALTITUDE equal to 0. For FP3 and FP4 the field of view boundaries are given in the pointing file for each observation by the arrays LONGITUDE and LATITUDE. For FP1 using the information on the FP1 field of view in (Flasar, 2004) or by using SPICE and Cassini SPICE kernels the circular field of view can be plotted instead of the octagonal one given by the LONGITUDE and LATITUDE in the pointing files.

If the pointing has been tweaked then the data will still have to be restricted to spectra that have their complete field of view on the surface. The latitude and longitude of each observation will be determined from the tweak.

The surface temperature correlated to each of the remaining spectra is determined by finding its best fitting black body temperature emission curve. A surface temperature map can then be created by combining the observations longitude, latitude and temperature information. Where data coverage overlaps the mean temperature in the overlap portion is used. For Mimas this process results in the creation of the map shown in Figure 32.

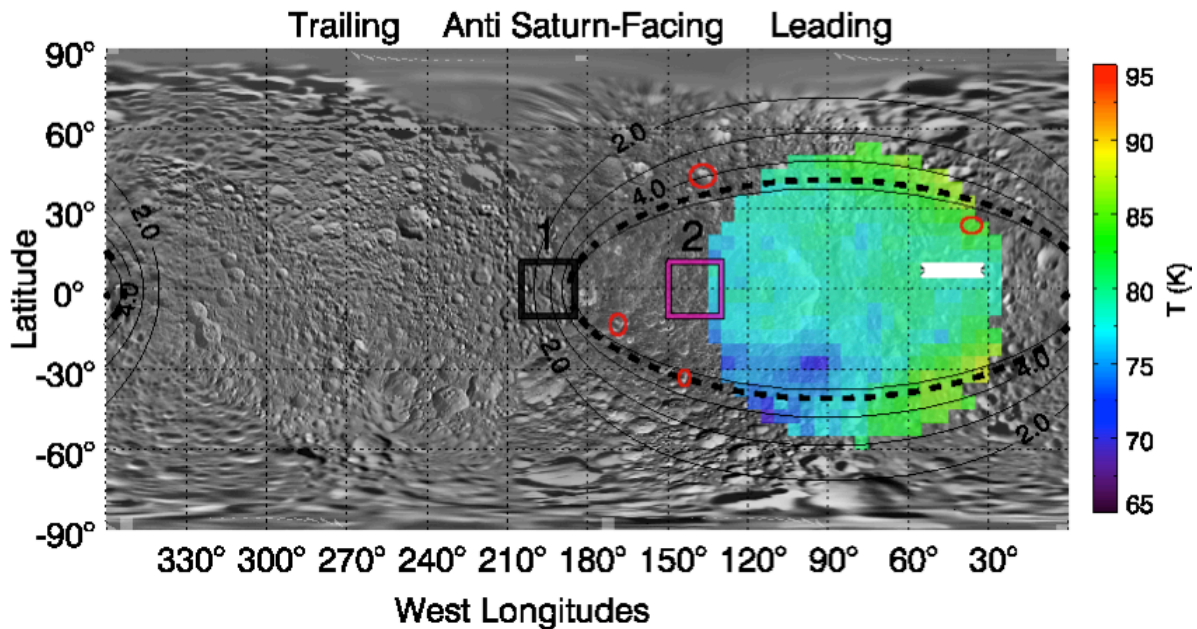


Figure 32 - Surface temperature map of Mimas, produced using Rev 144 data. For full description of this plot see Figure 2 of Howett et al., 2011.

## 5.3 Worked Example 2: Saturn Science

### 5.3.1 Overview

The Cassini Composite Infrared Spectrometer (CIRS) regularly provided 10-1400  $\text{cm}^{-1}$  (7-1000  $\mu\text{m}$ ) observations of Saturn's thermal emission throughout the prime and extended missions, allowing a detailed characterization of the seasonal evolution of the temperature and composition of a giant planet atmosphere. In this section, we describe the various types of Cassini Saturn data and their intended uses, and techniques for analyzing spectra from the three CIRS focal planes (FP1, FP3 and FP4). In general, FP1 is sensitive to tropospheric temperatures and para-hydrogen fraction via the collision induced absorption of  $\text{H}_2$  and He, and to the molecular abundances of phosphine ( $\text{PH}_3$ ), ammonia ( $\text{NH}_3$ ) and methane ( $\text{CH}_4$ ) via their rotational transitions. FP3 is generally used for upper tropospheric temperatures in the 600-680  $\text{cm}^{-1}$  region, and to determine various hydrocarbon species (mainly ethane,  $\text{C}_2\text{H}_6$ , and acetylene,  $\text{C}_2\text{H}_2$ ). Finally, FP4 is used to sound stratospheric temperatures via  $\text{CH}_4$  emission near 1300  $\text{cm}^{-1}$ , and the tropospheric distribution of  $\text{PH}_3$  near 1110  $\text{cm}^{-1}$ . The CIRS range also encompasses a multitude of trace species, isotopologues and aerosol features.

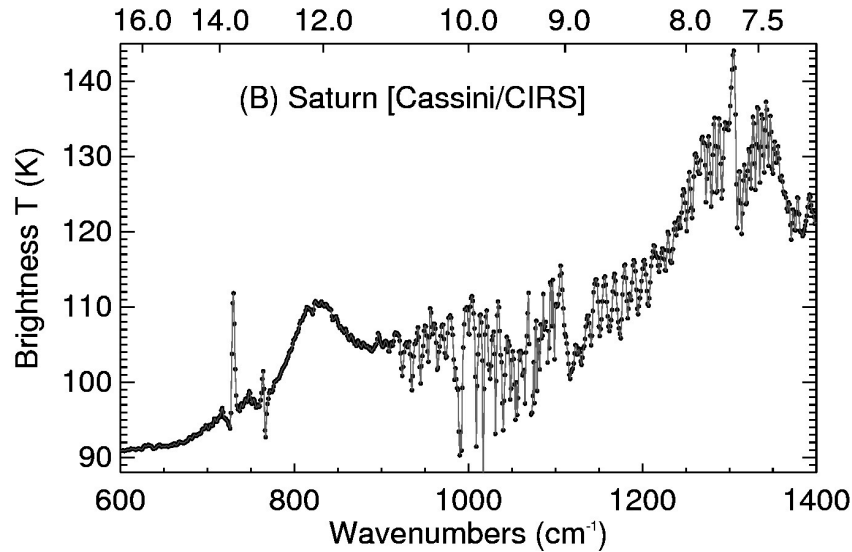


Figure 33: Example of CIRS 2.5 cm<sup>-1</sup> spectra of Saturn using the mid-infrared focal planes, FP3 and FP4. The upper abscissa shows wavelengths in μm. Emission features of CH<sub>4</sub> (7.7 μm), ethane (12.3 μm) and acetylene (13.8 μm) are visible, along with absorptions due to PH<sub>3</sub> and NH<sub>3</sub> (8-11 μm) and the collision-induced continuum of H<sub>2</sub> (15+ μm).

### 5.3.2 Saturn Data Selection

Nadir observations of Saturn come in four ‘flavors’ (excluding regional maps which are sometimes acquired in tandem with other instruments). The type of observations to be used is determined by the particular science application (i.e., temperature mapping, compositional measurements, etc.), with some examples given below. Particular data types can be selected via the RTI (real time interrupt) field, which determines the length of the interferograms, and hence the resolution of the spectrum. Data is collected in both the far- and mid-infrared focal planes simultaneously, despite the names given to the observations.

A useful list of all CIRS (indeed all Cassini observations) is contained in the \*TOL.ASC files contained in the INDEX/ directory of each PDS volume. In this file you can find the start and end date/time for each observation, useful when querying the database for a particular observational type. These date/times first need to be converted into Cassini SCET time (UT seconds since 00:00:00 Jan 1<sup>st</sup> 1970). The data can then be extracted using the following fields:

- SCET times (spacecraft elapsed time based on your selected observation)
- Detector numbers (0 for FP1, 1-20 for FP3, 21-40 for FP4).
- RTI (specifies the spectral resolution, see below).
- Target ID = 699, FOV Targets = 64.
- Select only open-shutter observations (closed-shutter is for calibration only)
- Select only observations with all q-points on the disc (otherwise one risks contamination from deep space).

### Low Resolution Mapping (FIRMAP)

These hemispherical mapping observations, obtained at  $15.0\text{ cm}^{-1}$  spectral resolution (36/37 RTI), are the only ones that provide complete ‘maps’ of Saturn’s thermal emission. All other observations sit and stare at a single latitude as Saturn rotates beneath (useful for high resolution spectroscopy, but not for latitudinal mapping). The FIRMAP observations require short integration times (because of the low spectral resolution), which allows the fields of view to be scanned over Saturn’s disc from a close proximity (17-37  $R_S$ , Saturn radii), providing a spatial resolution of  $6\text{-}8^\circ$  latitude in the far infrared and  $0.5\text{-}2^\circ$  latitude in the mid-infrared. The detectors are scanned from north to south along the central meridian as Saturn rotates either once or twice on its axis, so a full FIRMAP observation takes 10-20 hours as shown in Figure 34.

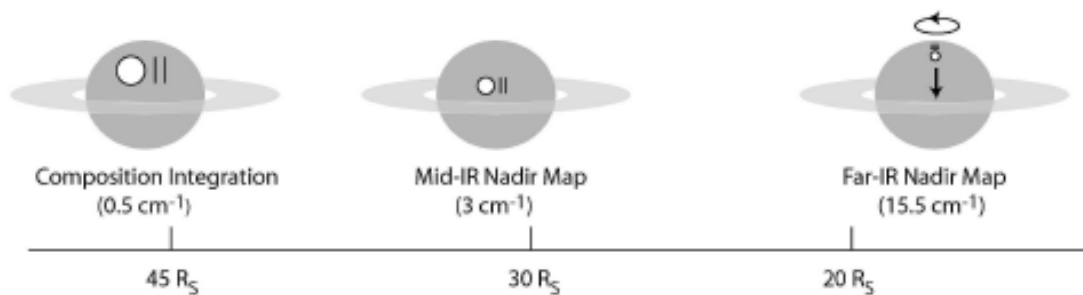


**Figure 34: diagram showing three types of observations used - COMPSIT  $0.5\text{ cm}^{-1}$  ‘sit-and-stare’ integrations at specific latitudes, MIRMAP  $2.5\text{ cm}^{-1}$  integrations using the same technique, and hemispherical FIRMAPs at  $15.0\text{ cm}^{-1}$  resolution where the arrays are scanned north-south over the central meridian.**

FIRMAPs are typically used for mapping atmospheric properties such as the tropospheric temperature and para-hydrogen distributions, as these affect the shape of the hydrogen-helium collisionally-induced continuum between  $250 - 680\text{ cm}^{-1}$  (FP1 and FP3), as well as the stratospheric temperatures from the methane emission in FP4. They also provide some estimate of the distribution of ethane and acetylene from FP3, albeit at a low spectral resolution. An example of a Saturn methane emission map from August 2011 is given in Figure 35.

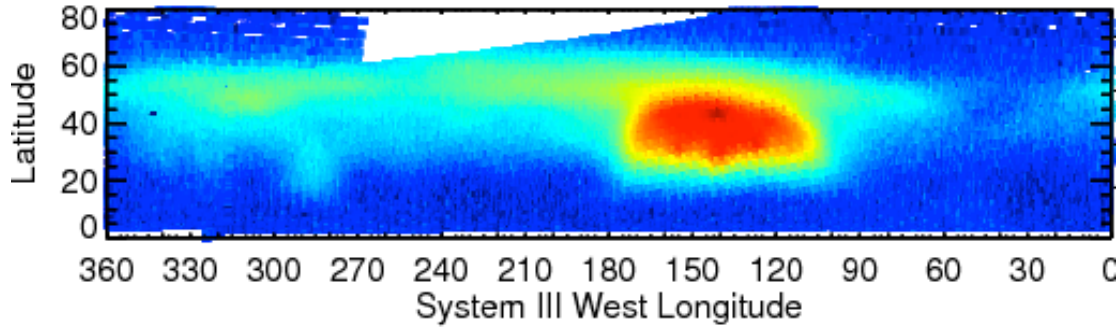


Figure 35: FIRMAPP 15 cm<sup>-1</sup> observations of Saturn's methane emission associated with the eruption of the storm in 2010 (Fletcher et al., 2011). Each FIRMAPP focuses on a single hemisphere, but captures all longitudes.

### Medium Resolution Composition (MIRMAP)

MIRMAPS are obtained by pointing at a single latitude and allowing Saturn's rotation to sweep the arrays over all longitudes. The 2.5 cm<sup>-1</sup> data (RTI 96/97) provide a useful compromise between spatial coverage, spectral resolution and signal to noise characteristics, being obtained from an orbital distance of approximately 30Rs. Latitudinal coverage must be built up slowly over the course of many months of repeated observations (see Fletcher et al., 2009, Icarus), and throughout the course of the Cassini prime and extended missions the latitudes were covered on several occasions.

The ability to resolve spectral features of PH<sub>3</sub>, NH<sub>3</sub>, C<sub>2</sub>H<sub>6</sub> and C<sub>2</sub>H<sub>2</sub> make these observations ideal for coaddition and determination of temperatures and abundances at a single latitude (assuming zonal homogeneity around a latitude circle). Furthermore, because the FP3 and FP4 arrays are oriented north-south during the sit and stare, these observations can be used as rudimentary maps of a 10-degree latitudinal swath (e.g., Figure 36, where two MIRMAPs are shown next to one another).

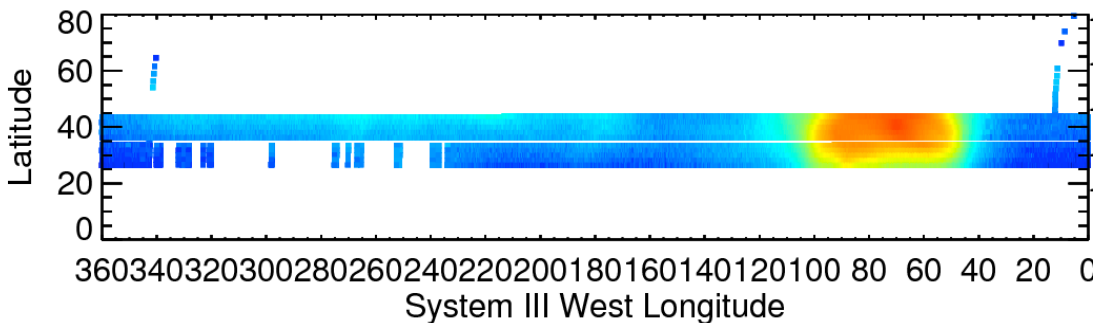
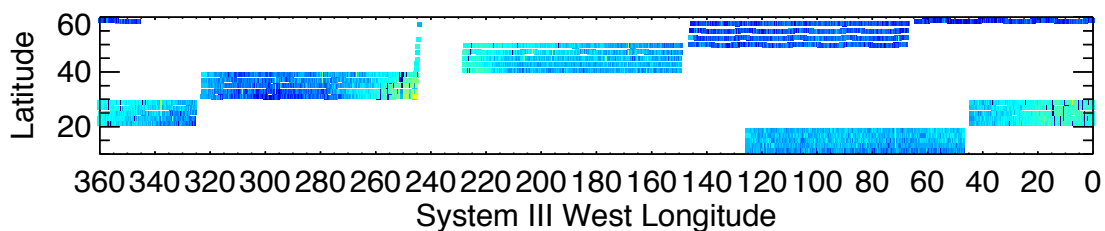


Figure 36: MIRMAPs can also be used to map out contrasts in thermal emission for a narrow latitudinal width. This figure shows two MIRMAPs from July 2011, focusing on methane emission from Saturn's storm.

### Medium Resolution Mapping (MIRTMAP)

From 2009 onwards, a compromise was needed between latitudinal mapping and spectral resolution, because the FIRMAPs were becoming less frequent and could not offer the possibility of tracking seasonal trends in chemical species. The MIRTMAPs have the same spectral resolution as the MIRMAPs ( $2.5\text{ cm}^{-1}$ , RTI 96/97), but are stepped across latitude bands with the arrays oriented north south. The resulting distribution of measurements is shown in Figure 37.



**Figure 37:** Example of MIRTMAP observations at  $2.5\text{ cm}^{-1}$  for the northern hemisphere, showing how the arrays are stepped from north to south as Saturn rotates beneath the spacecraft.

The MIRTMAP observations can be used to determine latitudinal distributions of temperatures,  $\text{PH}_3$ ,  $\text{NH}_3$ ,  $\text{C}_2\text{H}_6$  and  $\text{C}_2\text{H}_2$  at a single epoch, rather than waiting for a latitudinal map to be generated from the sequential MIRMAP observations.

### High Resolution Composition (COMPSIT)

The highest spectral resolution offered by CIRS are the  $0.5\text{ cm}^{-1}$  observations (RTI 400/401), acquired in the same fashion as the MIRMAPs (i.e., sitting and staring at a single latitude). Some COMPSITs use high emission angles to maximize the stratospheric emission from chemical species (i.e., utilizing the limb brightening effect), whereas others use a close-to-nadir geometry to maximize tropospheric absorption features. Long integration times are required to obtain a sufficient signal-to-noise ratio at this high resolution, so interferograms were measured from an orbital distance of 50-60 Rs, leading to an average field of view in the far-IR of  $10^\circ$  latitude, and  $2\text{-}4^\circ$  latitude in the mid-IR. Each observation focused on a single latitude, so north-south coverage must be acquired over many months.

COMPSIT observations are typically coadded for a particular latitude circle to enhance the signal-to-noise, then used to provide precise determinations of vertical temperature and compositional gradients. They are also used to resolve narrow features, such as rotational features of methane and HD or emission due to water and trace hydrocarbons. Many hundreds of spectra must be coadded to achieve a useable signal to noise, so COMPSITs are not suitable for spatial mapping.

#### 5.3.3 Estimation of Spectral Noise

Once the required observation is identified, we need to estimate the uncertainty on the measurements. This can be done in several steps:



- [1] Obtain the CIRS single-scan NESR (noise equivalent spectral radiance) and reduce this by the square-root of the number of target scans added together ( $\sqrt{N}$ ).
- [2] Calculate the standard deviation of the individual scans in the average (also useful for identifying spectral regions prone to noise spikes).
- [3] Calculate the noise on the deep space scans used for calibration (i.e., the CIRS NESR reduced by the number of deep space spectra ( $\sqrt{M}$ )). The number of target spectra typically exceeds the number of deep space calibration spectra, such that this dominates the uncertainty in the radiance.

The final uncertainty is taken to be the larger of [1]+[3] (added in quadrature) or the standard deviation, [2]. Once the spectral uncertainty is defined, one also needs to be aware of possible artifacts in the CIRS data that could corrupt interpretations.

**A note on coaddition:** In producing coadded spectra, it is wise to use data from a single observation type, as shifts in the instrument characteristics can subtly affect the calibration techniques used for each spectrum. So, rather than coadding all 401 RTI spectra for the month of August 2010, for example, it is better to isolate and individually coadd just the dedicated COMPSIT observations during that time period.

#### 5.3.4 Possible Systematic Errors

Below is a non-exhaustive list of some of the pitfalls found in Saturn CIRS data during the prime and extended mission (see also Section 2.5 Electrical interferences (spikes) and other data issues):

- **Clock Spike:** FP1 8-Hz spike (the clock spike) at  $191 \text{ cm}^{-1}$  in FP1, a result of the RTI count (which is  $1/8^{\text{th}}$  of a second). This also has low-power harmonics at 16 Hz ( $382 \text{ cm}^{-1}$ ) and 24 Hz ( $573 \text{ cm}^{-1}$ ), and in FP3 at 32 ( $768 \text{ cm}^{-1}$ ) and 40Hz ( $960 \text{ cm}^{-1}$ ).
- **BIU Spikes:** A repetitive series of 0.5 Hz spikes appear as a comb on the interferograms, resulting from the querying of the CIRS Bus Interface Unit (BIU) by the spacecraft Command Data Subsystem (CDS) every two seconds (every 16 RTIs) to transfer cached CIRS data. The BIU-spikes occur throughout the interferogram with a frequency 0.5 Hz, and are Fourier transformed to a regular comb of spikes in calibrated spectra with a spacing of approximately  $11.9 \text{ cm}^{-1}$ . These spikes were largely removed from 2006 onwards via new calibration techniques.
- **Sine Wave:** A sine ripple occurring on FP1 interferograms, suspected to be from a thermal source, leads to a large spike in calibrated FP1 spectra. Its frequency varies between 1 and 18 Hz over time, so its location is not well defined. Plotting the variance of the FP1 spectra is helpful to avoid regions of the spectrum contaminated by the sine wave.
- **Ripples:** Discontinuities in the interferograms, particularly at the transition between the double-sided region (symmetric about the ZPD) to the unique, single-sided region, and at the ends of interferograms, can cause ripples in calibrated spectra. These ripples are particularly acute in the low signal regions of FP3 ( $900\text{-}1100 \text{ cm}^{-1}$ ), making derivations of the tropospheric gas composition challenging here.

- **Negative FP4 radiances:** Thermal variations and laser mode shifts within the instrument between the times of deep space observations and the target observations can lead to inappropriate calibration references. These manifest themselves as baseline shifts for the radiances, and these are particularly visible in the 1100-1250  $\text{cm}^{-1}$  region of FP4. If the radiances are largely negative in this region, then the spectra are corrupt and a special calibration is required.
- **FP1 short-wavenumber issues:** The 10-50  $\text{cm}^{-1}$  region of FP1 may be prone to distortions associated with an as-yet unidentified thermal effect, leading to radiances and brightness temperatures which are non-physical. It is recommended to use this region in a line-to-continuum mode only (see Section "3.7.2 FP1 Long Wavelength Calibration").

### 5.3.5 Data Analysis

Once all sources of noise and systematic errors are accounted for, we proceed with inversion of the spectra to determine atmospheric temperatures and chemical composition. Several inversion techniques are available, including the multi-purpose NEMESIS optimal estimation retrieval code developed by Pat Irwin and colleagues at the University of Oxford (Irwin, 2008). The first-order product, whether it is from a spatially resolved FIRMAP observation, or a co-added MIRMAP/COMPSIT observation at a single latitude, will be the temperature field from the troposphere to stratosphere. These are then fixed and used to derive molecular abundances of a host of tropospheric and stratospheric species.

#### *Temperature Retrievals*

Figure 38 shows Saturn's mean zonal temperature field from the Cassini prime mission, 2004-2008, assembled by coadding all available FIRMAP observations (see Section 2.3.1). Tropospheric temperatures were derived from the 100-600  $\text{cm}^{-1}$  region of FP1, which provide a lower spatial resolution dataset that can then be updated with the higher spatial resolution of FP3 and FP4. Thus the FP3 600-680  $\text{cm}^{-1}$  spectrum (collision induced  $\text{H}_2$  absorption, sensitive to 80-200 mbar) and the FP4 1250-1350  $\text{cm}^{-1}$  spectrum (methane emission from the 0.5-10 mbar range) are used simultaneously to constrain the upper troposphere and stratosphere. Note that a good first-guess stratospheric profile is useful when retrieving temperatures from FP1, as the peaks of the collision induced absorption do have some sensitivity to lower stratospheric temperatures.



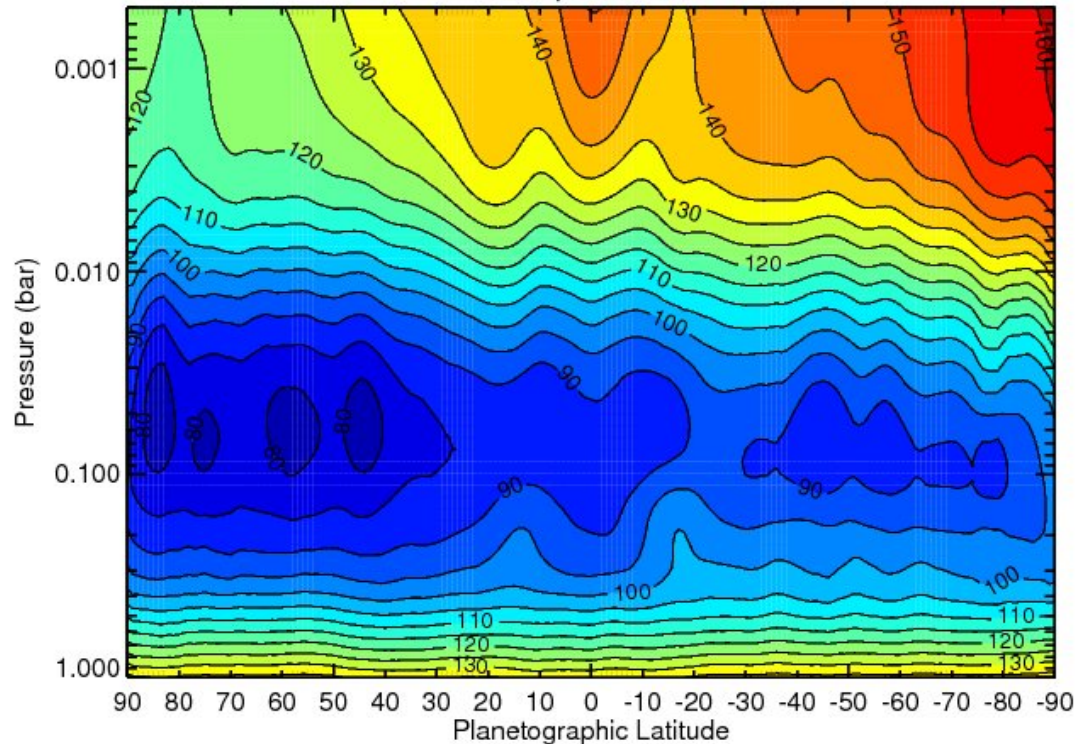


Figure 38: Saturn's temperature field derived from a co-addition of all available FIRMAP observations from the prime mission. The region between 10-80 mbar is a smooth interpolation between the two regions of CIRS sensitivity. Temperatures below 800 mbar are a smooth relaxation back to the a priori profile. See (Fletcher L. N., 2010) for details.

### Compositional Retrievals

Provided that the temperature profiles are defined for the vertical range of interest, gaseous composition can then be adjusted to fit emission and absorption features. Typical species of interest include  $\text{PH}_3$  (a disequilibrium tracer of tropospheric dynamics),  $\text{NH}_3$  (a condensable species in the upper troposphere, used to assess cloud condensation processes);  $\text{CH}_4$  (well-mixed, so can be used to estimate the C/H, D/H and  $^{12}\text{C}/^{13}\text{C}$  ratios in Saturn's bulk) and hydrocarbon species (principally  $\text{C}_2\text{H}_6$  and  $\text{C}_2\text{H}_2$ ). Trace species are also present and can be investigated in spectra with many thousands of coadded observations. Three different techniques are suggested, depending on the spectral resolution of the selected data (low resolutions limit the information content in a spectrum) and the desired speed of the spectral inversion:

- [1] Scaling reference profiles: Either obtain a theoretical profile for a species (e.g., the saturated vapour profile, or a photochemical profile) and scale it to fit the data.
- [2] Parametric profiles: For some species, define the profile in terms of a deep mole fraction, a reference pressure, and a fractional scale height above that level (the ratio of the gas scale height to that of the atmosphere). This technique has been successfully used for  $\text{PH}_3$  on Jupiter and Saturn (Figure 39) (Fletcher L. N., Phosphine on Jupiter and Saturn from Cassini/CIRS, 2009)

[3] Continuous profiles: For high spectral resolution data where multiple transitions are resolved, it is appropriate to derive a continuous vertical profile of species (e.g., ethane and acetylene) defined on multiple levels. This technique was used by (Howett C. e., 2007).

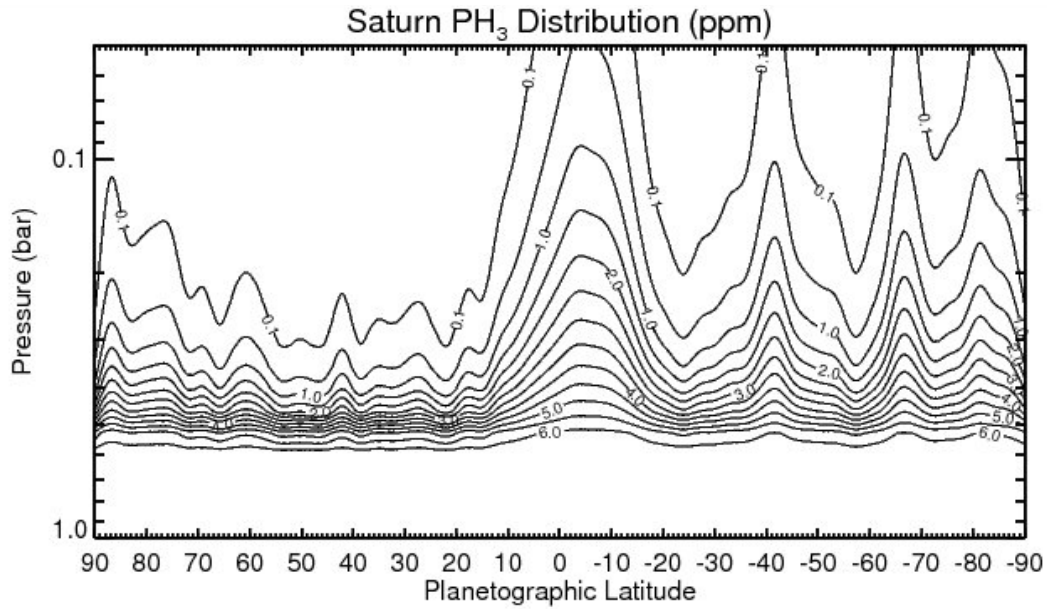


Figure 39: The meridional distribution of PH<sub>3</sub> derived from CIRS 1100-1200 cm<sup>-1</sup> FP4 observations at 2.5 cm<sup>-1</sup> using a parameterized profile (Fletcher L. N., Phosphine on Jupiter and Saturn from Cassini/CIRS, 2009).



## Further Information Sources

Hopefully, this document contains the majority of the information you are looking for. If not, please contact a CIRS representative listed in “Appendix E. Contact Information”, so long as the mission is continuing. After that time, someone at the PDS Atmospheres node may be able to help.



## Bibliography

- Achterberg, R. K., et al. (2011). Temporal variations of Titan's middle-atmospheric temperatures 2004-2009 observed by Cassini/CIRS. *Icarus*, 211, 686-698.
- Acton, C. (1996). Ancillary Data Services of NASA's Navigation and Ancillary Information Facility. *Planetary and Space Science*, 44, 65-70.
- Brasunas, J. C. (2002). Phase anomalies in Fourier-Transform Spectrometers: an absorbing beam splitter is neither sufficient nor necessary. *Applied Optics*, 41(13), 2481-2487.
- Carlson, R. C. et al. (2005). Vector Radiometric Calibration Model for the Cassini Composite Infrared Spectrometer (CIRS). OSA FTS Conference, Alexandria, VA.
- Coustenis, A. et al. (2010). Titan Trace Gaseous Composition From CIRS At The End of The Cassini-Huygens Prime Mission. *Icarus*, 207, 461-476.
- Flasar, F. M. et al. (2004). Exploring the Saturn System in the Thermal Infrared: The Composite Infrared Spectrometer. (C. Russell, Ed.) *Space Science Reviews*, 115 (1-4), 169-297.
- Fletcher, L. N. et al. (2009). Phosphine on Jupiter and Saturn from Cassini/CIRS. *Icarus*, 202(2), 543-564.
- Fletcher, L. N. et al. (2010). Seasonal change on Saturn from Cassini/CIRS observations 2004-2009. *Icarus*, 208(1), 337-352.
- Fletcher, L. N. et al. (2011). Thermal Structure and Dynamics of Saturn's Northern Springtime Disturbance. *Science*, 332, 1413-1417.
- Goody, R. M., and Yung, Y. L. (1989). *Atmospheric Radiation* (Second ed.). Oxford: Oxford University Press.
- Hanel, R. A. et al. (2003). *Exploration of the Solar System by Infrared Remote Sensing* (Second ed.). Cambridge: Cambridge University Press.
- Howett, C. J. A. et al. (2007). Meridional variations in stratospheric acetylene and ethane in the southern hemisphere of the Saturnian atmosphere as determined from Cassini/CIRS measurements. *Icarus*, 190, 556-572.
- Howett, C. J. A. et al. (2011). A high amplitude thermal inertia anomaly of probable magnetospheric origin on Saturn's moon Mimas. *Icarus*, 216, 221-226.
- Irwin, P. G. J. et al. (2008). The NEMESIS planetary atmosphere radiative transfer and retrieval tool. *JQSRT*, 109, 1136-1150.

Kunde, V. G. et al. (1996). Cassini infrared Fourier spectroscopic investigation. *Proc. SPIE* , 2803, 162-177.

Liou, K. N. (2002). *An Introduction to Atmospheric Radiation* (Second edition). Academic Press, San Diego.

Nixon, C. A. et al. (2009). Infrared Limb Sounding of Titan with Cassini CIRS. *Applied Optics* , 48 (10), 1912-1925.

Nixon, C. A. et al. (2009). Titan's Prolific Propane: The Cassini CIRS Perspective. *Planetary and Space Science* , 57, 1573-1585.

Press, W. H. et al. (2007). *Numerical Recipes in C++* (Third Edition). Cambridge University Press, Cambridge.

Rodgers, C. D. (2000). *Inverse Methods For Atmospheric Sounding* (First ed.). Singapore: World Scientific.

Teanby, N. A. et al. (2010). Mapping Titan's HCN in the far infrared: implications for photochemistry. *Faraday Discussions*, 147, 51-64.

Teanby, N. A., and Irwin, P. G. J. (2007). Quantifying the effect of finite field of view size on radiative transfer calculations of Titan's limb spectra measured by Cassini CIRS. *Astrophysics and Space Science* , 310, 293-305.

## Appendix

### A. Example PDT Designs For Observations

In this section we show example screenshots for the design of CIRS observations using the Cassini PDT software. Detailed descriptions are given in Section “2.3 Observation Strategies”.

#### A.1 SATURN

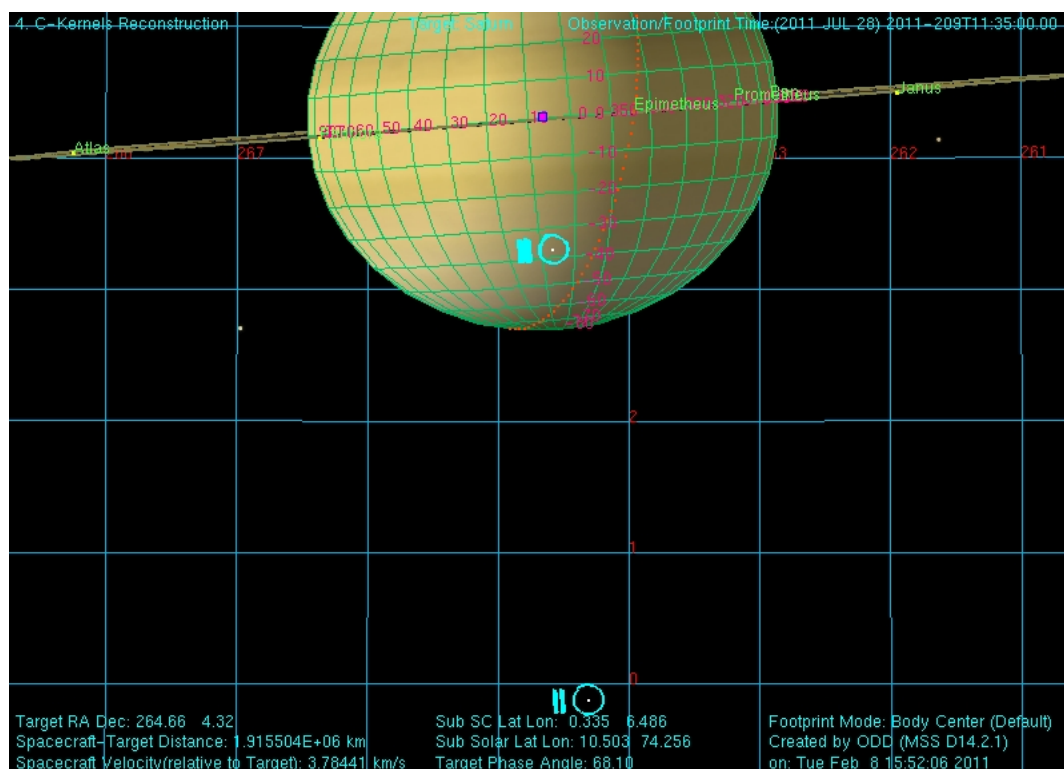


Figure 40: COMPSIT with the focal planes on the central meridian. Also shows the deep space position.



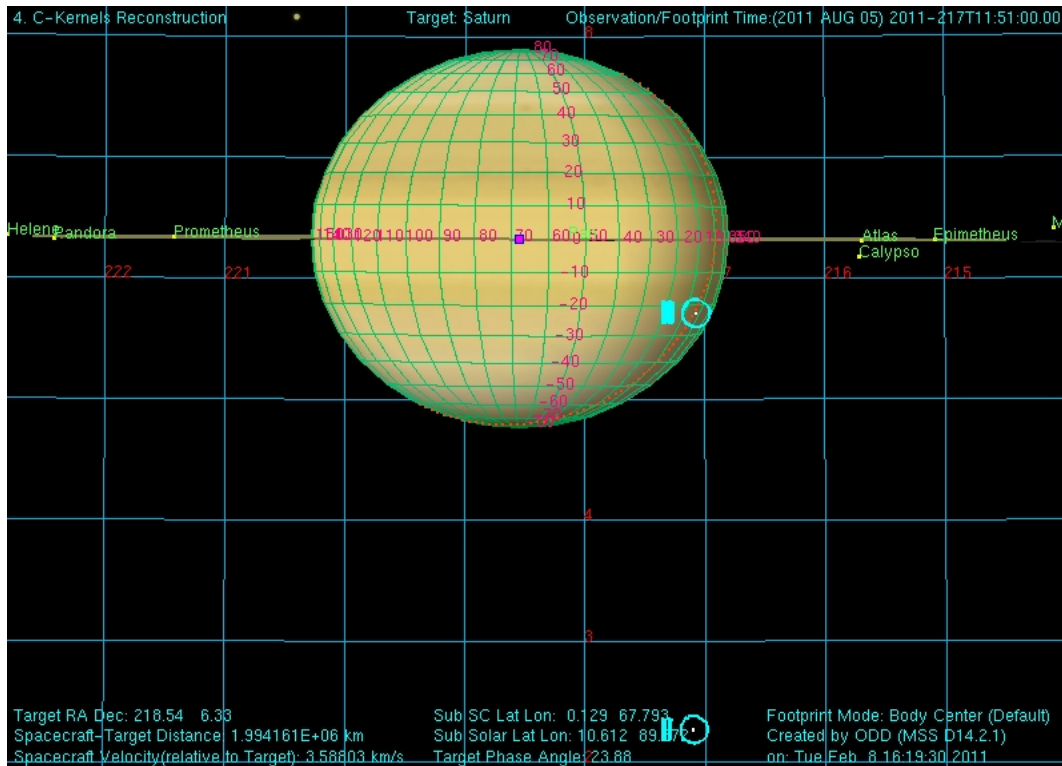


Figure 41: COMPSIT with FP1 offset for high emission angle studies. Also shows deep space position.

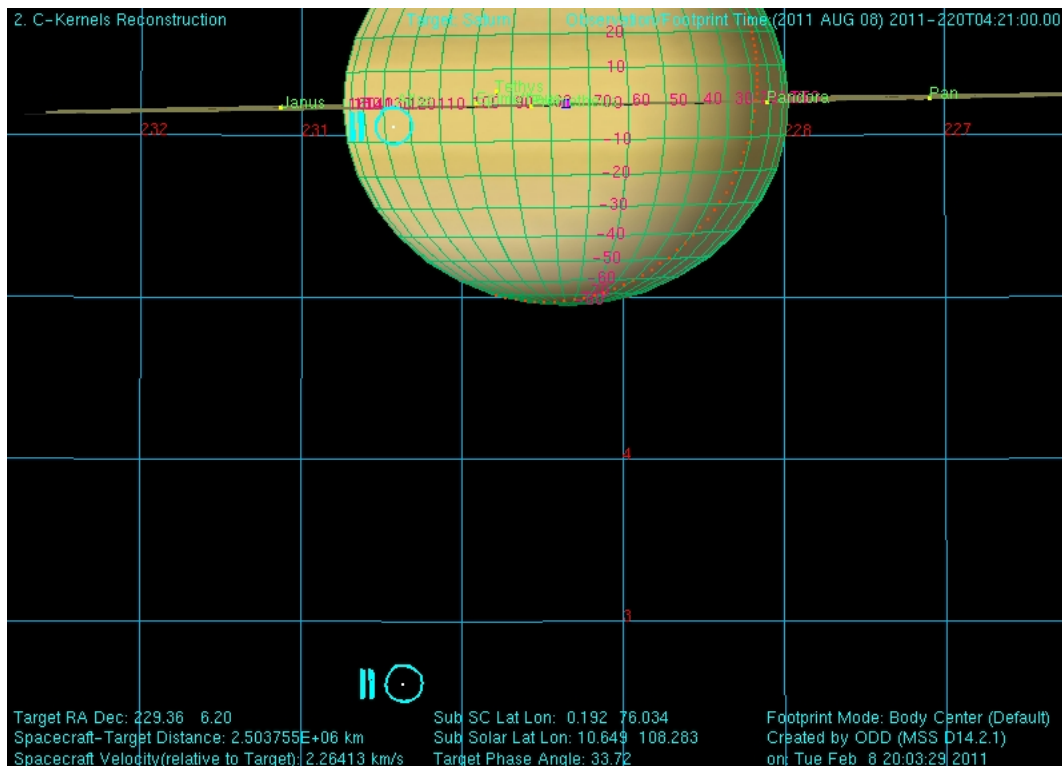


Figure 42: COMPSIT with FP3 offset for high-emission angle studies. Also shows deep space position.

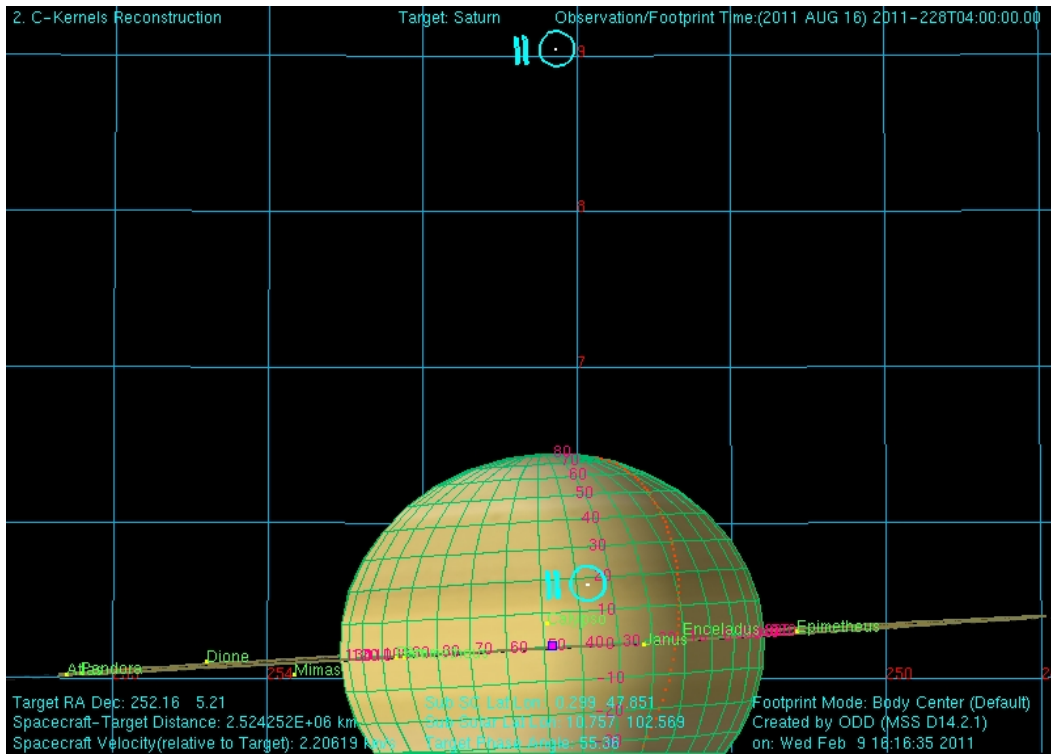


Figure 43: MIRMAPP on the central meridian. Also shows deep space position.

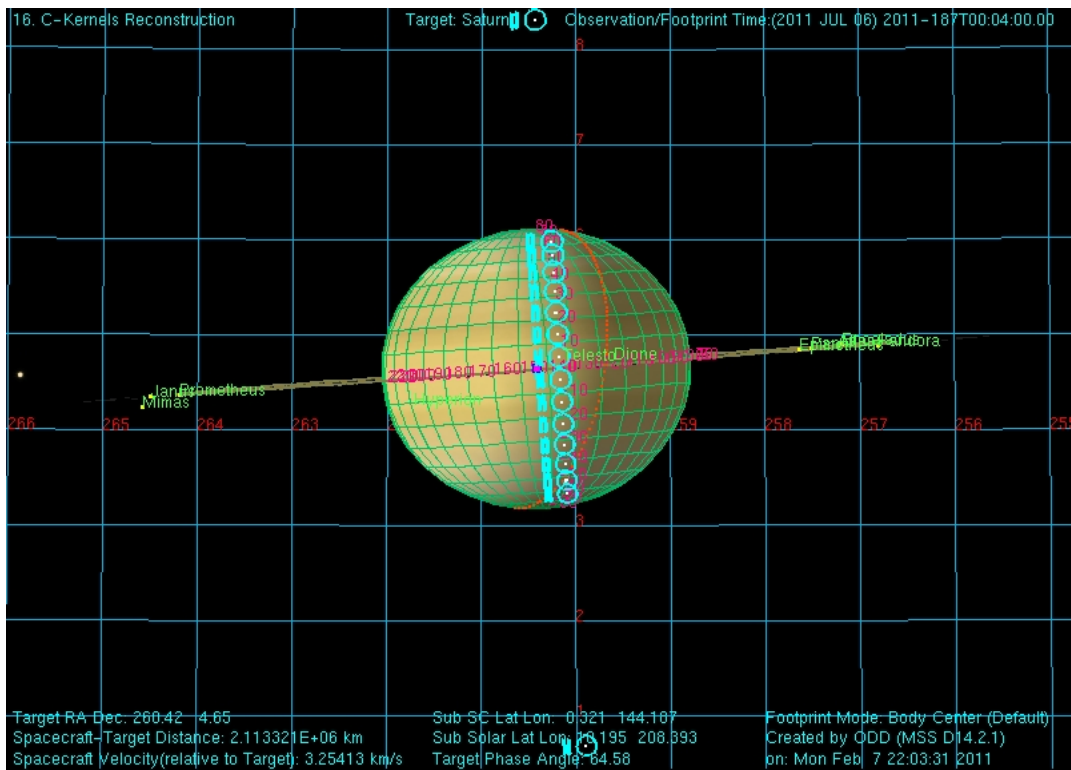


Figure 44: MIRMAPP with focal planes at multiple latitude positions on the central meridian. Also shows the deep space positions.

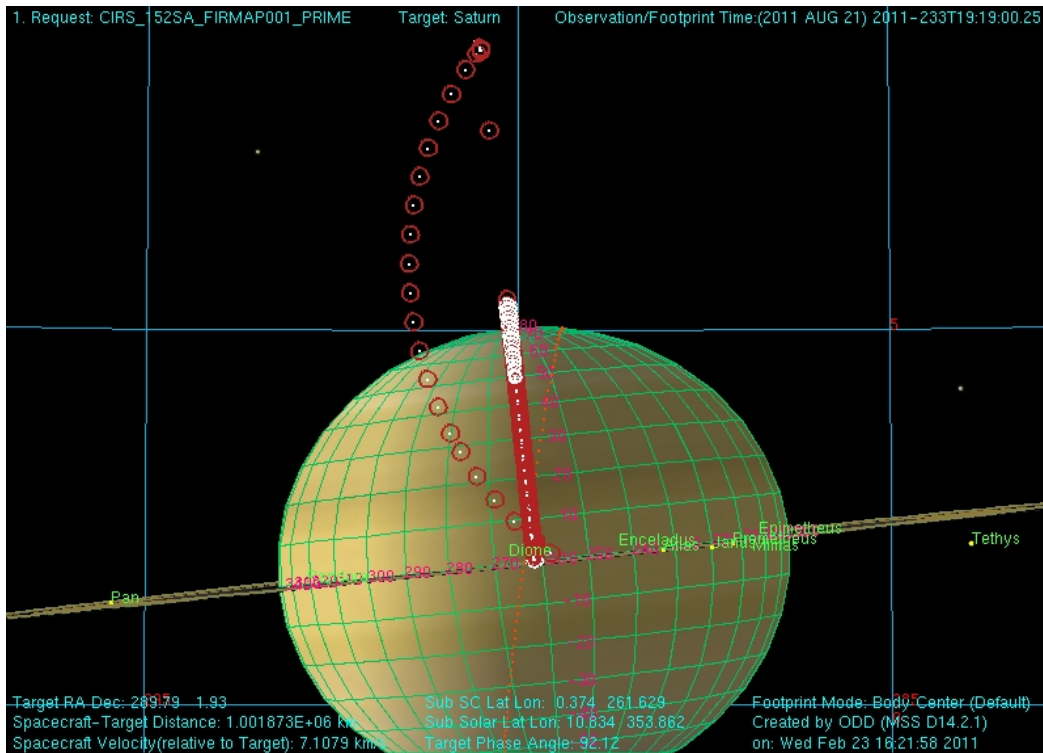


Figure 45: FIRMAP showing the targeting positions and deep space position.

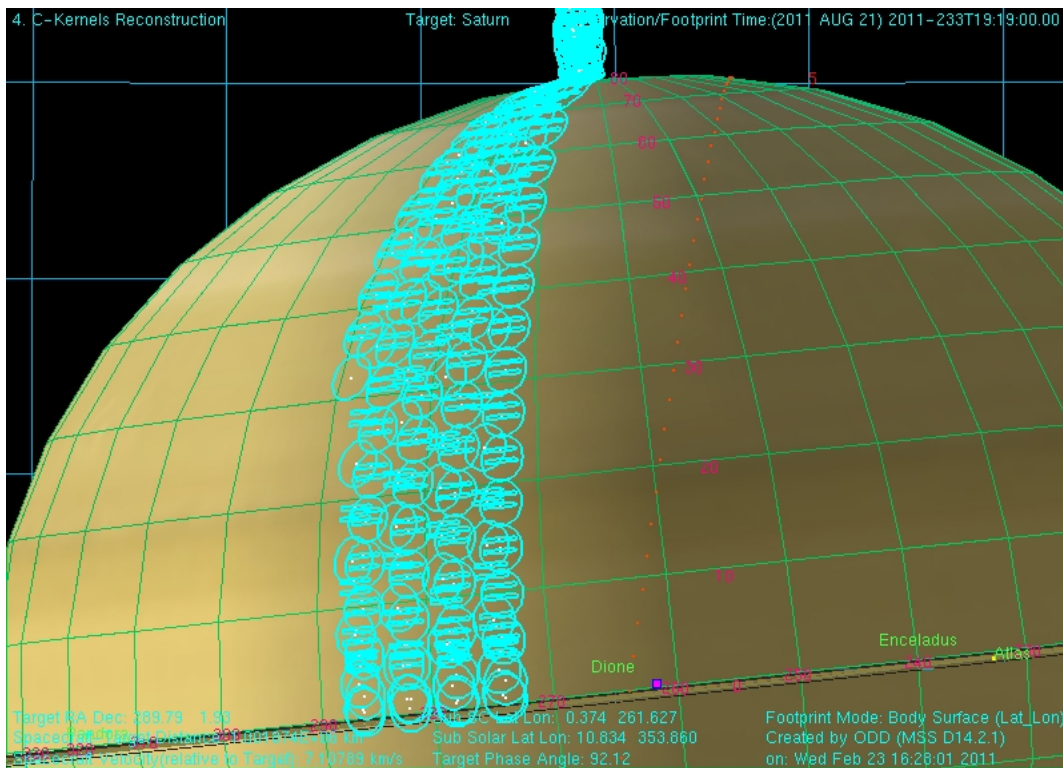


Figure 46: FIRMAP showing the focal planes for part of an observation. This shows the slewing across the northern hemisphere.

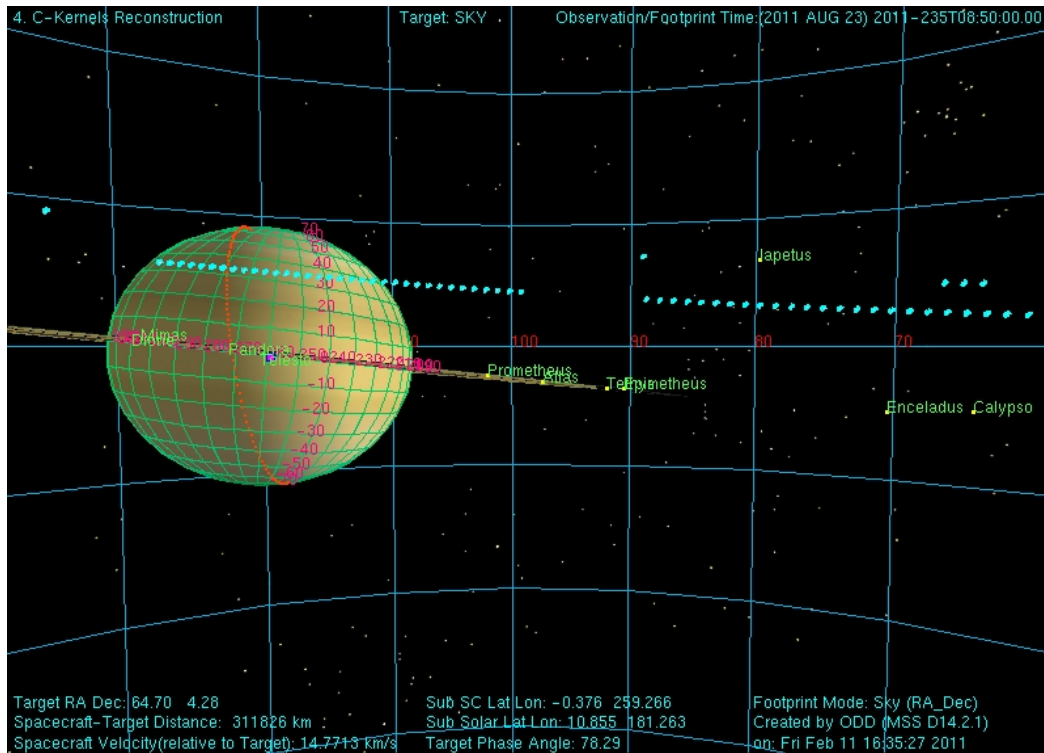


Figure 47: LIMBINT showing the entire observation and deep space position. Please note that LIMBMAP's also look like this except they have many target latitudes.

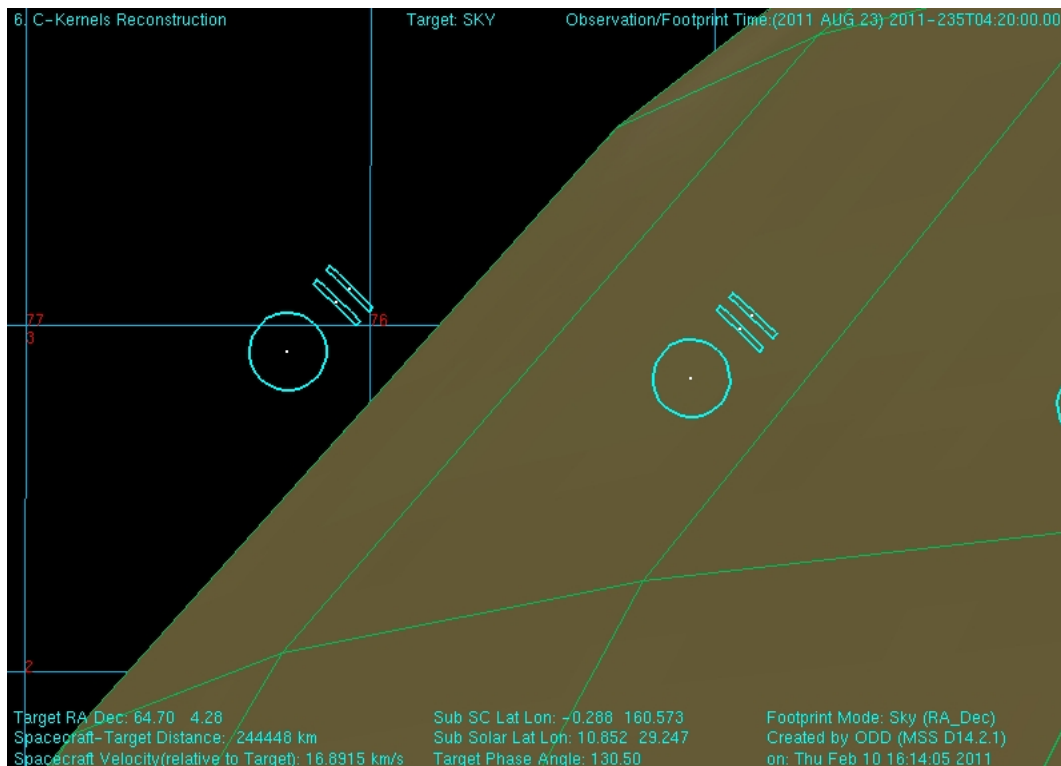


Figure 48: LIMBINT at altitude position 1. Focal planes are oriented normal to the local latitude limb to sound the first altitude position. This will be the same for LIMBMAP's.

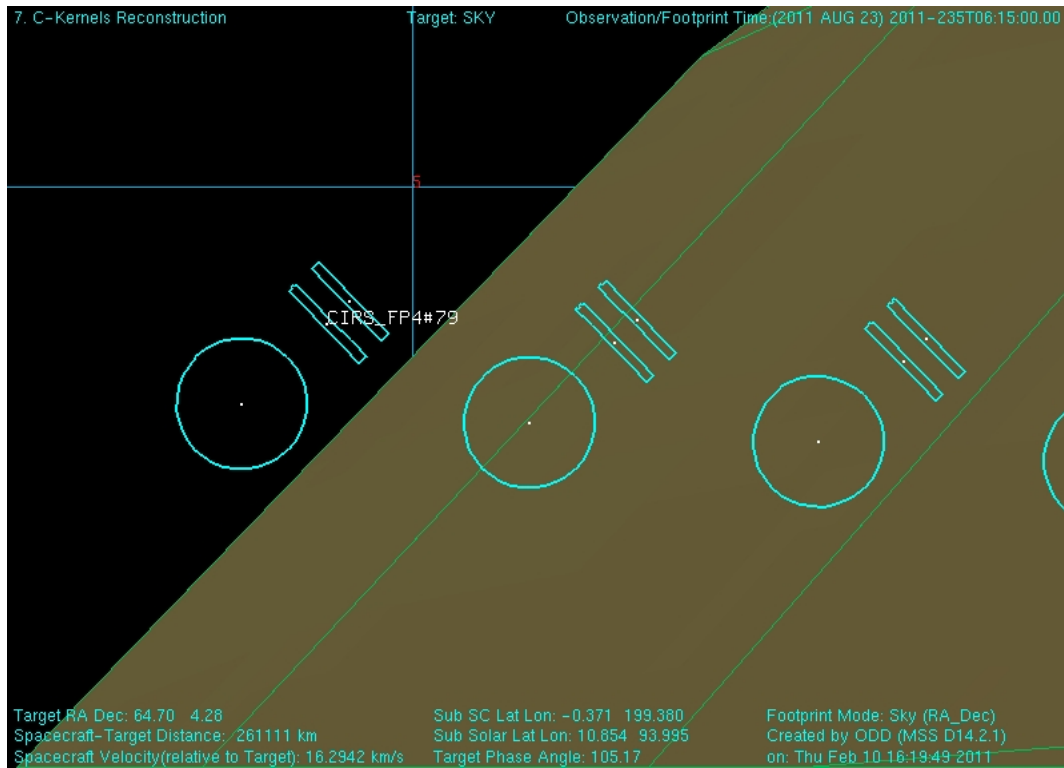


Figure 49: LIMBINT at the second altitude position.

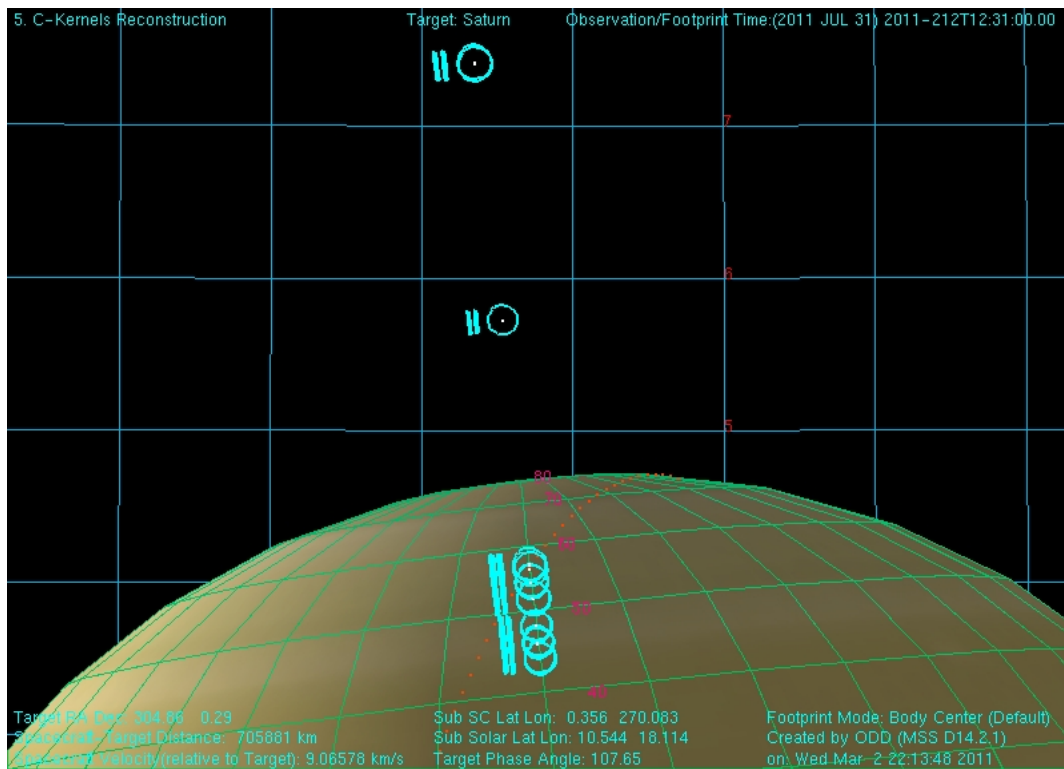


Figure 50: NADIROCC shown along with the deep space positions.

## A.2 RINGS

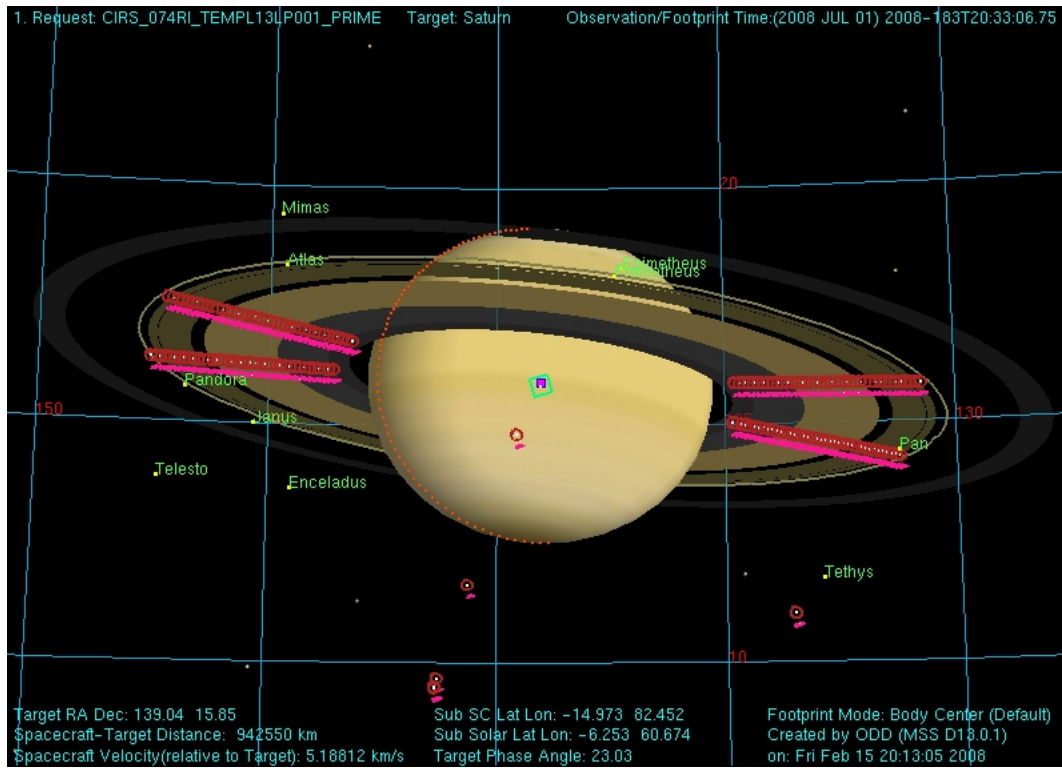


Figure 51 - A TEMP, CIRS\_074RI\_TEMPL13LP001\_PRIME, showing four radial scans taken from a relatively low spacecraft emission angle.



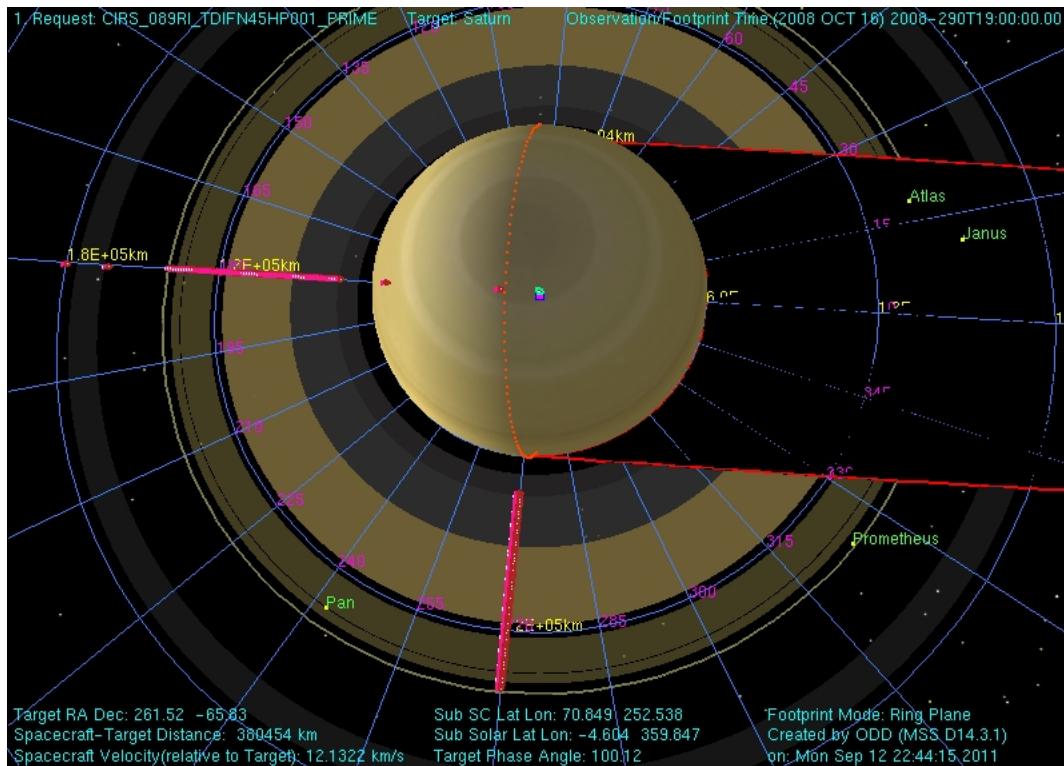


Figure 52 - A TDIF, CIRS\_089RI\_TDFN45HP001\_PRIME.

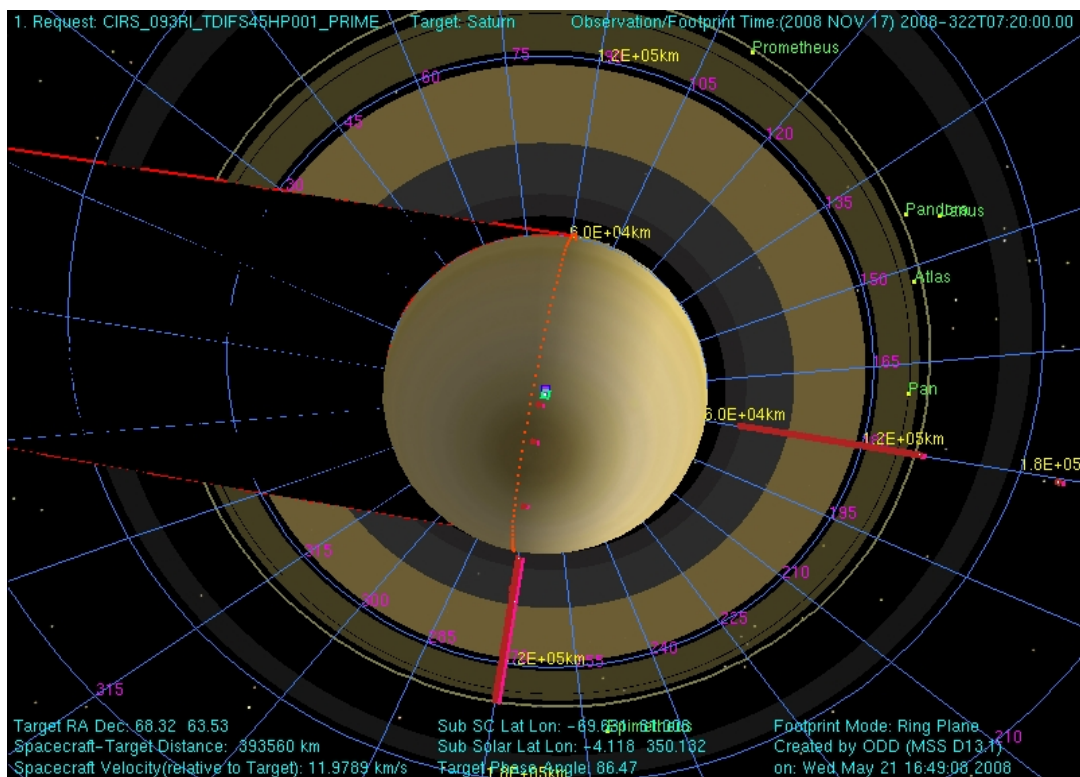


Figure 53 - A TDIF is composed of two scans: one on the lit side of the rings, the other on the unlit side of the rings but with an otherwise comparable geometry. In this case the rings have been scanned at a local hour angle of 12h and 18h from both the lit and unlit side of the rings.

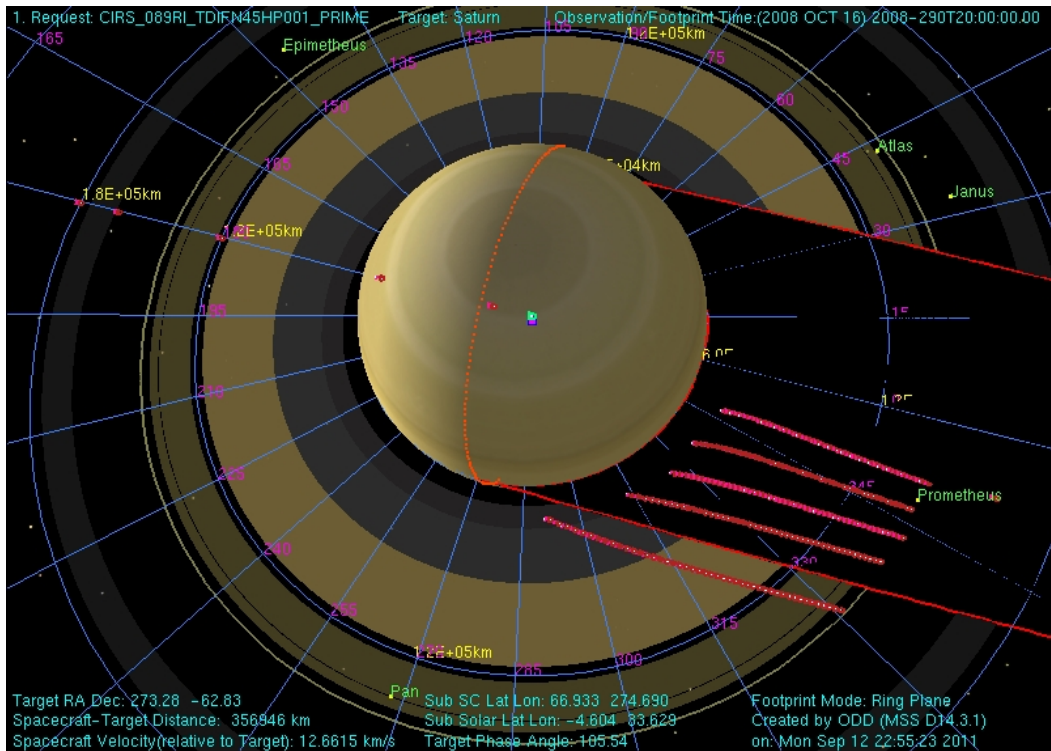


Figure 54 - Temperatures within Saturn's shadow are measured by scanning the FP1 detector in the vicinity of and within the planet's shadow. Each point in each scan is offset in longitude from the edge of the planet's shadow by an amount determined by the distance of that point from Saturn. The time it would take a ring particle moving on a circular Keplerian orbit to traverse the longitudinal offset at a given radial distance is identical across an individual scan. Offsets used in these PSHAD scans can be calculated relative to the egress or ingress shadow boundary.

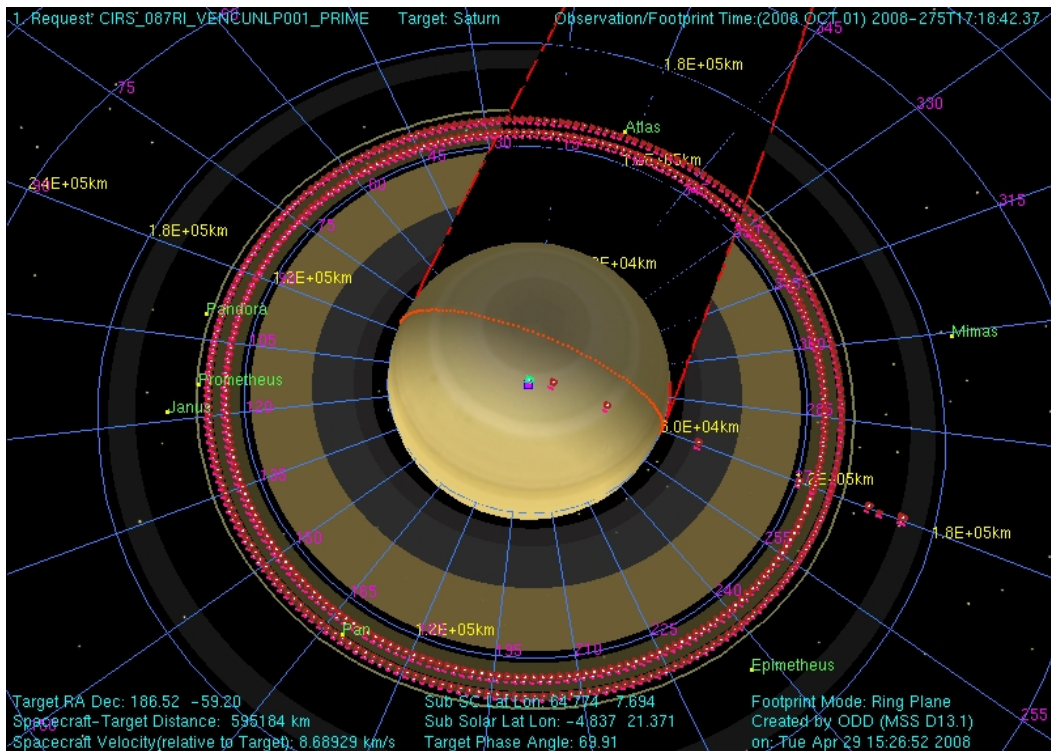




Figure 55 - Azimuthal scans reveal temperature variations in the course of an orbit around Saturn. Due to RBOT considerations, such long duration azimuthal scans are no longer performed.

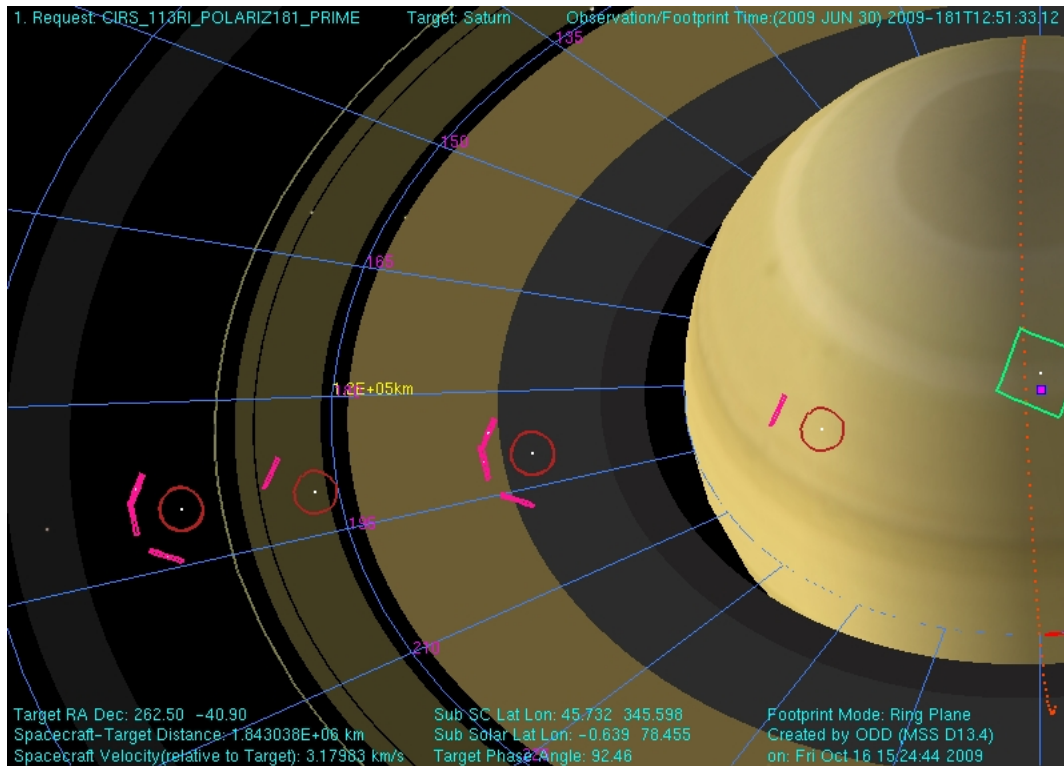


Figure 56 - During POLARIZ observations CIRS integrates on the rings from three distinct orientations in order to look for any polarization in the signal originating from the rings. The outer C ring is being targeted in CIRS\_113RI\_POLARIZ181\_PRIME. Deep space spectra are also obtained at the same three spacecraft orientations.

## A.3 TITAN

Figure 57: T6 FIRLMBT

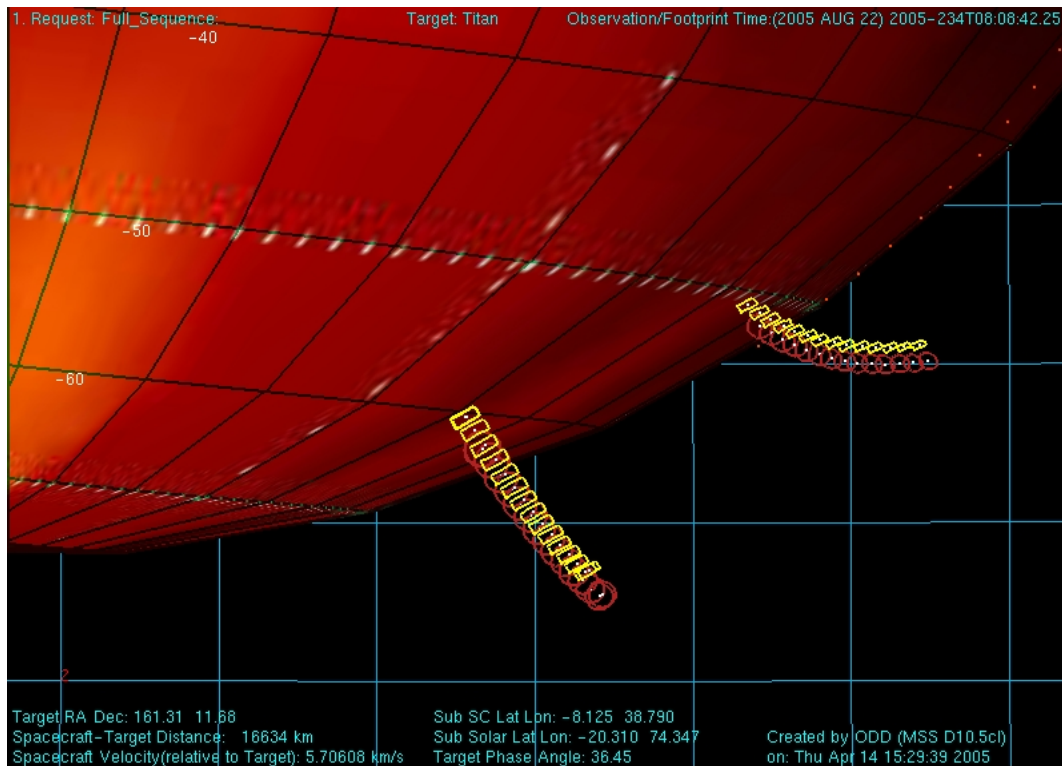


Figure 58: T6 FIRLMB AER

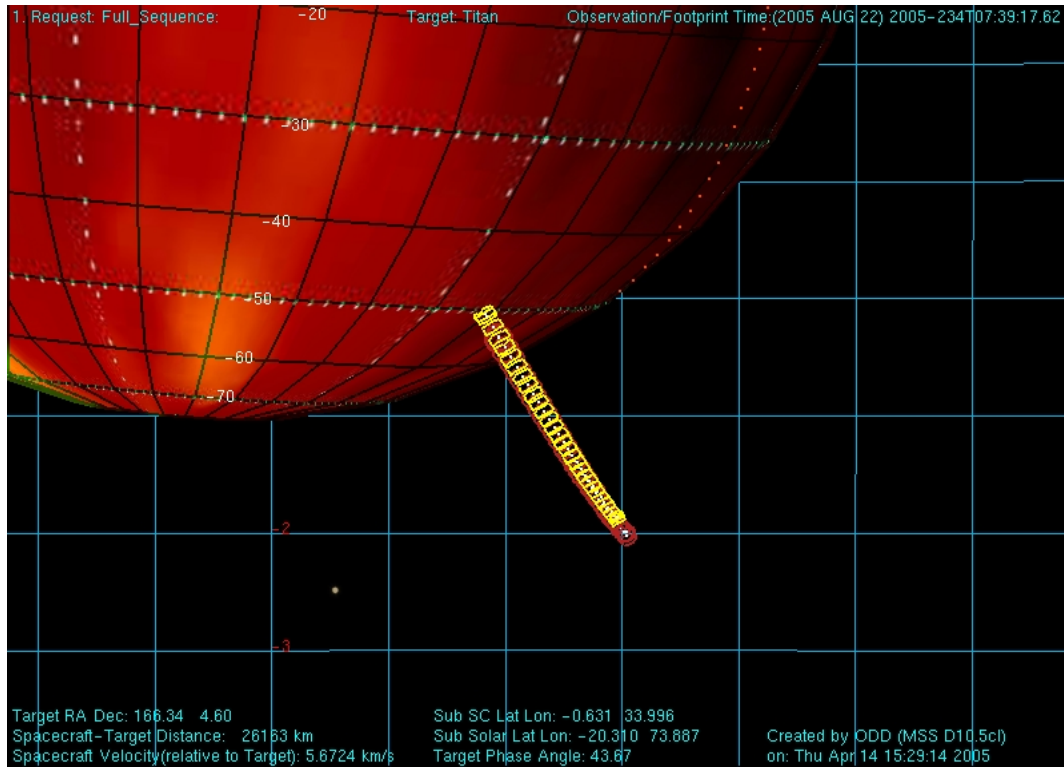


Figure 59: T6 FIRLMB INT

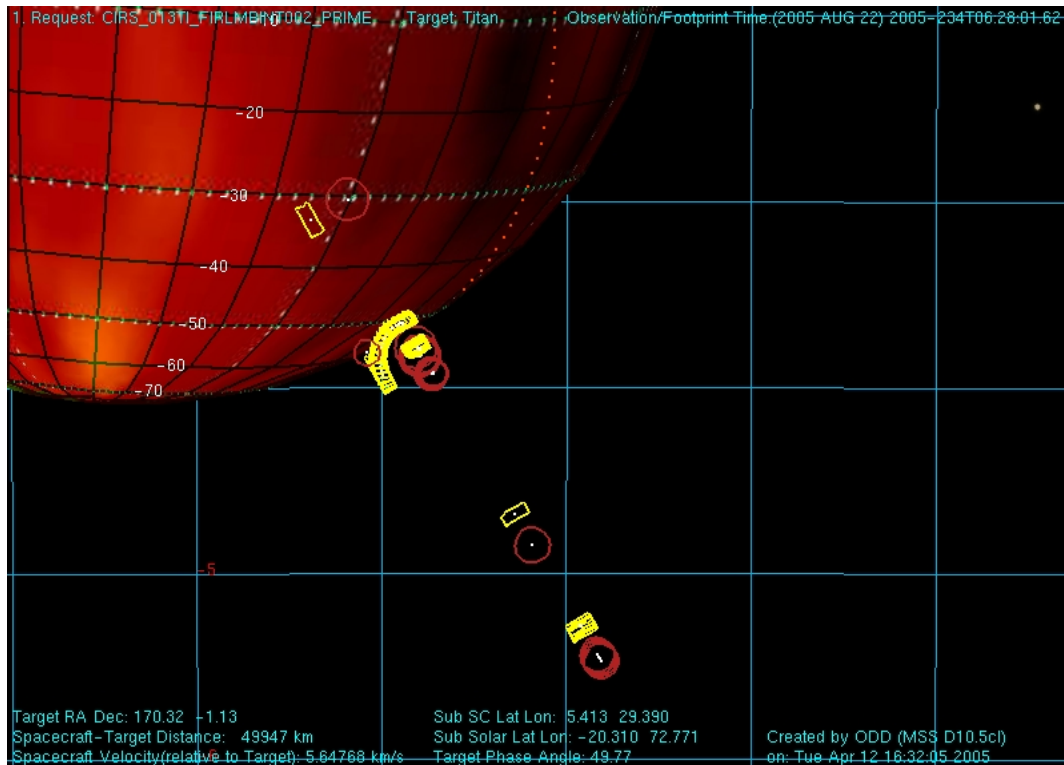


Figure 60: T6 FIRNADMAP

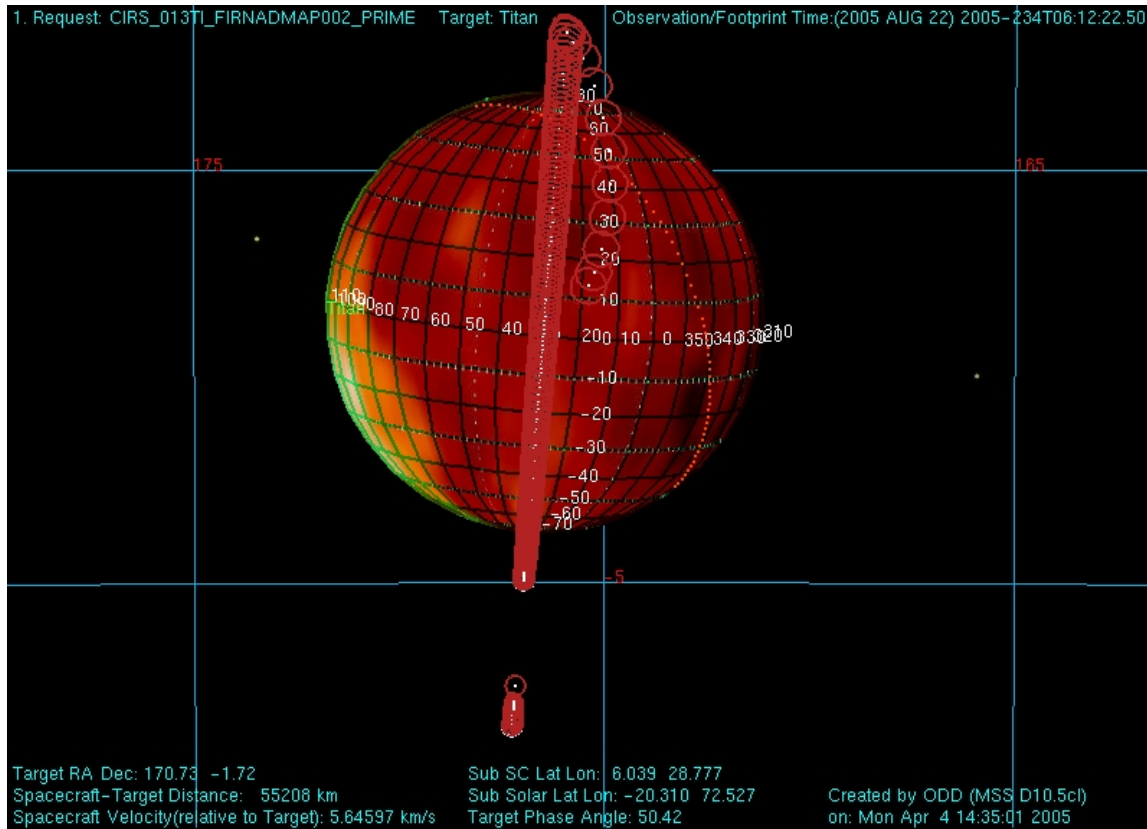


Figure 61: T6 MIRLMBINT

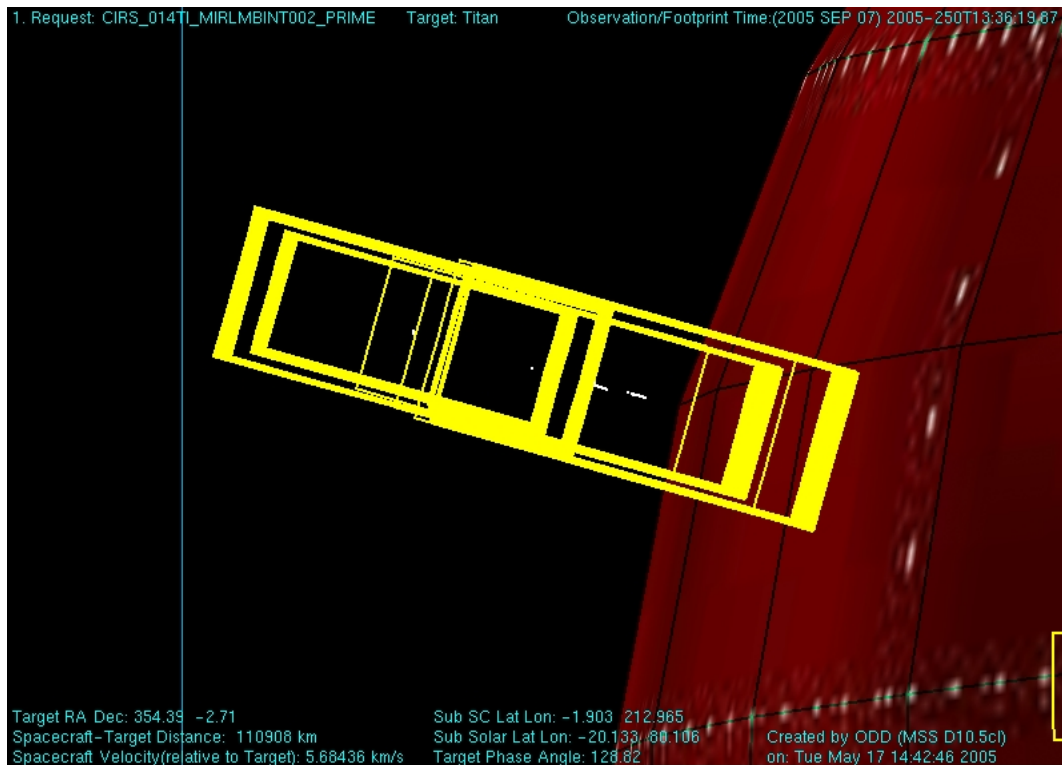


Figure 62: T6 MIRLMBMAP

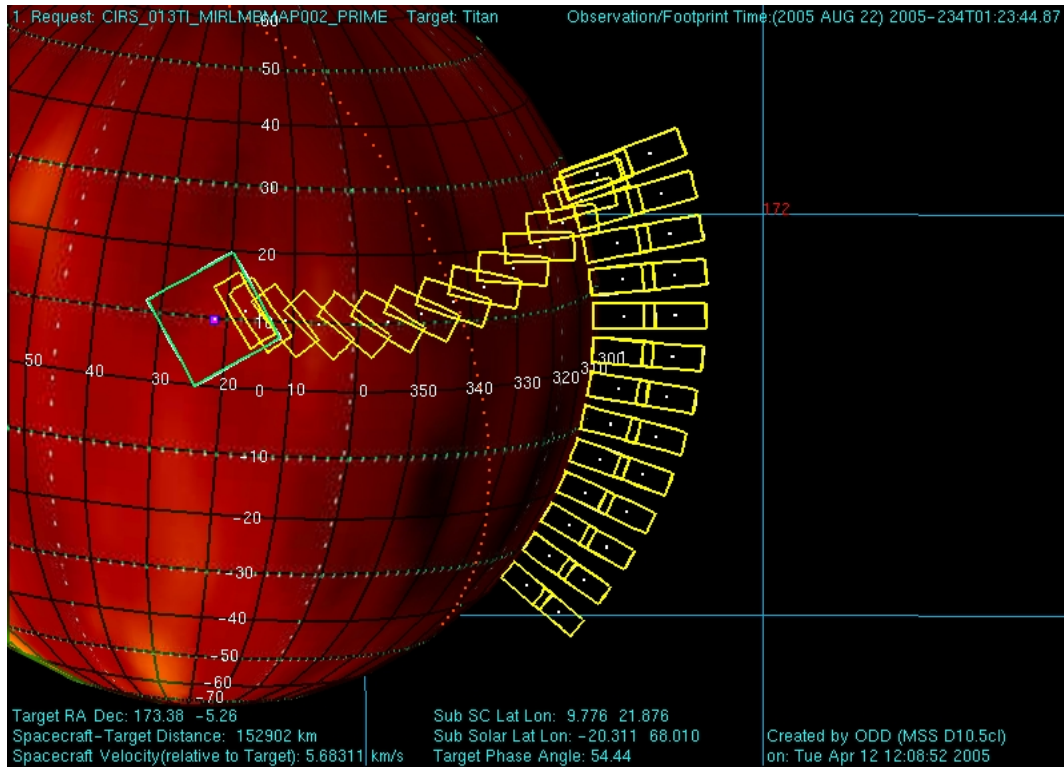
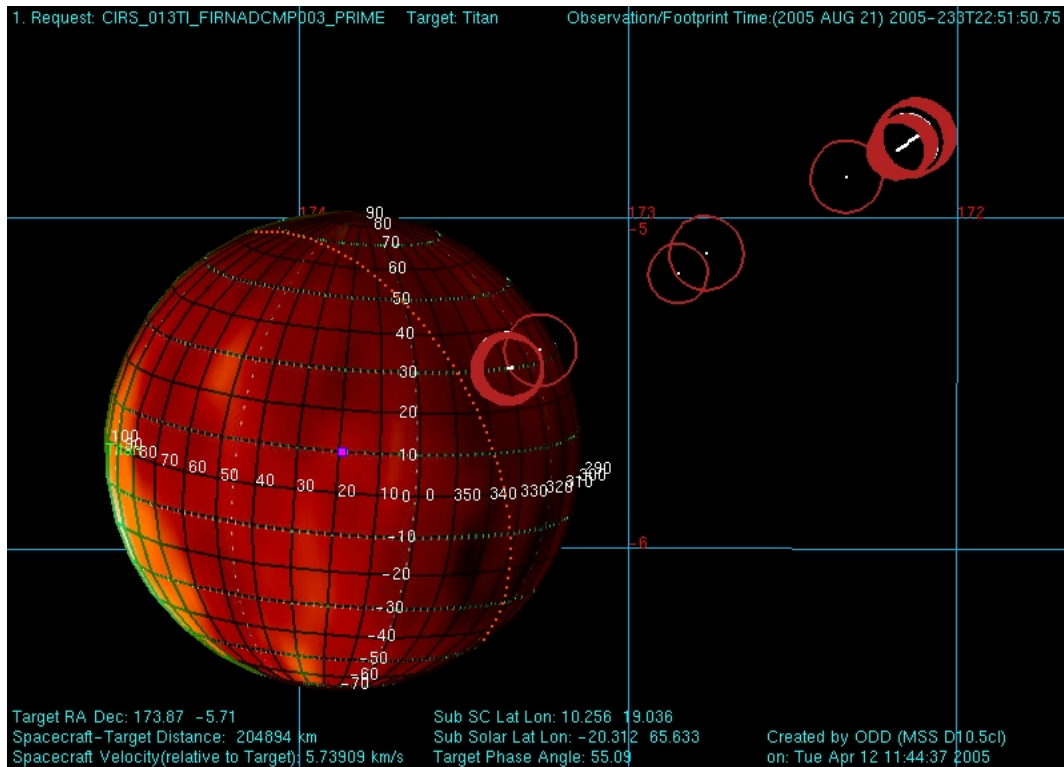


Figure 63: T6 FIRNADCMP



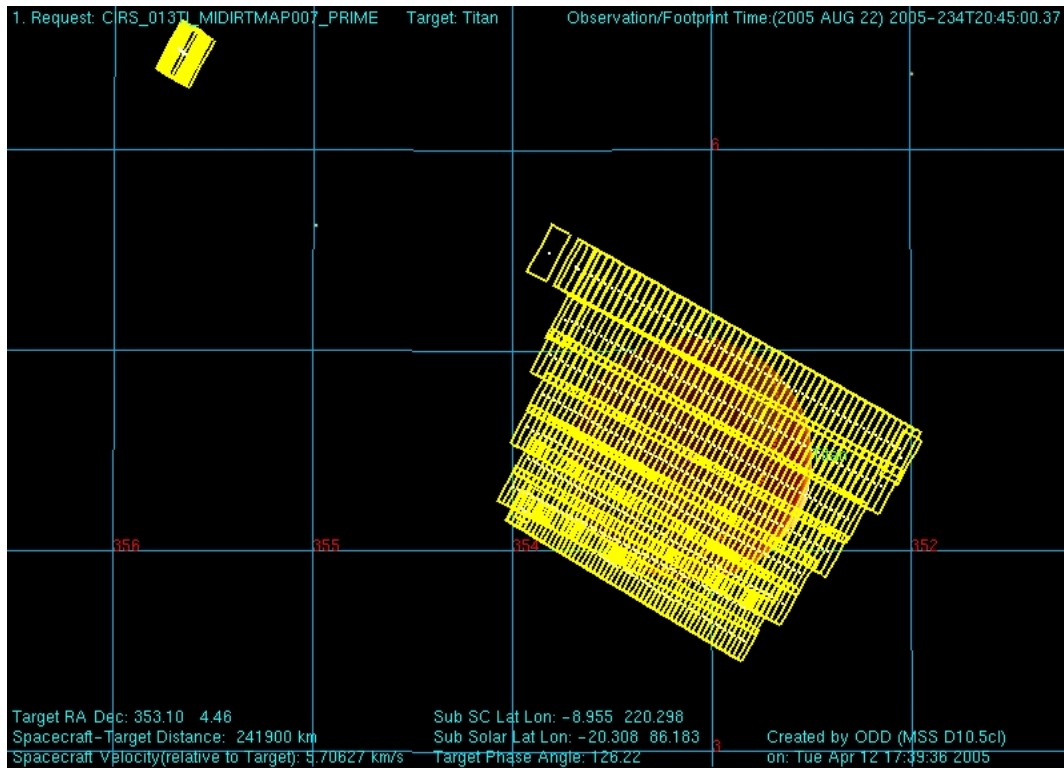


Figure 64: T6 MIDIRTMAP



## A.4 SATELLITES

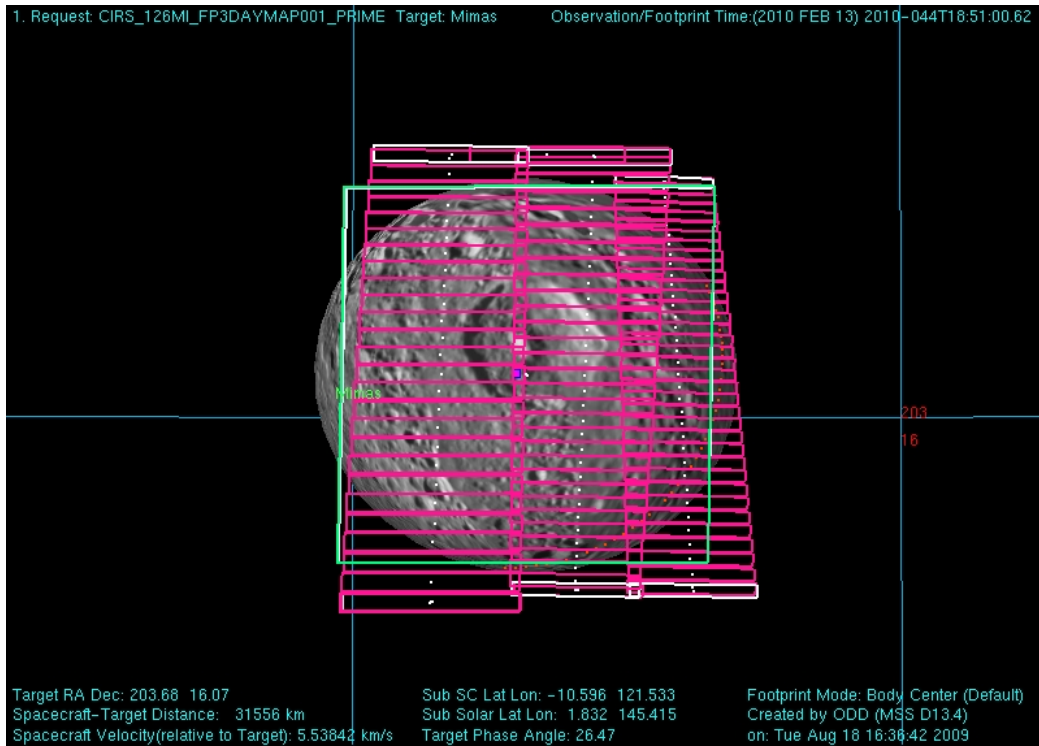


Figure 65: Mimas FP3DAYMAP in Rev 126A.4 SATELLITES

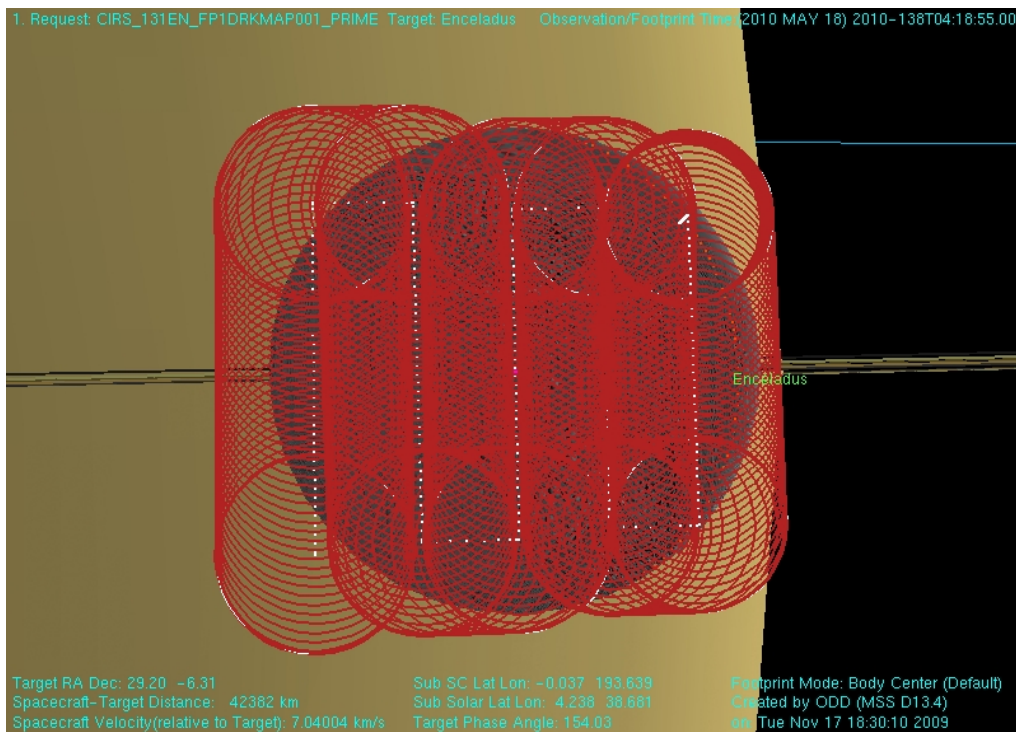


Figure 66: Enceladus FP1DRKMAP Rev 131

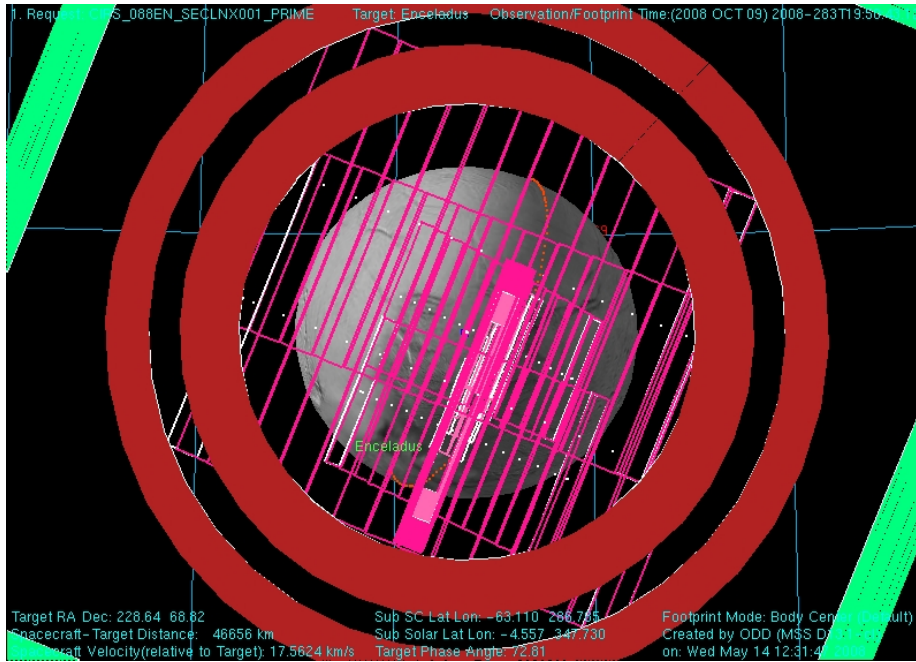


Figure 67: Enceladus SECLNX in Rev 8

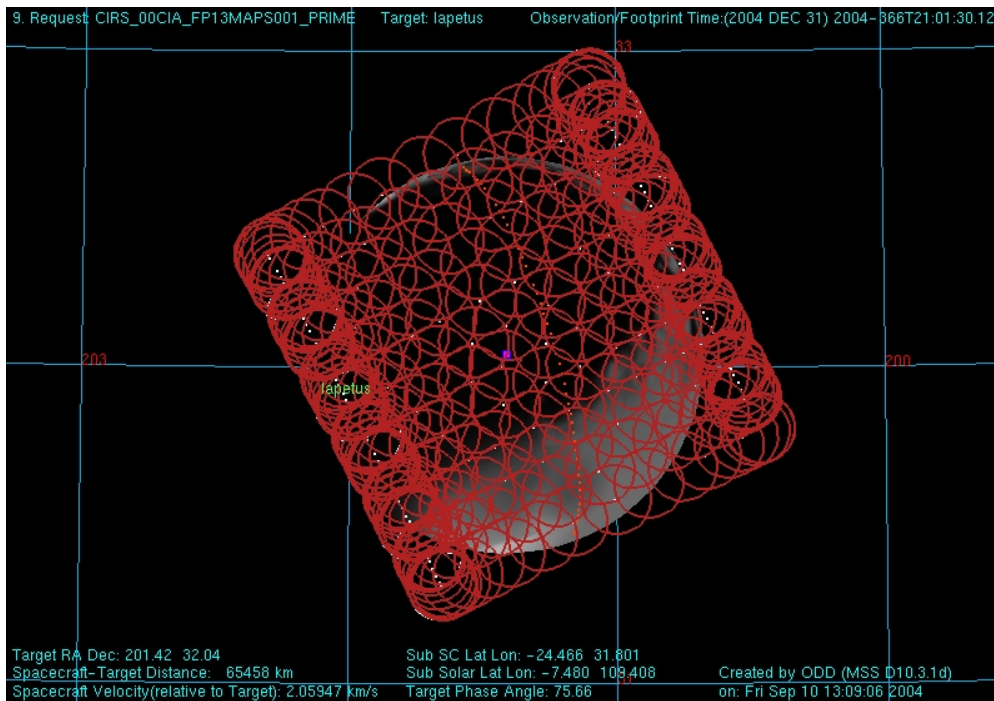


Figure 68: Iapetus FP13MAPS Rev 00C



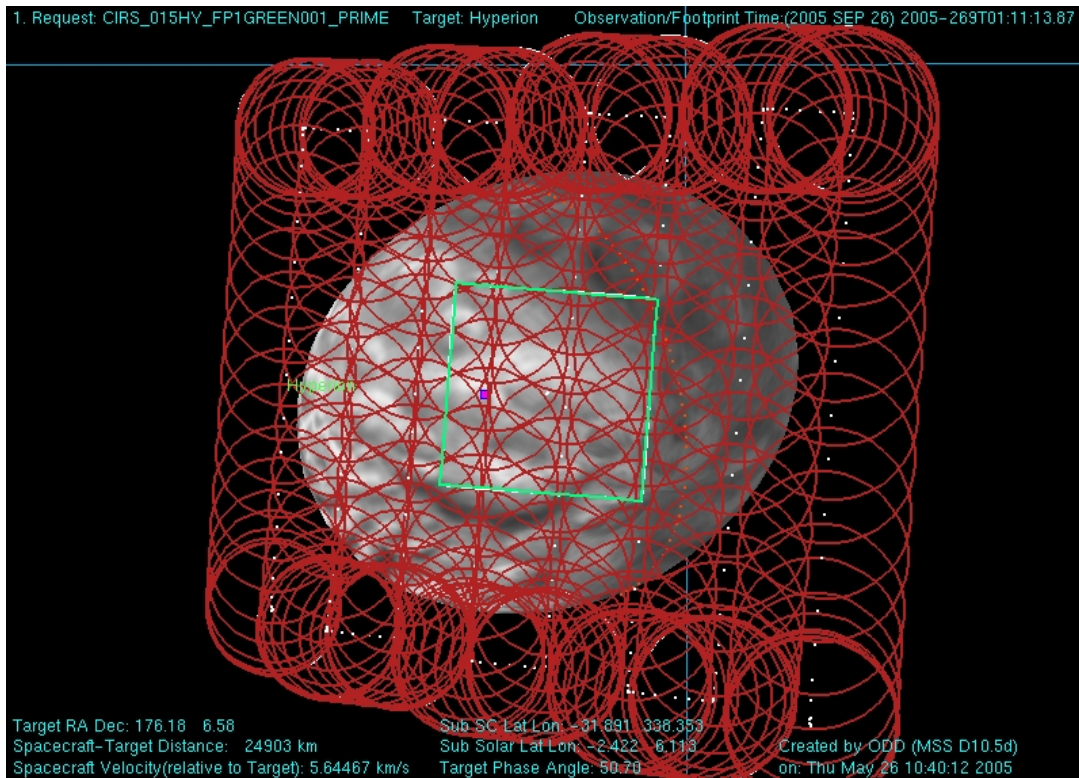


Figure 69: Hyperion FP1GREEN Rev 15

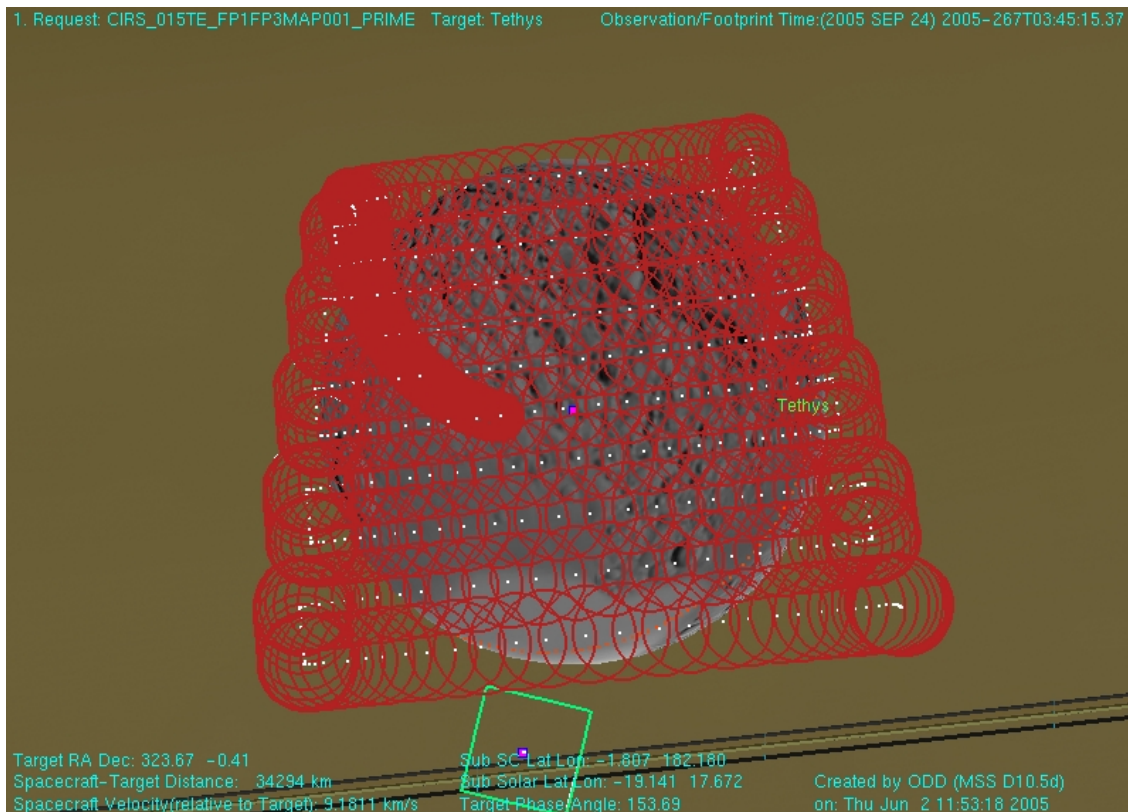


Figure 70: Tethys FP1FP3MAP Rev 15

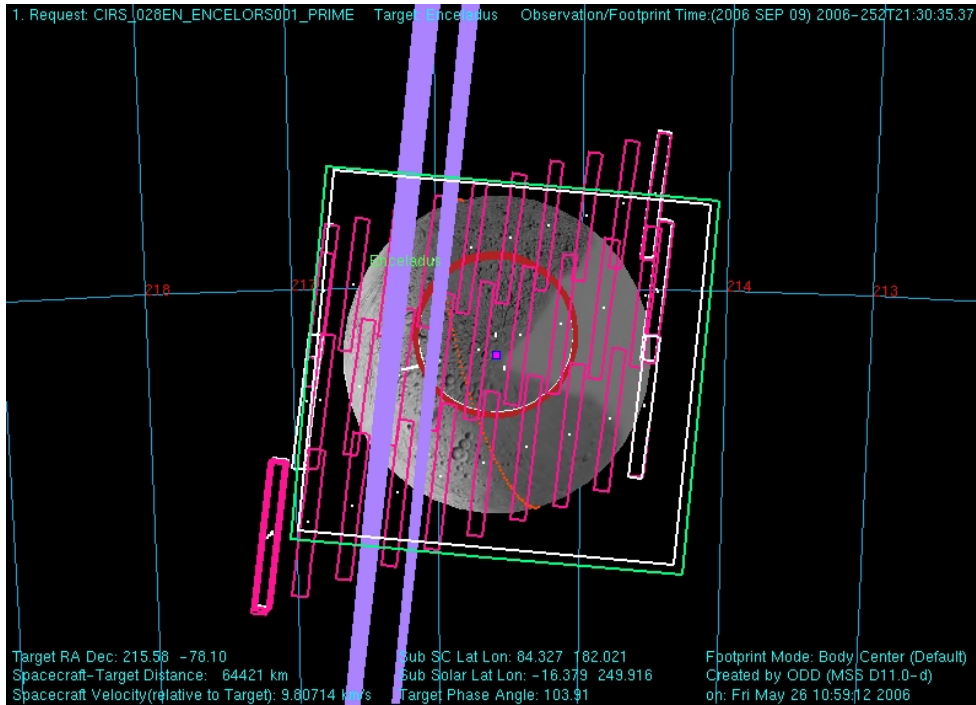


Figure 71: Enceladus Collaborative Observation taken in Rev 28. Includes ISS, UVIS, and VIMS pointing as well as CIRS FP1, FP3, and FP4.

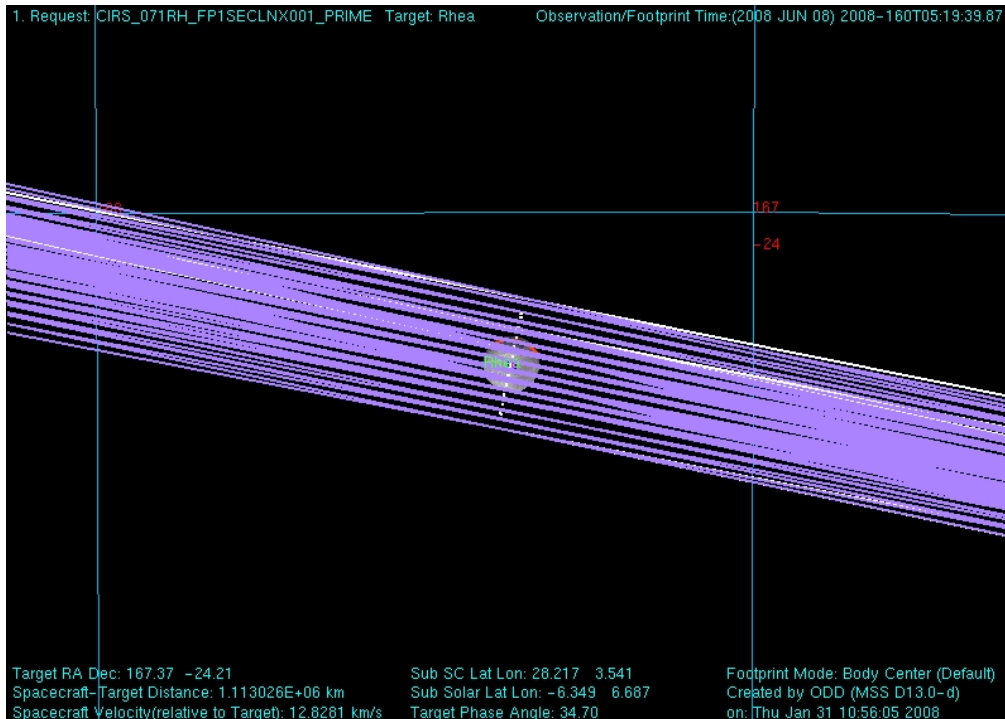


Figure 72: Rhea FP1SECLNX - Rhea eclipse exit on REV 71

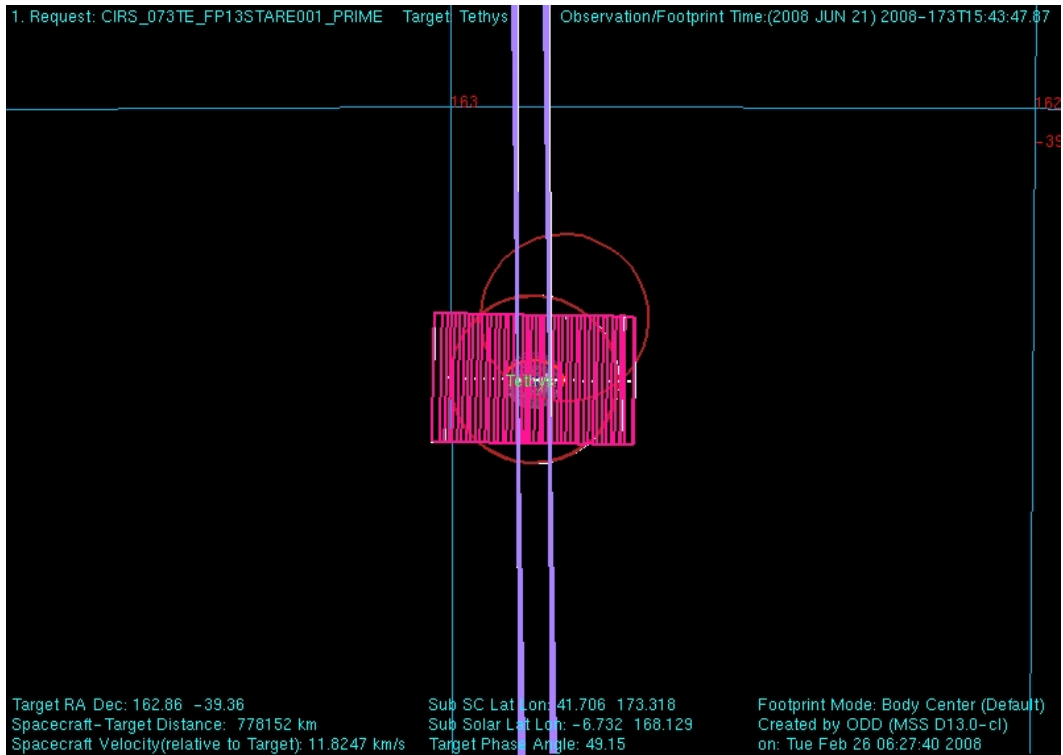


Figure 73: Tethys FP13STARE taken in Rev 73

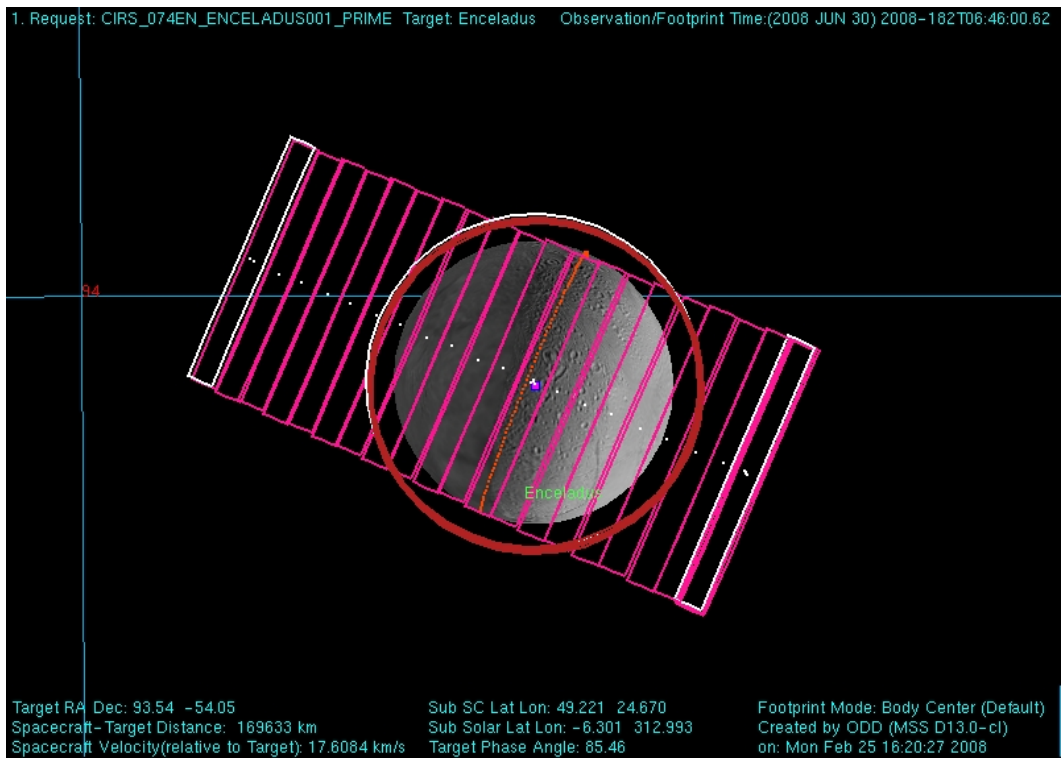


Figure 74: Enceladus distant FP3/4 map and FP1 Stare taken in Rev 74

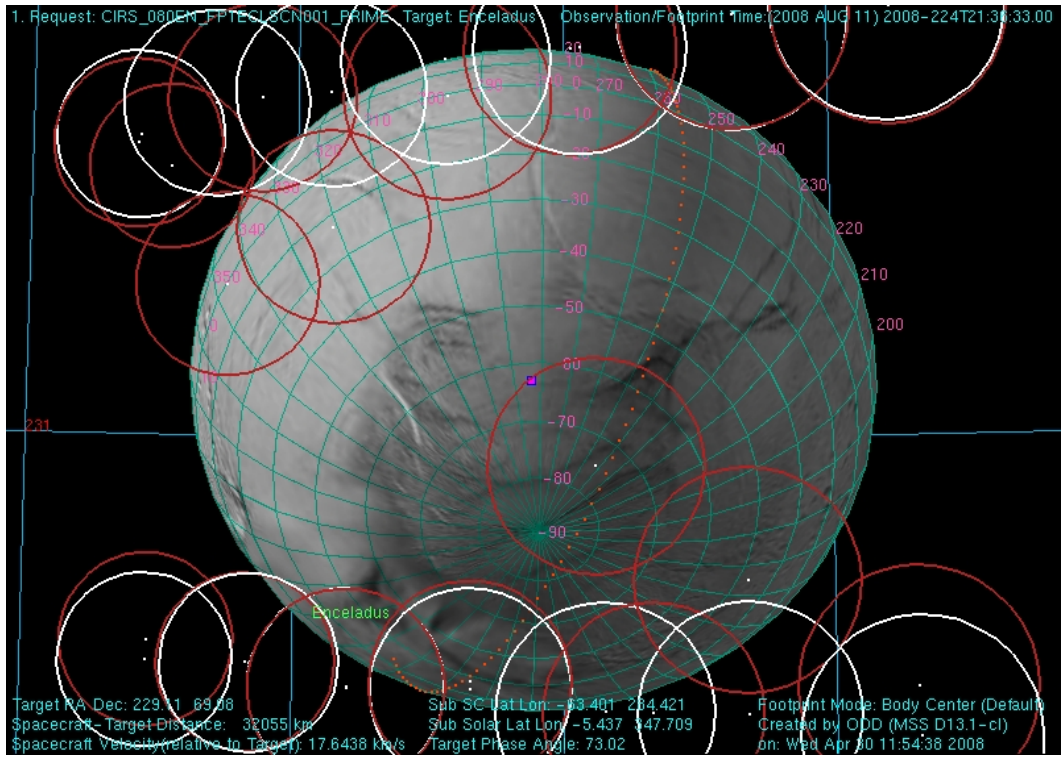


Figure 75: Enceladus FP1 Eclipse Scan/Map of the South Pole on Rev 80



## B. List of major data gaps

Table 21: list of major data gaps

<u>Observation name</u>	<u>Observation Start Time</u>	<u>Observation End Time</u>	<u>Expected Packets Received</u>
CIRS_C22JU_17ATM1X1265_ISS	11/2/2000 0:05:08	11/3/2000 3:23:11	0.00%
CIRS_000SA_MIRCMPSTA004_PRIME	6/8/2004 3:28:00	6/8/2004 5:28:00	0.00%
CIRS_000PH_FP13LTCRV004_PRIME	6/11/2004 4:40:00	6/11/2004 5:23:00	0.00%
CIRS_000RI_URIMPACT001_UVIS	7/4/2004 0:31:00	7/4/2004 2:31:00	0.00%
CIRS_000RI_COMP001_PRIME	7/4/2004 2:31:00	7/4/2004 12:41:00	0.00%
CIRS_00BDI_FP1DRKMAP001_PRIME	12/15/2004 1:40:00	12/15/2004 2:22:00	0.00%
CIRS_006RI_FMONITOR001_PRIME	4/19/2005 6:15:00	4/19/2005 14:30:00	0.00%
CIRS_013HY_GEOLOG009_ISS	8/17/2005 8:15:00	8/17/2005 8:35:00	0.00%
CIRS_013HY_GEOLOG011_ISS	8/17/2005 10:15:00	8/17/2005 10:35:00	0.00%
CIRS_013HY_GEOLOG013_ISS	8/17/2005 12:10:00	8/17/2005 12:30:00	0.00%
CIRS_014TI_MIDIRTMAP006_PRIME	9/6/2005 6:00:00	9/6/2005 11:00:00	0.00%
CIRS_014TI_FIRNADMAP005_ISS	9/7/2005 3:11:57	9/7/2005 7:20:57	0.00%
CIRS_014TI_FIRLMBBAER004_UVIS	9/7/2005 8:50:57	9/7/2005 9:35:57	0.00%
CIRS_014TI_MIRLMBINT002_PRIME	9/7/2005 13:51:57	9/7/2005 17:11:57	0.00%
CIRS_014TI_FIRNADCMP002_PRIME	9/7/2005 17:11:57	9/7/2005 20:11:57	0.00%
CIRS_014TI_MIDIRTMAP005_PRIME	9/7/2005 20:11:57	9/8/2005 2:23:49	0.00%
CIRS_015OT_ISSSPACE004_ISS	9/19/2005 6:25:00	9/19/2005 6:55:00	0.00%
CIRS_023TI_FIRNADCMP003_PRIME	4/30/2006 5:34:15	4/30/2006 11:58:15	0.00%
CIRS_023RE_E150PHASE001_VIMS	5/1/2006 23:10:00	5/2/2006 2:00:00	0.00%
CIRS_023RE_E150PHASE002_VIMS	5/2/2006 2:40:00	5/2/2006 3:50:00	0.00%
CIRS_023RE_E150PHASE004_VIMS	5/2/2006 5:35:00	5/2/2006 7:35:00	0.00%
CIRS_023RH_238W159PH001_ISS	5/2/2006 9:20:00	5/2/2006 10:30:00	0.00%
CIRS_023RE_E150PHASE007_VIMS	5/2/2006 13:20:00	5/2/2006 16:30:00	0.00%
CIRS_030IC_NORTH7CAL001_RADAR	10/7/2006 8:00:00	10/7/2006 9:45:00	0.00%
CIRS_030IC_DIORPX001_CDA	10/12/2006 3:15:00	10/12/2006 4:45:00	0.00%
CIRS_030RI_KAPSCOCC001_UVIS	10/13/2006 23:45:00	10/14/2006 7:50:00	0.00%
CIRS_030RA_VERTULMP001_PRIME	10/14/2006 7:50:00	10/14/2006 9:35:00	0.00%
CIRS_031IC_RPXING001_CDA	10/28/2006 2:30:00	10/28/2006 4:30:00	0.00%
CIRS_031IC_INMAGSCN001_INMS	10/28/2006 4:30:00	10/28/2006 6:00:00	0.00%
CIRS_032IC_ALPVIR001_UVIS	11/4/2006 3:12:00	11/4/2006 5:12:00	0.00%
CIRS_032IC_NORTH6CAL001_RADAR	11/4/2006 21:12:00	11/4/2006 22:42:00	0.00%
CIRS_032IC_LONG4CAL001_RADAR	11/6/2006 20:30:00	11/6/2006 22:00:00	0.00%
CIRS_032IC_NORTH4CAL001_RADAR	11/13/2006 21:14:00	11/13/2006 22:14:00	0.00%
CIRS_037IC_SOUTH3CAL001_RADAR	1/15/2007 16:30:00	1/15/2007 18:00:00	0.00%

CIRS_037IC_NORTH6CAL001_RADAR	1/18/2007 20:20:00	1/18/2007 21:50:00	0.00%
CIRS_037IC_NORTH3CAL002_RADAR	1/21/2007 1:45:00	1/21/2007 3:15:00	0.00%
CIRS_039TI_NIGHTNAC001_ISS	2/21/2007 11:23:25	2/21/2007 12:12:24	0.00%
CIRS_039TI_MIDIRTMAP001_PRIME	2/21/2007 12:12:24	2/21/2007 14:12:24	0.00%
CIRS_039TI_FIRNADCMP001_PRIME	2/21/2007 14:12:24	2/21/2007 17:12:24	0.00%
CIRS_039TI_PHOTOMWAC001_ISS	2/21/2007 17:12:24	2/21/2007 18:12:24	0.00%
CIRS_039TI_MIRLMBMAP001_PRIME	2/21/2007 18:12:24	2/21/2007 22:02:24	0.00%
CIRS_039TI_MONITORNA001_ISS	2/22/2007 14:12:24	2/22/2007 16:12:24	0.00%
CIRS_039TI_GLOBMAP001_VIMS	2/22/2007 16:12:24	2/22/2007 17:12:24	0.00%
CIRS_039TI_MIDIRTMAP002_PRIME	2/22/2007 17:12:24	2/23/2007 0:27:24	0.00%
CIRS_041TI_FIRLMBINT002_PRIME	3/26/2007 1:56:27	3/26/2007 2:38:27	0.00%
CIRS_043IA_TRAILSIDE111_ISS	4/21/2007 6:46:00	4/21/2007 7:50:00	0.00%
CIRS_043RB_VERTULMP002_PRIME	4/21/2007 7:50:00	4/21/2007 13:30:00	0.00%
CIRS_043RI_LATPHASE001_VIMS	4/21/2007 13:30:00	4/21/2007 20:45:00	0.00%
CIRS_046RI_LATPHASE001_VIMS	6/8/2007 10:40:00	6/8/2007 17:40:00	0.00%
CIRS_049IA_LIMBTOPOG001_ISS	9/9/2007 22:05:00	9/9/2007 22:25:00	0.00%
CIRS_050IC_CALSTAR3001_ISS	9/26/2007 21:51:00	9/27/2007 5:21:00	0.00%
CIRS_050RI_FMONITOR002_PRIME	9/27/2007 5:21:00	9/27/2007 9:36:00	0.00%
CIRS_050RI_SHADBOUND001_ISS	9/30/2007 22:30:00	9/30/2007 23:20:00	0.00%
CIRS_050RI_SUBMU04LP001_PRIME	9/30/2007 23:20:00	10/1/2007 3:20:00	0.00%
CIRS_050TI_MEDRES001_VIMS	10/2/2007 9:52:43	10/2/2007 12:42:43	0.00%
CIRS_050TI_GLOBMAP001_ISS	10/2/2007 12:42:43	10/2/2007 13:22:43	0.00%
CIRS_050TI_PHOTOMWAC002_ISS	10/2/2007 13:22:43	10/2/2007 13:42:43	0.00%
CIRS_050OT_SLEEP001_PRIME	10/6/2007 19:55:00	10/6/2007 20:00:00	0.00%
CIRS_052TI_FIRLMBT002_RIDER	11/19/2007 1:08:25	11/19/2007 1:31:25	0.00%
CIRS_052TI_HIRESNAC001_VIMS	11/19/2007 1:31:25	11/19/2007 2:47:25	0.00%
CIRS_058RI_RPXMOVIE001_VIMS	2/10/2008 16:06:00	2/10/2008 19:36:00	0.00%
CIRS_065RI_SUBMU60MP001_PRIME	4/20/2008 7:32:00	4/20/2008 12:20:00	0.00%
CIRS_066ST_RLEOCC001_VIMS	5/2/2008 4:40:00	5/2/2008 7:40:00	0.00%
CIRS_097RH_020W151PH001_ISS	12/17/2008 9:30:00	12/17/2008 11:43:00	0.00%
CIRS_105RI_LATPHASE108_VIMS	3/12/2009 11:45:00	3/12/2009 20:55:00	0.00%
CIRS_105RI_SATELLORB015_ISS	3/12/2009 20:55:00	3/12/2009 21:55:00	0.00%
CIRS_105RI_SURVEYPTG005_CAPS	3/13/2009 16:45:00	3/13/2009 18:45:00	0.00%
CIRS_105RI_SPKMVLFLP001_ISS	3/13/2009 18:45:00	3/14/2009 1:10:00	0.00%
CIRS_105RI_DEEPSPACE073_SP	3/14/2009 1:10:00	3/14/2009 1:50:00	0.00%
CIRS_105RI_EGPHASE119_VIMS	3/15/2009 4:00:00	3/15/2009 16:20:00	0.00%
CIRS_105RI_SATELLORB024_ISS	3/15/2009 16:20:00	3/15/2009 16:50:00	0.00%
CIRS_106TI_M60R2CLD075_ISS	3/16/2009 4:00:00	3/16/2009 5:15:00	0.00%
CIRS_106RI_SURVEYPTG001_CAPS	3/16/2009 5:45:00	3/16/2009 7:45:00	0.00%
CIRS_106RI_TMAPN20LP001_PRIME	3/16/2009 7:45:00	3/16/2009 17:45:00	0.00%
CIRS_106RI_DEEPSPACE076_SP	3/17/2009 3:20:00	3/17/2009 4:00:00	0.00%
CIRS_106RI_APOMOSU128_VIMS	3/17/2009 4:00:00	3/17/2009 17:25:00	0.00%
CIRS_108TI_M120R2HZ106_ISS	4/16/2009 9:13:00	4/16/2009 10:28:00	0.00%
CIRS_108RF_FMOVIE001_ISS	4/16/2009 10:28:00	4/16/2009 20:33:00	0.00%

CIRS_108IC_OPNAV061_NAV	4/16/2009 22:03:00	4/16/2009 23:32:00	0.00%
CIRS_109RI_LRHPENKMV001_ISS	4/17/2009 12:00:00	4/17/2009 20:00:00	0.00%
CIRS_109RI_MNRNGSHAD002_ISS	4/17/2009 22:00:00	4/17/2009 22:53:00	0.00%
CIRS_109TI_FIRNADCMP001_PRIME	4/19/2009 9:13:42	4/19/2009 14:20:45	0.00%
CIRS_109TI_PHOTOMWAC001_ISS	4/19/2009 14:20:45	4/19/2009 15:20:45	0.00%
CIRS_109TI_GLOBCLOUD001_VIMS	4/19/2009 15:20:45	4/19/2009 19:20:45	0.00%
CIRS_109TI_GLOBMAP001_ISS	4/20/2009 8:50:45	4/20/2009 9:20:45	0.00%
CIRS_109TI_GLOBMAP001_VIMS	4/20/2009 9:20:45	4/20/2009 14:20:45	0.00%
CIRS_109TI_MIDIRTMAP002_PRIME	4/20/2009 14:20:45	4/20/2009 22:20:45	0.00%
CIRS_109RI_SATELLORB004_ISS	4/24/2009 21:00:00	4/24/2009 21:33:00	0.00%
CIRS_110RI_LRHPENKMV001_ISS	5/4/2009 0:26:00	5/4/2009 8:42:00	0.00%
CIRS_110RI_SPKMVDFHP002_ISS	5/4/2009 14:42:00	5/4/2009 21:36:00	0.00%
CIRS_116TI_FIRNADCMP001_PRIME	8/9/2009 2:01:49	8/9/2009 4:03:53	0.00%
CIRS_116TI_PHOTOMWAC001_ISS	8/9/2009 4:03:53	8/9/2009 5:03:53	0.00%
CIRS_116TI_EUVFUV001_UVIS	8/9/2009 5:03:53	8/9/2009 8:53:53	0.00%
CIRS_116TI_TRANS001_ENGR	8/9/2009 14:29:53	8/9/2009 14:51:53	0.00%
CIRS_116TI_REGMAP001_ISS	8/9/2009 14:51:53	8/9/2009 16:11:49	0.00%
CIRS_117RI_HIPHASE001_VIMS	8/27/2009 2:45:00	8/27/2009 6:45:00	0.00%
CIRS_117RI_ALPORIOCC101_VIMS	8/27/2009 6:45:00	8/27/2009 9:10:00	0.00%
CIRS_117RI_URPI4ORIO01_UVIS	8/27/2009 9:10:00	8/27/2009 11:30:00	0.00%
CIRS_117RI_RNGMNSHAD001_ISS	8/27/2009 11:30:00	8/27/2009 12:30:00	0.00%
CIRS_117RI_LOWPHASE001_VIMS	8/27/2009 15:00:00	8/27/2009 17:00:00	0.00%
CIRS_117RI_EQXSHADOW013_ISS	8/27/2009 17:00:00	8/27/2009 20:45:00	0.00%
CIRS_117RI_POSTEQXB001_VIMS	8/27/2009 20:45:00	8/28/2009 0:45:00	0.00%
CIRS_117RI_EQLBN001_PRIME	8/28/2009 0:45:00	8/28/2009 6:45:00	0.00%
CIRS_117RI_POSTEQXB002_VIMS	8/28/2009 16:40:00	8/28/2009 20:40:00	0.00%
CIRS_117RI_TMAPN10LP002_PRIME	8/28/2009 20:40:00	8/29/2009 2:40:00	0.00%
CIRS_117RI_4STARCAL001_VIMS	8/29/2009 2:40:00	8/29/2009 7:00:00	0.00%
CIRS_117TI_M9OR3CLD241_ISS	8/29/2009 16:40:00	8/29/2009 17:55:00	0.00%
CIRS_117RI_RCOLSCEQX001_ISS	8/29/2009 20:25:00	8/30/2009 5:49:00	0.00%
CIRS_117RI_SPKMVLFP001_ISS	8/30/2009 16:40:00	8/31/2009 6:18:00	0.00%
CIRS_117TI_M9OR3CLD243_ISS	8/31/2009 16:35:00	8/31/2009 17:50:00	0.00%
CIRS_117RI_SPKMVLFP003_ISS	8/31/2009 20:20:00	9/1/2009 14:15:00	0.00%
CIRS_127TI_M6OR3CLD065_ISS	3/6/2010 19:29:00	3/6/2010 20:44:00	0.00%
CIRS_130OT_1STAROBS001_PRIME	4/18/2010 16:13:00	4/18/2010 23:13:00	0.00%
CIRS_134TI_GLOBMAP001_VIMS	7/7/2010 9:22:45	7/7/2010 14:22:45	0.00%
CIRS_134TI_GLOBMAP002_VIMS	7/7/2010 14:22:45	7/7/2010 17:57:45	0.00%
CIRS_141SA_COMPSIT001_PRIME	12/4/2010 5:00:00	12/4/2010 17:00:00	0.00%
CIRS_141RI_ERNGVERC001_ISS	12/4/2010 17:00:00	12/5/2010 6:00:00	0.00%
CIRS_148TI_M3OR2CLD131_ISS	5/11/2011 9:12:00	5/11/2011 10:42:00	0.00%
CIRS_050TI_MONITORNA001_ISS	10/2/2007 15:42:43	10/2/2007 17:42:43	0.06%
CIRS_000TI_FIRNADCMP005_VIMS	7/3/2004 3:15:00	7/3/2004 4:00:00	0.15%
CIRS_050TI_PHOTOMWAC001_ISS	10/1/2007 18:42:43	10/1/2007 19:42:43	0.17%
CIRS_109TI_REGCLDMAP001_VIMS	4/19/2009 19:20:45	4/19/2009 21:20:45	0.21%

CIRS_102RI_ALPTRAOCC105_VIMS	2/1/2009 5:07:00	2/1/2009 14:22:00	0.47%
CIRS_109RF_FRSTRCHAN001_ISS	4/24/2009 9:55:00	4/24/2009 21:00:00	4.27%
CIRS_104RI_DEEPSPACE058_SP	2/27/2009 4:35:00	2/27/2009 5:10:00	5.30%
CIRS_076RI_SUBMU45MP001_PRIME	7/13/2008 12:22:00	7/13/2008 15:22:00	6.88%



## C. The CIRS FP1 Spike Suppression Algorithm: Methodology

The FP1 spike suppression algorithm can be summarized as follows:

- “Pure” FP1 0.5 Hz and 8.0 Hz spike combs are constructed from “global” large averages of deep-space interferograms recorded over a several-month time period.
- The 0.5 Hz and 8.0 Hz spike combs, the target interferograms (Saturn, Titan, rings, satellites, etc.), and the deep-space interferograms are first over-sampled by a factor of 8. The 8X over-sampled spike combs are then independently adjusted in position and amplitude to fit the 0.5 Hz and 8.0 Hz spike patterns in the 8X over-sampled target and deep-space interferograms.
- The 8X over-sampled position- and amplitude-adjusted spike combs are then subtracted from the 8X over-sampled target and deep-space interferograms in order to calculate 8X over-sampled spike-free interferograms.
- The 8X over-sampled spike-free target and deep-space interferograms are down-sampled to their original number of samples.
- The down-sampled spike-free target and deep-space interferograms are used to calculate spike-free radiometrically-calibrated spectra.

The logic of the algorithm is illustrated in Figure 76. The “sine wave” suppression is not included in the present data base release. It will appear in a future release.

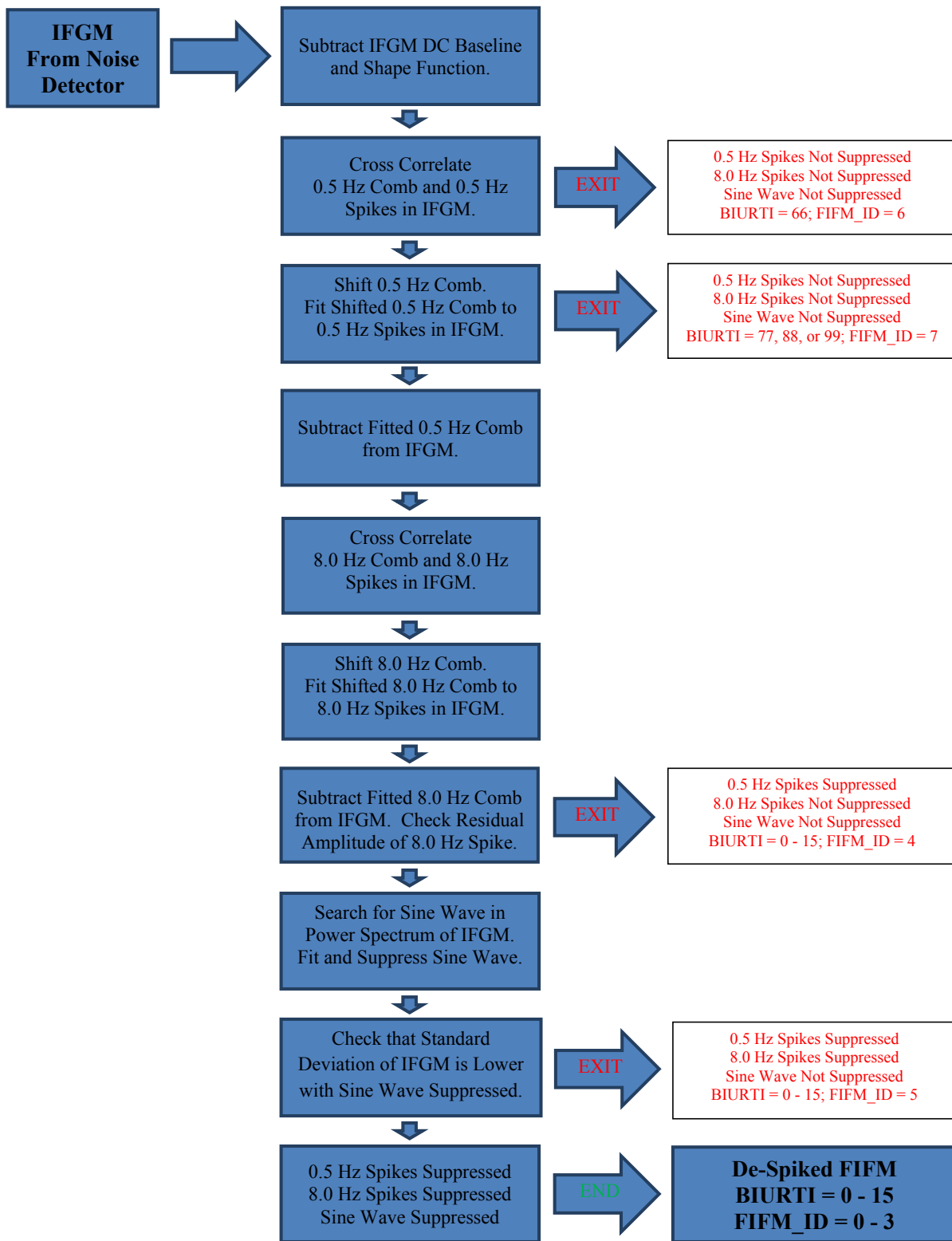


Figure 76: CIRS spike suppression algorithm block diagram

## C.1 Calculation of the 0.5 Hz and 8.0 Hz reference waveforms (“combs”)

Separate FP1 0.5 Hz and 8.0 Hz spike combs are constructed from “global” averages of deep-space interferograms. The interferograms in each average are carefully selected to be free of external noise effects, such as transient spikes, ZPD shifts, laser mode drifts, and velocity variations. The CIRS interferogram noise detector is used in conjunction with restricting the lengths of the interferograms to assure optimal quality. The 0.5 Hz and 8.0 Hz combs are calculated separately from each of 16 average 401 RTI deep-space interferograms with the same 0.5 Hz BIURTI offset value. The 0.5 Hz BIURTI offset = the number of RTIs that have elapsed from the beginning of sampling until the appearance of the first 0.5 Hz spike in the interferogram. An individual interferogram will therefore have one of 16 possible BIURTI offsets = 0, 1, 2, 3, ..., 15 RTI.

The D. C. baseline and the 401 RTI FP1 interferogram shape function are first subtracted from each of the 16 average deep-space interferograms (BIURTI offsets = 0 - 15 RTI). The shape function is calculated by twice Gaussian-filtering an average of 48,475 401 RTI deep-space interferograms that were recorded during the CIRS Saturn mission. Each interferogram is then over-sampled by the factor  $F = 8$  and now has 8 times as many points as it had originally. The “flat” region of each over-sampled average interferogram is defined to begin at the over-sampled sample number  $N = n * F = 345 * 8 = 2760$  and is far enough beyond the interferogram’s ZPD region to be fairly uniform in D. C. level. The 0.5 Hz and 8.0 Hz spike patterns in the “flat” region are now separated to form the respective spike combs. Each comb is then extrapolated from the “flat” region to cover the entire interferogram range, plus ~ 410 samples (after down-sampling) beyond the normal length of a 401 RTI interferogram. The extra length ensures that a 0.5 Hz comb of any BIURTI offset may be fitted to an interferogram of the same or any other BIURTI offset for the spike suppression. The fifteen 0.5 Hz combs with BIURTI offsets = 1, 2, 3, ..., 15 RTI are next shifted to coincide with the comb with BIURTI offset = 0, and the sixteen coincident combs are averaged. The sixteen 8.0 Hz combs are averaged without being shifted. Next, each 0.5 Hz spike in the averaged extrapolated comb is replaced by the average of the 0.5 Hz spikes in the “flat” region. The “global” 0.5 Hz and 8.0 Hz spike combs that were used to de-spike all of the spectra in the current PDS database were calculated from the following deep-space interferograms: 401 RTI, interferogram length = 2770 - 2780 samples, DSCAL = 1, BIURTI offset = 0 - 15 RTI, 8,758 interferograms averaged from 10/01/2005 - 02/28/2006, CIRS reference laser mode = 02.

## C.2 Calculation of de-spiked filtered interferograms (FIFMs)

The D. C. baseline and the FP1 interferogram shape function are first subtracted from a single or average interferogram that is to be de-spiked. If an average interferogram is to be de-spiked, then each interferogram in the average must have the same 0.5 Hz BIURTI offset

value. The interferogram is then over-sampled by the factor  $F = 8$ . The 0.5 Hz and 8.0 Hz Spike combs are already over-sampled.

The BIURTI offset value of the over-sampled interferogram that is to be de-spiked is first determined by a cross-correlation between the interferogram's 0.5 Hz spike pattern and the spike pattern in the over-sampled 0.5 Hz comb with BIURTI offset = 0. The 0.5 Hz comb is then shifted by the number of samples required to make its 0.5 Hz spikes coincide with the spikes in the interferogram. A similar cross correlation and shift of the 8.0 Hz spike pattern is subsequently performed.

"Flat" regions of the shifted over-sampled 0.5 Hz and 8.0 Hz spike combs and the interferogram are now defined. The "flat" regions begin at the over-sampled sample number  $N = n * F = 345 * 8 = 2760$  and are far enough beyond the interferogram's ZPD region to be fairly uniform in D. C. level.

The "flat" regions of the shifted 0.5 Hz and 8.0 Hz over-sampled spike combs are independently adjusted in position and amplitude to fit the 0.5 Hz and 8.0 Hz spike patterns in the "flat" regions of the over-sampled interferogram. In the course of this process, which is performed iteratively, the 0.5 Hz and 8.0 Hz spike patterns in the interferogram are separated from each other in order to be independently fitted to the 0.5 Hz and 8.0 Hz spike combs, respectively. It was found that only two iterations are required to closely match the positions and amplitudes of the 0.5 Hz and 8.0 Hz spikes in the combs to the corresponding spikes in the interferogram. If a single interferogram is being de-spiked, some of the 0.5 Hz spikes may be missing or greatly reduced in amplitude due to noise. Therefore, the correlation is verified by calculating the sample numbers and negative amplitudes of the interferogram's 0.5 Hz spikes that occur within  $\pm F/2 = \pm 8/2 = \pm 4$  samples of the position of each 0.5 Hz spike in the shifted 0.5 Hz comb. A minimum of twelve 0.5 Hz spikes with amplitudes  $< 4.0$  standard deviations from the mean must be present in the "flat" region of a 400 or 401 RTI interferogram in order for the correlation to be considered successful. The adjusted amplitude of the 0.5 Hz comb is calculated from the ratio of the average spike amplitudes in the shifted comb and the interferogram. The adjusted amplitude of the 8.0 Hz comb is calculated from the square root of the ratio of the 8.0 Hz power spectra of the comb and interferogram, including the 16.0 Hz and 24.0 Hz harmonics.

The "flat" regions of the over-sampled, shifted, and amplitude-adjusted 0.5 Hz and 8.0 Hz spike combs are extrapolated to the samples range of the entire over-sampled interferogram = ZPD region + "flat" region. The entire over-sampled, shifted, and amplitude-adjusted 0.5 Hz and 8.0 Hz spike combs (ZPD region + "flat" region) are then subtracted from the entire over-sampled interferogram. Finally, the de-spiked over-sampled filtered interferogram (FIFM) is down-sampled to its original length and is now ready to be included in the calibration process.

## D. Effective Integration Times

The method for calculating an effective integration time for a scan of a given spectral resolution was developed by L. Herath. CIRS interferograms are not purely one-sided or two-sided, since data sampling is initiated  $\sim 1.5$  seconds before the carriage reaches the ZPD point ( $x = L_1$ ). The data sampled before ZPD will be averaged with the corresponding data sampled after ZPD in the  $\sim$  symmetrical two-sided region centered about ZPD. The total number of data samples acquired after ZPD determines the spectral resolution. The pre- and post-ZPD interferogram regions are illustrated in Figure 77, which is an average of FP1 deep space interferograms recorded December 6 - 9, 2000.

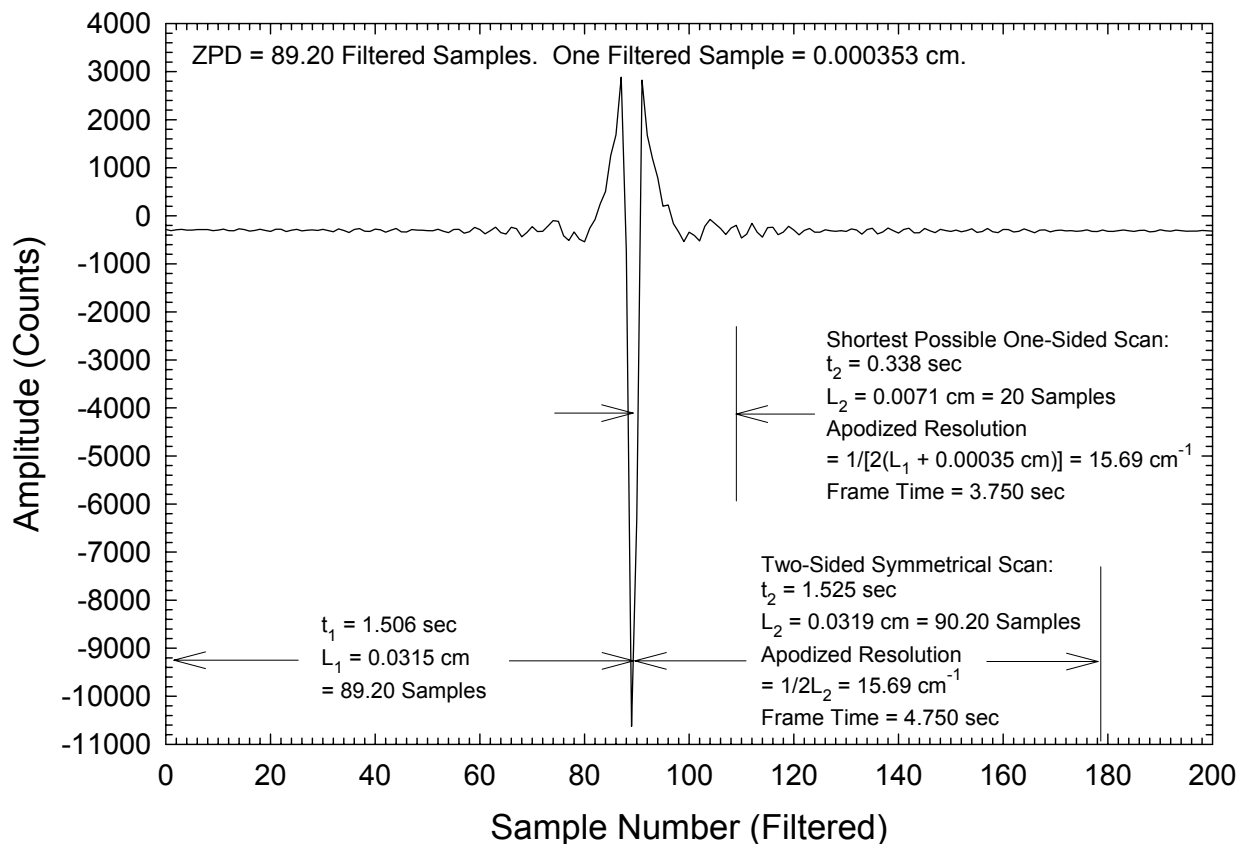


Figure 77: anatomy of an asymmetric interferogram

All interferogram data do not contribute equally to the spectral noise when apodization is applied. Data near ZPD ( $x = L_1$ ) contribute the most to the noise, whereas data at maximum path difference ( $x = L_1 + L_2$ ) contribute very little. Conversely, adding integration time near ZPD contributes more to reducing the spectral noise than does adding integration time near maximum path difference. Therefore, the extra 1.5 seconds of integration time before the carriage reaches the ZPD point contributes more than the interferogram average to reducing the spectral noise and results in an effective integration time  $\equiv t_{\text{eff}}$  that is slightly

greater than the total scan time =  $t_1 + t_2$ . This effective integration time is used to calculate NESRs for single and averaged scans. The NESRs thus calculated have been verified by comparisons with standard deviations of large averages of deep-space spectra.

The effect of apodization is expressed as a factor  $q$ , with the spectral noise proportional to  $\sqrt{q}$ :

$$q = \frac{1}{L_1 + L_2} \int_0^{L_1+L_2} |f(x)|^2 dx \quad (D.1)$$

$f(x)$  = apodization function

$L_1$  = scan length before ZPD (cm)

$L_2$  = scan length from ZPD to the end of scan (cm)

Equation (D.1) may be expressed in terms of time as:

$$q = \frac{1}{t_1 + t_2} \int_0^{t_1+t_2} |f(t)|^2 dt \quad (D.2)$$

$A(t)$  = apodization function

$t_1$  = scan time before ZPD (sec)

$t_2$  = scan time from ZPD to the end of scan (sec)

To evaluate the effective integration time, we shall compare  $q$  calculated by Equation (D.3) to that of a one-sided scan  $\equiv q_0$ , beginning at the ZPD point and ending at  $t_2$ :

$$q_0 = \frac{1}{t_2} \int_0^{t_2} |f(t)|^2 dt \quad (D.4)$$

We now average the pre-ZPD side of the interferogram from 0 to  $t_1$  with its counterpart on the post-ZPD side from  $t_1$  to  $2t_1$ , thereby reducing the noise in the interval 0 to  $t_1$  by  $\sqrt{2}$ .  $q$  then becomes:

$$q_1 = \frac{1}{t_2} \left[ \int_0^{t_1} \left| \left( \frac{1}{\sqrt{2}} \right) f(t) \right|^2 dt + \int_{t_1}^{t_2} |f(t)|^2 dt \right] \quad (D.5)$$

The effective integration time is then:

$$t_{\text{Eff}} = t_2 (q_0 / q_1) \quad (D.6)$$

For the CIRS instrument a Hamming apodization function is used to calculate  $t_{\text{Eff}}$ :

$$f(t) = 0.54 + 0.46 * \cos\left(\frac{\pi t}{t_{\max}}\right) \quad (D.7)$$

$t_{\max}$  = maximum carriage travel time from ZPD to the end of scan =  $t_2$  (sec)

It was desired to derive an empirical relationship between  $t_{\text{Eff}}$  and apodized spectral resolution  $\equiv R_{\text{Apod}}$ . To this end,  $t_{\text{Eff}}$  was calculated individually for 14 different resolutions from  $0.50 \text{ cm}^{-1}$  to  $20.291 \text{ cm}^{-1}$  using Equations (D.6) and (D.7). The FP1 pre-ZPD scan time  $t_1 = 1.506$  seconds was used in the calculations. The 14 pairs of  $\{t_{\text{Eff}}, R_{\text{Apod}}\}$  values were then fitted to an inverse 5<sup>th</sup> order polynomial in order to empirically determine  $t_{\text{Eff}}$  as a function of  $R_{\text{Apod}}$ :

$$t_{\text{Eff}} = a_0 + \frac{a_1}{R_{\text{Apod}}} + \frac{a_2}{R_{\text{Apod}}^2} + \frac{a_3}{R_{\text{Apod}}^3} + \frac{a_4}{R_{\text{Apod}}^4} + \frac{a_5}{R_{\text{Apod}}^5} \quad (11)$$

The inverse polynomial fits are illustrated in Figure 78, and the coefficients are listed in Table 22. Values of  $t_{\text{Eff}}$  for selected spectral resolutions are included in Table 17.

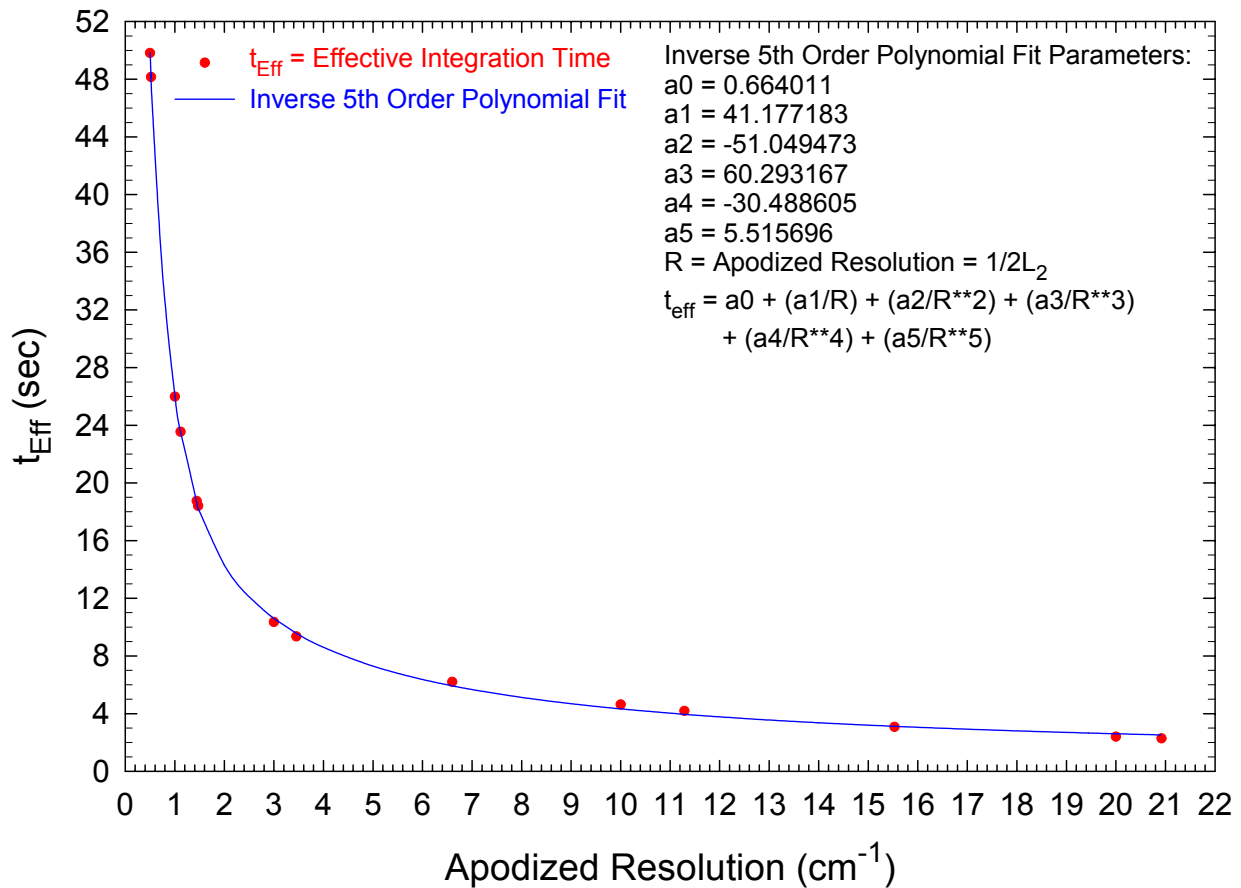


Figure 78: inverse polynomial fit of scan time to spectral resolution

**Table 22: Coefficients for the inverse 5th order polynomial fit to effective integration time as a function of spectral resolution**

Coefficient	Value
a0	0.664011
a1	41.177183
a2	-51.049473
a3	60.293167
a4	-30.488605
a5	5.515696

## E. Contact Information

### CIRS Team Authors:

Conor A. Nixon,  
NASA Goddard Space Flight Center Code 693, Greenbelt, MD 20771, USA  
301-286-6757; [conor.a.nixon@nasa.gov](mailto:conor.a.nixon@nasa.gov)

Monte S. Kaelberer  
NASA Goddard Space Flight Center Code 693, Greenbelt, MD 20771, USA  
301-286-0560; [monte.s.kaelberer@nasa.gov](mailto:monte.s.kaelberer@nasa.gov)

Nicolas Gorius  
NASA Goddard Space Flight Center Code 693, Greenbelt, MD 20771, USA  
301-286-0021; [Nicolas.gorius@nasa.gov](mailto:Nicolas.gorius@nasa.gov)

### PDS Atmospheres Node (master PDS database copy)

Lyle R. Huber  
Astronomy Department, New Mexico State University, P. O. Box 30001, Dept 4500.  
Las Cruces, NM 88003.  
575-646-1862; [lhuber@nmsu.edu](mailto:lhuber@nmsu.edu)

### PDS Rings Node (including ASCII database version)



Mark Showalter  
SETI Institute, 189 Bernardo Ave., Suite 100, Mountain View, CA 94043, USA  
650-810-0234; [mshowalter@seti.org](mailto:mshowalter@seti.org)